

# THE INFLUENCE OF DISABLING INJURIES ON THE DESIGN OF THE VEHICLE FRONT END FOR PEDESTRIAN SAFETY

---

A Dissertation  
Presented to  
The Faculty of the School of Engineering and Applied Science  
University of Virginia

---

In Partial Fulfillment  
of the Requirements for the Degree  
Doctor of Philosophy  
Mechanical and Aerospace Engineering

---

by  
Varun Bollapragada  
August 2019

---

Accepted by:  
Dr. Jason R. Kerrigan, Committee Chair  
Dr. Jeff R. Crandall, Advisor  
Dr. Taewung Kim, Co-Advisor  
Dr. Timothy L. McMurry  
Dr. Matthew B. Panzer  
Dr. Thomas Hartka

# Abstract

Pedestrians struck by motor vehicles constitute a global health problem accounting for nearly 270,000 deaths and 10 million injuries worldwide annually. This dissertation addresses one aspect of this global health problem from an engineering standpoint. Although pedestrian safety regulations exist, they have been criticized for only representing a narrow range of crash scenarios.

Most pedestrian crashes occur with the front of the vehicle impacting the pedestrian. The design of a vehicle front end and potential countermeasures to improve pedestrian safety is a challenging problem owing to both the complex nature of the design space as well as the risk of injury depending on the speed, stature, stance, impact location, geometry and stiffness of the front end. The complexity and breadth of the problem necessitates a comprehensive but efficient approach to the design of countermeasures. Multibody models have the potential to serve as excellent tools for such optimization studies owing to their computational efficiency, however, the biofidelity of these models is under question.

Traditionally, in the design of vehicles, the focus has been on minimizing the risk of fatalities. As countermeasures, regulations, and infrastructure are developed there is a trend towards fewer fatalities but injuries, albeit at potentially a lower severity, still exist. Many of these injuries have long-term consequences for the pedestrian survivors. The current pedestrian safety regulations rely on subsystem-based

procedures. Experimental test devices have been developed that represent the head, thigh-pelvis, and lower extremities. Given the complexity of the pedestrian kinematics, the subsystem procedures alone are insufficient to evaluate the protection provided by the countermeasures. Additionally, there is a lack of a comprehensive cost model that can detect the effects of local design changes on the overall risk arising from a vehicle to pedestrian impact. Also, the influence of disabling injuries on the design of the vehicle front end remains unexplored.

This dissertation provides a framework for the assessment of disabling injuries on the design of the vehicle front end for pedestrian safety. Firstly, a multibody model of a pedestrian representing the 50<sup>th</sup> percentile male is developed and its biofidelity is assessed by a series of component level impact tests in conjunction with whole-body impacts with a generic pedestrian buck. Field data from pedestrian databases is analyzed to identify the representative pedestrian injuries based on frequency, and their injury mechanisms are identified. With the aid of the Monte Carlo approach a cost function is developed to quantify the influence of both fatal and disabling injuries. The developed cost function in conjunction with the validated multibody pedestrian model is used to explore the primary objective of understanding the influence of disabling injuries on vehicle design (for pedestrian crashes). A design of experiment (DOE) is conducted by using a parameterized vehicle model representing a sedan impacting a 50<sup>th</sup> percentile male pedestrian at speeds of 40 km/hr and 25 km/hr.

The influence of disabling injuries on the vehicle design diminishes with increase in the speed of impact due to a higher risk of fatalities. In a hypothetical scenario where there are no head injuries (which are the leading cause of pedestrian fatalities) the cost associated with disability is more influential in affecting the vehicle design. Hence, it is important to consider the disability outcome while designing the countermeasures. While this dissertation focuses on pedestrian crash scenarios,

the framework developed here can be applied during the design of a vehicle for other crash modes like frontal, rear, and oblique impacts.

## **Dedication**

This dissertation is dedicated to my parents, brother and my wife for their unconditional love and support at various stages of my life.

## Acknowledgments

I would like to thank my advisor Dr. Jeff R. Crandall for providing me the opportunity to work with him and for the guidance and support which led to the successful completion of this dissertation. He has served as an inspiration and a role model to achieve excellence. In the nascent stages of my graduate career, Dr. Taewung Kim (co-advisor) took me under his wing and introduced me to the field of multibody dynamics and modeling. We have worked on several projects together and it was an excellent opportunity to work under his guidance. I would also like to express my gratitude for the members of my advisory committee Dr. Jason Kerrigan, Dr. Mathew Panzer, Dr. Tim McMurry and Dr. Tom Hartka who helped mold the dissertation and improve its quality. I would also like to thank Dr. Gerald Poplin for guiding me through the epidemiological work presented in this dissertation. I would also like to express my gratitude to Kasia Rawska who helped me setup and run MADYMO simulations in various projects associated with this dissertation. I would also like to thank Dr. Bronek Gepner for introducing me to parallel computing, and always lending a helpful hand in streamlining my simulation runs in this study.

I would also like to like to express my gratitude to all my friends and co-workers at the Center for Applied Biomechanics who helped me navigate my graduate career at the lab. I appreciate the friendship of Sourabh Boruah, Jacek Toczyski, Dani Perez, Salvador Acosta, Gwansik Park, and Joseph Ash who made my stay in Charlottesville

memorable and also extended their help and support through discussions and projects. I am also thankful to other members at the lab Taotao Wu, Lee gabler, BingBing Nie, and Hamed Joodaki for their collaboration in projects with their help and expertize. At various points I have received help from Jason Forman, Greg shaw, Sara Heltzel, and David Lessley with their expertise in their specialties.

I would also like to thank my brother Vikas Bollapragada for his help provided in reviewing this dissertation. I also acknowledge the thoughtful review of the manuscript by Tim Gillespie.

# Table of Contents

<b>Title Page</b> . . . . .	<b>i</b>
<b>Abstract</b> . . . . .	<b>ii</b>
<b>Dedication</b> . . . . .	<b>v</b>
<b>Acknowledgments</b> . . . . .	<b>vi</b>
<b>List of Tables</b> . . . . .	<b>xi</b>
<b>List of Figures</b> . . . . .	<b>xiii</b>
<b>1 Introduction</b> . . . . .	<b>1</b>
1.1 Background and Motivation . . . . .	1
1.2 Summary . . . . .	10
<b>2 Central Idea of Research</b> . . . . .	<b>12</b>
<b>3 Task 1: Field Data Analysis</b> . . . . .	<b>15</b>
3.1 Population and Demographic Characteristics . . . . .	15
3.2 Fatalities . . . . .	16
3.3 Hospitalized Pedestrians . . . . .	17
3.4 Injury Distributions . . . . .	17
<b>4 Injury Mechanisms and Risk functions</b> . . . . .	<b>20</b>
4.1 Head . . . . .	20
4.2 Nij . . . . .	24
4.3 Neck . . . . .	25
4.4 Face . . . . .	26
4.5 Upper Extremities . . . . .	27
4.6 Abdomen . . . . .	30
4.7 Pelvis . . . . .	31
4.8 Thigh and Leg . . . . .	32
4.9 Knee . . . . .	33

4.10	Foot/Ankle . . . . .	34
<b>5</b>	<b>Socio Economic Costs Associated With Injuries . . . . .</b>	<b>35</b>
5.1	Economic Costs . . . . .	36
5.2	Medical Costs . . . . .	36
5.3	Work Losses . . . . .	37
5.4	Health Status and Impairment . . . . .	38
5.5	Injury Impairment Index (III) . . . . .	40
5.6	Functional Capacity Index (FCI) and Whole Body FCI (WBFCI) . . . . .	41
5.7	Maximum AIS (MAIS) and New Injury Severity Score . . . . .	43
<b>6</b>	<b>Task2: Development and Validation of the UVAPED Model - Component Level Validation . . . . .</b>	<b>45</b>
6.1	Head . . . . .	48
6.2	Neck . . . . .	49
6.3	Shoulder Lateral . . . . .	52
6.4	ISO9790 Lateral Shoulder Impact . . . . .	54
6.5	Thorax . . . . .	54
6.6	Abdomen . . . . .	59
6.7	Pelvis . . . . .	62
6.8	Lower Extremities . . . . .	63
6.9	Discussion . . . . .	64
<b>7</b>	<b>Task2: Development and Validation of the UVAPED Model - Whole Body Validation . . . . .</b>	<b>69</b>
7.1	Introduction . . . . .	69
7.2	Scaling and Positioning . . . . .	70
7.3	Results . . . . .	75
7.4	Discussion . . . . .	91
<b>8</b>	<b>Task3: Injury Metric for Cost Estimation in the Optimization Problem . . . . .</b>	<b>94</b>
8.1	Introduction . . . . .	94
8.2	Methodology . . . . .	95
8.3	Monte Carlo Method of MAIS Estimation . . . . .	97
8.4	Assigning Specific AIS Codes (Monte Carlo Simulation II) . . . . .	100
8.5	Poly-trauma Injury Loss Metric Values . . . . .	102
8.6	Sanity Check . . . . .	103
8.7	Convergence Study . . . . .	104
8.8	Discussion . . . . .	105
8.9	Conclusion . . . . .	107
8.10	Limitations . . . . .	108

<b>9 Task4: DOE Exploration for The Design of Front End of a Vehicle for Pedestrian Impact Using Multiple Objective Functions . . . . .</b>	<b>109</b>
9.1 Introduction . . . . .	109
9.2 Methodology . . . . .	110
9.3 Results . . . . .	113
9.4 Discussion . . . . .	128
<b>10 Conclusions . . . . .</b>	<b>141</b>
10.1 Concluding Remarks . . . . .	141
10.2 Limitations and Future Work . . . . .	143
10.3 Contributions . . . . .	144
<b>Appendices . . . . .</b>	<b>146</b>
A Model Description . . . . .	147
B Component Validation . . . . .	155
C Whole-body evaluation . . . . .	172
D CIREN Case-Series Analysis . . . . .	193
E MacKenzie’s Original Description of FCI Dimension Impairment (1996)	208
F Mapping of AIS Code to Body Region and Injury Metric . . . . .	212
<b>Bibliography . . . . .</b>	<b>225</b>

# List of Tables

3.1	United States Frequency of Fatal and Non-Fatal MVC Victims Seeking Medical Treatment in 2012 . . . . .	16
4.1	Peak Limits and Nij Intercepts . . . . .	24
6.1	List of References for Validations of Responses Under Blunt Impacts .	47
6.2	Summary of ISO Ratings for Component Level Validation of UVAPED Model . . . . .	65
7.1	Comparison of Average ISO Rating Across Three Tests . . . . .	85
7.2	Comparison of Injury Reported in Experiments and Model Predictions for PMHS 2370 . . . . .	88
7.3	Comparison of Injury Reported in Experiments and Model Predictions for PMHS 2371 . . . . .	89
7.4	Comparison of Injury Reported in Experiments and Model Predictions for PMHS 2374 . . . . .	90
8.1	List of Injury Metrics Mapped to Their Associated Body Regions . .	97
8.2	Convergence Study of the Monte Carlo Simulations for ISS, WBFCI, and LYL . . . . .	104
9.1	Description and Bounds of Design Variables . . . . .	112
9.2	Contact Area to Scale the Force . . . . .	113
9.3	Summary of Range of Variation in Life Years Lost Across the Design Space . . . . .	115
9.4	Linear Regression Model of LYLC at 40 Km/hr . . . . .	122
9.5	Linear Regression Model for LYLC at 25 Km/hr . . . . .	124
9.6	Loss Metric Summary for the Best and the Worst Designs . . . . .	136
9.7	Design Parameters for the Best and the Worst Designs . . . . .	136
9.8	Injury Metric Summary for the Best and the Worst Designs . . . . .	136
9.9	A Comparison of Interquartile Range of Life Years Lost With and Without Head Trauma . . . . .	139
9.10	Variation in Poly-trauma Metrics with End Time at 40 km/hr for the Best Designs . . . . .	140

D.1	Summary of Included CIREN Cases*	194
D.2	Injury Frequency and Cost Summary	197
D.3	Injury and Disability and Probability of Fatality Scores	200
D.4	Individual Capacity Scores Across The Ten Dimensions of Function, FCI201	
D.5	Comparison of Most Severe and Most Disabling Injuries	202
D.6	Summary of Estimated Vehicle Speed	203
E.1	MacKenzie's original Description of FCI Dimension Impairment (1996) - Impairment Levels A,B,C	208
E.2	MacKenzie's original Description of FCI Dimension Impairment (1996) - Impairment Levels D,E,F,G	210
F.1	Mapping of AIS Code to Body Region and Injury Metric	212

# List of Figures

1.1	Motor Vehicle Crash Related Fatalities in United States, 2000-2012 . . . . .	2
1.2	Distribution of Pedestrian Injuries in Pedestrian-Vehicle Crashes (left) and Frequency of Injury Caused by Different Vehicle Regions (right). [adapted from <a href="#">Crandall et al. (2002)</a> ] . . . . .	3
1.3	Human Pedestrian Models . . . . .	5
1.4	Distribution of Injury Severity in Pedestrians (left) and Percentage of Adult Discharged Pedestrians Who Have Some Form of Functional Limitation One-Year Post Discharge (right) [adapted from <a href="#">Arregui-Dalmases et al. (2010)</a> ] . . . . .	10
2.1	Flowchart of Tasks Proposed For This Dissertation . . . . .	14
3.1	Distribution of Injury Severities (AIS 2+) . . . . .	18
3.2	Body Region Injury Distribution (AIS 2+) . . . . .	19
4.1	Six Regions for Nij Calculation . . . . .	25
4.2	Calculation of Cmax Using Lateral Chest Deflection . . . . .	29
4.3	Impactor Areas for Viano and Walfisch Risk Functions . . . . .	31
4.4	Area Where Pelvis Contact Force Was Measured . . . . .	32
6.1	UVAPED Baseline Model . . . . .	46
6.2	Head Frontal Impact Test Setup . . . . .	48
6.3	Lloyd Head Impact Test Setup . . . . .	49
6.4	NBDL Volunteer Neck Flexion Experiment ( <a href="#">Thunnissen et al. (1995)</a> ) . . . . .	50
6.5	Model Setup for Frontal and Lateral Test . . . . .	51
6.6	Input Acceleration Pulses for Frontal and Lateral Test of Neck ( <a href="#">GESAC (2005)</a> ) . . . . .	51
6.7	Compigne Lateral Shoulder Impact Test and Simulation Setups ( <a href="#">Compigne et al. (2004)</a> ) . . . . .	52
6.8	Subit Lateral Shoulder Impact Test and Simulation Setups ( <a href="#">Subit et al. (2010)</a> ) . . . . .	54
6.9	ISO/Meyer Lateral Shoulder Impact test and Simulation Setups ( <a href="#">ISO (1997)</a> ; <a href="#">Meyer and Bonnoit (1994)</a> ) . . . . .	55
6.10	Viano Thoracic Impact Test and Simulation Setups ( <a href="#">Viano et al. (1989)</a> ) . . . . .	56
6.11	ISO Thoracic Lateral Impact Test and Simulation Setups . . . . .	57

6.12	Impact Location, Lateral Impact Test, and Simulation Setups (Subit et al. (2010)) . . . . .	58
6.13	Simulation Setup for Thorax Frontal Impact . . . . .	59
6.14	Viano Lateral Abdominal Impact Test and Simulation Setups (Viano et al. (1989)) . . . . .	60
6.15	Abdomen Frontal Impact Test and Simulation Setups (Cavanaugh et al. (1986)) . . . . .	61
6.16	Viano Lateral Pelvis Impact Simulation (Viano et al. (1989)) . . . . .	62
6.17	Thigh and Leg Test and Simulation Setups (Kerrigan (2008a)) . . . . .	64
7.1	Generic Pedestrian Buck . . . . .	71
7.2	Scaled UVAPED Models . . . . .	71
7.3	Scaled TNOEL Models . . . . .	72
7.4	Schematic Overview of Positioning Procedure . . . . .	72
7.5	Comparison of Positioned Model UVAPED to Vicon Data at Anatomical Land Marks for PMHS V2370 . . . . .	73
7.6	Comparison of Positioned Model Uvaped to Vicon Data at Anatomical Land Marks for PMHS V2371 . . . . .	73
7.7	Comparison of Positioned Model Uvaped to Vicon Data at Anatomical Land Marks for PMHS V2374 . . . . .	74
7.8	Comparison of Pedestrian Impact Sequences for Test V2370 (Posterior View) . . . . .	75
7.9	Comparison of Pedestrian Impact Sequences for Test V2370 (Superior View) . . . . .	76
7.10	Comparison of Pedestrian Impact Sequences for Test V2371 (Posterior View) . . . . .	77
7.11	Comparison of Pedestrian Impact Sequences for Test V2371 (Superior View) . . . . .	78
7.12	Comparison of Pedestrian Impact Sequences for Test V2374 (Posterior View) . . . . .	79
7.13	Comparison of Pedestrian Impact Sequences for Test V2374 (Superior View) . . . . .	80
7.14	Trajectories of the Head, T1, T8 and Pelvis in Buck Ref Frame for the UVAPED model . . . . .	82
7.15	Trajectories of the Head, T1, T8 and Pelvis in Buck Ref Frame for THUMS PFEM model . . . . .	83
7.16	Trajectories of the Head, T1, T8 and Pelvis in Buck Ref Frame for TNOEL model . . . . .	84
7.17	Summary of Average ISO Scores for Different Signals . . . . .	87
7.18	Pictorial Representation of Injuries (Forman et al. (2015)) . . . . .	87
8.1	Injury Mapping for UVAPED Model From Field Data . . . . .	96
8.2	Injury Mapping for UVAPED Model From Field Data . . . . .	96

8.3	Monte Carlo Simulation 1 (MC1)	98
8.4	Example of Monte Carlo Sampling of MAIS for the Skull Body Region	99
8.5	Generation of M virtual Pedestrians With Prescribed MAIS Levels for Each Body Region	99
8.6	Sorting Real World Pedestrian Injury Data Into Body Regions Categorized by MAIS Level	101
8.7	Assignment of Injury to Specific Body Regions Through Random Sampling From Categorized MAIS Bins From the Pedestrian Database	101
8.8	Mapping Injury Patterns Based on MAIS Levels in Body Regions	102
8.9	Histogram of the WBFCI From the Real-world Database (Mapped Injuries Only) and the Monte Carlo Sampling II	105
9.1	Parametrization of Vehicle Front Shape	112
9.2	Contact Stiffness Characteristics of Bumper, Grill, and Hood	113
9.3	DOE Exploration of Life Years Lost at 40 km/hr	114
9.4	DOE Exploration of Life Years Lost at 25 km/hr	114
9.5	Range of Variation in Life Years Lost	115
9.6	Distribution of Whole Body FCI With Respect to NISS	116
9.7	Distribution of Normalized Design Variables Categorized by Cumulative Life Years Lost at 40 km/hr	118
9.8	Distribution of Normalized Design Variables Categorized by Cumulative Life Years Lost at 25 km/hr	119
9.9	Frequency of Vehicle Designs Grouped by Number of Cumulative Life Years Lost	119
9.10	Relative Ranking of Body Regions in Terms of Cumulative Life Years Lost	120
9.11	Relative Ranking of Body Regions in Terms of Life Years Lost Due to Fatality	121
9.12	Relative Ranking of Body Regions in Terms of Life Years Lost Due to Disability	121
9.13	DOE Exploration of Life Years Lost (weighted)	126
9.14	Distribution of WBFCI With Respect to (weighted)	126
9.15	Distribution of Design Variables Categorized by Cumulative Life Years Lost (Weighted)	128
9.16	Frequency of Vehicle Designs Grouped by Cumulative Number of Life Years Lost (Weighted)	128
9.17	Sensitivity of HIC36 With Normalized Windshield Peak Force	130
9.18	Sensitivity of UBrIC With Normalized Bonnet Length	130
9.19	Sensitivity of UBrIC With Normalized Bonnet Angle	131
9.20	Sensitivity of UBrIC With Normalized Windshield Peak Force	131
9.21	Range of Nij	132

9.22	Sensitivity of Anterior-Posterior Thorax Compression With Normalized Bonnet Angle . . . . .	132
9.23	Sensitivity of Pelvis Contact Force With Normalized Bonnet Leading Edge Height . . . . .	133
9.24	Sensitivity of Maximum Bending Moment in Femur With Normalized Bumper Lead . . . . .	133
9.25	Sensitivity of Maximum Bending Moment in Tibia With Normalized Bumper Force2 . . . . .	134
9.26	Sensitivity of Maximum Bending Moment in Tibia With Normalized Bumper Def2 . . . . .	134
9.27	DOE Exploration of Life Years Lost in Absence of Head Trauma (Weighted)	138
A.1	Schematic of Head and Face in UVAPED Model . . . . .	147
A.2	Schematic of Neck in UVAPED Model . . . . .	148
A.3	Schematic of Shoulder Structure . . . . .	149
A.4	Schematic of Thorax . . . . .	150
A.5	Mode Shapes of Thorax . . . . .	150
A.6	Schematic of Pelvis . . . . .	151
A.7	Lower Extremity Kerrigan (left) UVAPED (right) . . . . .	152
A.8	Schematic of Ankle/Foot Structure . . . . .	154
B.1	Head Frontal Impact (Melvin et al. (1985)) (a) 2 m/s (b) 5.5 m/s . . . . .	155
B.2	Forehead Drop Test (Lloyd et al. (2012)) (a) 1.1 m/s (b) 2.4 m/s . . . . .	155
B.3	Lateral Shoulder Impact (ISO (1997)) (a) 4.5 m/s (b) 5.5 m/s . . . . .	156
B.4	Lateral Shoulder Impact 1.5 m/s (Compigne et al. (2004)) . . . . .	156
B.5	Lateral Shoulder Impact 3 m/s (Compigne et al. (2004)) . . . . .	157
B.6	Lateral Shoulder Impact 1 m/s (Subit et al. (2010)) . . . . .	158
B.7	Lateral Shoulder Impact 3 m/s (Subit et al. (2010)) . . . . .	159
B.8	Frontal Thoracic Impact (Kroell et al. (1971)) (a) 4.3 m/s (b) 6.7 m/s . . . . .	160
B.9	Lateral Thoracic Oblique Impact (Viano et al. (1989)) 4.4 m/s . . . . .	160
B.10	Lateral Thoracic Oblique Impact (Viano et al. (1989)) 6.5 m/s . . . . .	161
B.11	Lateral Thoracic Mid Impact (Subit et al. (2010)) 1 m/s . . . . .	161
B.12	Lateral Thoracic Mid Impact (Subit et al. (2010)) 3 m/s . . . . .	162
B.13	Lateral Thoracic Up Impact (Subit et al. (2010)) 1 m/s . . . . .	162
B.14	Lateral Thoracic Up Impact (Subit et al. (2010)) 3 m/s . . . . .	163
B.15	Lateral Thoracic AL 15 deg Mid Impact (Subit et al. (2010)) 3 m/s . . . . .	163
B.16	Lateral Thoracic AL 15 deg Up Impact (Subit et al. (2010)) 3 m/s . . . . .	164
B.17	Lateral Thoracic PL 15 deg Mid Impact (Subit et al. (2010)) 3 m/s . . . . .	164
B.18	Lateral Thoracic PL 15 deg Up Impact (Subit et al. (2010)) 3 m/s . . . . .	165
B.19	Abdomen Frontal Impact (Cavanaugh et al. (1986)) 6.1 m/s . . . . .	165
B.20	Abdomen Lateral Impact (Viano et al. (1989)) (a) 4.8 m/s (b) 6.8 m/s . . . . .	166
B.21	Pelvis Lateral Impact (Viano et al. (1989)) (a) 4.5 m/s (b) 9.6 m/s . . . . .	166
B.22	Mid-Thigh Three Point Bending (Kerrigan et al. (2004)) 1.5 m/s . . . . .	167

B.23	Distal Thigh Three Point Bending (Kerrigan et al. (2004)) 1.5 m/s	168
B.24	Proximal Leg Three Point Bending (Kerrigan et al. (2004)) 1.5 m/s	169
B.25	Mid Leg Three Point Bending (Kerrigan et al. (2004)) 1.5 m/s	170
B.26	Distal Leg Three Point Bending (Kerrigan et al. (2004)) 1.5 m/s	171
C.1	Force Measurement Location and Coordinate System	172
C.2	Head Resultant Acceleration	173
C.3	T1 Resultant Acceleration	173
C.4	T8 Resultant Acceleration	174
C.5	Pelvis Resultant Acceleration	174
C.6	RFemur Resultant Acceleration	175
C.7	RTibia Resultant Acceleration	175
C.8	LTibia Resultant Acceleration	176
C.9	LFemur Resultant Acceleration	176
C.10	Head Angular Velocity (X)	177
C.11	T1 Angular Velocity (X)	177
C.12	Pelvis Angular Velocity (X)	178
C.13	RFemur Angular Velocity (X)	178
C.14	RTibia Angular Velocity (X)	179
C.15	LTibia Angular Velocity (X)	179
C.16	Head Angular Velocity (Y)	180
C.17	T1 Angular Velocity (Y)	180
C.18	Pelvis Angular Velocity (Y)	181
C.19	RFemur Angular Velocity (Y)	181
C.20	RTibia Angular Velocity (Y)	182
C.21	LTibia Angular Velocity (Y)	182
C.22	Head Angular Velocity (Z)	183
C.23	T1 Angular Velocity (Z)	183
C.24	Pelvis Angular Velocity (Z)	184
C.25	RFemur Angular Velocity (Z)	184
C.26	RTibia Angular Velocity (Z)	185
C.27	LFemur Angular Velocity (Z)	185
C.28	LTibia Angular Velocity (Z)	186
C.29	Hood Edge Passenger Side (Z)	187
C.30	Hood Edge Driver Side Force (Z)	187
C.31	Grill Passenger Side Force (Z)	188
C.32	Grill Driver Side Force (Z)	188
C.33	Upper Bumper Passenger Side Force (Z)	189
C.34	Upper Bumper Driver Side Force (Z)	189
C.35	Lower Bumper Passenger Side Force (Z)	190
C.36	Lower Bumper Driver Side Force (Z)	190
C.37	Hood Edge Passenger Side (Y)	191
C.38	Hood Edge Driver Side Force (Y)	191

C.39 Grille Passenger Side Force (Y) . . . . .	192
C.40 Grill Driver Side Force (Y) . . . . .	192
D.1 Comparison of Hospital Costs vs Estimated Costs. (Blincoe et al. (2015))	198
D.2 Hospital Medical Cost vs Number of AIS2+ Injuries (Survivors) . . .	198
D.3 Frequency Distribution of All (a) and AIS 2+ Injuries Based on Body Region . . . . .	199
D.4 Proportion and Magnitude of Functional Impairment Among Pedes- trian Case Series . . . . .	200
D.5 Comparison of Case Estimated Impact Speed to Reported Corridor Results in Bhalla et al. (2002) . . . . .	203

# Chapter 1

## Introduction

### 1.1 Background and Motivation

The World Health Organization estimates that about 22% of road traffic fatalities are pedestrians, accounting for nearly 270,000 deaths and 10 million injuries worldwide (WHO (2013)) annually. The proportion of pedestrian fatalities is even higher in lower or middle-income countries where they represent at least one-third of the road fatalities. Trauma data in the United States (U.S.) indicates that while the overall number of fatalities from motor vehicle crashes (MVCs) has decreased over the last 5 years, pedestrian fatalities have actually risen during the same period (Figure 1.1). For example, Retting and Rothenberg (2016) indicate that the number of fatalities increased by 10% between 2014 and 2015. While the number of fatalities are in themselves staggering, in the U.S., for every one pedestrian fatality, 13 people survive with injuries (Traffic safety facts, 2015 data). In addition to the loss of lives, pedestrian injuries also pose a great burden on society in terms of economic loss. Miller et al. (2004) estimated that the comprehensive lifetime costs including work losses, household productivity loss, and medical and legal costs accounted for \$40 billion (year 2000 dollars) for pedestrian and pedal cyclist injuries sustained in the

year 2000.

In adult pedestrians, the head and the lower extremities are the most commonly injured body parts, with head injury being the main cause of fatality (Figure 1.2). The windscreen and the bumper represent the two main sources of injury in pedestrian crashes (Crandall et al. (2002)).

Pedestrians struck by motor vehicles constitutes a global health problem requiring a multi-faceted solution like improvements to road infrastructure, pedestrian education, public policy, and vehicle countermeasures (Crandall et al. (2006)). From an engineering standpoint, the potential solutions for improving the safety of pedestrians is through the development of pedestrian safety standards, experimental research, and the use of computational models and surrogates during the design phase of a vehicle to improve the structure and develop countermeasures.

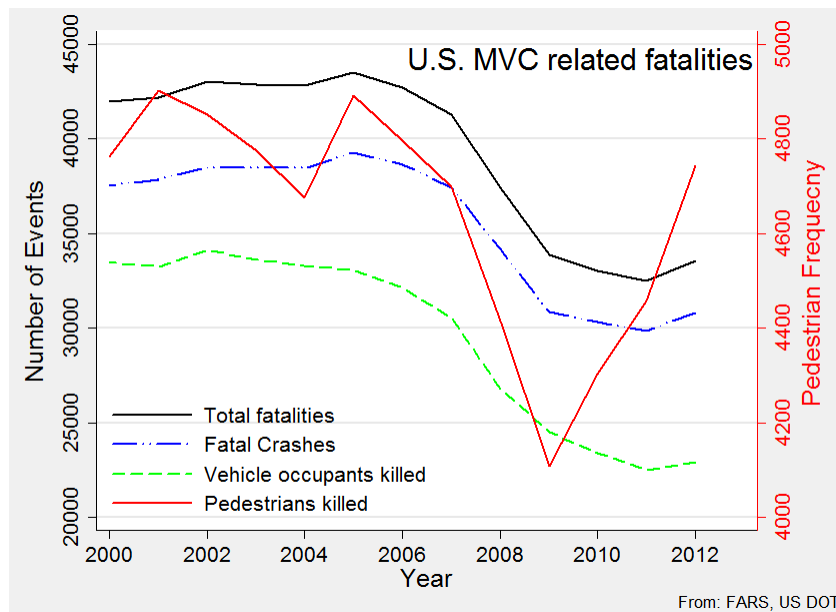


Figure 1.1: Motor Vehicle Crash Related Fatalities in United States, 2000-2012

The European Enhanced Vehicle Safety Committee (EEVC (1998)), the International Organization for Standardization (ISO (2002)) and the International Har-

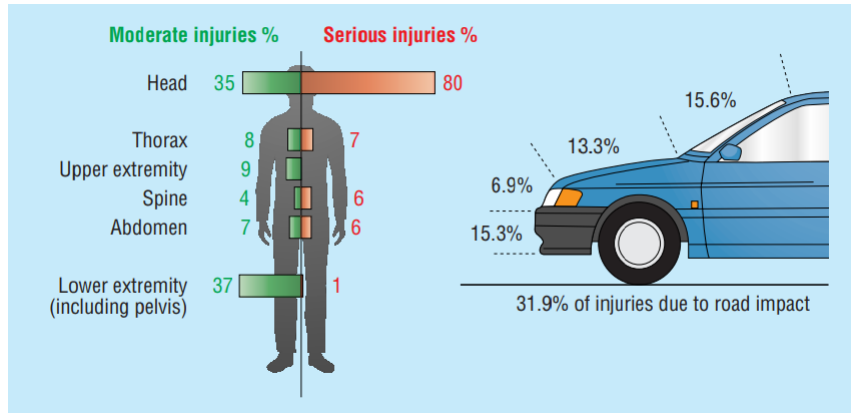


Figure 1.2: Distribution of Pedestrian Injuries in Pedestrian-Vehicle Crashes (left) and Frequency of Injury Caused by Different Vehicle Regions (right). [adapted from Crandall et al. (2002)]

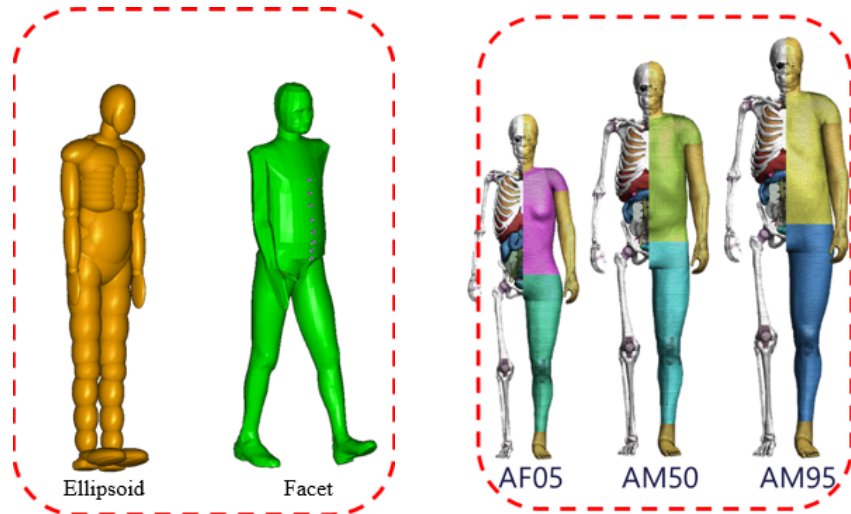
monized Research Activities (IHRA) (Mizuno and Ishikawa (2001)) were the main bodies established for developing pedestrian test standards. A series of sub-system impactor tests to mimic a 40 km/h pedestrian car crash have been developed by the EEVC and have established a rating system to rank the front end of the vehicle based on the sub-system impacts. The European parliament and Council adopted the Directive 2003/102/EC which provides for the introduction of requirements for leg injuries, and adult and child head injuries in the form of the European New Car Assessment Program (EuroNCAP). Injury thresholds were established and the front structures of vehicles were evaluated with the aid of sub-system impacts (Martinez et al. (2007)). IHRA in coordination with the pedestrian safety working group (PS) drafted the Global Technical Regulation (GTR) (UNECE (2008)). GTR omitted the inclusion of the testing of the windshield area for head form impactor tests and also excluded a potential upper leg-form test citing the lack of a biofidelic impactor. GTR had a larger threshold for HIC and similar leg form test specifications when compared to EURONCAP. The Japanese government has introduced a regulation for pedestrian protection with regards to small cars and trucks under a gross weight of

2500 kg (JNCAP). These sub-system impactor tests have been widely criticized in the literature for lacking the biofidelity to model the pedestrian-vehicle impacts ([Matsui et al. \(2002\)](#); [Bhalla et al. \(2003\)](#); [Kerrigan et al. \(2008\)](#)). Also, the focus on testing and regulations representing a crash scenario of 40 km/h limits the applicability of sub-system tests.

Along with the development of pedestrian testing standards, significant efforts have been made to develop the Polar pedestrian dummy that can be used to study whole-body pedestrian impacts under repeatable scenarios ([Akiyama et al. \(2001\)](#)). [Kerrigan et al.](#) noted that while the Polar-II dummy exhibited kinematic biofidelity (based on trajectory of the head, T1, and T8) relative to Post Mortem Human Surrogate (PMHS) tests, the differences in stature and neck stiffness between the PMHS and the dummy affected head dynamics before and during head impacts ([Kerrigan et al. \(2005\)](#), [Kerrigan et al. \(2009\)](#)). Pedestrian crashes involve different demographics, especially with regards to age, and size. The limited anthropometry of the Polar-II pedestrian dummy to the 50<sup>th</sup> percentile male hampers its utility for broader studies of pedestrian safety.

The design of a vehicle front end and potential countermeasures to improve pedestrian safety is a challenging problem owing to the complex nature of the design space (speed, anthropometry, stance, location, geometry and stiffness of the front end) ([Yang \(2002\)](#)). Computational models have the potential to be excellent tools for optimization of vehicle front end stiffness and geometry to improve pedestrian safety. They offer a cheaper way of running numerous vehicle to pedestrian impact tests instead of expensive and time consuming experiments. The computational human models can be broadly classified into two different categories based on their modeling approach: Multi-Body (MB) models and Finite Element (FE) models ([Figure 1.3](#)). While the FE human body models are considered to be the most

accurate computational human surrogates, its computational time is extensive (Kerrigan (2008b)). On the other hand, while unable to represent detailed geometries or material level responses, pedestrian MB models continue to be used extensively by both auto manufactures and researchers to predict and analyze the kinetics and kinematics of vehicle-pedestrian impacts, especially for running iterative optimization routines to explore the design space (Leglatin et al. (2006)). In addition, a combined approach can be used with the MB models used initially to narrow down the design space and FE models used later to refine the vehicle designs (Ito et al. (2008)). There is also a hybrid approach where a coupled simulation can be run with the front end of a vehicle, modeled using the FE method and impacted with a MB human model to capture the vehicle deformation during the impact (Happee et al. (2003); Leglatin et al. (2006)).



(a) MADYMO MB Human Models (b) THUMS FE Human Models

Figure 1.3: Human Pedestrian Models

There has been considerable advancement in the development and validation of computational human body models of pedestrians in the last decade (Chen et al. (2015); Poulard et al. (2015, 2016); Kerrigan (2008a)). Although pedestrian finite

element models (PFEM) are well validated (Poulard et al. (2015); Wu et al. (2017)), it is challenging to use these in iterative optimization problems owing to the complexity of the models and large computational time. MADYMO multibody facet and ellipsoid models (TNO (2013)) have been used in crash reconstruction (Untaroiu et al. (2009); Van Rooij et al. (2003)), optimization studies (Sankarasubramanian et al. (2016)), and sensitivity analyses (Simms et al. (2011); Gupta and Yang (2013)) to study pedestrian crashes owing to their faster computational speed and ease of positioning. MADYMO multibody human models have been validated under limited test conditions (van Hoof et al. (2003)). Elliott et al. (2012) studied the predictive capabilities of the MADYMO multibody pedestrian model and concluded that they can reproduce staged cadaver and dummy tests in terms of head trajectory (within 10%), longitudinal offset (within 17%), transverse offset (0 and 19%), impact location of the head, head impact time (mean absolute difference of 8.7 ms), and head impact velocity (with mean absolute difference of 1.8 m/s). Elliot also concluded that the model has shown to be largely unaffected by changes in vehicle stiffness and vehicle-pedestrian friction. This suggests that the model might be insensitive to design changes of the front end of the vehicle and its biofidelity needs to be further investigated.

Newer biomechanical test data and multibody pedestrian models have been introduced into the literature since the development of MADYMO pedestrian models. Kerrigan et al. (2009) developed a new multibody model of thigh and leg validated under three point bending. Subit et al. (2010) performed lateral impact studies of the human torso under moderate and low impact speeds of 1.5 m/s and 3 m/s. New injury risk criterion for medio-lateral bending have been developed for the lower extremities using bending moment as the predictor variable (Kerrigan et al. (2004)). A standardized generic pedestrian buck has been developed (Pipkorn et al. (2012, 2014)) and used in a series of three PMHS tests (Forman et al. (2015), Forman et al.

(2015)). In light of the new biomechanical data it is necessary to update the existing MADYMO multibody models in order to use them in vehicle design.

Although significant advances have been made in the field of pedestrian safety, one of the main challenges with regards to the design of the vehicle front end is the lack of a comprehensive cost function that could calculate the overall *risk* to a pedestrian based on an impact scenario. The design of the front end of a vehicle can affect the injury risks of all body regions and it is difficult to quantify this given the differences in injury severity, disability, and cost (Han et al. (2012)). Few researchers have attempted to optimize the front end geometry and vehicle structures and their objectives have been limited to reducing the injury risk to particular body regions like the head (Kausalyah et al. (2014); Carter et al. (2005)), the knee (Lee et al. (2014)), and the chest (Linder et al. (2004)). Sankarasubramanian et al. (2013) developed a methodology to quantify the threat to the pedestrian using Injury Cost measure (IC) by mapping injury indices to a score based on the Abbreviated Injury Scale (AIS) and then mapping them to cost implications. However, arbitrary thresholds for injury indices were used to determine the maximum AIS level (MAIS). There were five injury indices included in the study: head injury criterion (HIC), viscous criterion (VC), peak resultant chest acceleration, and peak forces observed in the femur and tibia for the lower extremities. Their methodology was similar to the Whole Body Injury Metric proposed by Bose and Crandall (Bose and Crandall (2008)). Bose and Crandall calculated a weighted sum of the medical and Quality of Life costs for different AIS levels in body regions with the probability of occurrence of an AIS level injury calculated from injury risk functions. The medical and Quality of Life costs were derived from the works of Miller et al. (Miller (1993); Miller et al. (2004); Naumann et al. (2010); Blincoe et al. (2015)). The Abbreviated Injury Scale (AIS) is a method of ranking anatomic injury in nine body regions along a six-point scale of

severity formulated in 1971 by the Association for the Advancement of Automotive Medicine (AAAM) (Gennarelli and Wodzin (2006)) and was updated in 2015. One of the major drawbacks of using the data from Miller et al. was their attribution of the medical and other auxiliary costs to the Maximum AIS (MAIS) injury for each individual. There is an expected relationship between the medical costs and injury severity as described by the Injury Severity Score (ISS) in addition to work related disability (Sears et al. (2013)). Pedestrians suffer from a complex array of injuries (Crandall et al. (2002)), occurring to various body regions often influenced by the stature, shape, speed and orientation. With concomitant injuries it is not clear how the injury costs can be based purely on MAIS for the body regions sustaining injuries.

The Functional Capacity Index (FCI) was developed in the early 1990s (MacKenzie et al. (1994); MacKenzie et al. (2002)). Ten dimensions of everyday human functioning were described: eating, excretory, sexual ambulation, hand and arm function, bending and lifting, visual, auditory, speech and cognitive functions. For each defined dimension, three to seven levels of function were defined with an increasing degree of limitation. A group of clinical experts mapped each AIS (1990) injury code to a vector of impairment level representing the expected impact the injury would have one-year post-injury on one of the ten functional dimensions. Recently the FCI has been reintroduced into the literature. (McMurry et al. (2015)). The most recent version of the FCI measures disability using a standard gamble technique which asks subjects whether they would prefer to live with long term impairment or undergo a procedure that would either result in death or complete cure with a pre-defined probability. With the aid of a standard gamble approach, it was found that on average subjects were never willing to accept less than a 60% chance of cure, so in practice, the FCI scores for survivors range from 60 to 100.

In a recent study of occupants in frontal and side impact crashes from the

2000-2013 National Automotive Sampling System – Crashworthiness Data System (NASS-CDS), [McMurry et al. \(2015\)](#) noted that frontal crashes produce a large number of disabling injuries, particularly to the lower extremities, and these crashes are estimated to account for approximately 400,000 life years lost to disability in comparison with 500,000 life years lost to fatality. McMurry concluded that the burden of disabling injuries to car crash survivors should be considered when setting vehicle safety design priorities. With lower extremities being one of the frequently injured body regions, it can be expected that injuries to the lower extremities in pedestrians would contribute a significant proportion to the life years lost due to disability as shown by [McMurry et al. \(2015\)](#). [Arregui-Dalmases et al. \(2010\)](#) analyzed hospital discharge data from eight European countries which amounted to 100.4 million Europeans in the year 2004 and selected pedestrian cases based on their ICD-9 and ICD-10 codes. AIS 2 level injuries were the most severe accounting for 50% of the total injuries seen in the European data (Figure 1.4a). Regarding the predicted functional limitations analysis of those 18-year-old or older who were discharged alive, 14.7% of patients had AIS codes that could not be matched to pFCI –AIS due to their lack of specificity. Among the patients about whom they had sufficient information concerning injuries, 46% were expected to be fully functional 1 year after the injury, with the remaining subjects sustaining varying degrees of functional limitations. Among body regions, hip injuries and injuries to the lower extremity lead the ranking, presenting the largest percentage of individuals with some residual disability 1 year after the crash at around 80-90% of victims (Figure 1.4b). As noted earlier, there are about 13 injured pedestrians for every pedestrian fatality in the United States, so it is imperative that we look at a metric that would address not only the immediate threat to life during vehicle design but also the disability associated with injuries.

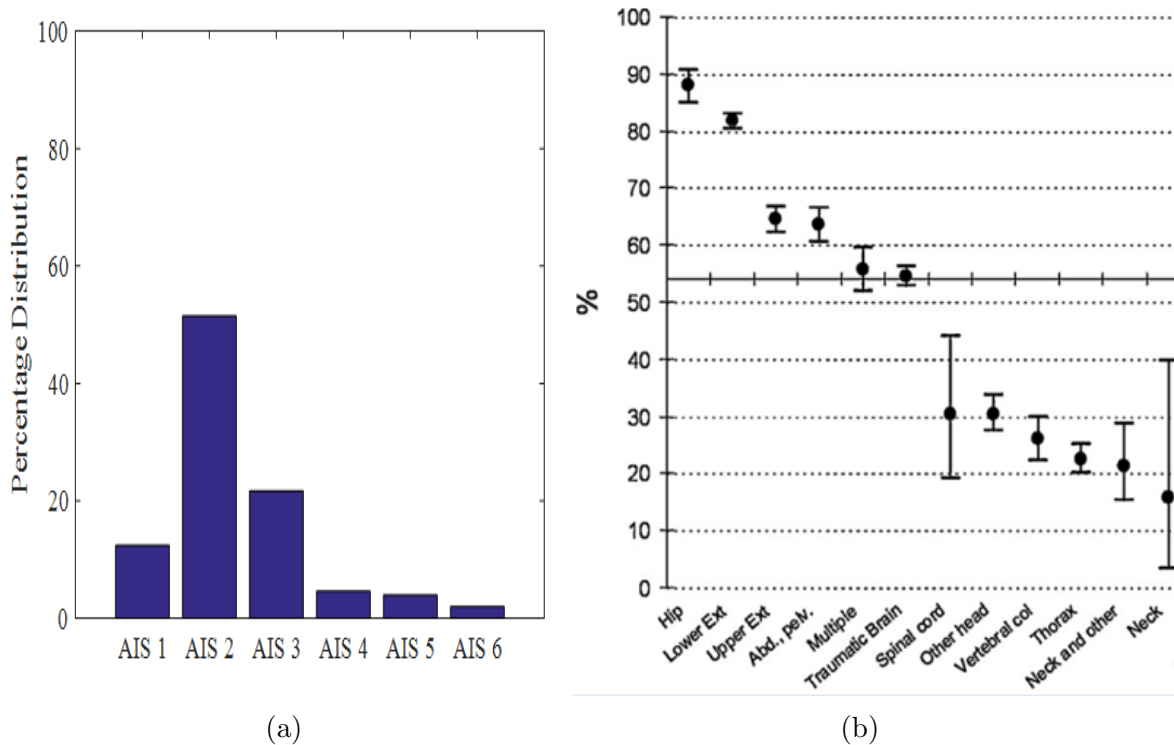


Figure 1.4: Distribution of Injury Severity in Pedestrians (left) and Percentage of Adult Discharged Pedestrians Who Have Some Form of Functional Limitation One-Year Post Discharge (right) [adapted from Arregui-Dalmases et al. (2010)]

## 1.2 Summary

1. Vehicle to pedestrian accidents are one of the leading causes of fatalities in road traffic accidents and also pose an economic burden on the society due to the disabling nature of the concomitant injuries that occur in the crashes.
2. Existing safety regulations and standard /and pedestrian dummies used for testing encompass only specific accident scenarios or pedestrian demographics.
3. Although validated PFEM models exist they prove to be challenging to use in optimization studies.

4. Multibody models offer faster computational times but the validity of the commercially existing models is under question. In light of new biomechanical data and lower extremity models, it is necessary to update and validate the MADYMO multibody pedestrian model for use in optimization studies.
5. Traditionally the design of vehicles has focused on minimizing the risk of fatalities, however, there is a lack of a comprehensive cost model that can detect the effects of local design changes on the overall risk arising from an impact. Additionally, the influence of disabling injuries on the design of the vehicle front end remains unexplored.

## Chapter 2

### Central Idea of Research

The central idea of research for this dissertation is to develop a framework that will assess the effect of disabling injuries on the design of the front end of vehicles for pedestrian safety. A field data analysis of pedestrian injuries is done to identify the representative injuries and delineate the injury mechanisms accompanying the injury. A literature review is performed to identify the injury risk functions that can assess the risk of representative injuries in the field. In order to address the primary objective, a multibody pedestrian model had to be developed; henceforth known as the UVAPED model. This model is validated under both component and full-scale impact tests. Virtual sensors have been incorporated into the UVAPED model to make it capable of predicting representative field injuries with the aid of injury risk functions. An injury cost metric is developed that takes into account a priori distribution of representative field injuries to output a cost based on the chance of occurrence of a fatality, the chance of occurrence of a disabling injury, or both. The developed cost metric in conjunction with the validated UVAPED model is used to optimize the front end of a parametric vehicle model in MADYMO to produce three vehicle designs each based on minimizing the risk of fatality, the risk of disabling injuries and both. The three optimal designs for the front end of the vehicle is analyzed to evaluate the influence

of disabling injuries on the design of the front end of a vehicle. Figure 2.1 summarizes the outline for the research tasks proposed in this study.

## Research Objectives

1. Examine the existing pedestrian databases to identify the most frequent and representative injuries, map them to existing injury risk functions from the literature and define outputs from the UVAPED model capable of predicting these injuries.
2. Develop a multibody pedestrian model capable of representing the most frequent pedestrian injuries observed in the field during a frontal impact. This objective is achieved by performing a component and whole-body level of the UVAPED model.
3. Develop an injury cost function capable of assessing the risk of fatal and disabling injuries.
4. Demonstrate the utility of incorporating disabling injuries while prioritizing body regions during the design of vehicle front end for pedestrian safety. This task involves designing an optimization study to optimize the front end of a parametric vehicle model in MADYMO using the cost metric developed in task 3 and study the influence of disabling injuries on the outcome of vehicle design for pedestrian impacts.

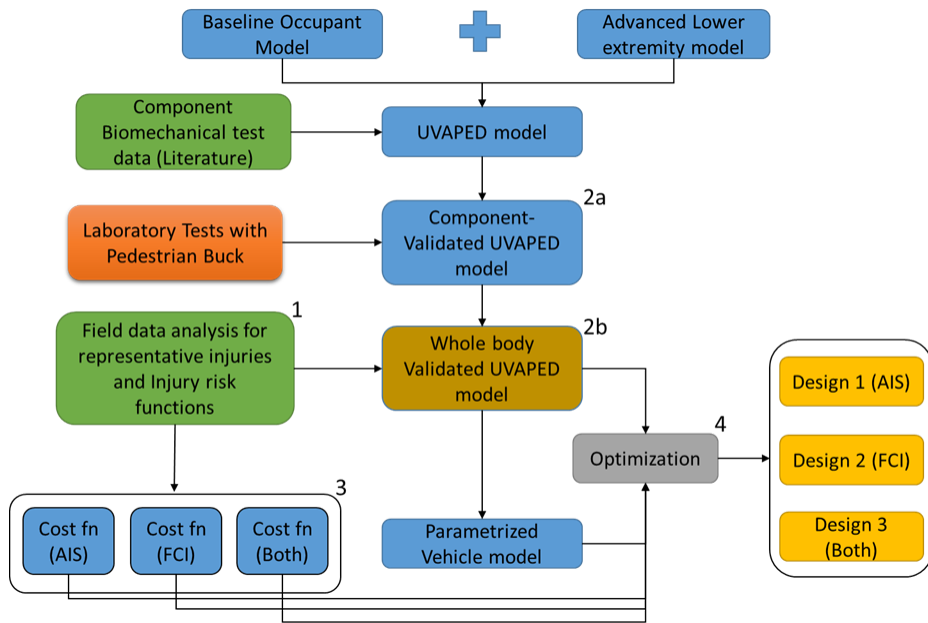


Figure 2.1: Flowchart of Tasks Proposed For This Dissertation

## Chapter 3

### Task 1: Field Data Analysis

Fatal and non-fatal data were collected for the year 2012 on individuals involved in motor vehicle collisions (MVCs) that sought care at a trauma center. The National Vital Statistics System (NVSS) provides a census of fatally injured individuals involved in an MVC, including pedestrians. Two databases from the Healthcare Cost and Utilization Project (HCUP) were used to describe non-fatally injured pedestrians. The National Inpatient Sample (NIS) is used to characterize hospitalized patients, while the Nationwide Emergency Department Sample (NEDS) records patients that are treated and released from the hospital during the initial visit. Each data source is designed and weighted to be nationally representative, and samples include approximately 90% of the states from where they are obtained.

#### 3.1 Population and Demographic Characteristics

NVSS, NIS and NEDS data were compiled for the year 2012 to describe the frequency of fatal, hospitalized and non-hospitalized motor vehicle crashes, respectively, including MVCs involving a struck pedestrian (Table 3.1). As reported by death certificate records captured within the NVSS, 35,353 MVC-related fatalities

were reported in 2012, while weighted estimates of hospital data indicate that 224,120 individuals were hospitalized as a result of an MVC, with an additional 2.9 million patients treated and released from an emergency department facility. Of this MVC patient population, struck pedestrians accounted for 14.6%, 11.0%, and 3.9% of fatal, hospitalized and non-hospitalized MVC victims, respectively.

Table 3.1: United States Frequency of Fatal and Non-Fatal MVC Victims Seeking Medical Treatment in 2012

	Fatalities		Hospital Admitted		ED Treated & Released	
	N† (%)	Obs.	Nwt* (%)	Obs.	Nwt* (%)	
MVC Occupant	10,068 (28.48)	28,216	141,080 (62.95)	561,090	2,439,486 (82.08)	
MVC Motorcyclist	4,603 (13.02)	7,697	38,485 (17.17)	31,105	136,273 (4.59)	
MVT Pedal cyclist	624 (1.77)	1,425	7,125 (3.18)	11,290	49,272 (1.66)	
MVC Pedestrian	5,169 (14.62)	4,932	24,660 (11.00)	26,795	117,713 (3.96)	
MVC Unspecified	14,876 (42.08)	2,253	11,265 (5.03)	50,973	212,796 (7.16)	
MVC Other	13 (0.04)	301	1,505 (0.67)	3,911	16,365 (0.55)	
Total	35,353	44,824	224,120	685,164	2,971,905	

†Census count \*Weighted frequency

## 3.2 Fatalities

Of the 5,169 pedestrian fatalities in 2012, the mean age of the victims was 46.5 years. Males accounted for 69.6% ( $n = 3,600$ ) of fatal cases. The hospital inpatient, outpatient, or emergency room were recorded as the most frequent places of death (52.6%). Aside from having multiple body regions contribute to the fatality, the head and neck (28.8%) were the most frequently injured body regions listed on the death certificate.

### 3.3 Hospitalized Pedestrians

Unless otherwise noted, the following descriptions of injury distributions and loss are focused on the 4,932 hospitalized observations from NIS, which when weighted, represents approximately 24,660 hospitalized pedestrians for the year 2012. Given that the 2012 sampling weights for NIS were all equally valued at 5.0, many of the distributions are presented at the observed, unweighted level. NIS captures about 20% of the inpatient discharges from the population of hospitals sampled. Information on the sampling redesign that took place in the 2012 NIS sample to provide more stable and precise national estimates can be found [online](#) by the U.S. Agency for Healthcare Research and Quality ([Houchens et al. \(2014\)](#)).

The average age of the hospitalized population was 41.5 years (IQR: 22-58). The distribution of hospitalized children (aged  $\geq 15$  years) was slightly skewed left with a median age of 10 years, while the median age of adults ( $> 15$  years) was 47 years. The adult population was also observed to have a bimodal distribution with peaks around 22 and 54 years of age. Children  $< 15$  years of age were excluded from the list of hospitalized injuries considered in task3 for the development of a comprehensive injury metric.

### 3.4 Injury Distributions

Including all injury severity levels (AIS 1-6), there were 20,847 injuries sustained by 4,867 pedestrians (injuries from 65 pedestrians could not be mapped to AIS). With the exception of concussions without loss of consciousness (LOC), restricting to moderate or worse injuries (AIS 2+) resulted in a database of 13,261 injuries observed by 4,867 pedestrians. Using the sampling weights, this represents

66,305 injuries experienced by 22,085 hospitalized pedestrians. Depending on the AIS version, concussion with no LOC may be coded as a minor or moderate injury severity. Given the relevance of concussion-related injuries, all instances were considered to be of moderate (AIS 2) injury severity.

Nearly 64% of weighted injuries were moderate (AIS2) and 28% were serious (AIS3) in severity (Figure 3.1). Injuries to the lower extremities were the most frequent among moderate (AIS2) injuries, while injuries to head, thorax and lower extremities were the most frequent among serious (AIS3) and severe (AIS4) injuries (Figure 3.2).

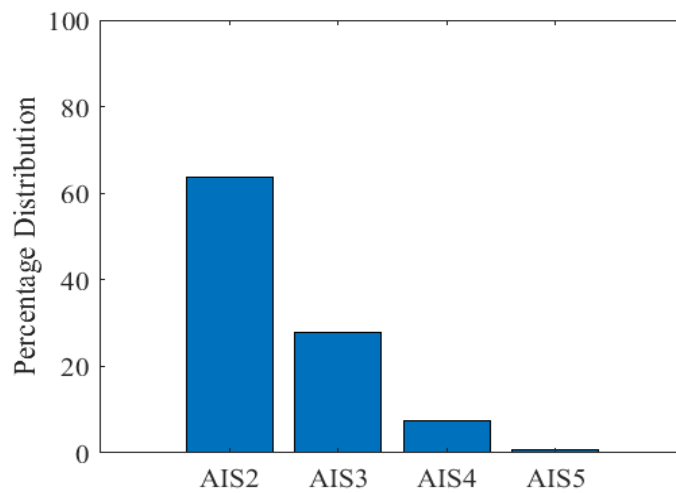


Figure 3.1: Distribution of Injury Severities (AIS 2+)

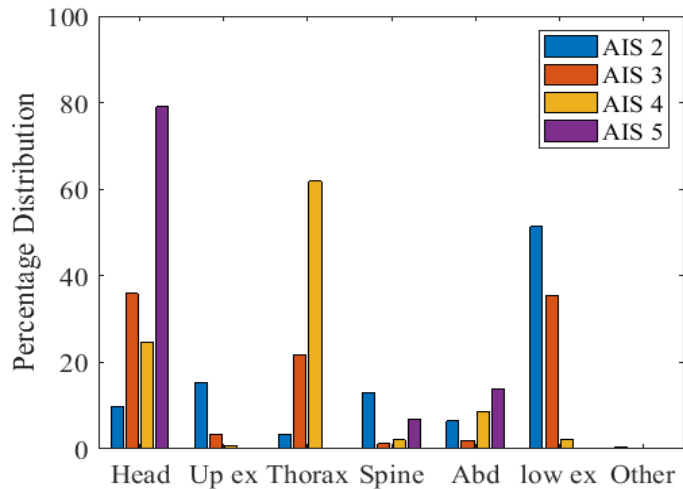


Figure 3.2: Body Region Injury Distribution (AIS 2+)

When the injuries from the PIRE database were filtered for adults (age >15), it resulted in 182 unique MAIS2+ injuries. Limiting the scope to AIS codes that occurred more than twice resulted in 143 different injuries, which were assigned to one of the 17 body regions considering their relevance to the injury metrics (Table F.1). This process ended up mapping injury metrics to 126 unique MAIS2+ injuries. Throughout this dissertation, these injuries are referred to as mapped injuries. Note that minor injuries (AIS1) were ignored during the mapping process of AIS codes to injury metrics as most of the injury risk functions available in literature are for AIS2+ injuries.

## Chapter 4

### Injury Mechanisms and Risk functions

In the field of Biomechanics several hypotheses are proposed and tested, and the one that most consistently produces the same injury emerges as the injury mechanism (King (2000)). The most frequently injured body regions in pedestrian crashes are head, and lower extremities (Crandall et al. (2002)), however, being a poly-traumatic event, injury to other body regions is also quite common in severe crashes. Following the AIS injury coding the human body has been divided into 7 gross body regions representing the Head, Neck, Upper extremity, Thorax, Abdomen, Spine and Lower extremity. Each gross body region has been further subdivided into multiple body regions leading to a total of 17 body regions in order to make the prediction of injury risk in a pedestrian crash as specific as possible.

#### 4.1 Head

The most common head injuries are scalp lacerations, skull fractures, brain injuries, and basilar skull fracture.

### 4.1.1 Scalp Laceration

The occurrence of scalp lacerations and skull fractures are influenced by a range of exogenous and endogenous influences, including the shape of the bony support, the local thickness of the overlying soft tissues, the impact geometry of the causative implement and the velocity of the impact (Sharkey et al. (2012)). Given the limitations of MADYMO modeling and a lack of injury risk function that incorporates all of these factors, a simple force relationship has been developed and used in this study (Equation 4.1).

Equation 4.1: Injury Risk of Scalp Laceration Based on Contact Force

$$P(\textit{Laceration AIS1}) = \frac{1}{2} \left( 1 + \textit{ERF} \left( \frac{\textit{Force}(N) - 3047}{982.5\sqrt{2}} \right) \right) \quad (4.1)$$

### 4.1.2 Brain Injuries and Skull Fractures

The time history of linear acceleration is used in the estimation of the Head Injury Criterion (HIC) (Equation 4.2), which is currently the most widespread metric in the estimation of head injuries. The HIC was developed from the Wayne State Tolerance Curve (WSTC) which showed that the linear acceleration required for skull fracture is inversely related to impact duration (Lissner et al. (1960)). In the UVA pedestrian model, linear head acceleration was measured at the center of gravity of the head and HIC was calculated for the time windows of 15 ms and 36 ms. The injury risk functions for the prediction of head injuries were presented in the National Highway Traffic Safety Administration (NHTSA) report ‘INJURY CRITERION FOR SIDE IMPACT DUMMIES’ (Kuppa (2004)) based on the analysis of head drop test data documented by Prasad and Mertz (Prasad and Mertz (1985)) using a parametric

survival method assuming a lognormal distribution (Equation 4.3).

Equation 4.2: Head Injury Criterion (HIC)

$$HIC = \left\{ \left[ \frac{1}{t_2 - t_1} \int_{t_1}^{t_2} a(t) dt \right]^{2.5} (t_2 - t_1) \right\}_{max} \quad (4.2)$$

Equation 4.3: Head Injury Risk Due to HIC

$$P(head\ injury) = cdf \left( \frac{\ln(HIC) - \mu}{\sigma} \right) \quad (4.3)$$

where  $\mu = 6.96352$  and  $\sigma = 0.844664$  for AIS 2+ head injuries,  $\mu = 7.45231$  and  $\sigma = 0.73998$  for AIS 3+ head injuries, and  $\mu = 7.65605$  and  $\sigma = 0.60580$  for AIS 4+ head injuries.

### 4.1.3 Brain Injuries Due to Rotation

Brain tissue is essentially an incompressible material with high bulk modulus and low shear stiffness. The major mechanisms of brain injury are pressure and shear stress due to the pressure gradients or the relative motion of brain with respect to the skull (King (2000)). A major flaw in the HIC is that it only accounts for linear acceleration. While it may have applicability for prediction of skull fracture, HIC has been shown to be unsuitable for the prediction of shear strain induced brain injuries like the diffuse axonal injury (DAI) or subdural hematoma (Zhang et al. (2001)). Recently the focus has been on the use of finite element models to study brain injuries. (Takhounts et al. (2003)) developed the simulated injury monitor (SIMon) and proposed a Cumulative Strain Damage Measure (CSDM) to predict DAI and other brain injuries caused due to rotation. (Gabler et al. (2018)) recently developed the Universal Brain Injury Criterion (UBrIC) and showed its efficacy in

the prediction of Maximum Principal Strain (MPS) and CSDM over a broad range of kinematics encountered in automotive crashes and sports. This is a metric developed based on the response of a second order system and relates rotational head kinematics to strain based brain injury metrics aka MPS and CSDM. The rotational kinematic history of the head from the MADYMO model has been used to calculate the CSDM based on UBrIC and the injury risk functions (Equation 4.4) proposed by (Takhounts et al. (2013)) were used to predict the probability of brain injuries with shear strain as an injury mechanism.

Equation 4.4: Probability of Brain Injury Using Shear Strain as a Predictor Proposed by Takhounts et al. (2013)

$$P(\text{Brain injury}) = 1 - e^{\left(-\left(\max\left(\frac{CSDM}{\alpha}, 0\right)\right)^{1.8}\right)} \quad (4.4)$$

where  $\alpha = 0.3, 0.49, 0.6,$  and  $0.624$  for AIS2+, AIS3+, AIS4+, and AIS5+ respectively.

#### 4.1.4 Basilar Skull Fracture

For the basilar process of the occipital bone, the mechanism is tension applied by ligaments and tendons to the foramen magnum (McELHANEY et al. (1995)). The tension component of  $N_{ij}$  can be used to obtain the risk of basilar skull fracture. The mean fracture force of basilar skull ring fractures is  $4300 \pm 350$  N. The injury risk functions developed by Eppinger et al. are used in the estimate of the risk of basilar skull fracture (Equation 4.5).

Equation 4.5: Injury Risk Function for Basilar Skull Injuries

$$P(\text{Basillar skull fracture}) = \frac{1}{1 + e^{(\alpha - \beta \times \max(NTF, NTE))}} \quad (4.5)$$

where  $\alpha = 2.05, 3.227, 2.693,$  and  $3.817$  and  $\beta = 1.195, 1.969, 1.195$  and  $1.195$  for AIS2+, AIS3+, AIS4+ and AIS5+ respectively. NTF: Nij based on tensile force and flexion moment. NTE: Nij based on tensile force and extension moment.

## 4.2 Nij

Nij uses two criteria: one is force-based and the other is a combination of force and moment. In the injury risk calculation for the UVA pedestrian model, the force-moment domain was divided into 6 regions (Figure 4.1) to consider peak limits (Table 4.1) in a continuous manner instead of a threshold value. For region I to IV, combined force and moment was used to calculate Nij (Equation 4.6), and the ratio of the force from the simulation and peak limit was used as Nij value if the force and moment state falls into the region V or VI as shown in Equation 4.7.

Table 4.1: Peak Limits and Nij Intercepts

Dummy size	Peak Limits				Nij intercepts	
	Tension (N)	Comp (n)	Tension (N)	Comp (N)	Flexion (N m)	Exten (N m)
CRABI	780	960	1460	1460	43	17
3 YO	1430	1380	2340	2120	68	30
6 YO	1890	1820	3096	2800	93	42
5F	2620	2520	4287	3880	155	67
50M	4170	4000	6806	6160	310	135
95M	5030	4830	8216	7440	415	179

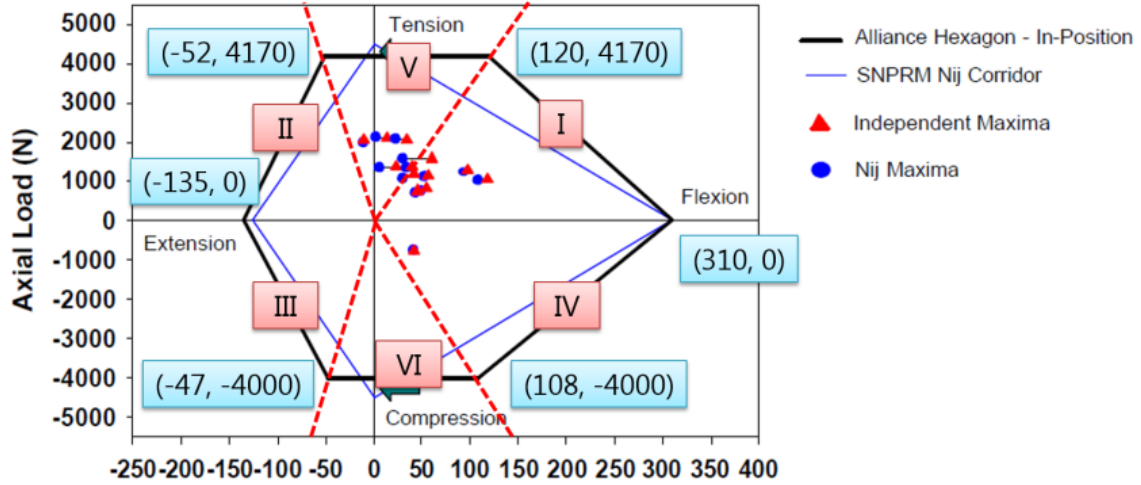


Figure 4.1: Six Regions for Nij Calculation

Equation 4.6: Nij for Region I to IV

$$N_{ij} = \frac{F_{CFC600}}{F_{intercept}} + \frac{M_{CFC600}}{M_{intercept}} \quad (4.6)$$

Equation 4.7: Nij for Region V and VI

$$N_{ij} = \frac{F_{CFC600}}{F_{peaklimit}} \quad (4.7)$$

## 4.3 Neck

### 4.3.1 Cervical Spine Fracture

The mechanism for cervical spine injury is axial compression or tension and flexion or extension. The formulation of Nij proposed by Eppinger et al. (2000) is currently used for the Hybrid III dummies. The injury risk function (Equation 4.8) developed by Eppinger et al. (2000) is used for estimating the risk of neck fractures.

Equation 4.8: Probability of neck injury using  $N_{ij}$

$$P(\text{Neck injury}) = \frac{1}{1 + e^{(\alpha - \beta \times N_{ij})}} \quad (4.8)$$

where  $\alpha = 2.05, 3.227, 2.693,$  and  $3.817$  and  $\beta = 1.195, 1.969, 1.195,$  and  $1.195$  for AIS2+, AIS3+, AIS4+ and AIS5+ respectively.

## 4.4 Face

### 4.4.1 Facial Skin Laceration

The tensile forces generated in the skin as a result of blunt force trauma are predicted using a cumulative density function (assuming normal distribution) developed using the impact force data by (Sharkey et al. (2012)) as a predictor variable.

Equation 4.9: Probability of a laceration (Facial) with contact force as predictor

$$P(\text{Laceration AIS1}) = \frac{1}{2} \left( 1 + \text{ERF} \left( \frac{\text{Force}(N) - 1316}{672\sqrt{(2)}} \right) \right) \quad (4.9)$$

### 4.4.2 Facial Fracture

With regards to facial injuries, maxilla fractures, orbital fractures and zygoma fractures are commonly observed in pedestrian-to-vehicle impacts. The mechanism of these injuries has been identified as the anterior posterior contact force (Porta et al. (1995); Cormier et al. (2011))

## 4.5 Upper Extremities

### 4.5.1 Shoulder

Clavicle fracture due to axial compression is one of the most common shoulder injuries during a vehicle to pedestrian impact. The axial compression force measured at the Clavicle-Scapula joint in the UVA pedestrian model was used to calculate the injury risk (Equation 4.10) of shoulder fracture (Zhang et al. (2013)).

Equation 4.10: Injury Risk of Clavicle Fracture Due to Axial Compression

$$P(AIS2 + clavicle injury) = 1 - e^{-e^{(3.5978 \cdot \ln(F(N)) - 27.8538)}} \quad (4.10)$$

### 4.5.2 Humerus Fracture

The mechanism of failure of the humerus shaft is load applied during lateral bending. The bending moment measured at the humerus was used to predict the risk of AIS2+ injuries (Santago et al. (2008)).

Equation 4.11: AIS2 + Risk of Humerus Fracture

$$P(AIS2 + humerus fracture) = 1 - e^{-(0.0036 \times M(Nm))^{4.871}} \quad (4.11)$$

### 4.5.3 Radius and Ulna Fracture

Bending is an accepted mechanism of the failure of the bones in the forearm (ulna and radius). The average failure tolerance of these bones is 108 Nm (Duma et al. (2002)). The risk of AIS2+ fracture of radius and ulna is estimated using the bending moment metric (Equation 4.12).

Equation 4.12: Injury Risk Function for the Failure of Radius or Ulna Bones

$$P(Ais2 + radius/ulna fracture) = 1 - e^{-\left(\frac{M(Nm)}{117.281}\right)^{3.842421}} \quad (4.12)$$

#### 4.5.4 Thorax

Lateral compression or impact and anterior-posterior compression are the two injury mechanisms for thoracic injuries. For lateral compression, a linear combination of age and normalized average half deflection were the best predictors of injury (Kuppa (2004)). The chest lateral deflection was measured along the y-axis of a local coordinate system constructed based on the positions of vertebral bodies at each thoracic level. The Cmax was calculated by normalizing the deflection amount using its initial length. For the left(right) side normalized average deflection was calculated using Cmax at 20%, 25%, and 30% (70%, 75%, and 80%) (Figure 4.2), and injury risk was calculated for multiple AIS levels using the normalized average Cmax (Equation 4.13).

Equation 4.13: Injury Risk Function for Thoracic Injury Due to Lateral Loading

$$P(Thoracic injury : lateral load) = \frac{1}{1 + e^{(\alpha - age \times \beta - \gamma \times Cmax_{avg})}} \quad (4.13)$$

where  $\alpha = 6.363, 9.092937, \text{ and } 10.96565$ , and  $\beta = 0.057, 0.03705, \text{ and } 0.03705$ , and  $\gamma = 25.97, 36.8232, \text{ and } 36.8232$  for AIS 2+, AIS 3+, and AIS 4+ injury risks respectively.

In the case of a-p loading, normalized Cmax was calculated using deflection of thorax measured near sternum. Kent and Patrie (2005) showed that chest deflection tolerance to blunt anterior loading is sensitive to age but not load distribution. Injury risk for Multiple AIS levels due to a-p loading (Kent and Patrie (2005)) was estimated

using the normalized Cmax (Equation 4.14).

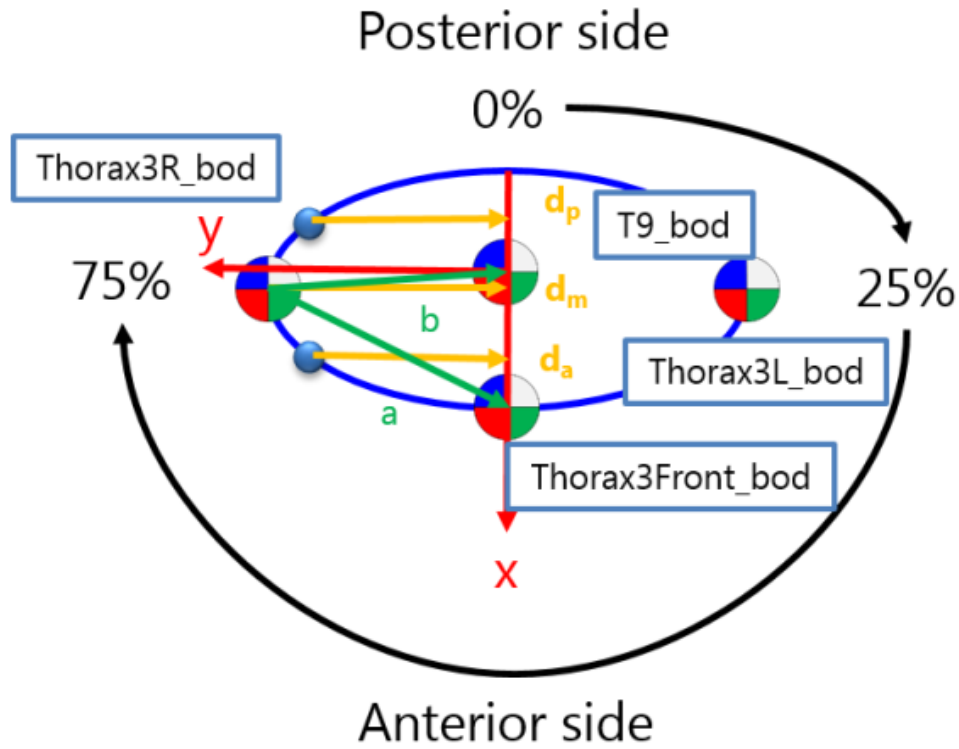


Figure 4.2: Calculation of Cmax Using Lateral Chest Deflection

Equation 4.14: Injury Risk Function for Thoracic Injury Due to a-p Loading

$$P(\text{Thoracic injury} : a - p \text{ load}) = \frac{1}{1 + e^{(-\alpha - age \times \beta - \gamma \times Cmax)}} \quad (4.14)$$

where  $\alpha = -6.7508, -6.406, -5.851, \text{ and } -9.3189$  and  $\beta = 0.720, 0.068, 0.054, \text{ and } 0.0474,$  and  $\gamma = 0.1302, 0.120, 0.121, \text{ and } 0.1818$  for AIS 1+, AIS 2+, AIS 3+, and AIS 4+ injury risks respectively.

## 4.6 Abdomen

Lateral compression and a-p compression are two injury mechanisms of the abdomen. For the lateral compression, contact force and VCmax are widely used to predict injury. [Viano et al. \(1989\)](#) developed abdominal injury risk functions using various metrics including lateral impact force. [Kuppa \(2004\)](#) proposed abdominal injury risk functions using lateral impact force based on [Walfisch et al. \(1980\)](#) test data (Equation 4.15). Since the size of the impactor differed in the cases of Viano and Walfisch, both injury risk functions were considered in the UVA pedestrian model by using different contact areas to measure contact forces. [Viano et al. \(1989\)](#) also proposed abdominal injury function based on VCmax for AIS4+ injuries (Equation 4.16).

Equation 4.15: Abdominal Injury Risk Function – Contact Force

$$P(\text{Abdomen injury} : \text{lateral}) = \frac{1}{1 + e^{(\alpha - \beta \times F)}} \quad (4.15)$$

where  $\alpha = 1.785$  and  $2.231$ , and  $\beta = 0.000346$  and  $0.000388$  for AIS2+ and AIS3+ respectively using [Viano et al. \(1989\)](#) test data and  $\alpha = 6.04044$  and  $9.282$ , and  $\beta = 0.002133$  for AIS3+ and AIS4+ respectively using [Walfisch et al. \(1980\)](#) test data.

Equation 4.16: Abdominal Injury Risk - VCmax

$$P(\text{Abdomen injury} : \text{lateral}) = \frac{1}{1 + e^{(8.639 - VCmax \times 3.814)}} \quad (4.16)$$

For a-p abdominal loading, [Untaroiu et al. \(2012\)](#) developed injury risk functions under lap belt loading for the lower abdomen. While the authors proposed the combination of belt pulling force and normalized abdominal deflection as the best predictor for abdominal injuries, VCmaxCmax was chosen as a new predictor (since

it is an internal measure independent of impacting object) and injury risk functions were developed (Equation 4.17) using the test data from Untaroiu et al. (2012).

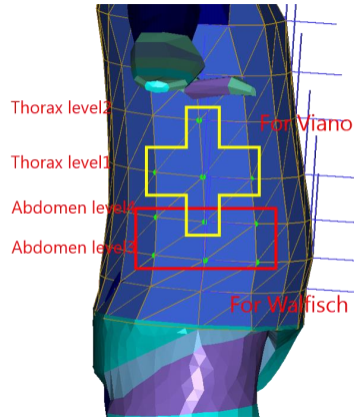


Figure 4.3: Impactor Areas for Viano and Walfisch Risk Functions

Equation 4.17: Abdominal Injury Risk Function Due to Anterior-Posterior Loading

$$P(\text{Abdomen injury} : a - p) = \frac{e^{(-\alpha + \beta \times VCmaxCmax)}}{1 + e^{(-\alpha + \beta \times VCmaxCmax)}} \quad (4.17)$$

where  $\alpha = 5.55$ , and  $14.02$ , and  $\beta = 2.004$ , and  $3.55$  respectively for AIS2+ and AIS3+ injury risks respectively.

## 4.7 Pelvis

Injury risk for pelvic fracture due to lateral impact is predicted using pelvic deformation or lateral impact force (Viano et al. (1989)). In the UVA pedestrian model, lateral impact force measured on the side of the pelvis skin (Figure 4.4) was used to calculate injury risk (Equation 4.18).

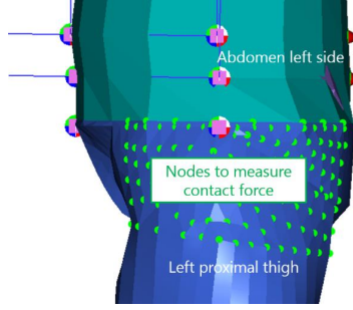


Figure 4.4: Area Where Pelvis Contact Force Was Measured

Equation 4.18: Pelvic Injury Risk Due to Lateral Loading

$$P(\text{Pelvic injury}) = \frac{1}{1 + e^{(\alpha - \beta \times \text{age} - \gamma \times F)}} \quad (4.18)$$

where  $\alpha = 6.806$ , and  $9.7023$ , and  $\beta = 0.0089$ , and  $0.04678$ , and  $\gamma = 0.0007424$ , and  $0.0005$  for AIS2+ and AIS3+ injury risks respectively.

In addition, lateral impact on the pelvic region causes fracture at femoral neck due to axial compression (Roberts et al. (2010)). Injury risk function for femoral neck fracture (4.19) has been developed in this study using mean and standard deviation of axial force on the femoral neck measured at hip joint from male subjects reported by Roberts et al. (2010).

Equation 4.19: Femoral Neck Fracture Risk Due to Axial Loading

$$P(\text{AIS3+ femoral neck fracture}) = \frac{1}{2} \left( 1 + \text{ERF} \left( \frac{F - 4882}{\sqrt{2} \times 2202} \right) \right) \quad (4.19)$$

## 4.8 Thigh and Leg

Tensile or compressive stress caused due to bending is considered as an injury mechanism for thigh and leg. Kerrigan et al. (2004) performed 3-point bending tests

using thigh and leg specimens and developed injury risk functions (Equation 4.20, Equation 4.21) using bending moment as the injury metric.

Equation 4.20: Femur Injury Risk Due to Bending

$$P(AIS3 + thigh\ injury) = 1 - e^{(-e^{6.24242 \times \ln M - 36.4101 - 0.90267 - 1.14485 \times \alpha})} \quad (4.20)$$

where  $\alpha = 0$  in case of proximal and distal thigh, or 1 in case of mid shaft.

Equation 4.21: Leg Injury Risk Due to Bending

$$P(AIS2 + leg\ fracture) = 1 - e^{-e^{5.69112 \times \ln M - 33.05211}} \quad (4.21)$$

## 4.9 Knee

Femoral condyle fractures, tibial plateau fractures caused due to axial compression and knee ligament tear caused due to varus/ valgus bending have been grouped under injuries to the knee complex. For femoral condyle fractures the axial compressive force (Equation 4.22) measured at the knee joint along the local direction of femur was used to calculate the injury risk (Rupp et al. (2010)).

Equation 4.22: Femoral Condyle Fracture Risk Due to Axial Load

$$P(Femoral\ condyle\ fracture) = \frac{1}{2} \left( 1 + ERF \left( \ln F - \frac{0.0081 \times mass - 0.00124 \times age + 2.6224}{0.4519} \right) \right) \quad (4.22)$$

For tibial plateau fracture the mean and standard deviation of axial compressive force measured at the knee joint along the local direction of tibia from Hirsch and Sullivan (1965) was used to develop the injury risk function (Equation 4.23).

Equation 4.23: Tibial Plateau Fracture Risk Using Axial Force

$$P(\text{Tibial plateau fracture}) = \frac{1}{2} \left( 1 + \text{ERF} \left( \frac{F - 730}{230\sqrt{2}} \right) \right) \quad (4.23)$$

For the knee ligament tear, the varus/valgus angle measured at the knee joint (Equation 4.24) was used to calculate injury risk (Ivarsson et al. (2004)).

Equation 4.24: Knee Ligament Risk Due to Varus/Valgus Bending

$$P(\text{Knee ligament tear}) = 1 - e^{-e^{-10.7034 \times \ln \phi - 28.541198}} \quad (4.24)$$

## 4.10 Foot/Ankle

Funk et al. (2002) proposed Xversion and axial compressive forces as a combined loading injury metric for the ankle region. The Xversion angle and the axial force measured at the ankle joint in the tibia local coordinate system were used to calculate the injury risk.

Equation 4.25: Ankle Injury Risk Due to Xversion and Axial Load

$$P(\text{AIS2+ ankle injury}) = 1 - e^{-e^{4.94 \ln \phi - 17.7 - 0.5 \times F(kN)}} \quad (4.25)$$

## Chapter 5

### Socio Economic Costs Associated With Injuries

The purpose of the field data analysis is to describe the nature and distribution of injuries to pedestrians struck by a motor vehicle. The units of measure quantifying the severity of injuries and the disability associated with them are dissimilar, hence, it is necessary to come up with a common measure that can quantify the outcomes either using life years lost or injury cost (monetary). The literature was reviewed in order to rank these injuries based on four outcome measures: maximum injury severity, injury severity score, injury impairment, and functional capacity. Relative rankings of these injuries can be made and compared across metrics for costs and functional impairment. Costs are estimated in the literature in terms of the medical, work loss, and indirect losses quantified by a quality of life dollar cost value (referred to as QALY dollars, \$QALY) (Blincoe et al. (2015); Spicer et al. (2011)). Impairment metrics include the Injury Impairment Index (III) and Functional Capacity Index (FCI), each estimated for 12-month impairment post injury event. Severity and disability associated with poly-traumatic events is characterized using the New Injury Severity Score (NISS) and Whole body FCI WBFCI).

## 5.1 Economic Costs

Medical, work loss and quality of life costs for each population are ascribed to each case using methods documented for the Web-based Injury Statistics Query and Reporting System (WISQARS) Cost of Injury Module ([Lawrence et al. \(2014\)](#)). The medical and work loss costs cover three mutually exclusive categories that reflect the severity of injury:

1. Injuries resulting in death, whether the death occurs inside or outside a health-care setting.
2. Injuries resulting in hospitalization with survival to discharge.
3. Injuries resulting an emergency department (ED) visit but not resulting in hospitalization or death.

## 5.2 Medical Costs

Fatal medical costs were calculated using costs per case by the scene of the crash or the healthcare facility in which the fatalities had occurred as per [Finkelstein et al. \(2006\)](#). These medical costs could include payments for the coroner, emergency medical transport, ED visit, and stays in the hospital, nursing home, or hospice.

The costing methods for non-fatal hospitalized injuries were originally based on the methodology described by [Finkelstein et al. \(2006\)](#), and were updated and applied to the latest acute care costs. The cost is comprised of facility component for inpatient stay, non-facility component, hospital readmission, short-to-medium term follow-up, follow-up beyond 18 months and up to seven years, hospital rehabilitation costs, nursing home costs, and transport and claims administration. Long-term costs

beyond seven years are applied to spinal cord injuries (SCI) and traumatic brain injuries (TBI).

The costs for injuries treated in an ED and released consisted of the ED visit, follow-up visits and medication during the first 18 months, follow-up costs beyond 18 months, emergency transport, and claims administration.

Documentation for the WISQARS injury costing methodology provides three examples for contextualizing how costs are estimated for a fatal, non-fatal hospitalized, and ED treated injury cases (Lawrence et al. (2014)).

### 5.3 Work Losses

Injuries can result in both temporary and permanent disability. Work losses due to injury may include loss of wages and accompanying fringe benefits, and the loss of ability to perform one’s normal household responsibilities. Fatal work losses represent the value of goods and services never produced due to premature death. Equation 5.1 (Finkelstein et al. (2006)) was used to compute the lifetime earnings based on age  $a$  and gender  $b$ .

$$Earn_{a,b} = \sum_{K=a}^{102} \left\{ P_{a,b}(k) \times Y_{k,b} \times \left( \frac{1+g}{1+d} \right)^{k-a} \right\} \quad (5.1)$$

where  $P_{a,b}(k)$  is the probability that someone of age  $a$  and gender  $b$  will live until age  $k$ ,  $Y_{k,b}$  is the average value of annual earnings (include fringe benefits) or of annual household production at age  $k$  for someone of gender  $b$ ,  $g$  is the productivity growth rate (0.01) for earnings and 0.00 for household production, and  $d$  is the discount rate (0.03).

Non-fatal work losses in WISQARS were stratified into two categories: short-

term losses, which represent the work loss occurring in the first six months after the injury, and the long-term losses, which represent the work losses occurring after six months from the time of the injury.

## 5.4 Health Status and Impairment

Quality adjusted life years (QALYs) are a measure of health status that accounts for both the quality and duration of a health state (Spicer et al. (2011)). It is a product of remaining life expectancy and the quality of life over the same period and is derived from a health model that accounts for multiple health dimensions, including physical, psychological, and social wellbeing. The loss of one QALY is equivalent to losing a full year of life due to premature death (Spicer et al. (2011)).

The QALY measure was first introduced by Zeckhauser and Shepard (1976) and gained popularity as a tool for evaluating health interventions, medical care, and technology (Sassi (2006); Gold et al. (2002)). A QALY is valued at 1.0 for perfect health and 0.0 for death, typically with negative values (fates worse than death) allowed. Evaluating the global burden of diseases relies on disability adjusted life years (DALYs), which are complementary to QALYs (i.e.,  $DALY = 1 - (QALY)$ ). Spicer et al. (2011) and Miller (2000) describe QALYs that have been regularly used to evaluate the efficacy and effectiveness of pharmaceutical drugs and other clinical trial interventions. The US Department of Transportation (DOT) mandates the use of QALY-based costs for benefit-cost analyses of road safety decisions.

The QALY values used by the DOT are constructed using the injury impairment index (III), which was originally developed for physician use to rate the consequences of injury (Hirsch and Eppinger (1984)). It is comprised of a six dimensional scale to assess the impact of an injury on the mobility, cognitive, self-care, pain,

sensory, and cosmetic aspects of living. The disability across each dimension due to a particular injury was categorized into four levels based on criterion defined by [Hirsch and Eppinger \(1984\)](#). Injury losses were rated by days, weeks, months and years for estimated time spent under a level of impairment in a particular dimension for all AIS 2-5 injury diagnosis in the Occupant Injury Code/ Abbreviated Injury Score 1985 (OIC/AIS85). They also noted the variation in impairment with the age of a person, if any, for each dimension. [Carsten \(1986\)](#) added estimates for new AIS-90 diagnoses and [Miller \(1995\)](#) added the estimates for injuries of maximum AIS level 1 (minor), while also defining an additional dimension of functionality – the ability to perform household responsibilities and wage work based on disability probabilities. Using a literature review, Miller developed impairment fraction to combine the physician ratings by dimension into a single rating of percentage of utility lost over time. The weights convert from functional capacity losses to utility losses, and reflect the relative importance of different aspects of functioning. This method calibrates functional capacity loss so that the utility of a year of life and a year of functioning are equal. Utility measures the value people place on their being alive (and in a particular health state).

The weighting method is multiplicative and assumes that the percentage of utility lost on each dimension to be a percentage of the utility remaining after the losses on prior dimensions are accounted for. The weighted six dimensional impairment equals (equation 5.2).

$$1 - \prod (1 - WTGi \times LOSSi) \tag{5.2}$$

where WTGi is the column of utility loss fractions associated with dimension  $i$  and LOSSi is the rated impairment level on dimension  $i$ .

This method yielded estimates of functional loss within three time periods post-injury: 1-2 years, 2-5 years, and beyond 5 years after initial injury. [Spicer et al. \(2011\)](#) updated these weights by reviewing all the disability metrics and measures developed until 2005. Multiple injuries of moderate (AIS 2) or greater were accounted for by treating the loss for each additional injury as a percentage loss of functioning remaining after the first injury ([Miller \(1993\)](#)). For multiple injuries of equal severity only one injury was considered for calculation of the functional loss.

## 5.5 Injury Impairment Index (III)

Noted above in the description for QALYs, quality-adjusted life years is a product of expected life remaining and one's health status. How an individual's health status is quantified depends on the outcome or disease of interest. Hence, several healthy utility indices exist that can be used to value various health states and may include direct and indirect methods for measurement. The III was originally developed for physician use to rate the consequences of injury ([Hirsch and Eppinger \(1984\)](#)). As described by [Spicer and Miller \(2010\)](#), the National Highway Traffic Safety Administration (NHTSA) uses the injury impairment index (III) as the health utility metric for calculating QALYs and in aiding regulatory analyses and for conducting cost-benefit analysis of safety and injury prevention efforts.

The III scale quantifies health utility based on six dimensions of functioning: mobility, cognition, activities of daily living, pain, sensory, and cosmetic. Within each dimension there are four levels of severity, which are derived from a literature review of preference weights used in other instruments. The most recent update to III utility weights was in 2011 ([Spicer et al. \(2011\)](#)). The cognitive dimension shows the highest gradient in the variation of disability weights across the four levels of disability.

## 5.6 Functional Capacity Index (FCI) and Whole Body FCI (WBFCI)

The Functional Capacity Index (FCI) was developed in the early 1990s under a cooperative agreement between the National Highway Traffic Safety Administration (NHTSA) and The Johns Hopkins University School of Hygiene and Public Health and is by [Mackenzie et al. \(1994\)](#); [MacKenzie et al. \(1996\)](#). Ten dimensions of everyday human functioning were described for: eating, excretory, sexual, ambulation, hand and arm function, bending and lifting, visual, auditory, speech, and cognitive functions. For each defined dimension, three to seven levels of function were defined with increasing degrees of limitation (Table [E.1](#), [E.2](#)). Pain and disfigurement are not human functions and were therefore excluded from the dimensions. Due to the FCI being developed as a measure of functional capacity reflected by limitations in physical and cognitive functions only, the psychosocial function was purposely excluded from the defined dimensions.

After a series of ratings and valuations (described by [Mackenzie et al. \(1994\)](#); [MacKenzie et al. \(1996\)](#)), a group of clinical experts assigned each AIS (1990) code a vector of impairment levels representing the impact the injury would be expected to have one year post-injury on one of the ten functional dimensions. [Appendix E](#) provides a condensed version of the definition of all the levels of function defined for the ten different dimensions. A complete description of all levels of function for the ten different dimensions can be found in [Mackenzie et al. \(1994\)](#). It should be noted that the original mapping of AIS codes to FCI scores described above was conducted based on four assumptions: 1) the individual survives the injury, 2) the individual is 18 to 34 years old and has no pre-injury morbidities, 3) the acute care and rehabilitation received is appropriate and timely, and 4) the injury described is

the only injury sustained by the individual.

FCI seeks to describe impairment 12 months post-injury, and it rates every injury in the AIS 2005 (2008 update) codebook on a 0 (dead) to 100 (full recovery) scale across each of 10 dimensions of everyday living described above. The impairments in these 10 dimension can be combined into an overall 0 to 100 FCI score for patients sustaining multiple injuries that may affect different functional dimensions. A brief literature review and detailed description of FCI can be found in [McMurry et al. \(2015\)](#).

The most recent version of the FCI (2005) measures disability using the standard gamble technique, which asks subjects whether they would prefer to live with long term impairment or undergo a procedure that would either result in death or complete cure with a pre-specified probability. The lowest probability of cure a subject is willing to accept is interpreted as the proportion of full life the subject is able to experience. When these updated FCI values were constructed, it was found that on average subjects were never willing to accept less than a 60% chance of cure, so in practice, FCI scores for survivors range from 60 to 100.

In case of poly-trauma it can be expected that different injuries effect multiple dimensions at the same time. [McMurry et al. \(2015\)](#) developed the Whole-Body FCI (WBFCI) metric to describe the cumulative impairment effects from poly-trauma across all functional dimensions. It takes the most worst disability accrued across each dimension and combines them according to the Equation 5.3.

$$WBFCI = 40 \times \prod_{d=1}^{10} \left( \frac{FCI_d - 60}{40} \right) + 60 \quad (5.3)$$

where  $FCI_d$  is the FCI score for the injury in the  $d^{th}$  dimension (e.g. bending and Lifting).

As mentioned by [McMurry et al. \(2015\)](#) Equation 5.3 “is slightly modified from the version published in [MacKenzie et al. \(1996\)](#) in order to accommodate subsequent revisions to FCI. First, the FCI scale was reversed to make higher scores correspond to less disability. Second, in the standard gamble approach no level of impairment caused subjects on average to be willing to accept more than a 40% chance of death, so FCI scores for survivors were adjusted to range from 60 to 100. . . Third, the dimension weights are incorporated into the individual  $FCI_d$ .”

## 5.7 Maximum AIS (MAIS) and New Injury Severity Score

Though not originally developed to be a measure of threat to life, the Abbreviated Injury Scale (AIS) is associated with mortality and is often assessed as the maximum injury severity sustained across all body regions (MAIS). Soon after AIS was developed, and given that the primary population of interest was motor vehicle occupants, it was observed that there were different mortality rates between body regions with the same AIS severity level (e.g., AIS 4 injuries between the head and lower extremity) and that individuals tended to have a higher mortality rate based on secondary injuries. Therefore, the Injury Severity Score (ISS) was developed in order to assess trauma patients with multiple injuries and to address some of the nonlinearity associated between AIS and mortality. ISS is calculated by the sum of squares of the highest severity levels in three separate AIS body regions, and has been demonstrated to be associated with mortality ([Baker and O’Neill \(1976\)](#)). Because the ISS calculation might exclude non-maximal but significant injuries in the same body region, the New Injury Severity Score (NISS) was later developed to overcome

that potential problem. NISS is simply the sum of squares of the three most severe injuries, regardless of body region injured, and has also been shown to be predictive of mortality and to be a slight improvement to ISS (Sullivan et al. (2003)). A case series evaluation of injury distribution and associated losses related to ten pedestrian classes that occur under similar impact scenarios and speeds is provided in [Appendix D](#).

## Chapter 6

### Task2: Development and Validation of the UVAPED Model - Component Level Validation

The baseline UVAPED model (Figure 6.1) of a 50<sup>th</sup> percentile male was developed by combining the lower limb models developed by UVA (Hall (1999); Kerrigan (2008a)) and the upper body portion of the existing scalable TNO-developed facet 50<sup>th</sup> percentile male occupant human model (TNOOCC). The most updated facet pedestrian model (version 3.0, TNO PED) from TNO was not scalable and cannot be converted into a scalable model due to data encryption (TNO (2013)). As an alternative, a scalable occupant human model (TNOOCC) provided by TNO was used for the baseline UVAPED model (facet occ. Ver 4.0). Since the occupant model was developed for simulating the occupant behavior during a crash, the quality of the upper body was relatively good compared to its lower body and was considered a good starting point. A short model description has been provided in Appendix A.

The biofidelity of the baseline UVAPED model was improved by validating it against various cadaveric blunt impact tests from the literature. Table 6.1 provides a list of the tests used to validate various body parts. The summary of component level validation has been included in Appendix B.

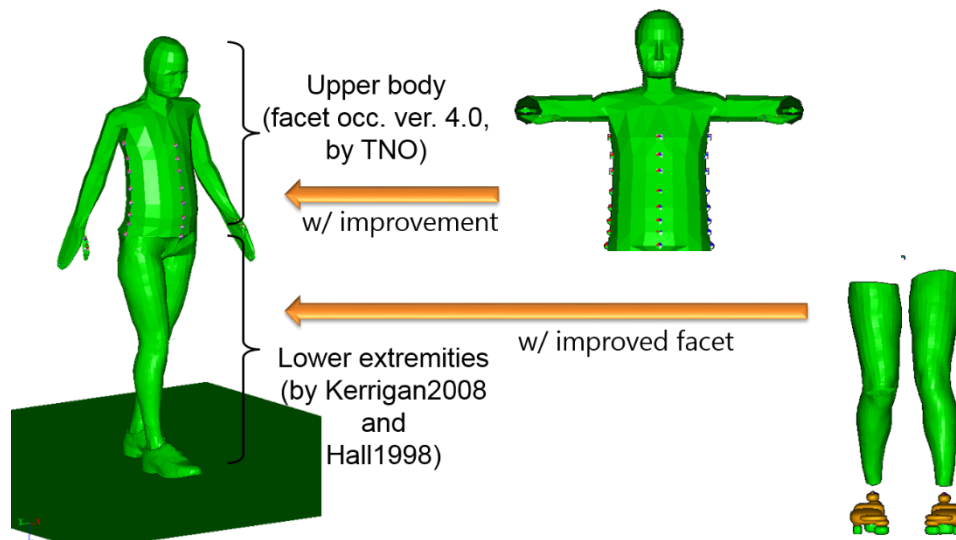


Figure 6.1: UVAPED Baseline Model

Table 6.1: List of References for Validations of Responses Under Blunt Impacts

Human Body Region	Reference
Head	AATD System Technical Characteristics, Design concepts and Trauma Assessment criteria (Melvin et al. (1985)) Impact Properties of Adult and ATD Heads (Loyd et al. (2012))
Neck lateral	Biomechanical Response Requirements of the Thor NHTSA Advanced Frontal Dummy GESAC (2005)
Neck frontal	Human volunteer head neck response in frontal flexion (Thunnissen et al. (1995))
Arm	Response corridors for the medial–lateral compressive stiffness of the human arm: Implications for side impact protection (Kemper (2013))
Shoulder lateral	Non-injurious and injurious impact response of the human shoulder three-dimensional analysis of kinematics and determination of injury threshold (Compigne et al. (2004)) Reponse of the torso to lateral and oblique constant velocity impacts (Subit et al. (2010)) Road vehicles – Anthropomorphic side impact dummy – lateral impact response requirements to assess the biofidelity of the dummy. Document N455 – revision 4, May, 1997 (ISO (1997)) Le choc latéral sur l'épaule: Mise en place d'un protocole expérimental en sollicitation dynamique (Meyer and Bonnoit (1994))
Thorax Frontal	Impact tolerance and response of the human thorax (Kroell et al. (1971))
Thorax lateral	Road vehicles – Anthropomorphic side impact dummy – lateral impact response requirements to assess the biofidelity of the dummy. Document N455 – revision 4, May, 1997 (ISO (1997)) Biomechanics of the human chest, abdomen, and pelvis in lateral impact. (Viano et al. (1989)) Reponse of the torso to lateral and oblique constant velocity impacts. (Subit et al. (2010))
Abdomen lateral	Biomechanics of the human chest, abdomen, and pelvis in lateral impact. (Viano et al. (1989))
Abdomen frontal	Lower Abdominal Tolerance and Response (Cavanaugh et al. (1986))
Pelvis lateral	Biomechanics of the human chest, abdomen, and pelvis in lateral impact (Viano et al. (1989))
Thigh	A computationally efficient mathematical model of the pedestrian lower extremity. (Kerrigan (2008a))
Knee*	A computationally efficient mathematical model of the pedestrian lower extremity. (Kerrigan (2008a))
Leg	A computationally efficient mathematical model of the pedestrian lower extremity. (Kerrigan (2008a))
Ankle*	Biomechanical characterization and multibody modeling of the human lower extremity. (Hall (1998))

\*Knee and ankle structural characteristics were determined based on component level cadaveric test. Therefore, it was assumed that those regions are biofidelic.

## 6.1 Head

### Frontal Impact Test

The corridors for the forehead frontal impact tests were developed by [Melvin et al. \(1985\)](#) by equating the impact energy in the head from head drop tests with the effective impact energy from an impactor. The impactor had a diameter of 152 mm, cylindrical shape, and 23.4 kg of mass. The test conditions were two impact velocities of 2 m/s and 5.5 m/s. The subject was tested in a sitting position with the legs horizontal and the arms raised (Figure 6.2). The head of the subject was placed so that the axis of the impactor was aimed at a point on the forehead on the mid-sagittal plane. The tilt of the model head/neck assembly was adjusted so that the normal vector of impacting area on the head was parallel to the impacting direction.

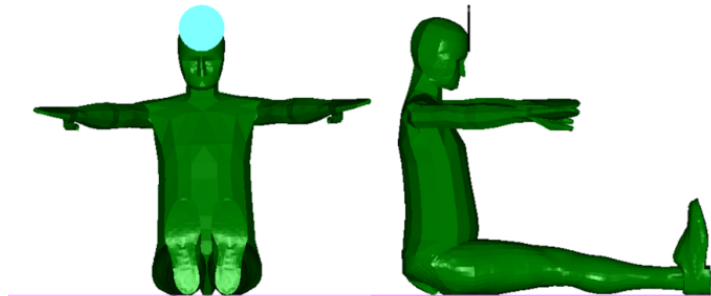


Figure 6.2: Head Frontal Impact Test Setup

### Forehead Drop Test

[Loyd et al. \(2012\)](#) performed component head drop tests with the mandible detached, and the considered drop heights were 15 cm and 30 cm, which are equivalent to 1.7 m/s and 2.4 m/s of drop speeds, respectively. Although the drop tests were

performed aiming at various impact locations on the head, forehead drop test data were used in this model evaluation. The authors did not provide any information regarding the orientation of the head so the isolated head drop model has been set up to impact the forehead area in the same way to the head impact test (Figure 6.3).

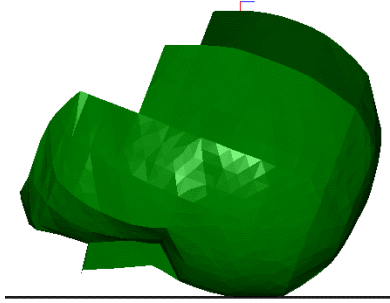


Figure 6.3: Lloyd Head Impact Test Setup

The head impact force or ground reaction force were reported either in the form of corridors or time histories in the literature (Melvin et al. (1985); Loyd et al. (2012)). The head contact force from the simulations were compared to the corridors and the force time histories.

## 6.2 Neck

### Whole Body Neck Flexion

During the NBDL test, the human volunteers were seated in an upright position on a sled which is adjusted to have the accelerations simulating frontal and lateral impacts (Thunnissen et al. (1995)) (Figure 6.4). The resultant three-dimensional motions of the volunteers' head and first thoracic vertebrae body (T1) were recorded by accelerators and photographic targets. During the impact experiments, the subjects were restrained by shoulder straps, a lap belt and an inverted V-pelvic strap tied to the lap belt. In the frontal test, an acceleration level of 15 g was used to develop the

response of the head and the T1, and an acceleration level of 8g was used to develop the responses. In the MADYMO simulation, the procedure was simplified by locking all the joints of the human model except the joints above the T1 location, and making the T1 joint duplicate the acceleration pulse observed in the NBDL test at the same location. Although there was discrepancy between the physical experimental setup and the MADYMO simulation setup because of the rotation of T1, [Thunnissen et al. \(1995\)](#) pointed out that the response differences between the rotated and non-rotated T1 coordinate system for all high severity human volunteer experiments were small. [Wang et al. \(2015\)](#) validated the neck of MADYMO pedestrian model and the optimized parameters from this study were used in the neck of UVAPED model.



Photo 1 The head-neck response during 15.6 G frontal impact. Experiment LX3983, subject H00134, 1982. From left to right 0 msec, 74 msec and 147 msec.

(a) Frontal Neck Flexion Test

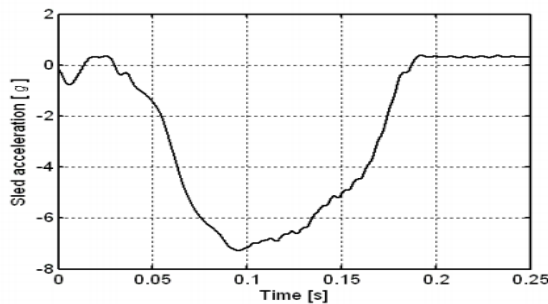


Figure 2.9: HYGE sled acceleration profile (ISO TR 9790)

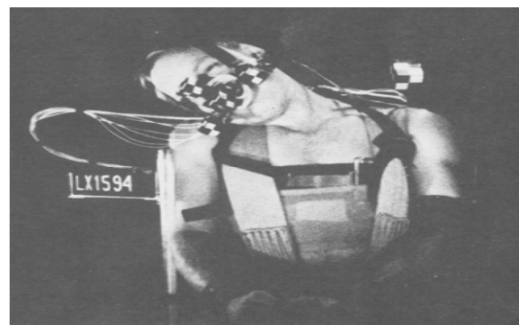


Figure 2.10 Maximum head excursion in a lateral NBDL test (Ewing et al., 1978)

(b) Lateral Neck Flexion Test

Figure 6.4: NBDL Volunteer Neck Flexion Experiment ([Thunnissen et al. \(1995\)](#))

The head angle, head resultant acceleration and the displacement of the center of gravity (CG) of the head observed in the test were selected to evaluate the neck mechanical characteristics by comparing them with the corresponding corridors. The T1 accelerations obtained from the volunteer tests were adopted as input acceleration pulse in the simulation of this study (Figure 6.5). Figure 6.6 shows the T1 acceleration curves for the frontal and the lateral tests separately. The mean acceleration from the frontal and lateral corridors was used as input.

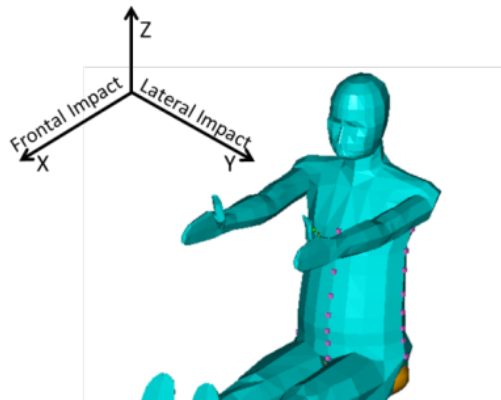


Figure 6.5: Model Setup for Frontal and Lateral Test

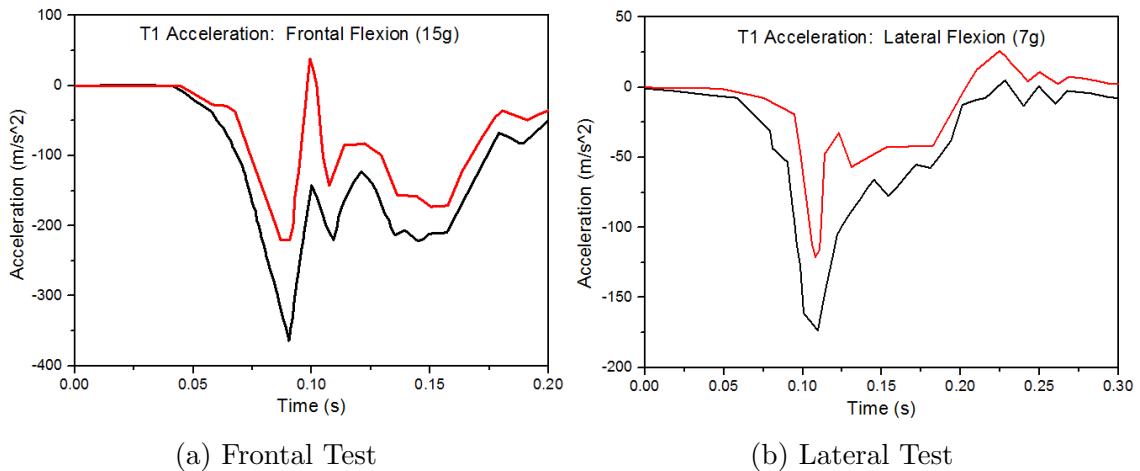


Figure 6.6: Input Acceleration Pulses for Frontal and Lateral Test of Neck (GESAC (2005))

## 6.3 Shoulder Lateral

### Lateral Shoulder Impact Test

Compigne et al. (2004) designed an experiment in which an impactor of mass 23.4 kg and dimensions of 150x80 mm was aligned at the center of the glenohumeral joint to strike the upright seated subject at two initial speeds of 1.5 m/s and 3 m/s. The model was positioned in an upright seated position with the impactor aligned to the glenohumeral joint to match Compigne's test setup (Figure 6.7). The authors normalized the impact force and shoulder deflection to those of the 50<sup>th</sup> percentile male since the weights (33-67 kg), height (148-165 cm), and shoulder widths (340-400 mm) of their subjects were quite different from those of the 50<sup>th</sup> percentile male, which are 75kg, 176cm, and 468mm, respectively. All subjects test data for 1.5 m/s and specimen #5 and #6 test data for 3m/s were used for the model evaluation. Compigne et al. (2004) calculated the impactor force by multiplying the impactor mass with its measured acceleration with inertial compensation. The acromion to acromion distance was measured by tracking targets attached to the shoulder blade through video analysis. For the model, the shoulder deflection was measured by using the relative displacement between the left and right scapulae.



Figure 6.7: Compigne Lateral Shoulder Impact Test and Simulation Setups (Compigne et al. (2004))

Subit et al. (2010) designed an experiment in which the subject was seated on a rigid chair. The seated surface was tilted  $11^\circ$  from the horizontal plane and the seat back was tilted  $21^\circ$  from the vertical plane. An impactor of 71.8 kg mounted on a linear guide struck the right-side shoulder (Figure 6.8). The impacting probe was a 75 (height) x 400 (width) x 60 (depth) mm hollow piece of aluminum with 10 mm of rounded edges (Subit et al. (2010)). The head of the subject was hung to a support frame using a spring, which had 1.3 kN/m of stiffness, to maintain its posture. Subject 427 was chosen for comparison as its anthropometry and body mass index were very close to the 50<sup>th</sup> percentile male (79 kg weight, 181cm height and 24.1 kg/m<sup>2</sup> BMI). Each MADYMO model was positioned in a sitting posture following the test condition to mimic the initial spine curvature of the PMHS. The model was rolled  $4.3^\circ$  of roll angle according to the initial posture of the subject 427 in the test (Figure 6.8), and the knee joint, hip joint, and elbow joint were also adjusted to meet the test setup. The spring for the head was considered during the simulation (Figure 6.8). The impactor height was adjusted to the glenohumeral joint. Prescribed motions from the experimental data were imposed to the impactor for the simulation. Subit et al. (2010) measured impact force using a load cell attached to the leading end of the transfer piston. The authors measured the motion of spine, sternum, scapulae, and impactor using a 3D motion tracking system. In the simulation, the shoulder impact force was measured using the contact force between the shoulder and the impactor. In the simulation, the displacements of the T1, sternum, and scapulae were measured and compared to those of Subit et al. (2010).

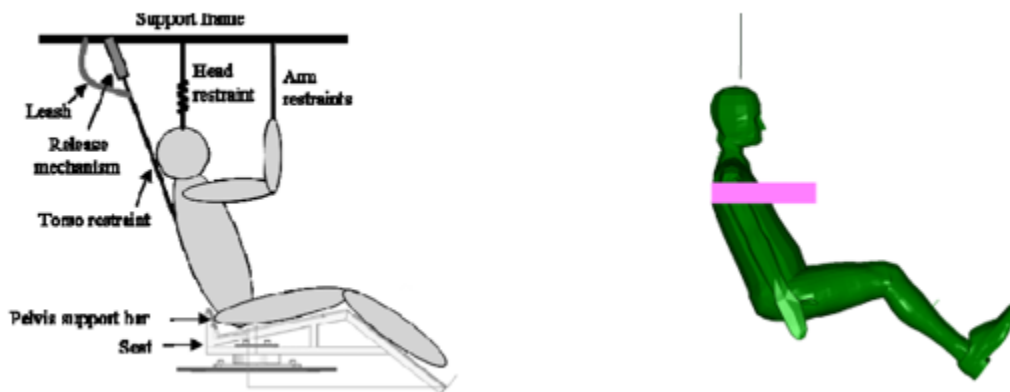


Figure 6.8: Subit Lateral Shoulder Impact Test and Simulation Setups (Subit et al. (2010))

## 6.4 ISO9790 Lateral Shoulder Impact

AN ISO9790 shoulder blunt impact test (ISO (1997)) was modeled using a pendulum (mass 14 kg and 152 mm diameter) striking the upright human body with the arm down, and the axis of the impactor (Figure 6.9) aligned with the center of the shoulder at an initial speed of 4.5 m/s. A similar configuration was set up with an initial speed of 5.5 m/s of the tests conducted by Meyer et al (1998) (Meyer and Bonnoit (1994)). For the ISO/Meyer tests, the shoulder impact forces time histories of the models were compared to the impact force response corridors.

## 6.5 Thorax

### Lateral Thoracic Impact

Viano et al. (1989) performed lateral thoracic impact tests using a 23.4 kg pendulum suspended by guide wires and accelerated to impact speeds of 4.5, 6.7 and

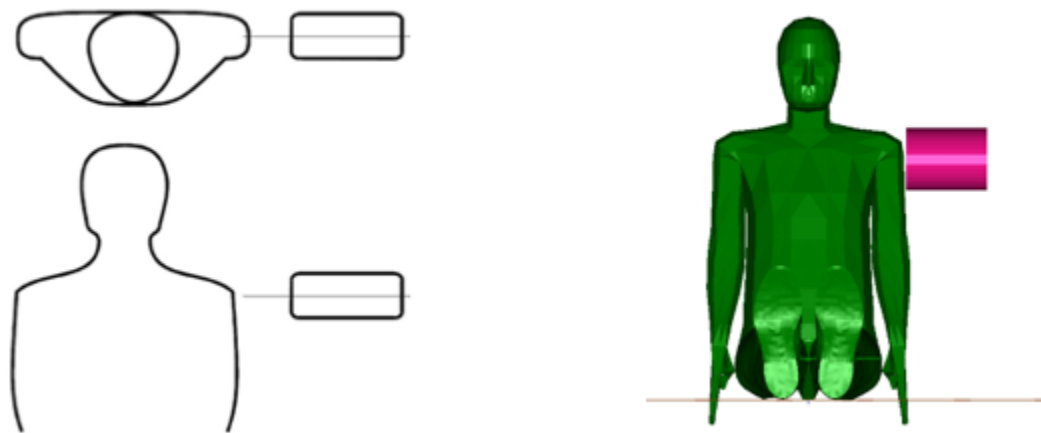


Figure 6.9: ISO/Meyer Lateral Shoulder Impact test and Simulation Setups (ISO (1997); Meyer and Bonnoit (1994))

9.4 m/s. The cadaver was suspended upright with hands and arms overhead. The specimen was rotated  $30^\circ$  so that the point of pendulum contact was lateral on the thorax. This protocol was used to assure that full lateral thoracic impact occurred with the axis of force through the center of gravity of the torso. The impactor was aligned with the xiphoid process 7.5 cm below mid sternum. The pendulum surface was a smooth, flat, 150 mm diameter circular disc with edges rounded (Figure 6.10). A suspension system for the arms was released prior to the impact. Two impact speeds of 4.5 and 6.7 m/s were considered for the evaluation of the pedestrian models. A uniaxial accelerometer was attached to the pendulum and its response was multiplied by the pendulum mass to give the force of impact. High-speed movies of the impact were taken from the frontal, posterior and overhead views. Corridors for impactor deflection were obtained through photo target analysis of the markers attached to the impactor and lumbar vertebrae. The relative displacement of the impactor and the L2 vertebrae was used to evaluate the impactor deflection in the model. The contact force was measured at the impact location.

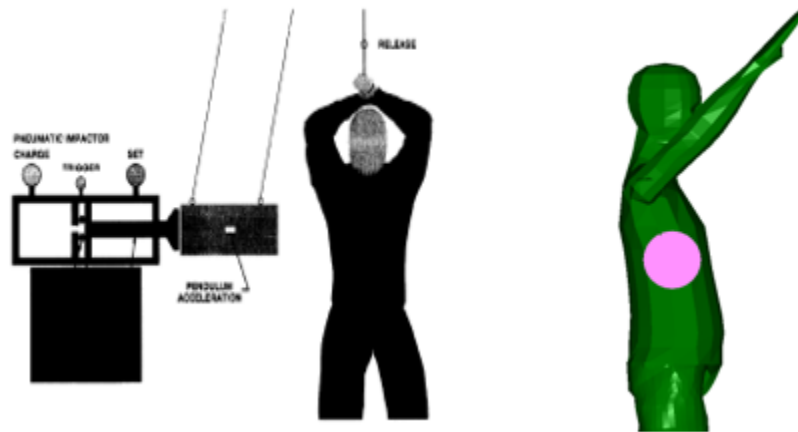


Figure 6.10: Viano Thoracic Impact Test and Simulation Setups (Viano et al. (1989))

## ISO9790 Lateral Thoracic Impact

Two series of cadaveric thorax lateral impact tests were conducted by HSRI (ISO (1997)). The cadavers were seated upright with one arm raised so that the lateral aspect of the thorax was directly impacted. The impactor had a flat, rigid impact surface which was 150 mm in diameter, and its mass was 23.4 kg (Figure 6.11). The impact velocity for the first series of the tests was 4.3 m/s. A second series of impact tests were carried out with the same impactor as the first series with 6.8 m/s of impactor speed, but the impacting direction was changed from pure lateral to 60° oblique to the mid-sagittal plane. Note that the authors concluded that the obliqueness of the impactor had little effect on the peak impact force and the duration of the impulse. Therefore, the response corridors from the oblique impacts at speeds of 6.8 m/s has been recommended for biofidelity comparison of dummies under pure lateral impact. For the ISO lateral thoracic impact simulation, both 4.3 m/s and 6.8 m/s lateral thoracic impact simulations were performed in pure lateral impact configuration. The contact force and T1 vertebrae body acceleration in the impact

direction from the model were compared to the experimental corridors.

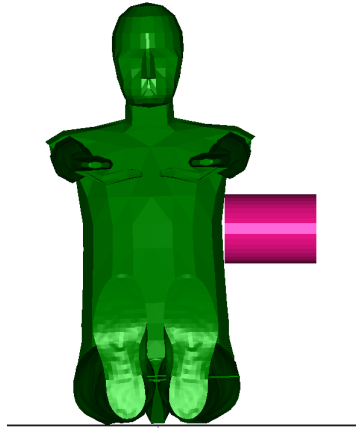


Figure 6.11: ISO Thoracic Lateral Impact Test and Simulation Setups

## Lateral and Oblique Thoracic Impact

The setup for lateral and oblique thoracic impact tests performed by [Subit et al. \(2010\)](#) was similar to that of the Subit shoulder impact tests in terms of the occupant posture, seat configuration, and dimensions and mass of impactors (Figure 6.12). The constant velocity impacts of 1 and 3 m/s were performed at three impacting angles ( $0^\circ$  lateral;  $-15^\circ$  anterolateral; and  $+15^\circ$  posterolateral) at two levels of thorax (Figure 6.12). The impact was defined as an upper-arm impact, when the impactor was just inferior to the posterior aspect of the upper arm and upper arm on the struck side was horizontal. If the impact was just inferior to the inferior angle of the scapula and the upper arm of the struck side was horizontal, it was called mid-chest impact. For the mid-chest impacts, the chest lateral deformation was directly defined as the variation of distance between the impactor and the spine. For the upper-chest impacts, the scapula was in between the impactor and the spine and any displacement of the scapula reduced the amount of chest deformation. Therefore,

the chest deformation for these tests was defined as the displacement of the impactor minus the displacement of the spine and scapula.

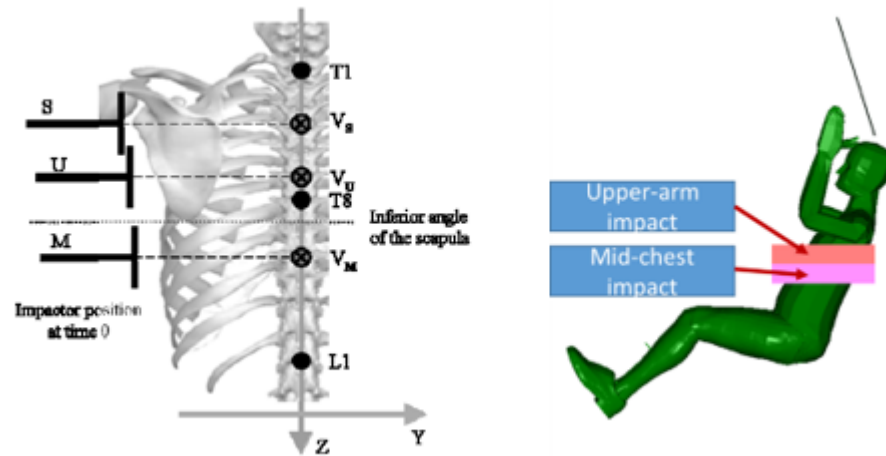


Figure 6.12: Impact Location, Lateral Impact Test, and Simulation Setups (Subit et al. (2010))

## Frontal Thoracic Impact

Nahum et al. (1970) conducted frontal thoracic impacts using a rigid 15.2 cm diameter cylindrical impactor striking the sternum at the 4<sup>th</sup> rib interspace. These test series were followed by another frontal impact test conducted by Kroell et al. (1971). This test configuration has been well-accepted as a standard to assess the biofidelity of the thorax. Two biofidelity corridors for low speed (4.3 m/s) and high speed (6.7 m/s) impact respectively were proposed by Lobdell et al. (1973) using impactor force vs deflection data from Nahum et al. (1970) and Kroell et al. (1971). These corridors only provided the skeletal deflection data and were updated by Lebarbé and Petit (2012) to include the total deflection of thorax. Additionally, more tests were added to the raw data (Trosseille et al. (2008)) and the biofidelity corridors were constructed

using recent normalization techniques [Mertz \(1984\)](#).

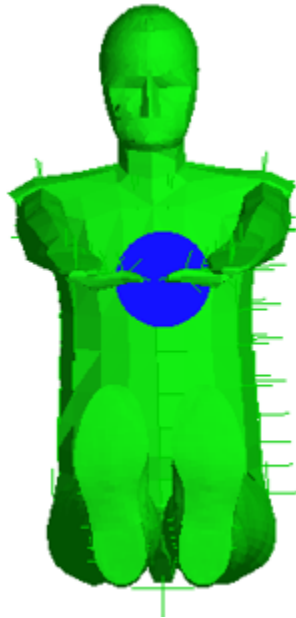


Figure 6.13: Simulation Setup for Thorax Frontal Impact

## 6.6 Abdomen

### Lateral Abdominal Impact

[Viano et al. \(1989\)](#) performed lateral abdominal impact tests using a 23.4 kg pendulum suspended by guide wires and accelerated to impact speeds of approximately 4.5, 6.7 and 9.4 m/s. The cadaver was suspended upright with hands and arms overhead. The specimen was rotated 30° so that the point of pendulum contact was lateral on the abdomen. This protocol was used to assure that full lateral abdominal impact occurred with the axis of force through the center of gravity of the torso. The impactor was aligned 7.5 cm below the xiphoid process and 15 cm below mid sternum. The pendulum surface was a smooth, flat, 150 mm diameter circular disc with edges rounded (Figure 6.14). A suspension system for the arms was

released prior to the impact. The impact speeds of 4.5 and 6.7 m/s were considered for the evaluation of the pedestrian models. A uniaxial accelerometer was attached to the pendulum and its response was multiplied by the pendulum mass to give the force of impact. High-speed movies of the impact were taken from frontal, posterior and overhead views. Corridors for impactor deflection were obtained through photo target analysis of the markers attached to the impactor and lumbar vertebrae. The relative displacement of impactor and L2 vertebra was used to evaluate the impactor deflection in the model. The contact force was measured at the impact location.

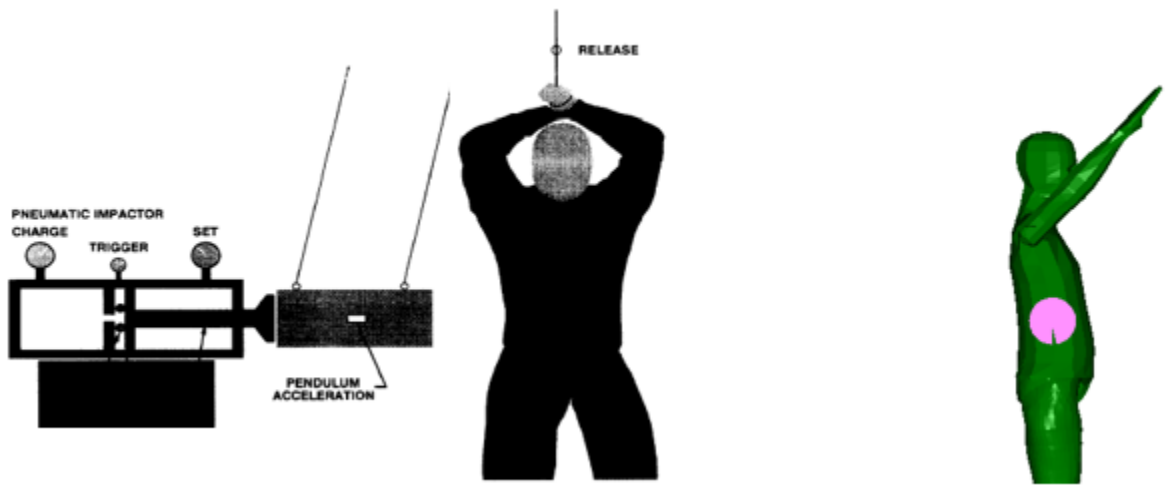


Figure 6.14: Viano Lateral Abdominal Impact Test and Simulation Setups (Viano et al. (1989))

## Frontal Abdominal Impact

Cavanaugh et al. (1986) performed 12 abdominal impacts with the cadaver seated in an upright position with legs parallel to each other and resting on a horizontal plane. The main axis of the torso was upright, at 90 degrees to the horizontal platform and the anterior side of the torso was facing the impactor (Figure 6.15). The

back of the subject was unrestrained so it was free to translate rearward on impact. The impact level was L3 lumbar vertebrae. The impactor mass used during the test series was essentially either 32 kg or 64 kg. The assembly used on the impactor face was an aluminum bar, 25 mm in diameter, 381 mm long, oriented so that the long axis of the bar was parallel to the width of the body (Figure 6.15). The impactor was instrumented with a uniaxial accelerometer and uniaxial load cell. Their sensitive axes were parallel to the direction of impact. The mass ahead of the impactor force transducer consisted primarily of the impactor bar assembly. The impactor load cell assembly was inertially compensated. The deflection data was obtained by analyzing the high speed camera film data. The impactor contact force was measured at the impact location in the model and the abdomen deflection was calculated based on the relative displacement between the impactor and L3 vertebrae bodies.

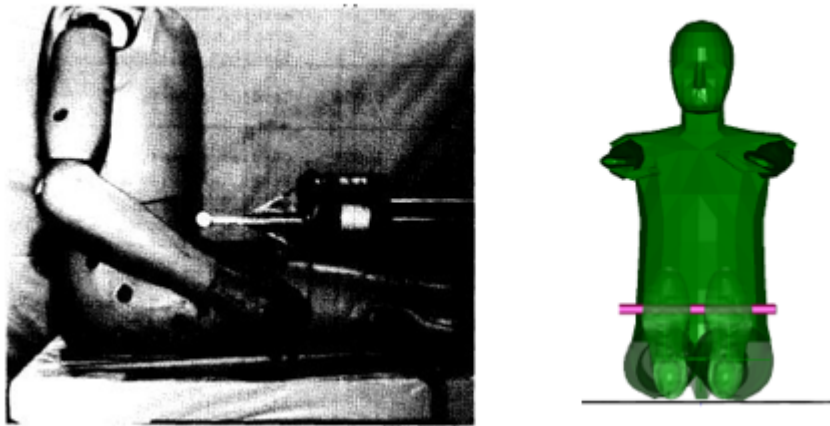


Figure 6.15: Abdomen Frontal Impact Test and Simulation Setups (Cavanaugh et al. (1986))

## 6.7 Pelvis

### Lateral Pelvis Impact

Viano et al. (1989) performed lateral pelvis impact tests using a 23.4 kg pendulum suspended by guide wires and accelerated to impact speeds of approximately 4.5, 6.7 and 9.4 m/s. (Figure 6.10). The location of the impact was on the greater trochanter on the right side of the model (Figure 6.16). The impactor force from the experiment has been compared to the contact force between the impactor and the skin surrounding the pelvis region. This includes the following parts: Hip gap, pelvis filler and pelvis skin.

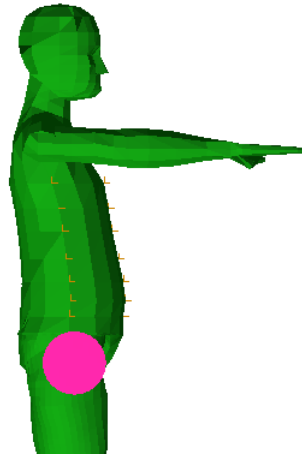


Figure 6.16: Viano Lateral Pelvis Impact Simulation (Viano et al. (1989))

## 6.8 Lower Extremities

### Thigh Lateral Beding and Leg Lateral Bending

Kerrigan (2008a) performed a series of 3 point (medial-lateral) bending tests on isolated components of PMHS lower extremities (thigh and leg) to evaluate the fracture tolerance of the thigh and leg to lateral bending. These tests were done on non-embalmed specimens and therefore accounts for the influence of flesh on the lateral bending of leg and thigh. The ends of the specimen were potted and fixed to the proximal and distal cups which were attached to roller supports (Figure 6.17a). An Instron machine was used to move the impactor at a rate of 1.5 m/s to simulate dynamic loading conditions until the bone fracture occurred. The specimens supported at both ends were loaded at either mid-diaphysis location, a third of their length measured from the distal end (distal), or a third of their length measured from the proximal end (proximal). For the thigh model, the knee and hip joints were fixed to the distal and proximal cups, respectively, using bracket joints. For the leg model, the ankle and knee joints were fixed to the distal and proximal cups, respectively, using bracket joints (Figure 6.17b). A multibody to multibody contact was defined between the rollers and the load cell plates. A finite element to multibody contact was defined between the indenter and the flesh of the thigh or leg models. Proximal and distal load cells were used to measure the support loads and moments and a uniaxial load cell was used to measure the impactor force. Two angular rate sensors were fixed to the proximal and distal cups to measure the rotation of the cups along the y-axis (Figure 6.17a). The indenter and support loads were measured at the same locations in the model and the rotation of the proximal and the distal cups were measured with respect to the global reference system.

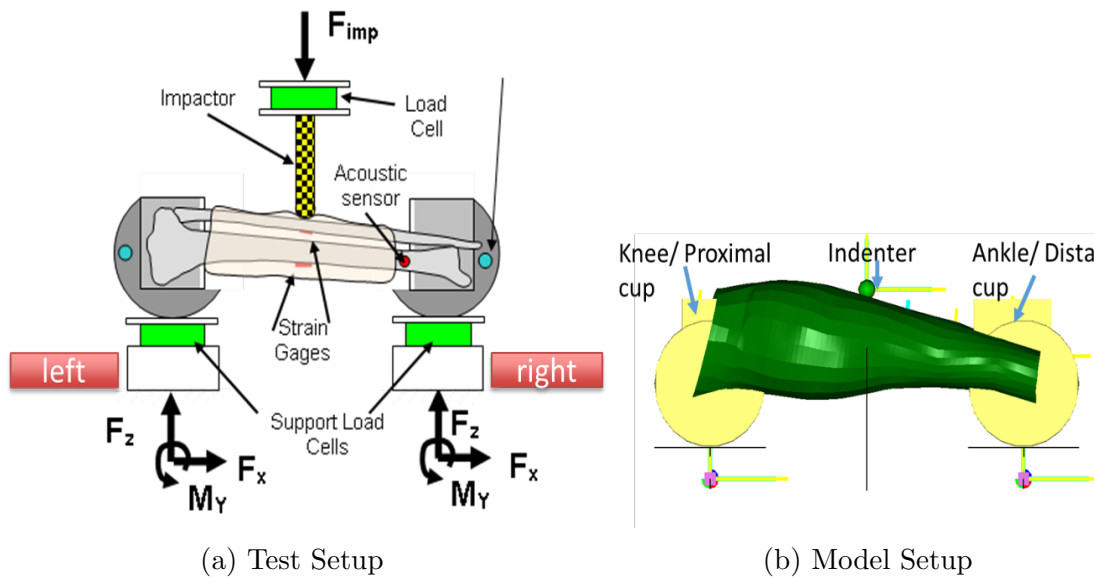


Figure 6.17: Thigh and Leg Test and Simulation Setups (Kerrigan (2008a))

## 6.9 Discussion

The UVAPED model showed improved biofidelity in head frontal impact, thorax frontal impact, pelvis lateral impact, abdomen lateral impact and lower extremities under lateral bending (Table 6.2). While the Cora scores for lateral shoulder impact under ISO test mode were lower for the UVAPED model it has to be noted that the responses fall within the biofidelity corridors established for the test mode. Compared to the Subit lateral impact tests which use a narrow impactor targeting a specific body region, the UVAPED model showed better match to the PMHS response in the Viano lateral impact, which uses a larger impactor. This is due to the approximation of the thorax in the UVAPED model which was modeled using four frontal and lateral bodies. The lower extremities of the UVAPED model were optimized to improve the repose of the model in Thigh and Leg lateral bending and therefore showed superior biofidelity.

Table 6.2: Summary of ISO Ratings for Component Level Validation of UVAPED Model

Body Region	Test Mode	Signal	Per test mode		Average per test mode	
			TNOPEd	UVAPED	TNOPEd	UVAPED
Head	HeadF_Melvin_2p0mps	ImpactFvsT	0.63	0.63	0.63	0.63
	HeadF_Melvin_5p5mps	ImpactFvsT	0.52	0.76	0.52	0.76
	HeadF_Loyd_1p7mps	ImpactFvsT	0.78	0.75	0.78	0.75
	HeadF_Loyd_2p4mps	ImpactFvsT	0.62	0.74	0.62	0.74
Shoulder	ShoulderL_ISO_4p5mps	FvsT	0.70	0.59	0.70	0.59
	ShoulderL_ISO_5p5mps	FvsT	0.54	0.43	0.54	0.43
	ShoulderL_Compigne_1p5mps	FvsT	0.53	0.74	0.59	0.63
	ShoulderL_Compigne_1p5mps	DvsT	0.64	0.53		
	ShoulderL_Compigne_3p0mps	FvsT	0.69	0.53	0.74	0.60
	ShoulderL_Compigne_3p0mps	DvsT	0.79	0.66		
	ShoulderL_Subit_1mps	FvsT	0.47	0.72	0.72	0.80
	ShoulderL_Subit_1mps	DSCvsT	0.60	0.67		
	ShoulderL_Subit_1mps	DSTvsT	0.88	0.86		
	ShoulderL_Subit_1mps	DT1vsT	0.87	0.90		
	ShoulderL_Subit_1mps	DT8vsT	0.80	0.87		
	ShoulderL_Subit_3mps	FvsT	0.74	0.60	0.78	0.76
	ShoulderL_Subit_3mps	DSCvsT	0.62	0.65		
	ShoulderL_Subit_3mps	DSTvsT	0.69	0.84		
ShoulderL_Subit_3mps	DT1vsT	0.93	0.86			
ShoulderL_Subit_3mps	DT8vsT	0.91	0.87			

Continued on next page

Table 6.2 – continued from previous page

Body Region	Test Mode	Signal	Per test mode		Average per test mode	
			TNOPED	UVAPED	TNOPED	UVAPED
Thorax	ThoraxF_Kroell_4p3mps	FvsD	0.54	0.82	0.54	0.82
	ThoraxF_Kroell_6p7mps	FvsD	0.44	0.69	0.44	0.69
	ThoraxL_Viano_4p4mps	FvsT	0.54	0.82	0.55	0.71
	ThoraxL_Viano_4p4mps	FvsD	0.57	0.59		
	ThoraxL_Viano_6p5mps	FvsT	0.52	0.87	0.49	0.81
	ThoraxL_Viano_6p5mps	FvsD	0.47	0.75		
	ThoraxL_Subit_Mid_1mps	FvsT	0.13	0.21	0.41	0.56
	ThoraxL_Subit_Mid_1mps	DT8vsT	0.68	0.91		
	ThoraxL_Subit_Mid_3mps	FvsT	0.32	0.42	0.50	0.61
	ThoraxL_Subit_Mid_3mps	DT8vsT	0.68	0.81		
	ThoraxL_Subit_Up_1mps	FvsT	0.34	0.25	0.53	0.42
	ThoraxL_Subit_Up_1mps	DT8vsT	0.72	0.60		
	ThoraxL_Subit_Up_3mps	FvsT	0.69	0.47	0.77	0.66
	ThoraxL_Subit_Up_3mps	DT8vsT	0.85	0.85		
	ThoraxL_Subit_AL_Mid_3mps	FvsT	0.26	0.39	0.35	0.56
	ThoraxL_Subit_AL_Mid_3mps	DT8vsT	0.45	0.72		
	ThoraxL_Subit_AL_Up_3mps	FvsT	0.51	0.36	0.60	0.52
	ThoraxL_Subit_AL_Up_3mps	DT8vsT	0.68	0.69		
	ThoraxL_Subit_PL_Mid_3mps	FvsT	0.73	0.62	0.61	0.53
	ThoraxL_Subit_PL_Mid_3mps	DT8vsT	0.49	0.43		
ThoraxL_Subit_PL_Up_3mps	FvsT	0.46	0.40	0.52	0.52	
ThoraxL_Subit_PL_Up_3mps	DT8vsT	0.59	0.64			

Continued on next page

Table 6.2 – continued from previous page

Body Region	Test Mode	Signal	Per test mode		Average per test mode	
			TNOPED	UVAPED	TNOPED	UVAPED
Abdomen	AbdomenF_Cavanaugh_6p1mps	FvsT	0.80	0.73	0.80	0.73
	AbdomenL_Viano_4p8mps	FvsT	0.03	0.35	0.03	0.35
	AbdomenL_Viano_6p8mps	FvsT	0.09	0.82	0.09	0.82
Pelvis	PelvisL_Viano_5p2mps	FvsT	0.39	0.77	0.39	0.77
	PelvisL_Viano_9p8mps	FvsT	0.27	0.83	0.27	0.83
Thigh	ThighL_Kerrigan_Mid_1p5mps	ImpactFvsT	0.67	0.81		
	ThighL_Kerrigan_Mid_1p5mps	ProxCupFvsT	0.64	0.91		
	ThighL_Kerrigan_Mid_1p5mps	DistCupFvsT	0.58	0.90	0.62	0.86
	ThighL_Kerrigan_Mid_1p5mps	ProxCupAngvsT	0.64	0.86		
	ThighL_Kerrigan_Mid_1p5mps	DistCupAngvsT	0.59	0.81		
	ThighL_Kerrigan_Dist_1p5mps	ImpactFvsT	0.49	0.88		
	ThighL_Kerrigan_Dist_1p5mps	ProxCupFvsT	0.42	0.68		
	ThighL_Kerrigan_Dist_1p5mps	DistCupFvsT	0.45	0.85	0.47	0.78
	ThighL_Kerrigan_Dist_1p5mps	ProxCupAngvsT	0.49	0.73		
	ThighL_Kerrigan_Dist_1p5mps	DistCupAngvsT	0.50	0.78		
Leg	LegL_Kerrigan_Prox_1p5mps	ImpactFvsT	0.74	0.63		
	LegL_Kerrigan_Prox_1p5mps	ProxCupFvsT	0.65	0.81		
	LegL_Kerrigan_Prox_1p5mps	DistCupFvsT	0.69	0.72	0.62	0.70
	LegL_Kerrigan_Prox_1p5mps	DistCupAngvsT	0.39	0.64		
	LegL_Kerrigan_Mid_1p5mps	ImpactFvsT	0.54	0.84		
	LegL_Kerrigan_Mid_1p5mps	ProxCupFvsT	0.58	0.75		
	LegL_Kerrigan_Mid_1p5mps	DistCupFvsT	0.52	0.79	0.52	0.79
	LegL_Kerrigan_Mid_1p5mps	DistCupAngvsT	0.43	0.79		

Continued on next page

Table 6.2 – continued from previous page

Body Region	Test Mode	Signal	Per test mode		Average per test mode	
			TNOPED	UVAPED	TNOPED	UVAPED
	LegL_Kerrigan_Dist_1p5mps	ImpactFvsT	0.43	0.82		
	LegL_Kerrigan_Dist_1p5mps	ProxCupFvsT	0.41	0.72		
	LegL_Kerrigan_Dist_1p5mps	DistCupFvsT	0.38	0.72	0.41	0.76
	LegL_Kerrigan_Dist_1p5mps	DistCupAngvsT	0.42	0.76		

## Chapter 7

### Task2: Development and Validation of the UVAPED Model - Whole Body Validation

#### 7.1 Introduction

The UVAPED model has been validated under various blunt impact conditions and it has demonstrated superior biofidelity to the commercially available multibody pedestrian models. The blunt impact validation lacks the ability to assess the interaction between various body regions and their effect on the injury risk. Therefore, evaluation of the biofidelity of the UVAPED model under whole-body pedestrian impact is a crucial step prior to using the model in pedestrian research for vehicle design, counter measures evaluation, and or crash reconstruction.

Few studies have evaluated the biofidelity of pedestrian multibody models under whole-body based pedestrian impact tests using a production car (Ishikawa *et al.* (1993); Yang *et al.* (2000)). While production cars have more realistic information about the geometry, the stiffness of the front end of the vehicle is largely unknown except to the vehicle manufacturers. Therefore, although a pedestrian model may show good correlation with the responses of cadavers, questions on the biofidelity of

the pedestrian model may still exist.

Recently, the University of Virginia Center for Applied Biomechanics performed cadaveric pedestrian impact tests using a generic vehicle buck (Figure 7.1) (Forman et al. (2015); Forman et al. (2015)). The buck is based on a sedan type vehicle, and was developed by the SAE Pedestrian Dummy Task Group (PDTG) for dummy and model biofidelity assessment (Pipkorn et al. (2014, 2012); Takahashi et al. (2014)). The bumper, hood and grill were constructed with the aid of simple engineering materials (polyethylene, sheet steel etc.) and were designed to represent a good rated vehicle in the EuroNCAP pedestrian impactor testing. The extensive kinematics (accelerations, trajectories, rotations of anatomical locations), kinetics (reaction forces measured between the bumper, hood, grill and buck frame (Figure 7.1b), and injury outcomes recorded during the tests will be used to assess the UVAPED model's performance under whole-body impact and it will be compared to its counterpart, which is the commercially available TNO ellipsoid model and also the THUMS pedestrian finite element model (PFEM). Wu et al. (2017) evaluated the biofidelity of the THUMS pedestrian model under whole-body impact with the generic pedestrian buck and the results from this study will be used to evaluate the biofidelity of the UVAPED model relative to THUMS and TNO ellipsoid model which is a scalable form of a commercially available pedestrian model.

## 7.2 Scaling and Positioning

The baseline pedestrian model has been mass scaled (Figure 7.2) to match the anthropometries of the three subjects (V2370, V2371, V2374) (Figure 7.2). The positioning procedure of the scaled model involved three steps. First, the pelvis orientation was matched to the Vicon data and then the lower extremities were positioned

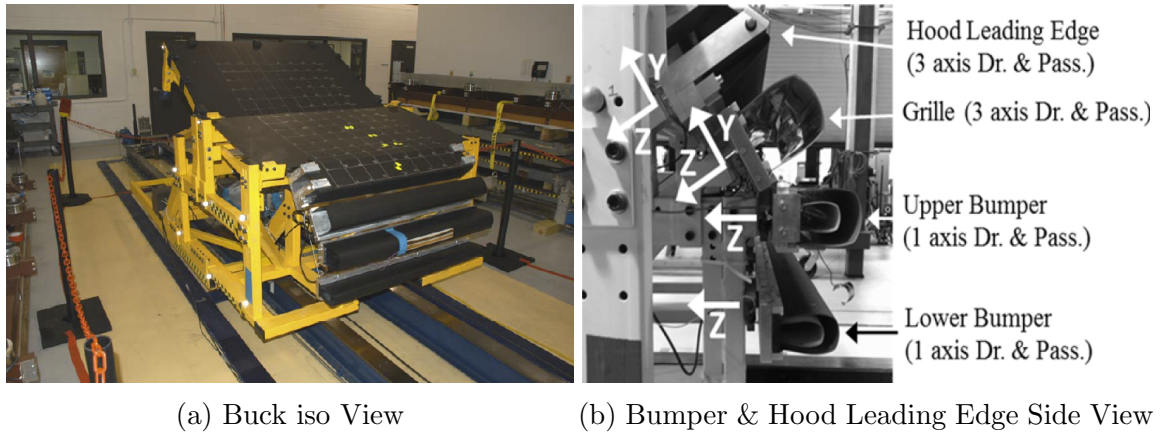


Figure 7.1: Generic Pedestrian Buck

by optimizing the roll and pitch angles at the hip joint and the pitch angle degree of freedom at the knee joint to match the femur and tibial local coordinate system from the Vicon data. The second step involved positioning the upper body to match the T1, and head relative positions with respect to the pelvis in the  $x$  direction to maintain the spinal curvature. The model is later shrugged and the arms are finally positioned to match the pre-test positioning posture (Figure 7.4).

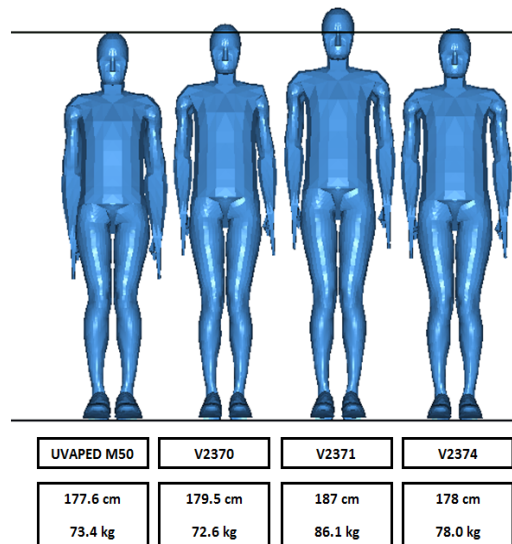


Figure 7.2: Scaled UVAPED Models

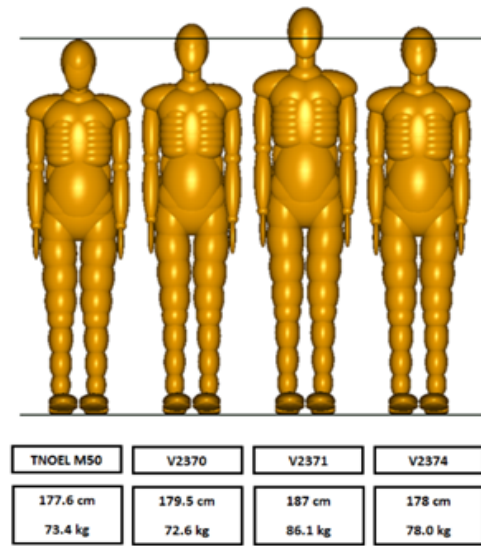


Figure 7.3: Scaled TNOEL Models

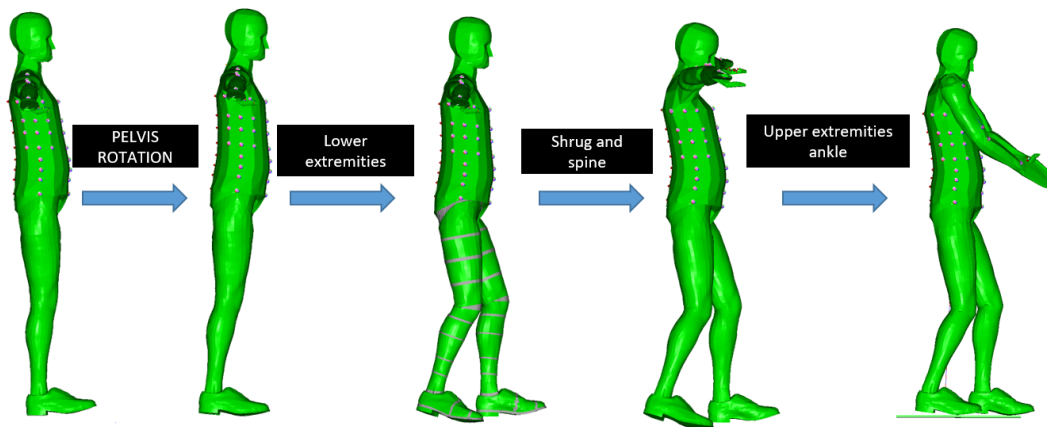


Figure 7.4: Schematic Overview of Positioning Procedure

A comparison of positioned Model UVAPED to Vicon data at anatomical land marks is shown in Figures 7.5, 7.6, and 7.7.

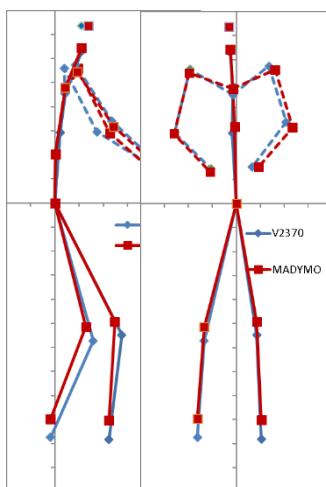


Figure 7.5: Comparison of Positioned Model UVAPED to Vicon Data at Anatomical Land Marks for PMHS V2370

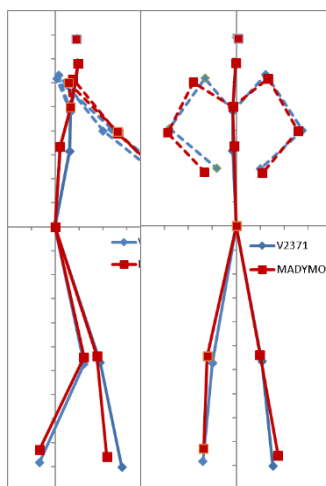


Figure 7.6: Comparison of Positioned Model Uvaped to Vicon Data at Anatomical Land Marks for PMHS V2371

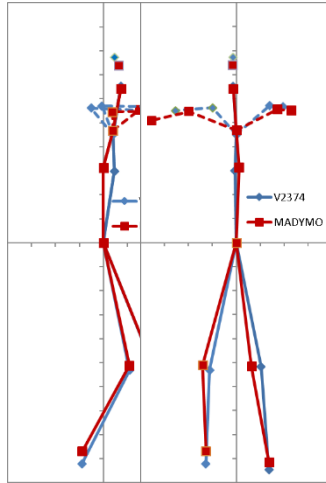


Figure 7.7: Comparison of Positioned Model Uvaped to Vicon Data at Anatomical Land Marks for PMHS V2374

The pedestrian models were positioned with respect to the buck to match the standing posture for each of the three PMHS from pedestrian sled tests with a generic vehicle buck. Each model's vertical position was adjusted to align the struck-side knee height to the target height obtained from the Vicon 3D motion tracking system. The lateral position was adjusted to get first contact between the struck-side leg and the buck close to time zero and the model was centered in between the buck to match the location of the pelvis with respect to the midsection of the buck.

## 7.3 Results

An overall comparison of the PMHS and UVAPED kinematics is provided in Figure 7.8 to Figure 7.13 for the 3 PMHS tests.

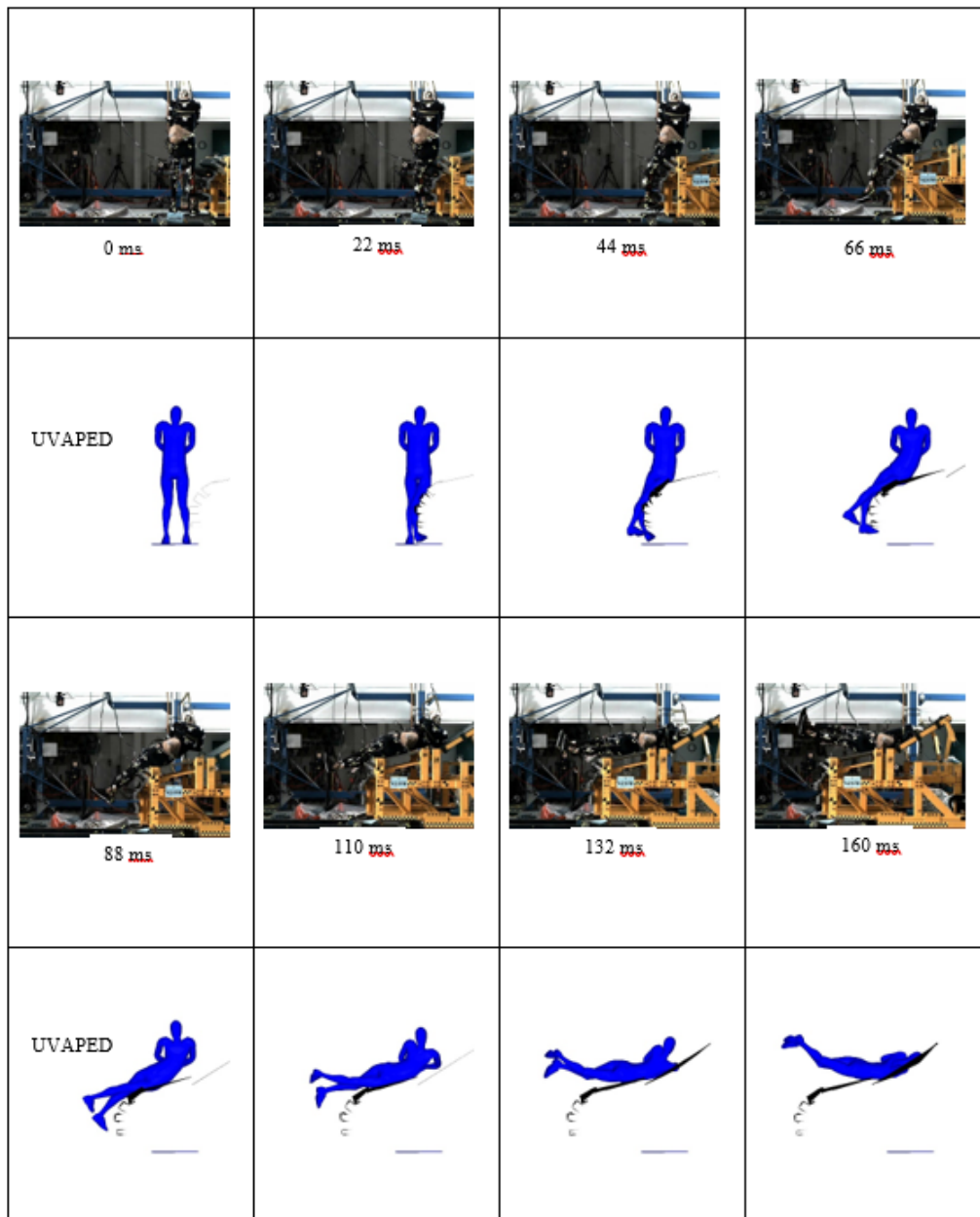


Figure 7.8: Comparison of Pedestrian Impact Sequences for Test V2370 (Posterior View)

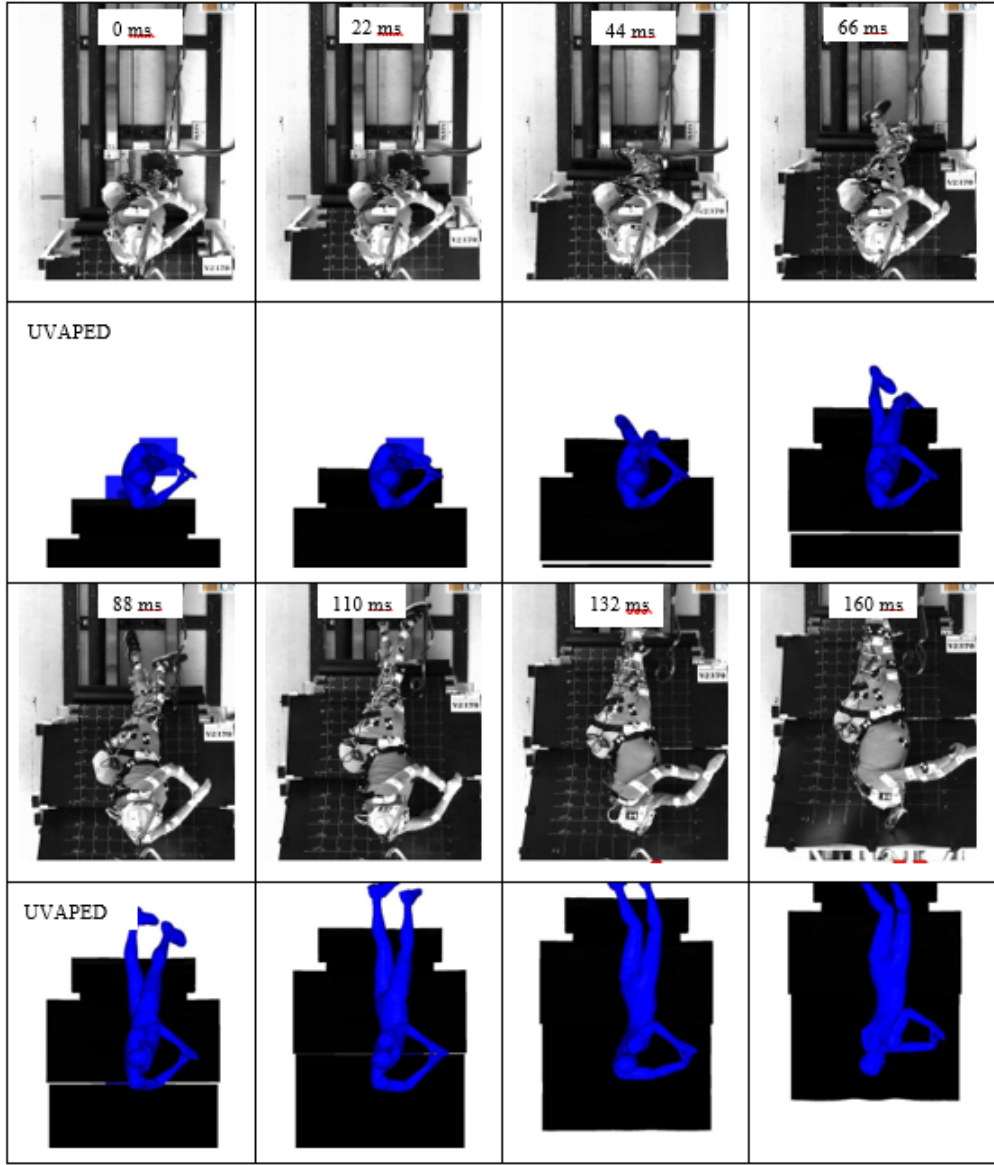


Figure 7.9: Comparison of Pedestrian Impact Sequences for Test V2370 (Superior View)

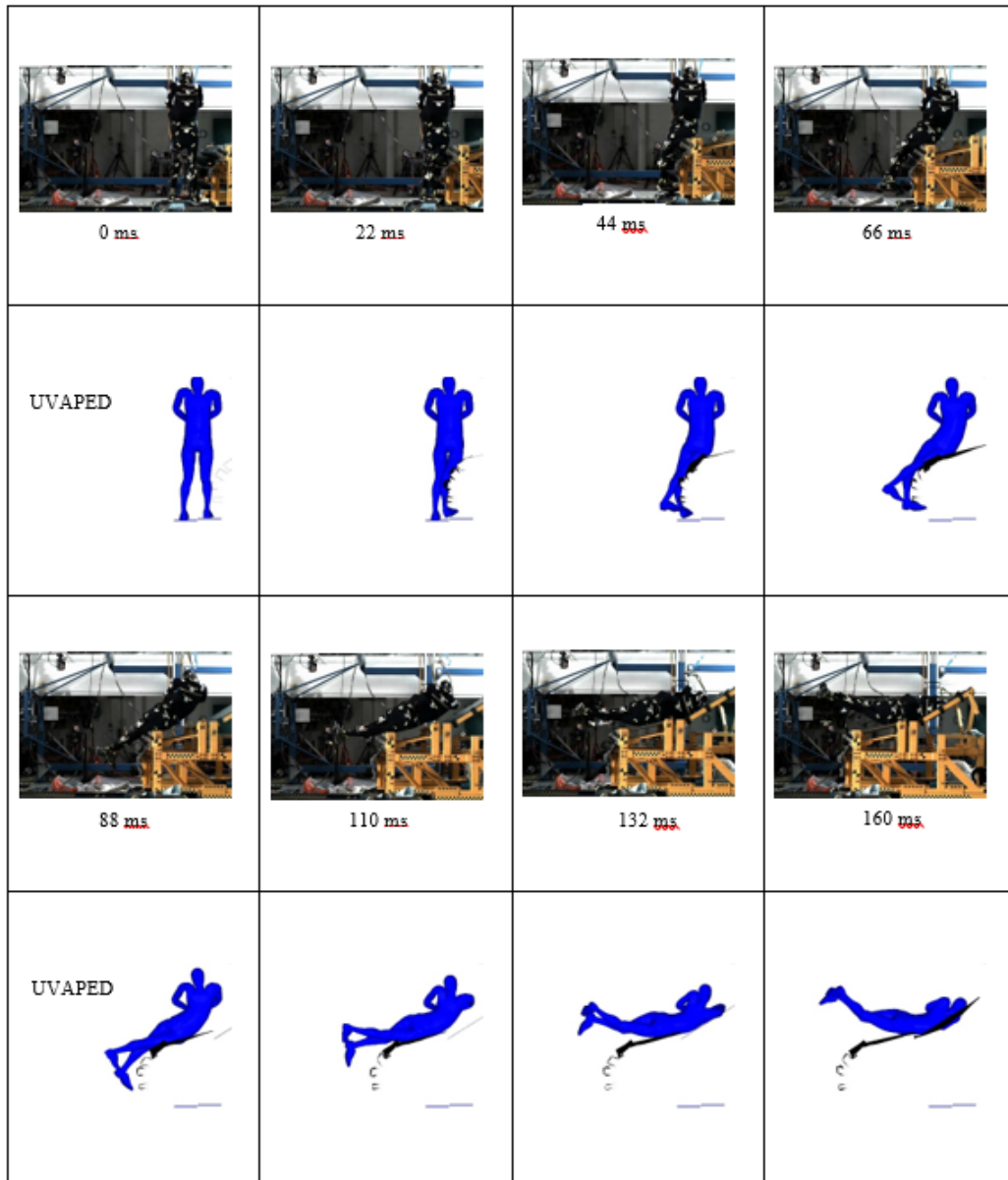


Figure 7.10: Comparison of Pedestrian Impact Sequences for Test V2371 (Posterior View)

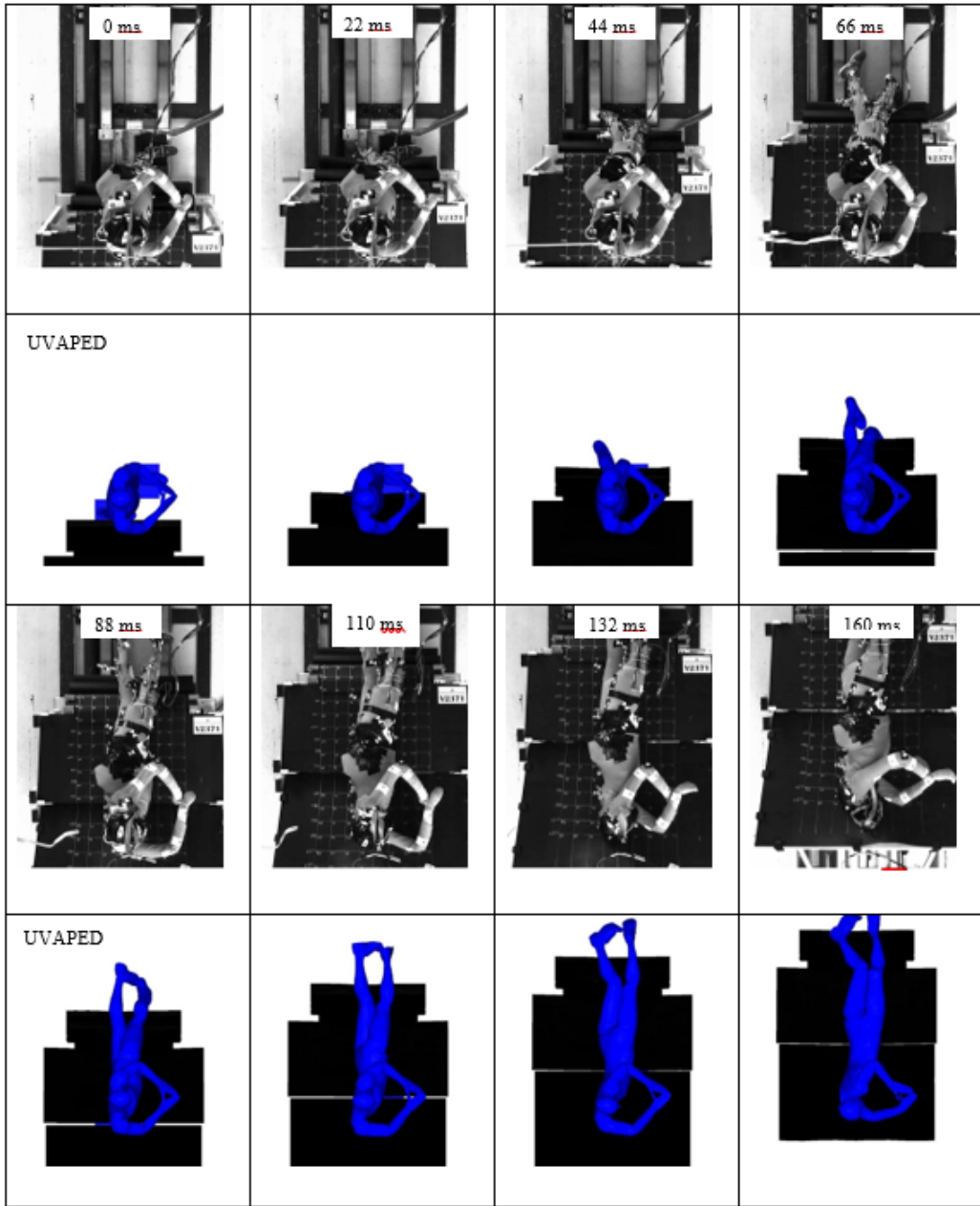


Figure 7.11: Comparison of Pedestrian Impact Sequences for Test V2371 (Superior View)

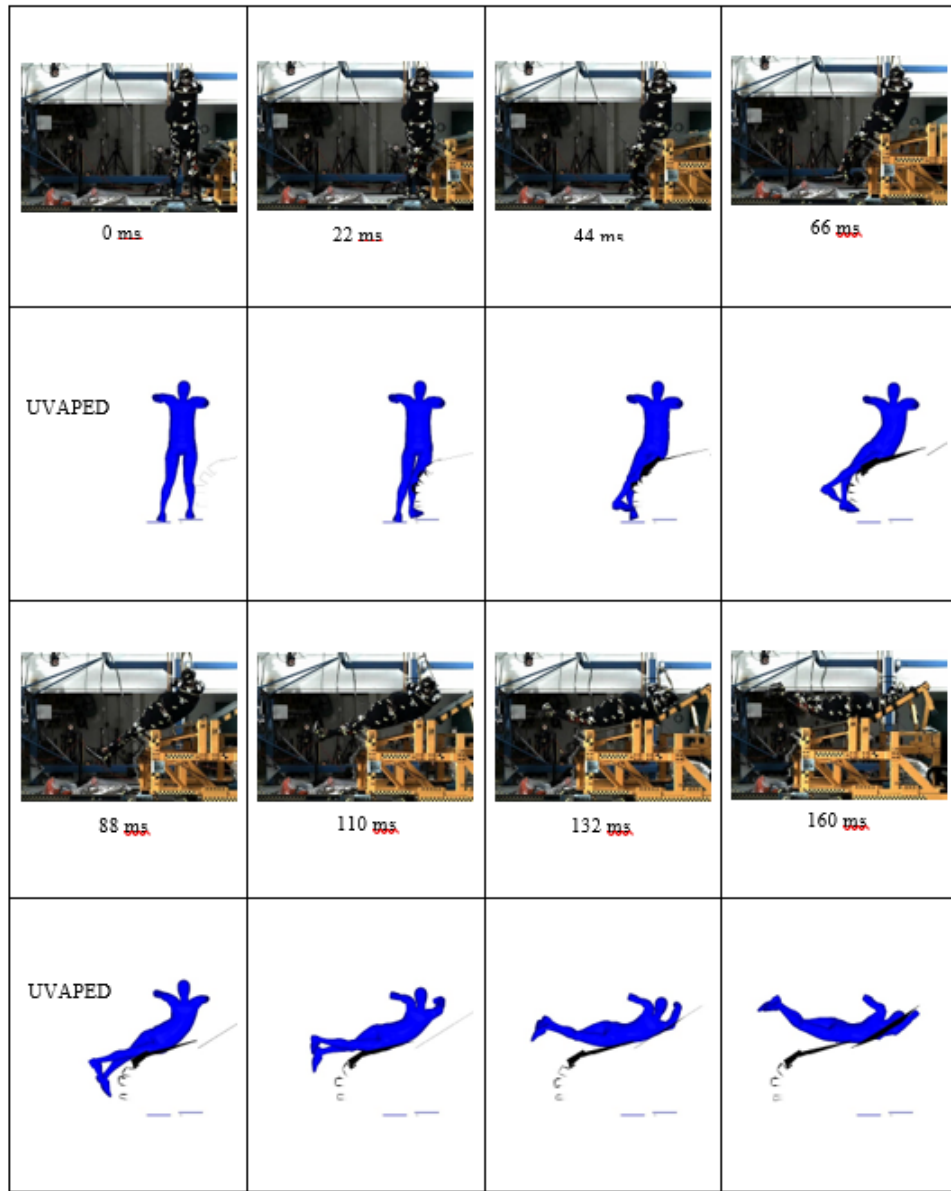


Figure 7.12: Comparison of Pedestrian Impact Sequences for Test V2374 (Posterior View)

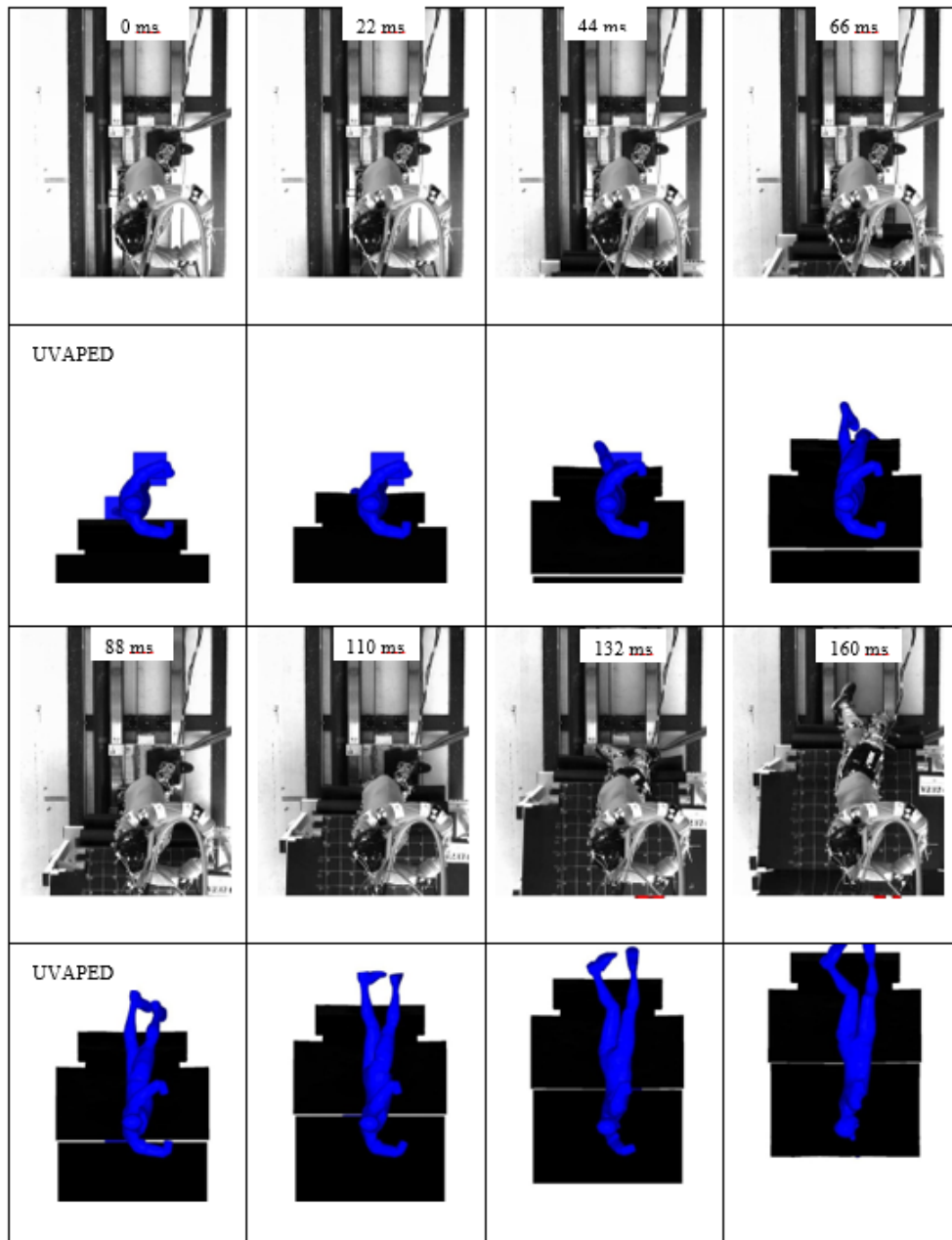


Figure 7.13: Comparison of Pedestrian Impact Sequences for Test V2374 (Superior View)

### 7.3.1 Trajectories

The trajectories of the head, T1, T8, pelvis, right distal femur, right distal tibia, left distal femur and left distal tibia in the YZ plane from the 3 models were compared with the trajectories of the PMHS specimens from the anatomical landmarks captured using Vicon 3D motion capture. Both THUMS PFEM and UVAPED followed the trajectories of the PMHS surrogates from the three test modes in the  $yz$  plane (Figure 7.14-Figure 7.16). The TNOEL model (Figure 7.16) showed a shorter wrap around distance compared to the UVAPED and THUMS PFEM models. This can be attributed to the crude model of spine of the TNOEL model with one joint.

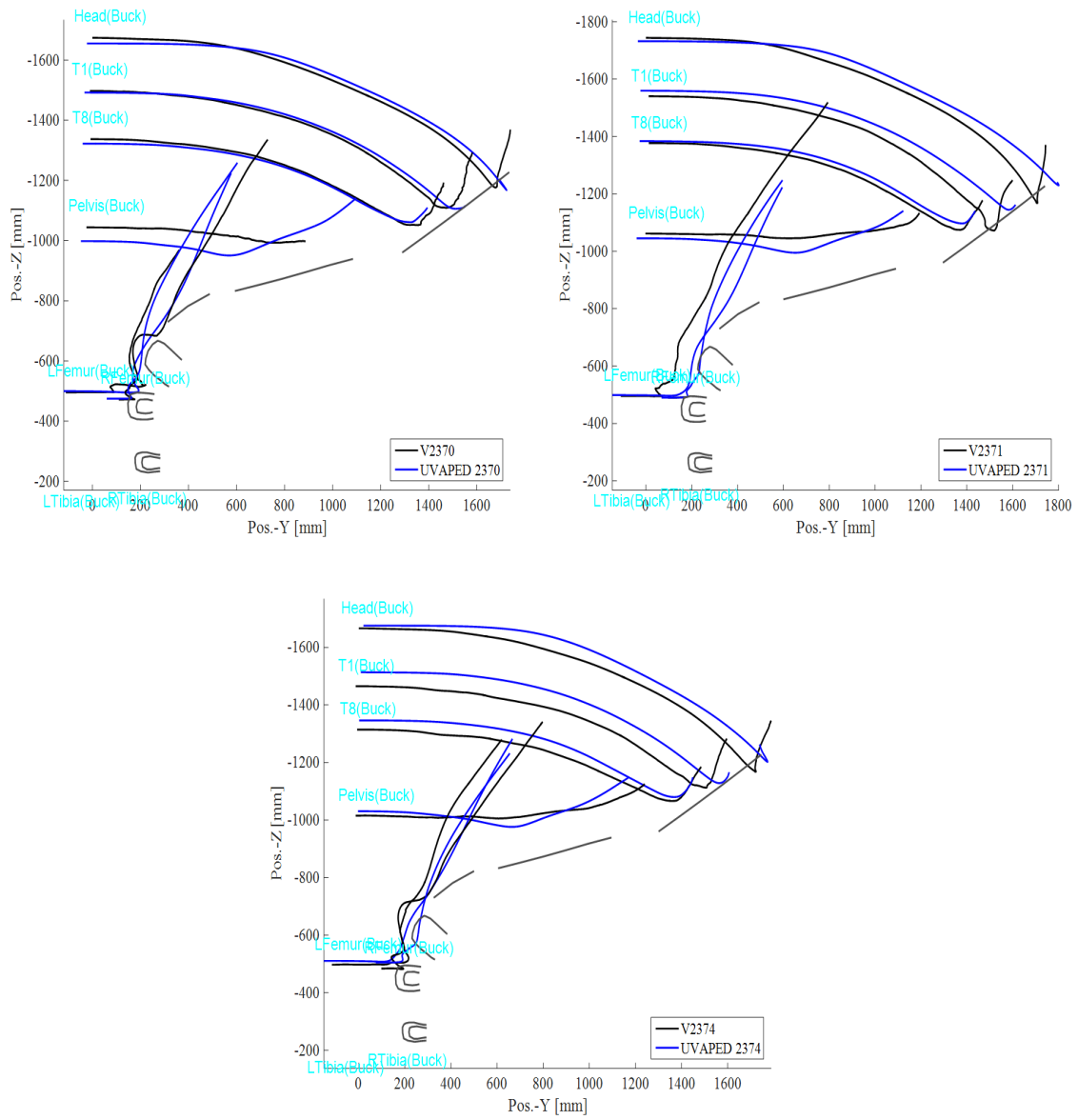


Figure 7.14: Trajectories of the Head, T1, T8 and Pelvis in Buck Ref Frame for the UVAPED model

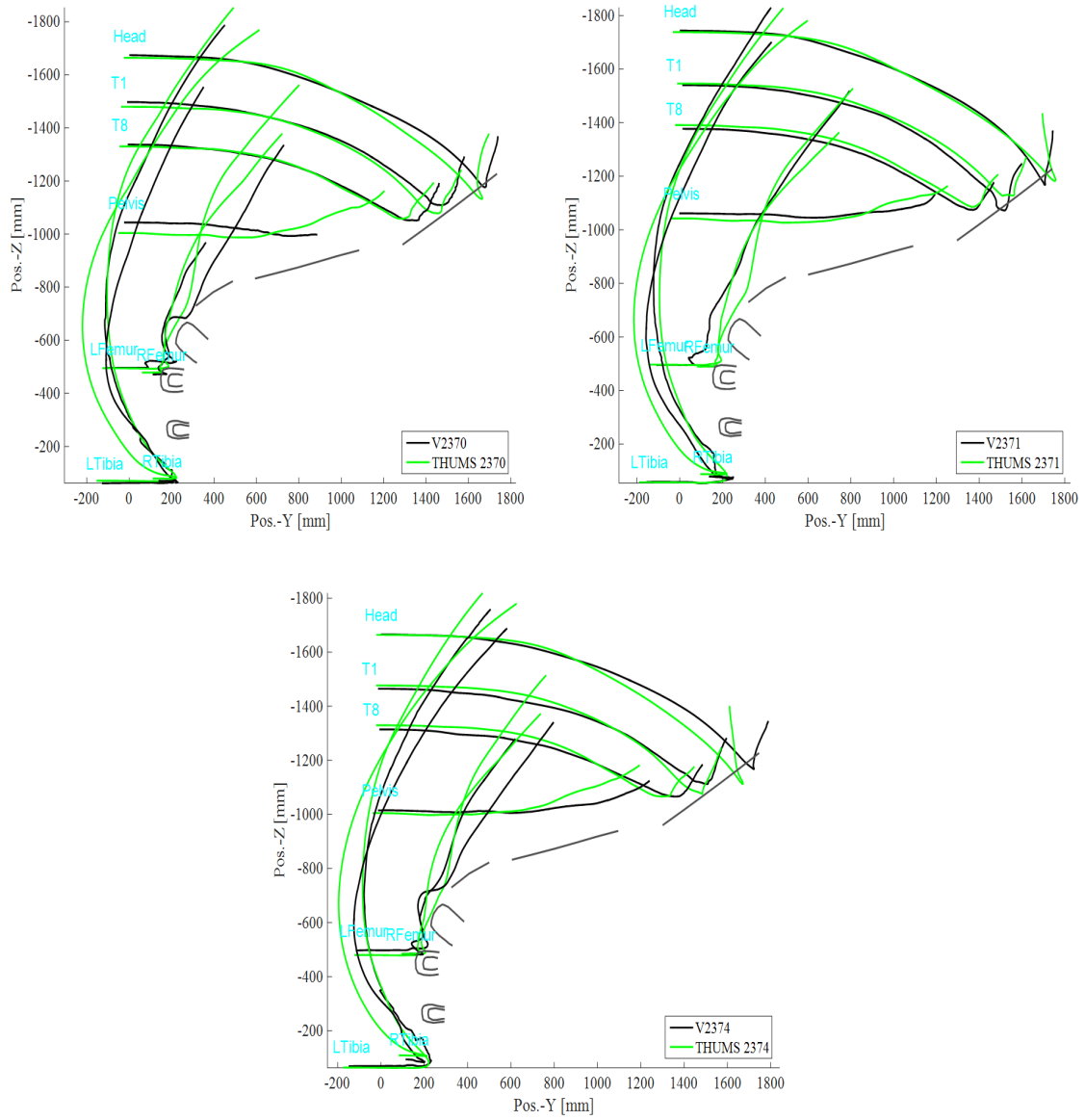


Figure 7.15: Trajectories of the Head, T1, T8 and Pelvis in Buck Ref Frame for THUMS PFEM model

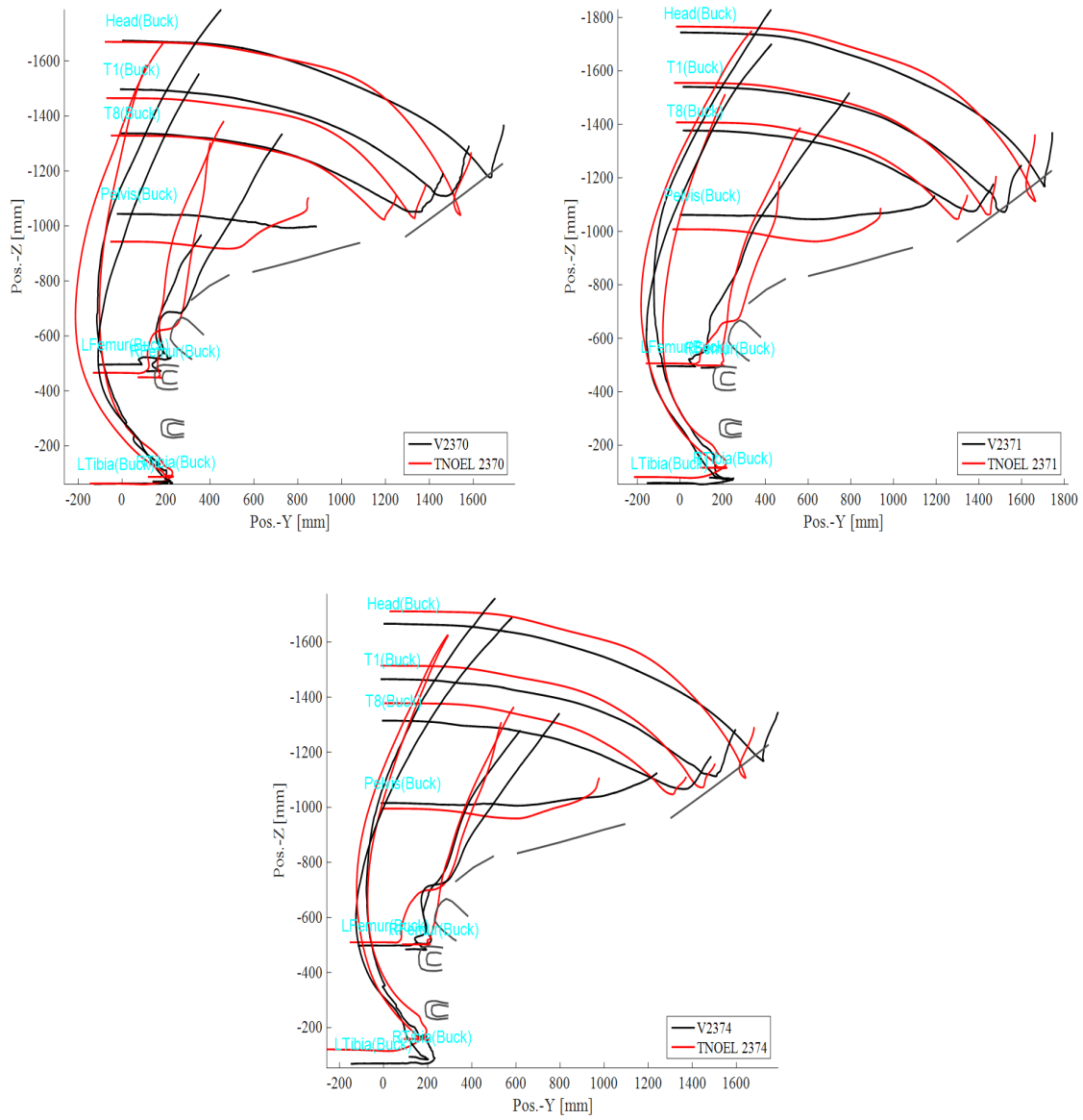


Figure 7.16: Trajectories of the Head, T1, T8 and Pelvis in Buck Ref Frame for TNOEL model

### 7.3.2 ISO Rating

The ISO rating methodology was used to quantitatively evaluate the correlation between the responses from the three models to the PMHS tests during the whole-body impact tests. The ISO rating evaluates the correlation between two signals in terms of corridor, magnitude, phase and shape scores. To calculate model scores the *MATLABISO\_tool-W7\_version.exe* was used. A summary of the resulting average ISO scores for each signal from the kinematics and kinetics comparisons between the three pedestrian models and PHMS response is shown in Table 7.1.

Table 7.1: Comparison of Average ISO Rating Across Three Tests

Acceleration	UVAPED	THUMS	TNOEL	Velocity	UVAPED	THUMS	TNOEL
Head	0.7	0.74	0.77	Head	0.82	0.83	0.82
T1	0.7	0.6	0.71	T1	0.85	0.75	0.89
Pelvis	0.66	0.49	0.69	T8	0.83	0.81	0.86
RFemur	0.74	0.71	0.64	Pelvis	0.92	0.91	0.82
RTibia	0.63	0.51	0.65	Average	0.85	0.83	0.85
LFemur	0.76	0.61	0.51	Omega x	UVAPED	THUMS	TNOEL
LTibia	0.76	0.53	0.66	Head	0.65	0.59	0.72
T8	0.65	0.63	0.65	T1	0.67	0.6	0.53
Average	0.7	0.6	0.66	Pelvis	0.53	0.52	0.7
FZ	UVAPED	THUMS	TNOEL	RFemur	0.66	0.32	0.64
FZ Hood PS	0.39	0.38	0.34	RTibia	0.24	0.16	0.52
FZ Hood DS	0.4	0.4	0.35	LTibia	0.56	0.25	0.19
FZ Grill PS	0.72	0.62	0.64	Average	0.55	0.41	0.55
FZ Grill DS	0.6	0.53	0.53	Omega y	UVAPED	THUMS	TNOEL
Fz UB PS	0.74	0.83	0.77	Head	0.38	0.46	0.58
FZ UB DS	0.8	0.79	0.79	T1	0.45	0.44	0.43
FZ LB PS	0.47	0.53	0.38	Pelvis	0.25	0.35	0.24
FZ LB DS	0.57	0.6	0.61	RFemur	0.25	0.24	0.46
Average	0.59	0.58	0.55	RTibia	0.23	0.22	0.19
FY	UVAPED	THUMS	TNOEL	LTibia	0.27	0.22	0.24
FY Hood PS	0.29	0.23	0.3	Average	0.31	0.32	0.36
FY Hood DS	0.31	0.3	0.34	Omega z	UVAPED	THUMS	TNOEL
FY Grill PS	0.35	0.33	0.29	Head	0.42	0.33	0.29
FY Grill DS	0.2	0.32	0.19	T1	0.24	0.35	0.2
Average	0.29	0.3	0.28	Pelvis	0.33	0.24	0.51
				RFemur	0.21	0.4	0.22
				RTibia	0.34	0.33	0.41
				LTibia	0.34	0.35	0.34
				Average	0.31	0.33	0.33

The three models showed a good match in terms of the ISO scores for the resultant velocity measured at the head, T1, T8 and pelvis (average ISO rating scores  $> 0.8$ ). All the three models showed a similar response in terms of T1, T8 and pelvis accelerations. THE UVAPED model with deformable lower extremities showed a good match for the acceleration histories from the lower extremities. The TNOEL model showed a large spike in the accelerations measured at the lower extremities (Figure C.2 - Figure C.9). Even though the spike did not reduce the ISO score substantially, it could lead to abnormal prediction of injury risks for the TNOEL models. All three models showed a good match in the angular rates measured at the anatomical locations along their local x axis which is the major rotational axis during the impact (Figure C.10 - Figure C.15). The three models did not show a good match in case of the angular velocities measured along the local y and z axes (Figure C.16- Figure C.28) which can be seen from their ISO scores (Figure 7.17). The three models showed a good match in the forces measured along the impact direction at the upper bumper and grill on both driver and passenger sides (Figure C.31 - Figure C.36). All three models showed lower forces on hood leading edge and this underestimation of forces was reflected in the poor rating form the hood forces measured at both driver and passenger sides (Table 7.1). All the models showed a poor match in terms of the shear force measured along the local y direction of the load cells at the hood and grille (Figure 7.17, Figure C.37 - Figure C.40).

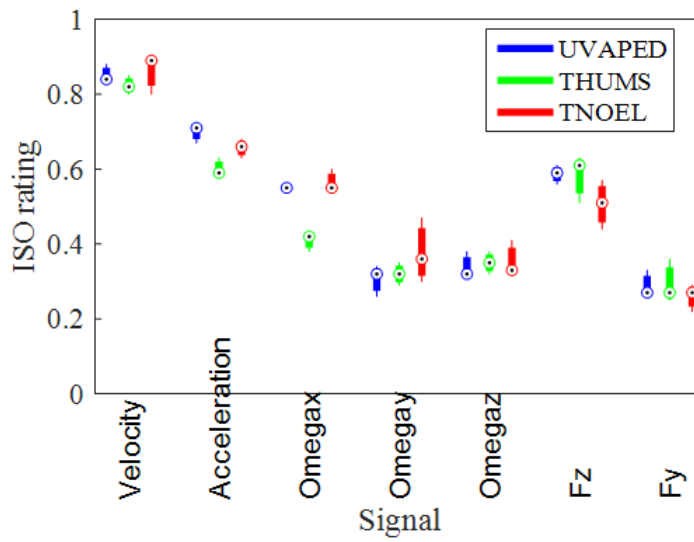


Figure 7.17: Summary of Average ISO Scores for Different Signals

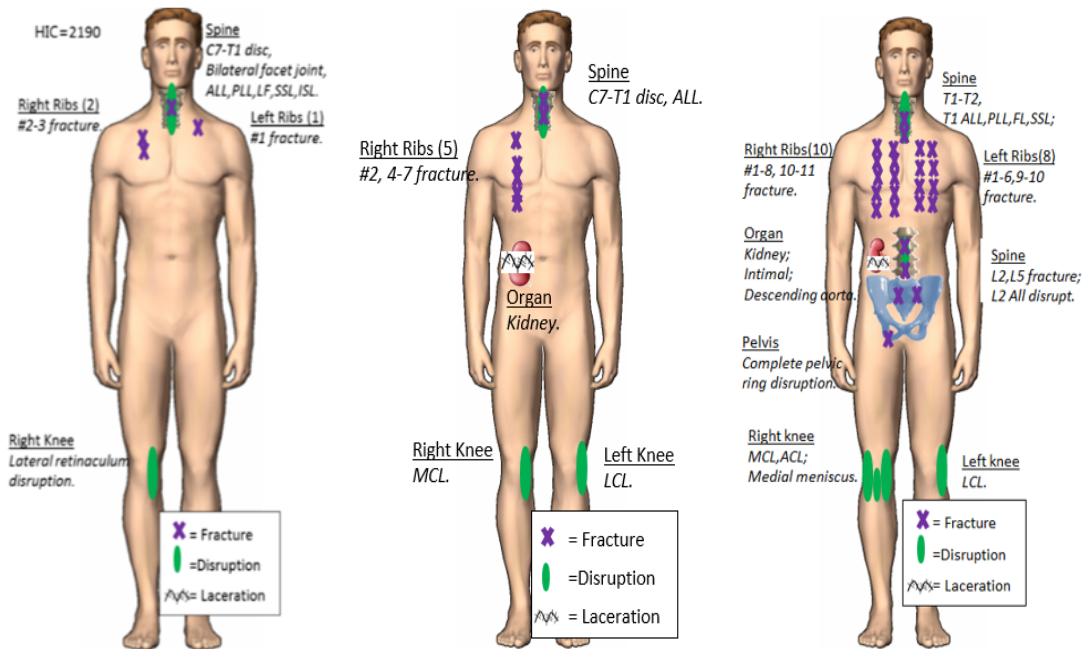


Figure 7.18: Pictorial Representation of Injuries (Forman et al. (2015))

### 7.3.3 Injuries

The injury predictions of the three models are summarized in Table 7.2 and were compared with the injuries sustained in the PMHS tests.

Table 7.2: Comparison of Injury Reported in Experiments and Model Predictions for PMHS 2370

PMHS Injury				Injury risk(%)		
Region	Injury	Measurement	Severity	THUMS	TNOEL	UVAPED
Head (AIS 2+)	No injury (HIC=2190)	HIC	AIS 2+	92% (2859)	90% (3143)	93% (3679)
Neck (soft)	C7-T1 spinous ligament injury (AIS 1), ALL PLL ISL SSL LF	Shear Force	AIS 2+	NE	NE	NE
Neck (bone)	C7-T1 disk injury (AIS 2); C7-T1 joint dislocation (AIS 3)	Nij	AIS 2+	NE	19%	21%
Thorax* R	2 rib (R2, R3) fractures (AIS 3)	Normalized deflection/TTI	AIS 2+	45% (3+)	NE	90%
Thorax* L	Rib dislocation at costovertebral joint (R1)		AIS 2+	3% (3+)	NE	14%
Thorax M	No Injury		AIS 2+	NE	NE	72%
Shoulder R		Clavicle axial force (N)	AIS 2+	NE	NE	42%
Shoulder L			AIS 2+	NE	NE	0
Pelvis		Lateral force (N)	AIS 2+	0	27%	0
R Thigh		Moment (Nm)	AIS 3+	0	18%	15%
L Thigh			AIS 3+	0	1	6
R Leg			AIS 3+	15%	84%	16%
L Leg			AIS 3+	0	78%	20%
R Knee (soft)		Lateral retinaculum disruption	Bending angle	AIS 2+	100%	30%
L Knee (soft)	No injury	Bending angle	AIS 2+	100%	24%	100%
R Ankle		Bending angle	AIS 2+	0	19%	0
L Ankle		Bending angle	AIS 2+	56%	30%	1%

Table 7.3: Comparison of Injury Reported in Experiments and Model Predictions for PMHS 2371

PMHS Injury				Injury risk		
Region	Injury	Measurement	Severity	THUMS	TNOEL	UVAPED
Head (AIS 2+)	No injury (HIC=3758)	HIC	AIS 2+	92% (3566)	94% (4023)	85% (2524)
Neck (soft)	C7-T1 spinous ligament injury (AIS 1), ALL LF (partial disruption)	Shear Force	AIS 2+	NE	NE	NE
Neck (bone)	C7-T1 disk injury (AIS 2); C7-T1 joint dislocation (AIS 3)	Nij	AIS 2+	NE	19%	21%
Thorax* R	5 rib (R2, R4-7) fractures (AIS 3)	Normalized deflection/TTL	AIS 2+	47%(3+)	NE	55%
Thorax* L	Strain at costovertebral joint (R1-3)		AIS 2+	35%(3+)	NE	5%
Thorax M	No injury (right kidney posterior transverse laceration was found in the experiment but the injury risk of internal organ was not assessed in this study)		AIS 2+	NE	NE	18%
Shoulder R		Clavicle axial force (N)	AIS 2+	NE	NE	46%
Shoulder L			AIS 2+	NE	NE	0
Pelvis		Lateral force (N)	AIS 2+	0	0.22	0
R Thigh		Moment (Nm)	AIS 3+	0	12%	44%
L Thigh			AIS 3+	1%	1%	10%
R Leg			AIS 3+	25%	93%	27%
L Leg			AIS 3+	3%	88%	64%
R Knee (soft)	Right knee MCL disruption	Bending angle (deg)	AIS 2+	100	39	97
L Knee (soft)	Left knee LCL disruption	Bending angle (deg)	AIS 2+	100	68	100
R Ankle	No injury	Bending angle (deg)	AIS 2+	0	20	0
L Ankle		Bending angle (deg)	AIS 2+	56	38	1

Table 7.4: Comparison of Injury Reported in Experiments and Model Predictions for PMHS 2374

PMHS Injury				Injury risk		
Region	Injury	Measurement	Severity	THUMS	THOEL	UVAPED
Head (AIS2+)	No injury (HIC=889)	HIC	AIS 2+	98% (6423)	81% (2253)	92% (3542)
Neck (soft)	C7-T1 spinous ligament injury (AIS 1), ALL SSL LF PLL	Shear force	AIS 2+	NE	NE	NE
Neck (bone)	T1 fracture (AIS 2); C7-T1 joint dislocation (AIS 3)	Nij	AIS 2+	NE	18%	22%
Thorax* R	11 rib (R1-8, R10-11, multiple fractures on R2) fractures (AIS 4); Strain at costovertebral joint (R9); T2 Process Fracture	Normalized deflection/TTL	AIS 2+	95%(3+)	NE	78%
Thorax* L	12 rib (L1-6, L9-10, multiple fractures on L4 and L5) fractures (AIS 4); Strain of costovertebral joints x2 (L1, L2)		AIS 2+	35% (3+)	NE	11%
Thorax M	No injury		AIS 2+	NE	NE	33%
Shoulder R		Clavicle axial force (N)	AIS 2+	NE	NE	19%
Shoulder L			AIS 2+	NE	NE	12%
Lumbar	ALL (AIS 1); L5 (AIS2); right kidney posterior transverse laceration and abdominal aorta disruption were found in the experiment but the injury risk of internal organ was not assessed in this study	-	-	NE	NE	NE
Pelvis	Pelvic ring fracture (AIS 3)	Lateral force (N)	AIS 2+	1	-	0
R Thigh	No injury	Moment (Nm)	AIS 3+	0	3	45%
L Thigh			AIS 3+	0	1	11%
R Leg			AIS 3+	18%	57%	5%
L Leg			AIS 3+	2%	86%	22%
R Knee (soft)	Right knee MCL disruption	Bending angle	AIS 2+	100%	9%	97%
L Knee (soft)	Left knee LCL disruption	Bending angle	AIS 2+	100%	60%	100%
R Ankle	No injury	Bending angle	AIS 2+	0	19%	0
L Ankle		Bending angle	AIS 2+	46%	34%	1%

## 7.4 Discussion

Due to the availability of limited experimental data using a standardized buck, the UVAPED model has been validated only under a 40 km/hr impact. Different impact speeds and vehicle geometries would generate different kinematics and injuries. The three PMHS tests exhibited consistent responses and were therefore considered in this study. The capability of UVAPED model in reproducing the PMHS responses for kinematics and contact forces has been shown with similar ISO ratings with the most advanced PFEM model. The UVAPED model demonstrated good kinematics in agreement with the experimental data. The major components of the model responses (Y component for translation, X component for rotation and Z component for impact forces) showed the highest rating scores (Figure 7.17).

The UVAPED model showed a delay in head impact (Figure C.2) with an average head impact time of 151.6 ms lagging behind the PMHS subjects by about 13.6 ms. The spine of the UVAPED model has not been validated and a sensitivity analysis of increasing the spine stiffness in bending and torsion improved the head impact timing. Additionally, the neck of the UVAPED model has been validated under the NBDL test conditions (chapter 6) which use the volunteer test data and therefore, there is a discrepancy in behavior of neck of the UVAPED model when compared to PMHS response.

The UVAPED model yawed about its  $z$  axis and this problem is reflected in poor omega  $z$  scores for the pelvis, femur and tibia respectively (Figure C.25, Figure C.26, and Figure C.24). The root cause of the problem was the initial contact of the bumper with the leg.

While the PMHS did not show any skull fractures, all three models predicted a greater than 90% risk of AIS2+ head injury for each PMHS test. Despite the

models showing good correlation for the linear velocity of the head with that of the PMHS data, all the models consistently predicted higher HIC values than the PMHS subjects. The PMHS experienced knee ligament failure without any bony fracture, cervical spinal injuries and ligament tear, and rib fractures without any external injuries to the skull. In the case of the bony fracture of the lower extremities (Femur AIS3+ and tibia AIS2+) the THUMS model showed the lowest risk of fracture. The knee injury risk evaluation based on the bending angle of the knee joint predicted 100% risk of injury (AIS2+) on the struck side of the leg in the cases of THUMS and UVAPED models. The UVAPED model also predicted knee ligament injuries on the left leg which has been documented during the tests. However, it has to be noted that for all the three test conditions the UVAPED model consistently predicted the maximum AIS2+ injury risk of 100% and therefore, raises question on the biofidelity of the knee joint stiffness characteristics under lateral bending. In the case of the thorax, the risk of AIS 2+ thoracic injury predicted by the UVAPED model varied between 40-70%. The UVAPED model underestimated the risk of thoracic injuries compared to the THUMS PFEM model. In case of the V2374 subject, 10+ rib fractures were observed on both sides of thorax. Additionally, the dxa scans of PMHS V2374 showed that the subject had the lowest mineral density among the three specimens and therefore sustained a larger number of rib fractures. Although BMD might be correlated with age it is not one of the predictor variables used to assess the injury risk of the thorax, therefore the UVAPED model was not be able to capture the large number of fractures sustained in the case of the V2374 test.

In conclusion, the biofidelity of UVAPED model was evaluated in the current chapter by reconstructing specific PMHS tests using a well characterized pedestrian buck, and its responses were compared to that of the other commercially available pedestrian models (THUMS PFEM and TNOEL). Though the major components

of the model responses demonstrated good agreement with the experimental data, the biofidelity of certain body regions like the knee is under question. Given the capability of reproducing the pedestrian kinematics and kinetics the UVAPED model and its performance being on similar level with the THUMS PFEM in terms of ISO rating shows that the UVAPED model can be used as a potential tool in designing better cars for pedestrian safety.

## Chapter 8

### Task3: Injury Metric for Cost Estimation in the Optimization Problem

#### 8.1 Introduction

Given that computational pedestrian models are being used to predict injury risk from multiple body regions with the aid of Injury Risk Functions (IRF) developed from PMHS data (Lobo et al. (2015); Wu et al. (2017)), a comprehensive metric that could be used to attribute a ‘cost’ to the outcome of a crash event is necessary to aid in the design of the front end of vehicles through optimization. Poly-trauma metrics such as New Injury Severity Score (NISS) (Osler et al. (2008)) and whole body functional capacity index WBFCI) (McMurry et al. (2015)) exist to estimate the probability of fatality or functional disability after an injurious event. However, the estimation of these metrics require the precise knowledge of injury in other words the specific AIS code used to define a particular injury. The use of injury risk functions can only provide the probability of injury of a particular AIS severity level and we may notice a disconnect when we try to estimate either of the poly-trauma metrics from simulation outcomes assessing injury via risk functions. A framework to estimate multi trauma

loss metrics from simulation results with the aid of frequently occurring real world crash patterns is presented in this chapter.

## 8.2 Methodology

One of the poly-trauma metrics used to estimate the severity of a poly-traumatic event and estimate the risk of fatality is NISS. It is defined as the sum of the squares of the Abbreviated Injury Scale (AIS) scores of each of a patient's three most severe AIS injuries regardless of the body region in which they occur. Therefore, to calculate the NISS value we need the top three maximum AIS scores from a simulation outcome, however, one can only estimate the probability of a given MAIS level injury for different body regions from a simulation outcome using IRF.

For a given crash scenario the UVAPED model is capable of predicting injury risks from 14 body regions which represent the most frequently observed injuries in the field (Figure 8.1). Because of the presence of multiple injury metrics for a same body region like head, the body regions are further divided to account for one injury metric per body region. For example, the head was subdivided into skull, brain and face which resulted in a total of 17 body regions (Table 8.1) .

From the simulation outcomes the top three MAIS injuries are unknown, but the probability of different MAIS+ injuries in each body region following an injury mechanism from the IRF can be calculated. Typically, IRF is available in the literature in the form of MAIS+, which is not suitable to predict a specific AIS level of injury. By assuming mutual exclusivity between different AIS levels, Equation 8.1 can be used to calculate the cumulative distribution function (cdf) of MAIS for each body region (Figure 42).

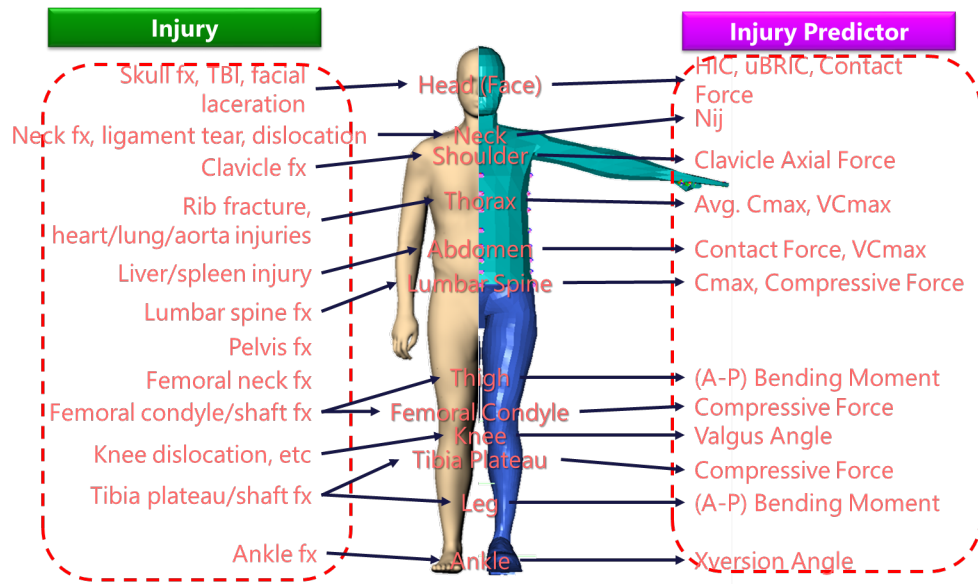


Figure 8.1: Injury Mapping for UVAPED Model From Field Data

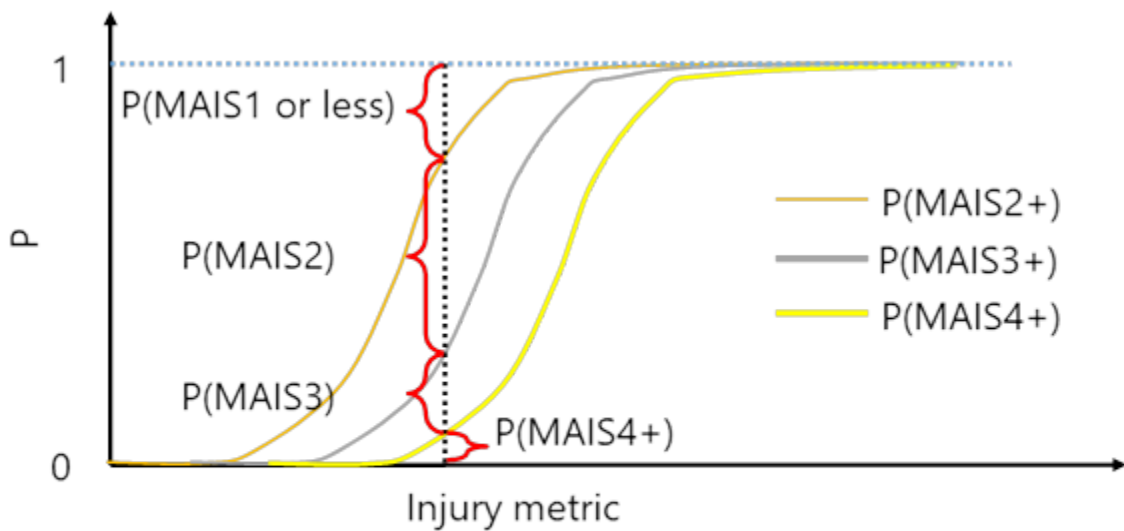


Figure 8.2: Injury Mapping for UVAPED Model From Field Data

Table 8.1: List of Injury Metrics Mapped to Their Associated Body Regions

Body Region (Loss Estimation)	Measuring Location in UVAPED	Metric
Skull	Head	HIC36
	Head	HIC15
	Head	NIJ (Tension only)
Brain	Head	BrIC
Face	Face	Force
Neck	Neck	NIJ
	Neck Lateral	NIJ
	Neck Lateral	Shear Force
Shoulder	Shoulder	Axial Force
Upper arm	Upper Arm	Bending Moment
Lower arm	Lower Arm	Bending Moment
Wrist	Wrist	Axial Force
Thorax	Thorax Lateral	Cmax Normalized
	Thorax Frontal	Cmax Normalized
Abdomen	Thorax Lateral	VCmax
	Abdomen Lateral	VCmax
	Abdomen Lateral (T12 level)	Force
	Abdomen Lateral (L2-L2 level)	Force
	Abdomen Frontal	VCmaxCmax
Lumbar	Lumbar Compression	Axial Force
	Lumbar Lateral	Cmax Normalized
Pelvis	Pelvis Lateral	Force
Femoral neck	Femoral Neck	Axial Force
Femoral shaft	Femur 1/3, mid, 2/3	Bending Moment
Knee	Femoral Condyle	Axial Force (Compression)
	Knee Lateral	Bending Angle
	Tibial Plateau	Axial Force
Tibial shaft	Tibia 1/3, mid, 2/3	Bending Moment
Ankle	Ankle	Bending Angle & Axial Force

### 8.3 Monte Carlo Method of MAIS Estimation

Monte Carlo methods are a class of computational algorithms that rely on repeated random sampling to obtain numerical results. It is a computer simulation that generates a large number of simulated samples of data based on an assumed

Data Generating Process (DGP) that characterizes the population from which the simulated samples are drawn. Patterns in such simulated samples can be studied or evaluated in terms of statistical properties like the estimation of mean.

Now with the aid of cumulative distribution function (cdf) for each body region as the DGP, we sample a random vector with 17 components each varying from 0-1 for each body region (Figure 8.3). For example, if we sample randomly sample a number ranging from 0-1 for the skull body region,  $[0.25, 0.60, \dots, 0.87]$ , then using the cdf we assign the MAIS levels of  $[MAIS1, MAIS2, \dots, MAIS3]$  respectively. This is repeated for each body region and each Monte Carlo sample generates a virtual pedestrian with MAIS levels prescribed to each body region (Figure 8.4). This process is repeated  $M$  times to create  $M$  virtual pedestrians (Figure 8.5).

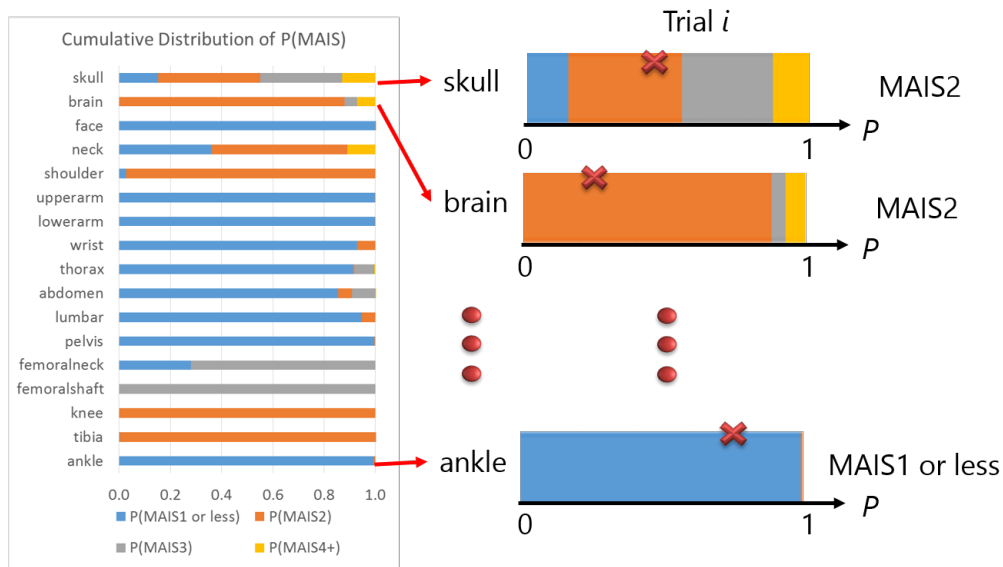


Figure 8.3: Monte Carlo Simulation 1 (MC1)

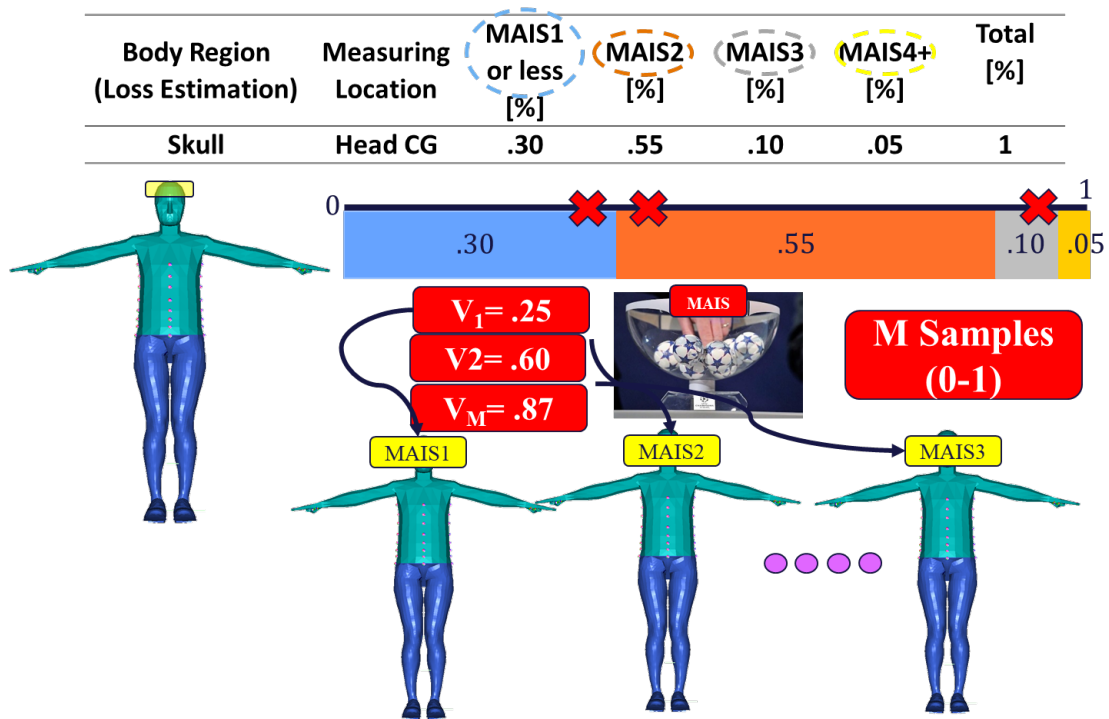


Figure 8.4: Example of Monte Carlo Sampling of MAIS for the Skull Body Region

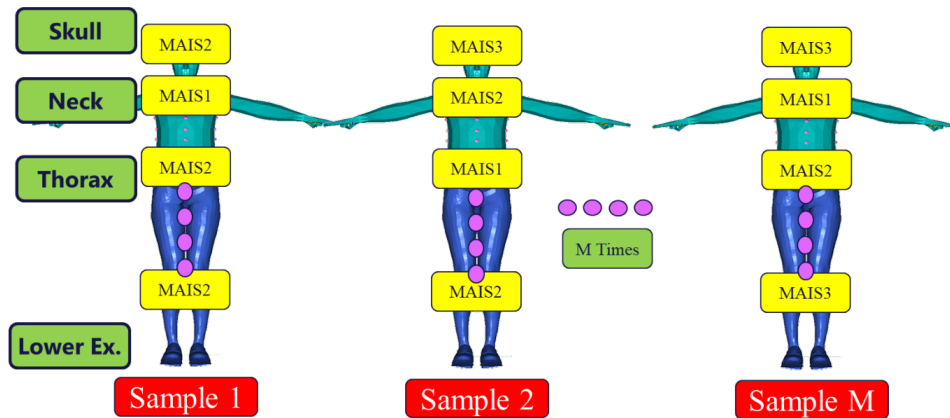


Figure 8.5: Generation of M virtual Pedestrians With Prescribed MAIS Levels for Each Body Region

## 8.4 Assigning Specific AIS Codes (Monte Carlo Simulation II)

To define the second poly-trauma metric, i.e., the functional disability outcome, it is necessary to have the full AIS code of an injury because of the mapping between AIS code and FCI (McMurry et al. (2015)). Injuries from the representative real world pedestrian database were sorted based on body regions that were being represented in the UVAPED model and the specific injury mechanisms in the body region (Figure 8.6). The major underlying assumption was that an injury pattern observed in a body region at a given MAIS level, is insensitive to vehicle designs and impact scenarios such that the distribution of injuries of a given AIS value within a body region would not change with the type of vehicle or impact scenario. After assigning body regions for each representative injury they were categorized based on MAIS level (Table F.1).

For each virtual pedestrian generated through MC1 (MAIS sampling), an injury was assigned from the categorized pedestrian database to each body region based on random sampling from the MAIS bin for the specific body region (Figure 8.7, Figure 8.8). Once AIS codes are assigned WBFCI and NISS can be calculated for each of the  $M$  virtual pedestrians generated through the Monte Carlo sampling process.

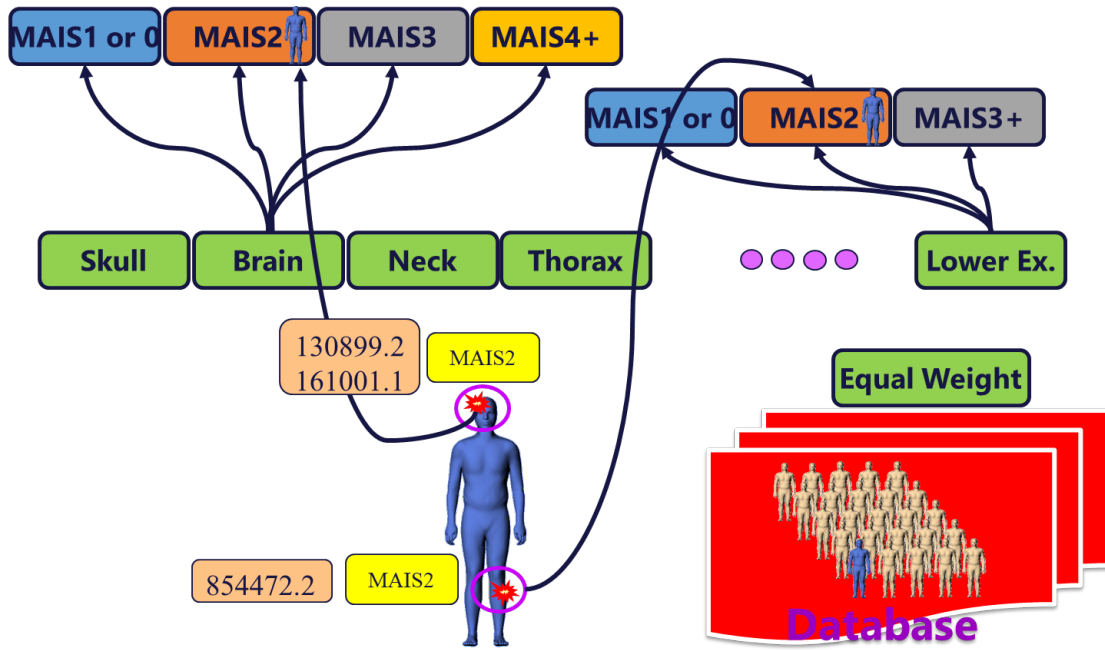


Figure 8.6: Sorting Real World Pedestrian Injury Data Into Body Regions Categorized by MAIS Level

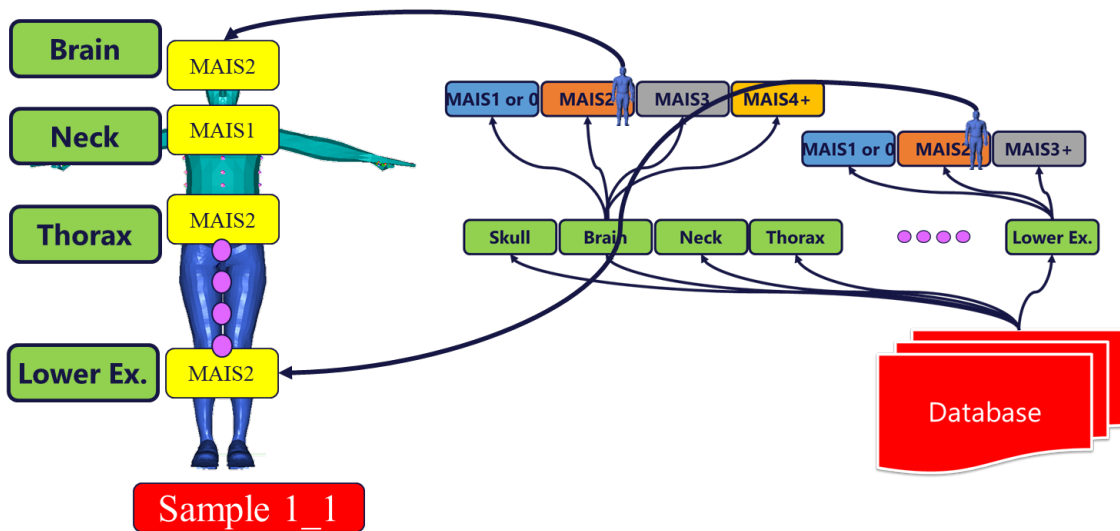


Figure 8.7: Assignment of Injury to Specific Body Regions Through Random Sampling From Categorized MAIS Bins From the Pedestrian Database

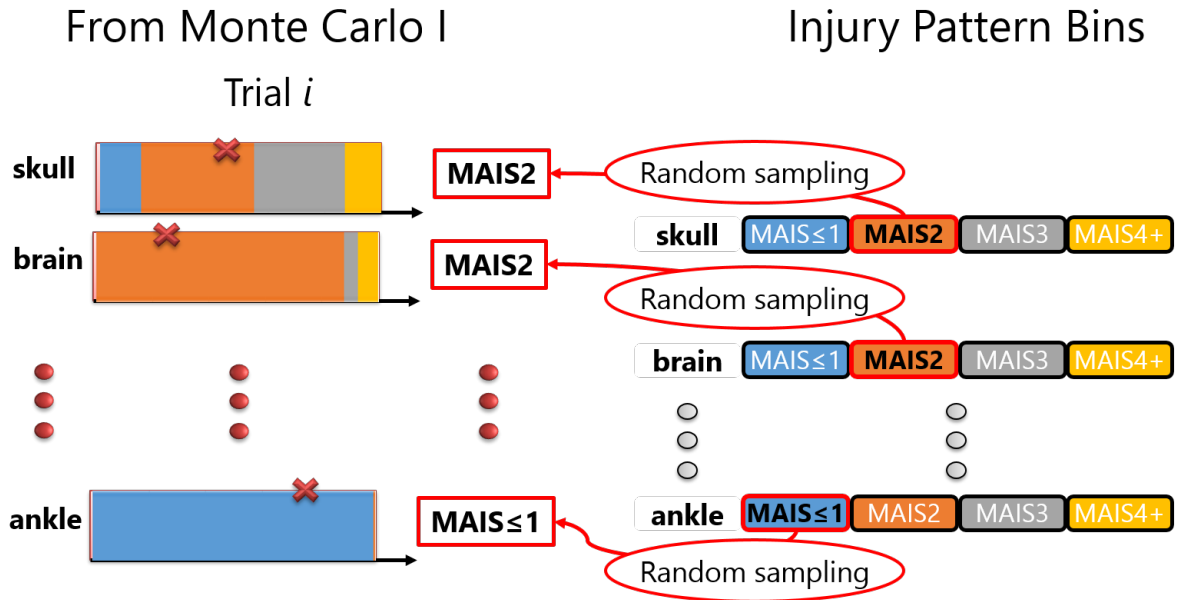


Figure 8.8: Mapping Injury Patterns Based on MAIS Levels in Body Regions

## 8.5 Poly-trauma Injury Loss Metric Values

After AIS code(s) are assigned to the 17 body regions for the  $M$  virtual pedestrians, any poly-trauma injury loss metrics that are functions of AIS codes can be calculated. Then, by taking the average of the  $M$  poly-trauma metric values, expected values of the poly-trauma injury loss metric can be obtained using Equation 8.1.

Equation 8.1: Expected Value of Poly-trauma Metric

$$E(\text{polytrauma metric}) = \frac{1}{M} \left( \sum_{i=1}^M \text{polytraumametric}_i \right) \quad (8.1)$$

There are three poly-trauma metrics that can be estimated using NISS and WBFCI: life years lost due to fatality (LYLF), life years lost due to disability (LYLD)

and cumulative life years lost (LYLC). NISS is a well-known predictor for probability of fatality (Meredith et al. (2002)) and the probability of fatality can be estimated using equations 8.2. LYLF, LYLD and LYLC can be estimated using equation 8.3, 8.4 and 8.5 respectively.

Equation 8.2: Probability of Fatality (Meredith et al. (2002))

$$P(\text{death}) = \frac{1}{\left[1 + e^{(4.746 - 0.934 \times NISS)}\right]} \quad (8.2)$$

Equation 8.3: Life Years Lost Due to Fatality

$$LYLF = (LE - Age) \times P(F) \quad (8.3)$$

where LE is the life expectancy and Age is the current age of an individual suffering from poly-trauma.

Equation 8.4: Life Years Lost Due to Disability

$$LYLD = (LE - Age) * (1 - P(F)) \times \left(1 - \frac{WBFCI}{100}\right) \quad (8.4)$$

Equation 8.5: Life Years Lost Due to Disability

$$LYLC = LYLD + LYLF \quad (8.5)$$

## 8.6 Sanity Check

A sanity check of the injury assignment was performed by utilizing the patient data that were used to build the body region-specific injury patterns. Treating their body region-specific MAIS level as the results of the Monte Carlo sampling I, WBFCI

values were estimated by performing Monte Carlo sampling II. Note that each patient data contained a full list of AIS codes so that poly trauma metrics for each patient are known. The distributions of the WBFCI values from the real-world pedestrian data and Monte Carlo sampling II were compared. For the subsets of the real-world pedestrians that have the same distribution of the body region-specific MAIS levels and consists of more than 30 samples, mean values of the WBFCI were compared with those of from the Monte Carlo sampling II.

## 8.7 Convergence Study

A convergence study using an exemplary vehicle design (design 25, chapter 9) at 40 km/hr impact showed converged values for the expected NISS, WBFCI and LYLC with number of iterations (Table 8.2).

Table 8.2: Convergence Study of the Monte Carlo Simulations for ISS, WBFCI, and LYL

number of MC samples	NISS	WBFCI	LYLC (Years)
500	23.62	73.87	11.08
1000	23.56	73.87	11.09
5000	23.64	73.79	11.14
10000	23.84	73.75	11.19
50000	23.82	73.7	11.2

The WBFCI from the MC2 exhibited that the mid-range values (around 77 to 86) were over-represented compared to the WBFCI from the real-world data, which were calculated excluding injuries that were not considered during the injury mapping process (Figure 8.9 and Table 8.2). Instead, the WBFCI values from the MC2 were under-represented in either of the extreme values, such as around 60 to 70 and around 90 to 100.

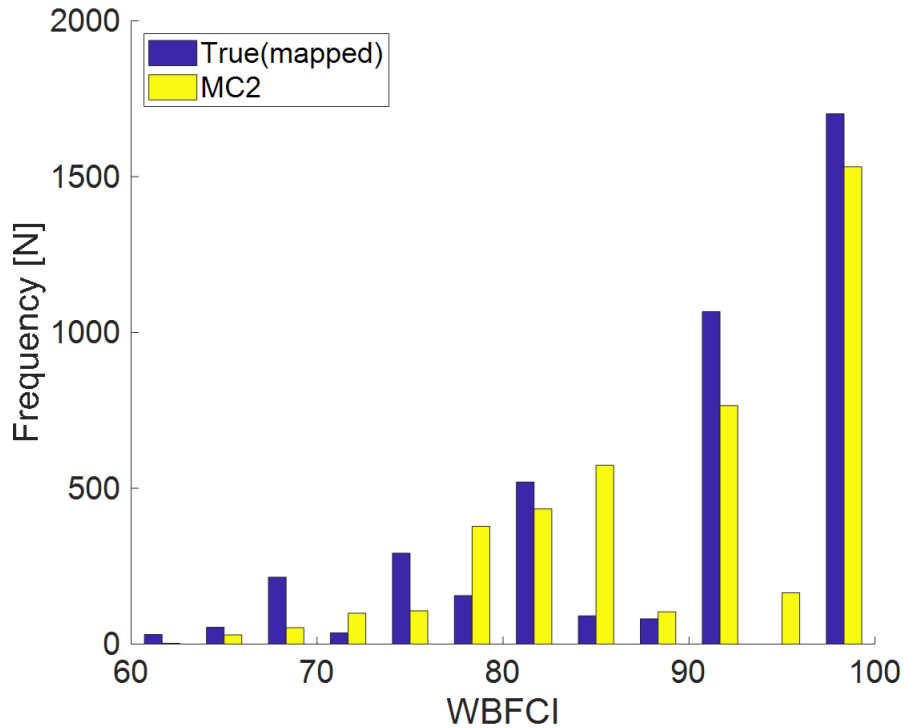


Figure 8.9: Histogram of the WBFCI From the Real-world Database (Mapped Injuries Only) and the Monte Carlo Sampling II

## 8.8 Discussion

The current study proposed a systematic procedure for estimating polytrauma injury loss metrics based on injury risk information from a computational human surrogate and real-world injury outcomes. To infer the AIS level information from the injury risk information, real-world data from the injuries that pedestrians sustained was utilized. The AIS codes were categorized into 17 groups, which is more specific than the nine AIS body regions (Gennarelli and Wodzin, 2008), considering the ability of a multibody pedestrian model to minimize the influence of the injury pattern of the real-world pedestrian data. While constructing bins for the body region-specific injury patterns, minor injuries (AIS1) were ignored because the impact of AIS1 injuries are minor and injury risk functions for MAIS1 is often unavailable from literature.

For a body region whose risk of injury can be predicted by multiple injury risk functions, the highest risk value was chosen for the MAIS level assuming all the injury risk functions are valid and trying to be conservative. When injury risk of the higher MAIS level was higher than the one of the lower MAIS level due to intersecting injury risk functions for a body region, the risk for the higher level injury was assigned as the risk for the lower severity injury as a conservative decision as well.

Monte Carlo samplings were performed based on injury risk across the body regions from a pedestrian impact simulation and resulted in expected values of poly-trauma metrics such as NISS and WBFCI. The results of the Monte Carlo samplings converged when the size of the sample was 50,000. The proposed method required one set of injury risk information across the body region, which can be obtained from a single pedestrian impact simulation. The Monte Carlo sampling is computationally cheap so that it can be done in a few minutes using a personal computer.

The MC II showed an averaging effect in estimating WBFCI because of the prediction of the WBFCI based on body region-specific MAIS levels. For the same level of MAIS, certain injuries can cause greater functional loss (or lower FCI values) than other injuries. For example, the FCI values for cerebrum subarachnoid hemorrhage associated with coma less than six hours (140695.3, 193 observations) is 68.2. In contrast, FCI values for other MAIS3 brain injuries such as cerebrum hematoma NFS (140629.3, 82 observations), cerebrum hematoma epidural or extradural NFS (140630.3, 12 observations), and cerebral concussion LOC one to six hours (161006.3, 8 observations) are 100. One of these injuries will be sampled for MAIS3 brain injuries during the MC2 step. The MC2 will estimate 79.2, which is weighted averages of the FCI values for the brain MAIS3 injury pattern. This estimate (79.2) is either an over-prediction for the pedestrian who sustained 140629.3 or an under-prediction for the one who sustained 140629.3, 140630.3, or 161006.3. This is the reason why the

cumulative distribution of the WBFCI from the MC II resulted in the greater proportions for the mid-range WBFCI values than those of the real-world pedestrians (Figure 8.9).

This limitation of the proposed method stems from its dependence on the body region specific MAIS levels for predicting AIS level injuries. This limitation will gradually be overcome as the injury prediction capability of computational human surrogate progress due to the advance in the injury prediction metrics or strain-based injury prediction capability. In addition, the current method assumes that each body region-specific injury patterns happens independently of the injury pattern of other body regions. It is possible that a certain skull fracture might be correlated to a certain brain injury. If a correlation is understood between different injuries, this correlation could be considered during the Monte Carlo sampling.

This method can simplify a vehicle design optimization process by estimating a loss due to injuries as a scalar value instead of a matrix quantity consisting of probabilities with respect to each MAIS level. Lastly, the proposed method can be applied to other human surrogates such as occupant models.

## 8.9 Conclusion

The current study proposed a method for estimating poly-trauma injury loss metrics using a computational human surrogate and real-world AIS-level injury data. While the proposed method exhibited an averaging effect in estimating WBFCI due to its reliance on MAIS levels information, the proposed method accurately predicted average WBFCI values of the real-world pedestrians with the same body region-specific MAIS distributions. This method can simplify a vehicle design optimization process by transforming multi-output optimization problem into a single output one.

## 8.10 Limitations

1. Multiple injury metrics for a single body region. As a conservative approach injury metric predicting the highest risk is chosen.
2. Limitation of injury metric. Not every possible field injury can be attributed to a single mechanism and we might be missing injuries with coupled mechanisms.
3. Crossing injury risk functions. As different authors publish AIS risk functions for a specific body region, there are potential cases where two injury risk functions can cross each other in a nonphysical way. Such cases have been identified and rectified.
4. Missing injury risk prediction. Some of the more severe risks, like AIS4+ for certain body regions like the pelvis, are missing from the literature. In such cases the probability of MAIS levels was calculated for MAIS2, and MAIS3+.
5. Insufficient description to assign a body region from AIS code. When assigning a body region was ambiguous such cases were omitted.

## Chapter 9

# Task4: DOE Exploration for The Design of Front End of a Vehicle for Pedestrian Impact Using Multiple Objective Functions

### 9.1 Introduction

The design of the front end of a vehicle is a challenging task owing to the complex nature of the design space. The risk of injury depends on the speed of the impact, anthropometry of the pedestrian, stance and orientation of the pedestrian, impact location on the vehicle, and the geometric and stiffness parameters of the front end which lead to many possible combinations of potential designs over the given design space. Vehicle designers have used computational models as an inexpensive and effective way of evaluating vehicle front end designs. For the purpose of illustration of influence of disabling injuries on vehicle design, a simplified design space is considered by limiting the anthropometry of struck pedestrians to the 50<sup>th</sup> percentile male struck laterally at the center of the vehicle.

A parametric vehicle model was developed in MADYMO to conduct a design of experiment (DOE) study to explore the given design space. 250 potential vehicle

designs were randomly generated using Latin hypercube sampling methodology (Stein (1987)) spanning across the entire design space. A pedestrian to vehicle crash was simulated in MADYMO using a 50<sup>th</sup> percentile male human model developed in task 2 with each of the generated vehicle designs under two speeds, 25 and 40 km/h. Each vehicle design was ranked using three different objective functions: life years lost due to fatality (LYLF), life years lost due to disability (LYLD), and cumulative life years lost (LYLC) and the relationship between the objective function and design factors were explored in this chapter.

## 9.2 Methodology

A parametric vehicle model was developed using 21 variables to characterize the geometry and structural stiffness of the front end of a sedan. The geometry of the vehicle was described by four regions (bumper, grill, hood, and windshield, Figure 9.1) using five landmarks. The geometric landmarks were defined using the parameters described by Mizuno (2005). The range of the geometric variables was selected (Table 9.1) to represent sedans based on the vehicle profile corridors of a fleet of vehicles (Nie and Zhou (2016)). The contact stiffness for the bumper, grill, and hood were characterized using four parameters F1, p1, F2 and p2 for a total of 12 variables (Table 9.1) and the bounds were selected based on the stiffness corridors for the European fleet (Martinez et al. (2007)). Zone I was modeled to represent the elastic deformation of the structure with stiffness F1/p1, zone II was modeled to represent the plastic deformation of the structure with stiffness F2/p2 and Zone III was modeled to represent the bottoming out of structure following plastic deformation due to contact with stiffer parts in the vehicle like engine block etc. (Figure 9.2). The peak force generated during the windshield deformation was determined to range between

6-10 kN (Martinez et al. (2007); Li et al. (2017)). A series of impactor simulations mimicking the test setup used by Martinez et al. (2007) was used to determine the contact area under the impactor tests to match the average force deflection corridors (Table 9.2) and the force for contact was scaled using the contact area to make the contact stiffness characteristic independent of contact object. In total this resulted in 21 design variables (Table 9.1) that parametrized both the geometry and the stiffness characteristic of the vehicle front end. To perform the Design of Experiment study, owing to the large number of design variables, a Latin Hypercube sampling methodology was used to sample 250 independent vehicle designs using the lhsdesign() function in MATLAB. The range of the variables was normalized (0-1) prior to the sampling and a set of 250 independent vectors each representing a unique vehicle design spanned across the design space were generated. Each of the vehicle designs was used to run a pedestrian impact simulation impacting the vehicle at the center in a stance following the experiments conducted at UVA (Forman et al. (2015)).

Accident studies indicate that the majority of pedestrians are struck by vehicles in urban and residential areas at crash speeds up to 40 km/hr (Ashton (1982); ETSC (1999); Mizuno and Ishikawa (2001)). Hence, the simulations were run at two impact speeds of 40 km/hr and 25 km/hr respectively to cover this range of impact speeds observed in the field. Only the vehicle to pedestrian contact was used to analyze the injuries. An end time-step of 200 ms and 250 ms was used for the high and low speed test cases respectively, to ensure head contact with the hood/windshield. The simulations produced the peak values and time histories of raw physical quantities that were used to process the injury metrics (Table 8.1). The Monte Carlo method of MAIS estimation and AIS code specification described in chapter 7 was used to determine the ‘cost’ related to each vehicle design based on LYLF, LYLD and LYLC.

Table 9.1: Description and Bounds of Design Variables

Variable	Design Variable	Parameter	Units	Lower Bound	Upper Bound
$v1$	P1(x)	Bottom depth	mm	0	51.9
$v2$	P1(z)	Bottom height	mm	197.6	301.4
$v3$	P2(z)	UBRL height	mm	521.2	667.6
$v4$	P3(x)	Bumper lead	mm	20.5	192.7
$v5$	P3(z)	BLERL height	mm	703.9	795.8
$v6$	P34L	Bonnet length	mm	814.6	1474.1
$v7$	P34 angle	Bonnet angle	deg	9	19
$v8$	P45 angle	Windshield angle	deg	21	31
$v9$	S1	Bumper force1	kN	1	9.5
$v10$	e1	Bumper def1	mm	10	20
$v11$	S2	Bumper force2	kN	0	30.5
$v12$	e2	Bumper def2	mm	40	130
$v13$	S1	Grill force1	kN	1.5	5
$v14$	e1	Grill def1	mm	20	40
$v15$	S2	Grill force2	kN	2	6.5
$v16$	e2	Grill def2	mm	110	130
$v17$	S1	Hood force1	kN	1.5	5
$v18$	e1	Hood def1	mm	10	20
$v19$	S2	Hood force2	kN	0	1
$v20$	e2	Hood def2	mm	15	80
$v21$	F	Windshield peak force	kN	6	10

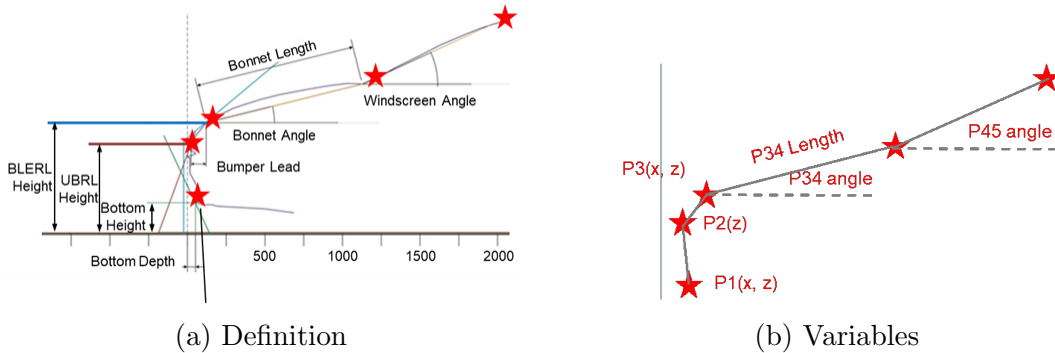


Figure 9.1: Parametrization of Vehicle Front Shape

Table 9.2: Contact Area to Scale the Force

Region	Contact area
Bumper	$0.098 \text{ m}^2$
Grill	$0.067 \text{ m}^2$
Hood	$0.04 \text{ m}^2$

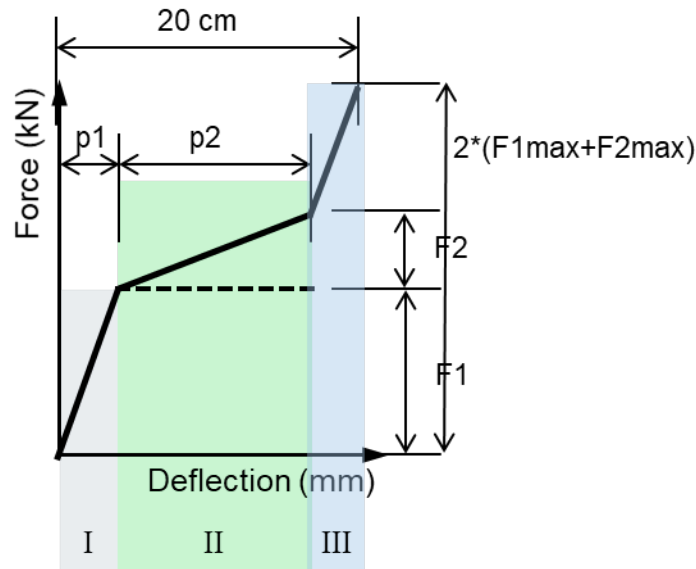


Figure 9.2: Contact Stiffness Characteristics of Bumper, Grill, and Hood

### 9.3 Results

Out of the 250 simulations at the high speed condition of 40 km/hr, 4 simulations terminated in an unexpected manner owing to numerical instabilities generated due to excessive contact forces from shoulder and head contact with the vehicle. These 4 vehicle designs have been omitted from the injury analysis under both impact speeds. LYL<sub>F</sub>, LYL<sub>D</sub> and LYL<sub>C</sub> were calculated for each vehicle design at the two impact speeds (Figure 9.3, Figure 9.4). Use of LYL<sub>F</sub> and LYL<sub>C</sub> as a ‘cost’ functions

led to the same optimal design at 40 km/hr. This vehicle design was also optimum at 25 km/hr (Table 9.6).

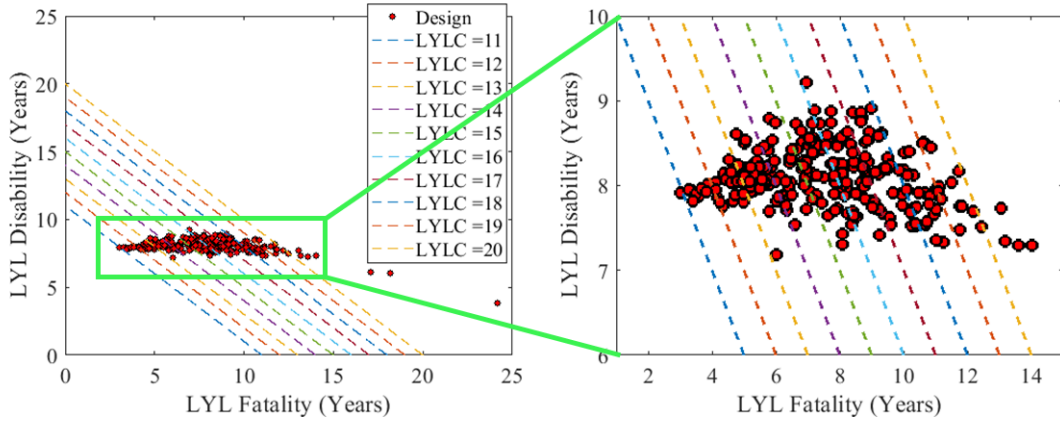


Figure 9.3: DOE Exploration of Life Years Lost at 40 km/hr

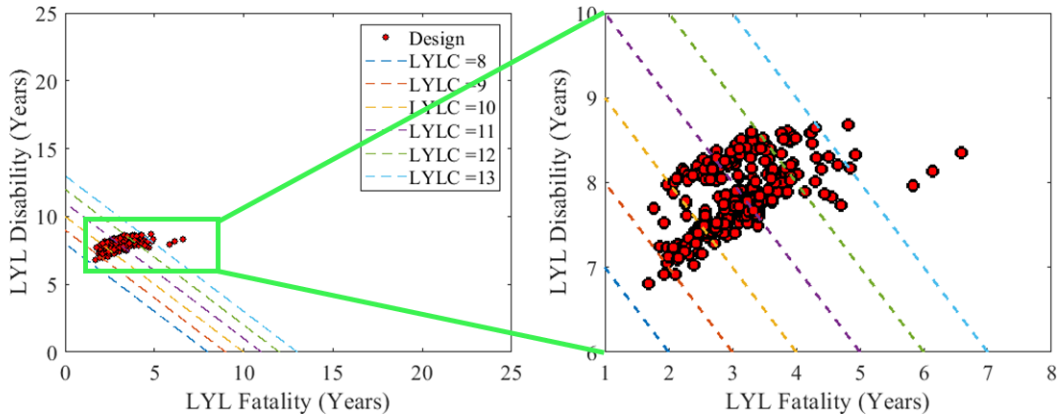


Figure 9.4: DOE Exploration of Life Years Lost at 25 km/hr

The influence of disabling injuries on the vehicle design was minimal at the impact speed of 40 km/hr (Figure 9.5, Table 9.3). Although the median values of LYLF and LYLD are similar in magnitude at 40 km/hr the interquartile range of LYLF was almost six times the interquartile range of LYLD suggesting that life years lost due to disability did not vary significantly across the design space when compared to the variation found in LYLF. At speed of 25 km/hr the interquartile

range of LYLD and LYLF were similar in magnitude indicating that as the severity of the injury decreased the contribution of LYLD to LYLC increased (Table 9.3).

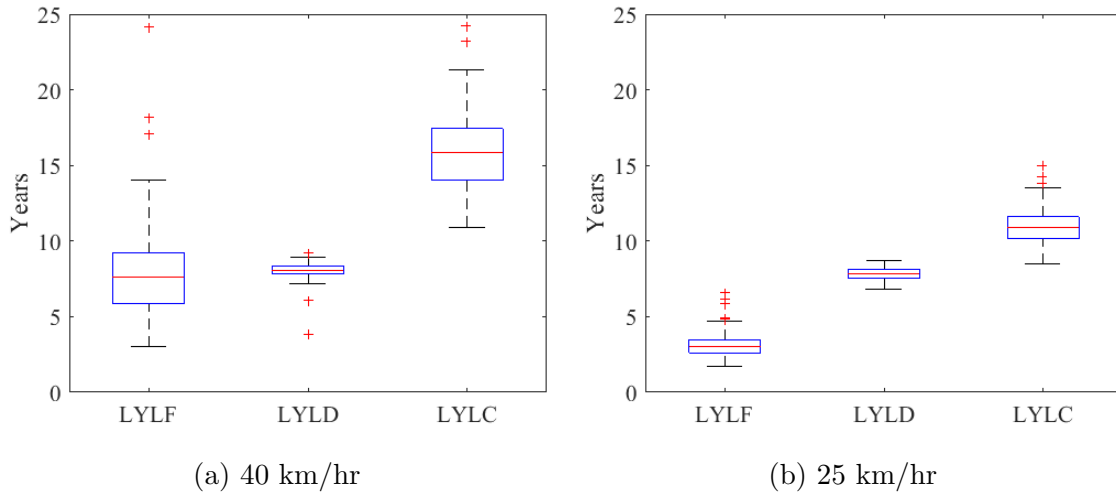


Figure 9.5: Range of Variation in Life Years Lost

Table 9.3: Summary of Range of Variation in Life Years Lost Across the Design Space

Variable	Inter quartile range		Median	
	40 km/hr	25 km/hr	40 km/hr	25 km/hr
LYLF	3.34	0.85	7.61	3.05
LYLD	0.47	0.63	8.07	7.81
LYLC	3.38	1.42	15.88	10.87

A negative correlation was observed between metrics WBFCI and NISS at the two impact speeds (Figure 9.6). This implies that within the design space as the severity of injuries increased (higher NISS) the disability associated with the injuries also increased (lower WBFCI). However, except at the tail ends of the data, there is a distribution of WBFCI at a given NISS value which shows the variation in disability associated with injuries at a given injury severity.

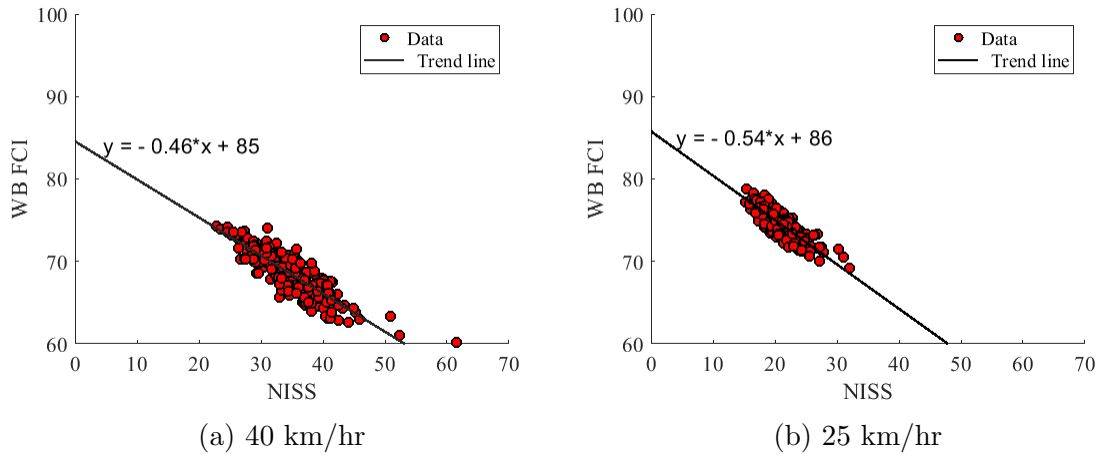
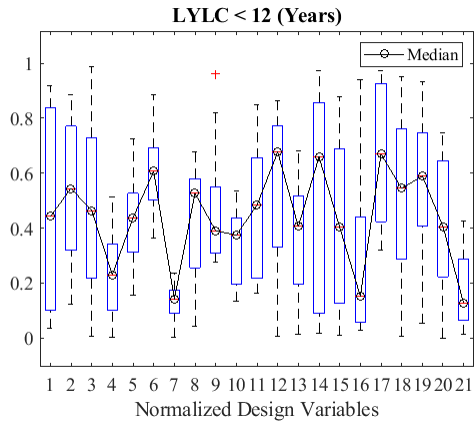
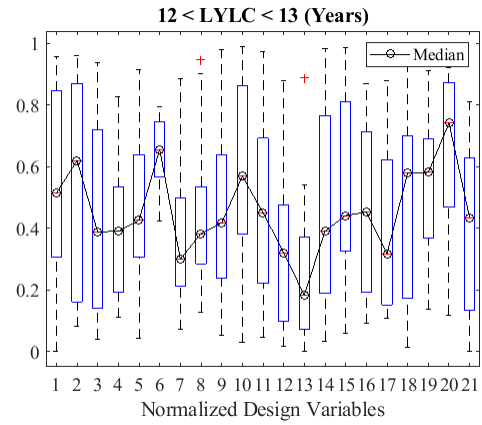


Figure 9.6: Distribution of Whole Body FCI With Respect to NISS

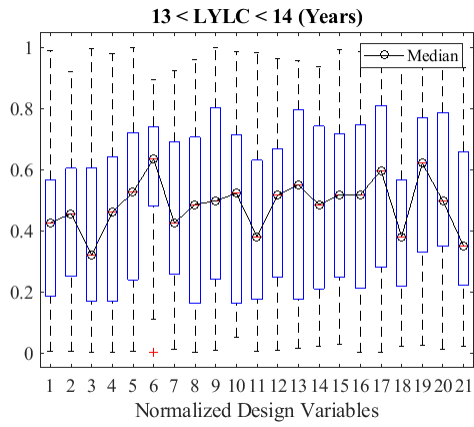
To gain insight into how the design variables affected the overall outcome of cumulative life years lost, the vehicle designs were binned based on LYLC and the distribution of the design variables pertaining to geometric and stiffness parameters were analyzed (Figure 9.7, Figure 9.8, Figure 9.15). At the speed of 40 km/hr, the vehicle designs for which the LYLC ranged between 13-16 years, the median values of the normalized design variables ranged between 0.4-0.6 (Figure 9.7). However, at the tail end of the distribution of vehicle designs in terms of LYLC ( $< 12$ ,  $12 - 13$ ) or ( $17 - 20$ ,  $> 20$ ) the median values of the design variables move closer to the extrema (0-1). For a set of common design parameters an opposite trend can be observed between good ( $< 12$ ,  $12 - 13$ ) and poor vehicle designs ( $17 - 20$ ,  $> 20$ ) in terms of LYLC. A similar trend can be observed at the speed of 25 km/hr (Figure 9.8). The frequency of vehicle designs follows a normal distribution in terms of cumulative life years lost LYLC (Figure 9.16, Figure 9.9). This shows that most designs provide a middle ground in terms of LYLC while very few designs provide either the best or worst outcome in terms of life years lost.



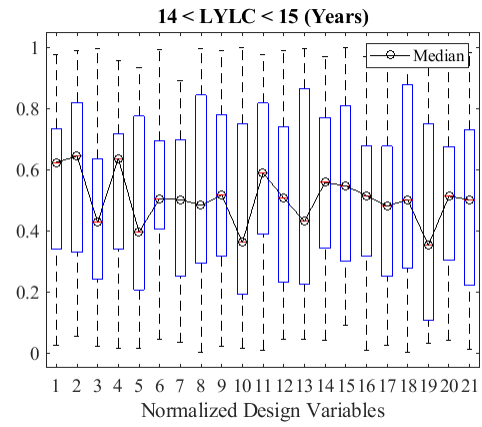
(a)



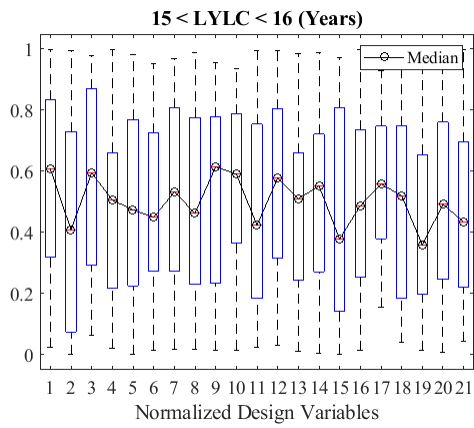
(b)



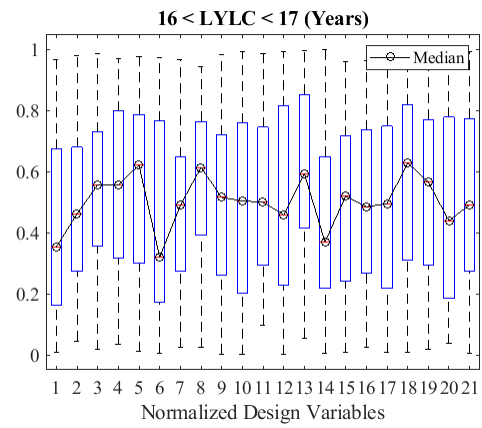
(c)



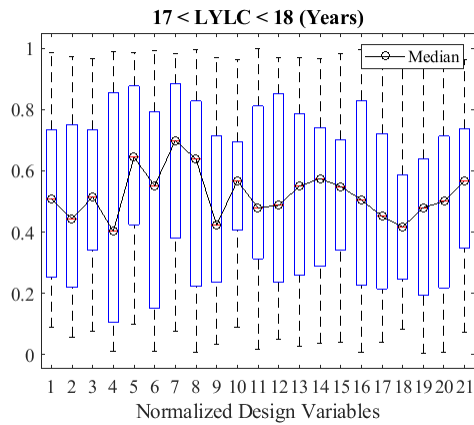
(d)



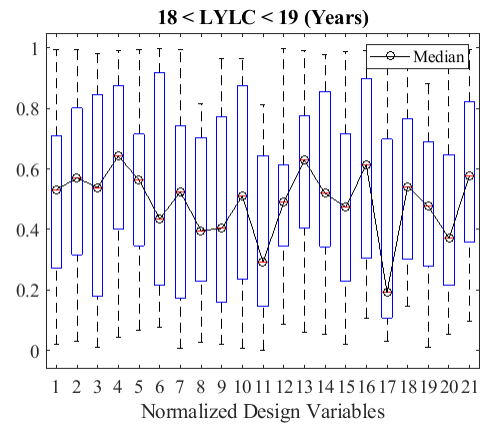
(e)



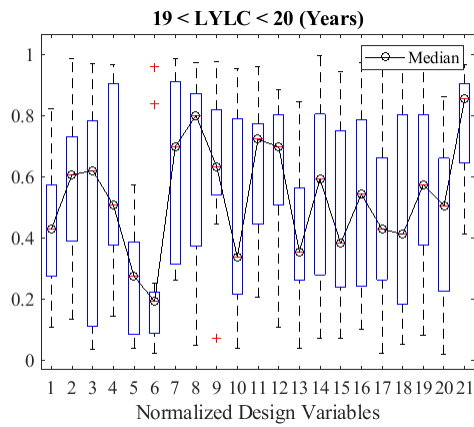
(f)



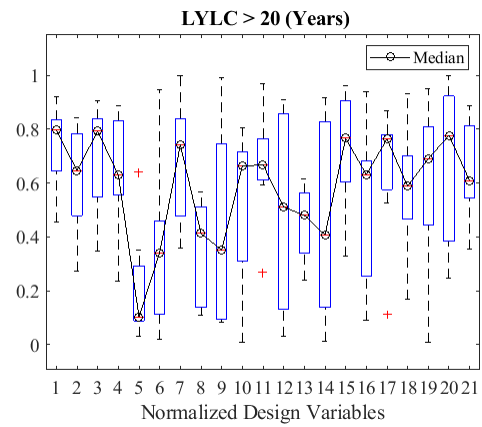
(g)



(h)

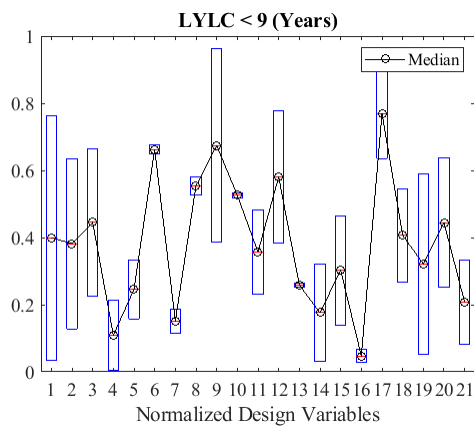


(i)

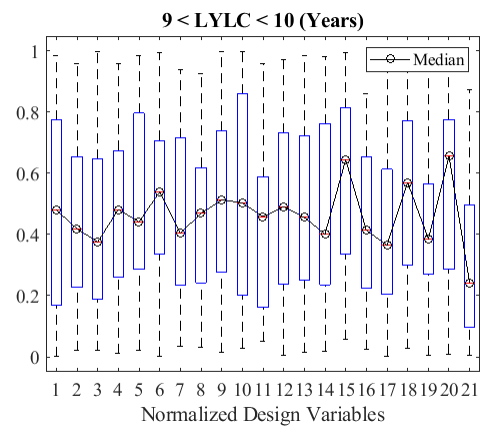


(j)

Figure 9.7: Distribution of Normalized Design Variables Categorized by Cumulative Life Years Lost at 40 km/hr



(a)



(b)

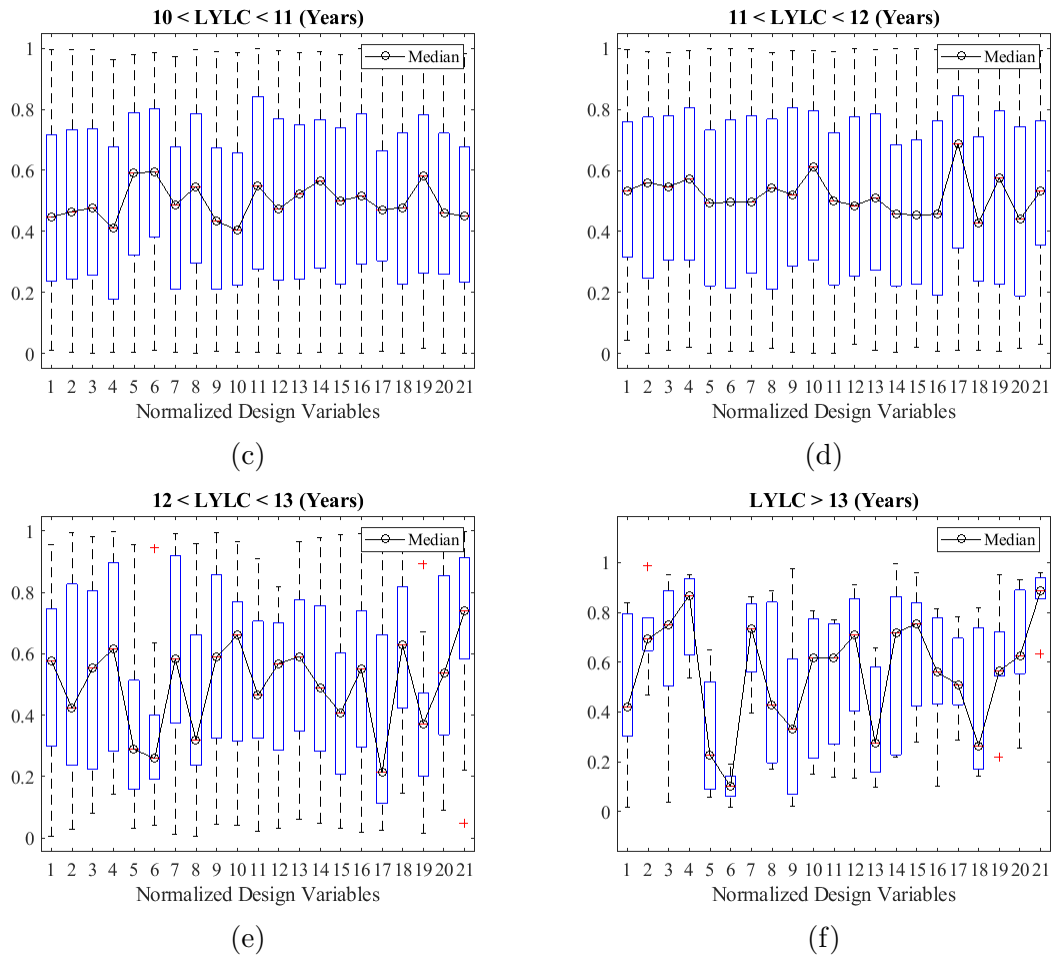


Figure 9.8: Distribution of Normalized Design Variables Categorized by Cumulative Life Years Lost at 25 km/hr

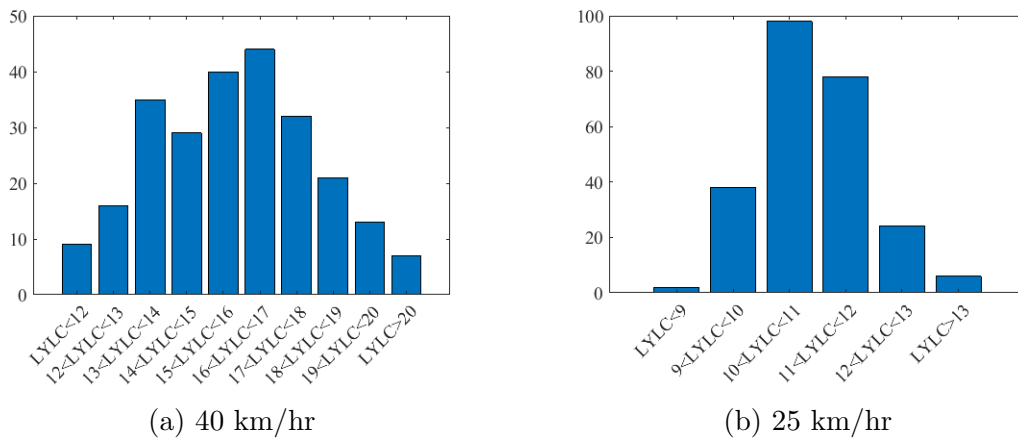


Figure 9.9: Frequency of Vehicle Designs Grouped by Number of Cumulative Life Years Lost

In order to calculate the relative ranking of body regions for a given metric (LYLC, LYL $F$ , LYLD), the injuries to each body region were omitted one at a time. The cost calculation using the Monte-Carlo methodology described in chapter 8 was repeated to estimate the expected value of a metric, given the omission of injuries from the particular body region. The ratio of the mean values of the metric with consideration of all injuries to the mean value of the metric from omission of injuries was used to rank the body regions for the given metric (Figure 9.10, Figure 9.11, Figure 9.12). A ratio of 1 indicates that a given metric was not influenced by the omission of injuries from a particular body region. Injuries to the brain were the most influential in affecting the LYL $F$  at both impact speeds ( Figure 9.11). At the speed of 25 km/hr knee injuries were most influential in affecting the LYLC and LYLD (Figure 9.10, Figure 9.12).

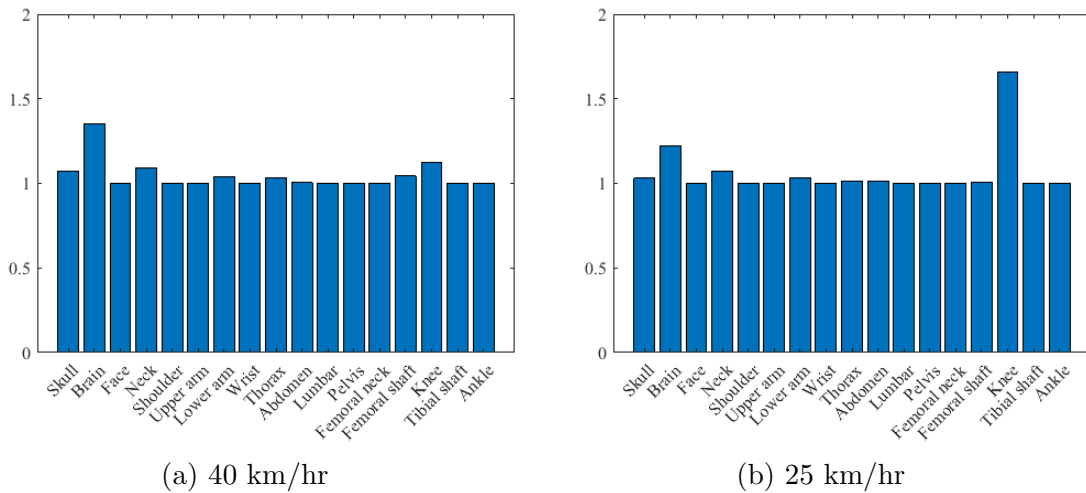
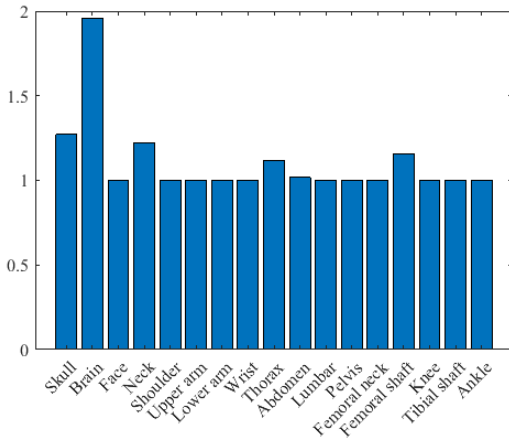
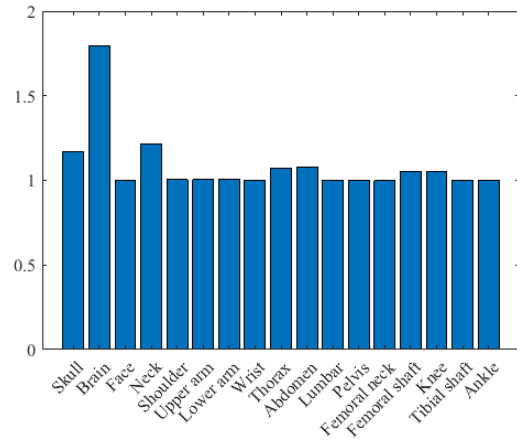


Figure 9.10: Relative Ranking of Body Regions in Terms of Cumulative Life Years Lost

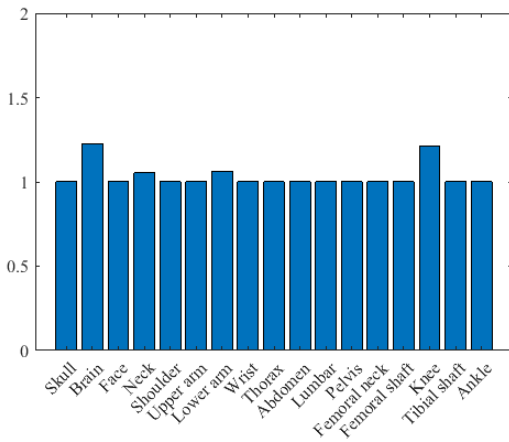


(a) 40 km/hr

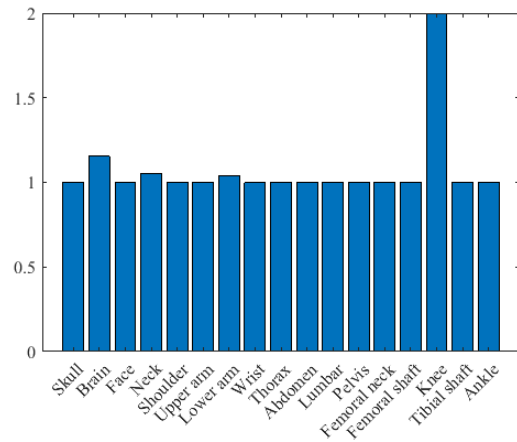


(b) 25 km/hr

Figure 9.11: Relative Ranking of Body Regions in Terms of Life Years Lost Due to Fatality



(a) 40 km/hr



(b) 25 km/hr

Figure 9.12: Relative Ranking of Body Regions in Terms of Life Years Lost Due to Disability

To assess the effect of design variables on LYLC a regression analysis was done using stepwise linear regression *stepwiselm* function in MATLAB. The stepwise linear regression models were fit to output of LYLC at the two design speeds of 40 km/hr (Table 9.4) and 25 km/hr (Table 9.5). While the design variable v21 (peak

force during windshield deformation) was statistically significant at the speed of 25 km/ hr (pvalue < 0.05), it was not statistically significant at the speed of 40 km/hr (pvalue > 0.05). This is because at the speed of 40 km/hr brain injuries were mostly contributing to the LYLC and LYLFF lost (Figure 9.10, Figure 9.11), while the stiffness of windshield only affected the prediction of HIC values which are the predictor for head injuries with linear acceleration as an injury mechanism (skull fractures).

Table 9.4: Linear Regression Model of LYLC at 40 Km/hr

Variable	Estimate	SE	tstat	pValue
(Intercept)	11.69	1.87	6.26	2.19E-09
v1	-0.64	1.21	-0.53	5.97E-01
v3	-0.12	0.77	-0.15	8.80E-01
v4	4.41	1.21	3.63	3.57E-04
v5	-1.7	1.06	-1.61	1.09E-01
v6	5.06	1.83	2.77	6.13E-03
v7	7.31	1.02	7.18	1.28E-11
v8	1.79	1.42	1.27	2.07E-01
v9	0.55	1.03	0.53	5.96E-01
v11	3.68	1.88	1.96	5.09E-02
v12	-6.71	1.46	-4.59	7.73E-06
v13	3	0.73	4.11	5.85E-05
v14	-1.6	0.76	-2.09	3.78E-02
v15	-3.4	1.11	-3.07	2.47E-03
v16	-2.79	1.02	-2.72	7.06E-03
v18	-2.54	0.96	-2.65	8.68E-03

Continued on next page

**Table 9.4 – continued from previous page**

Variable	Estimate	SE	tstat	pValue
v19	-3.86	1.17	-3.3	1.14E-03
v20	1.78	0.72	2.47	1.45E-02
v21	0.62	0.79	0.78	4.36E-01
v1:v8	-3.55	1.34	-2.65	8.78E-03
v1:v11	2.85	1.5	1.91	5.79E-02
v1:v15	4.22	1.38	3.06	2.50E-03
v3:v6	4.03	1.33	3.03	2.72E-03
v4:v7	-4.1	1.39	-2.94	3.68E-03
v4:v9	-4.81	1.31	-3.67	3.12E-04
v4:v19	2.8	1.36	2.06	4.05E-02
v5:v6	5.01	1.38	3.64	3.50E-04
v5:v11	-3.68	1.37	-2.69	7.74E-03
v6:v7	-5	1.32	-3.79	2.00E-04
v6:v8	-4.81	1.4	-3.43	7.33E-04
v6:v11	-7.32	1.43	-5.11	7.36E-07
v6:v20	-4.8	1.31	-3.67	3.15E-04
v8:v16	3.19	1.37	2.34	2.03E-02
v8:v18	3.71	1.4	2.64	8.81E-03
v9:v12	3.5	1.31	2.68	7.94E-03
v11:v12	2.99	1.39	2.16	3.23E-02
v11:v13	-4.47	1.29	-3.48	6.20E-04
v11:v19	3.34	1.32	2.53	1.23E-02

Continued on next page

**Table 9.4 – continued from previous page**

Variable	Estimate	SE	tstat	pValue
v12:v15	3.09	1.29	2.39	1.77E-02
v12:v16	3.58	1.31	2.73	6.89E-03
v14:v19	3.27	1.43	2.3	2.27E-02
v18:v21	3.56	1.39	2.57	1.10E-02

Table 9.5: Linear Regression Model for LYLC at 25 Km/hr

Variable	Estimate	SE	tstat	pValue
(Intercept)	6.99	0.55	12.82	2.69E-28
v1	1.21	0.46	2.64	8.87E-03
v3	-0.72	0.36	-2.01	4.59E-02
v4	0.74	0.29	2.52	1.25E-02
v5	1.77	0.42	4.26	3.06E-05
v6	2.43	0.53	4.57	8.18E-06
v7	2.56	0.34	7.44	2.45E-12
v8	-2.49	0.46	-5.37	2.03E-07
v9	0.67	0.28	2.41	1.70E-02
v10	-0.6	0.28	-2.16	3.22E-02
v11	0.66	0.3	2.25	2.56E-02
v12	0.48	0.28	1.7	9.03E-02
v13	0.27	0.14	1.92	5.57E-02
v16	0.91	0.28	3.25	1.36E-03
v17	0.41	0.14	2.89	4.20E-03

Continued on next page

**Table 9.5 – continued from previous page**

Variable	Estimate	SE	tstat	pValue
v19	0.52	0.29	1.79	7.52E-02
v20	-0.46	0.46	-0.99	3.21E-01
v21	4.76	0.36	13.32	7.27E-30
v1:v9	-1.54	0.5	-3.06	2.50E-03
v1:v10	1.26	0.49	2.6	9.97E-03
v1:v16	-1.8	0.5	-3.6	3.92E-04
v3:v8	1.48	0.47	3.13	2.00E-03
v3:v20	1.31	0.48	2.73	6.95E-03
v4:v11	-1.03	0.52	-1.99	4.75E-02
v5:v7	-2.24	0.5	-4.49	1.14E-05
v5:v21	-1.75	0.51	-3.44	6.89E-04
v6:v7	-1.76	0.5	-3.54	4.94E-04
v6:v8	1.76	0.54	3.28	1.21E-03
v6:v20	-1.97	0.48	-4.1	5.91E-05
v6:v21	-4.55	0.5	-9.18	3.81E-17
v8:v20	1.42	0.51	2.77	6.01E-03
v12:v19	-1.04	0.49	-2.14	3.31E-02

Based on NHTSA’s General Estimates System (GES), a nationwide probability sample of police reported crashes, the low speed crashes of 25 km/hr were four times as likely as the crashes at 40 km/hr (Leaf and Preusser (1999)). To consider the exposure to a given crash scenario, cost metrics of LYLC, LYLF and LYLD were re-evaluated by taking a weighted sum of individual metrics at the speeds of 25 km/hr

and 40 km/hr using the exposure ratio of 4:1 (Figure 9.13, Figure 9.14). The same vehicle design remained the optimum under weighted conditions and all the three ‘cost’ metrics led to the same optimal design. The range of design variables grouped by net LYLC followed a similar trend between weighted and unweighted scenarios (Figure 9.15). The frequency of vehicle designs remained a normal distribution with LYLC and this is to be expected given the underlying distributions at both speeds (Figure 9.16).

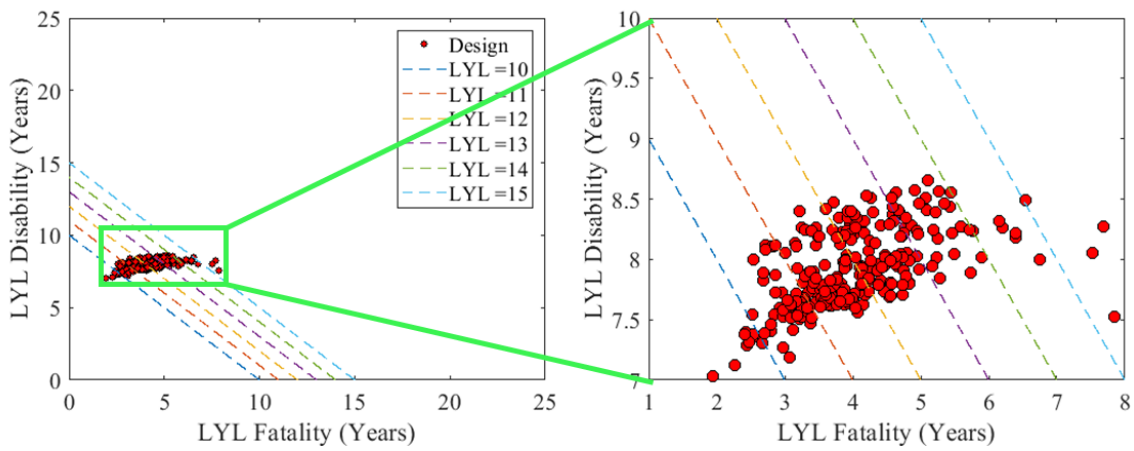


Figure 9.13: DOE Exploration of Life Years Lost (weighted)

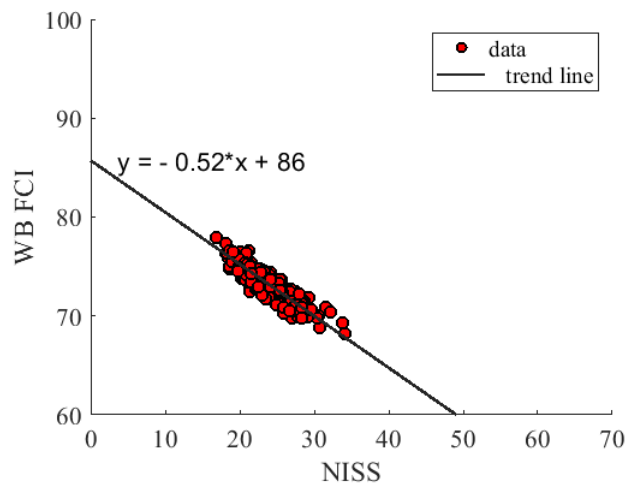
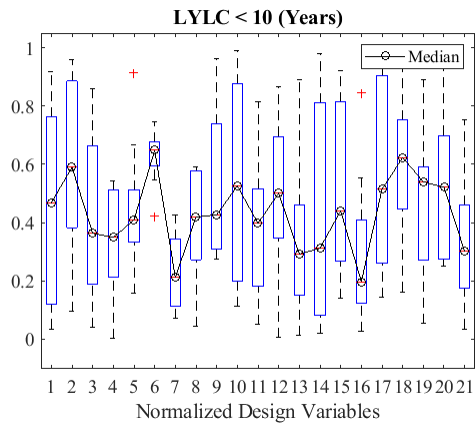
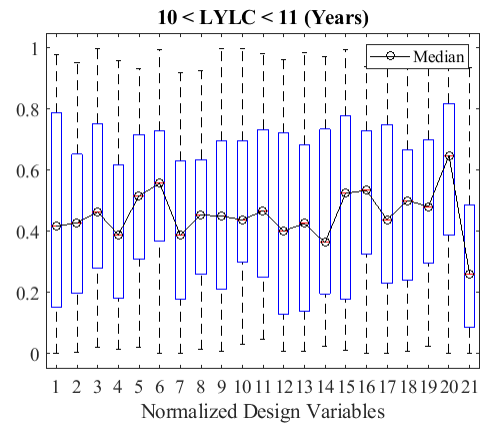


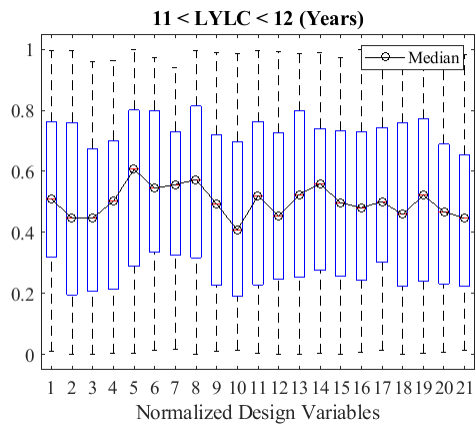
Figure 9.14: Distribution of WBFCI With Respect to (weighted)



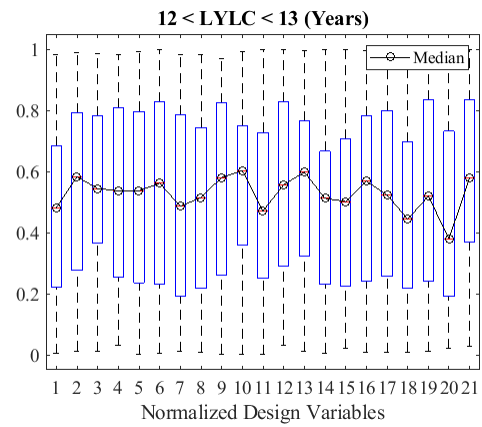
(a)



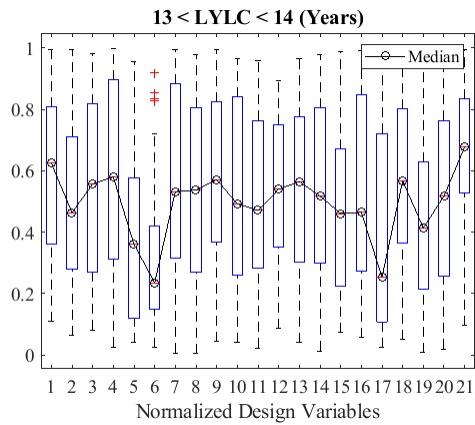
(b)



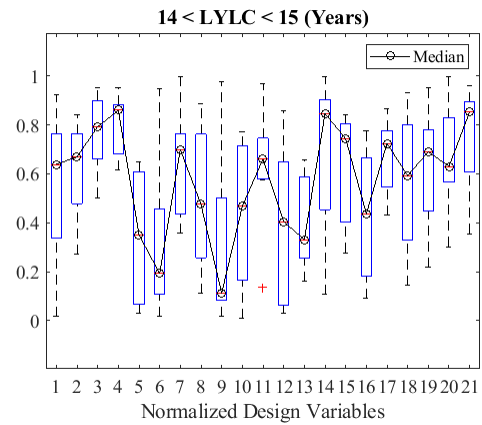
(c)



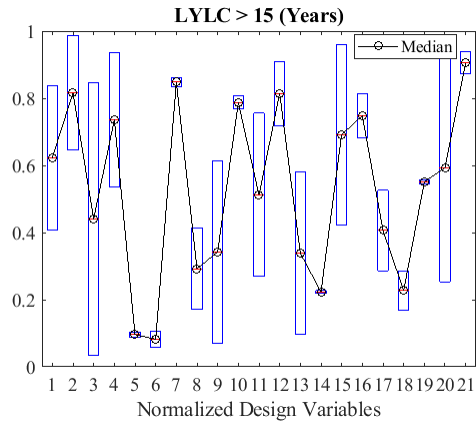
(d)



(e)



(f)



(g)

Figure 9.15: Distribution of Design Variables Categorized by Cumulative Life Years Lost (Weighted)

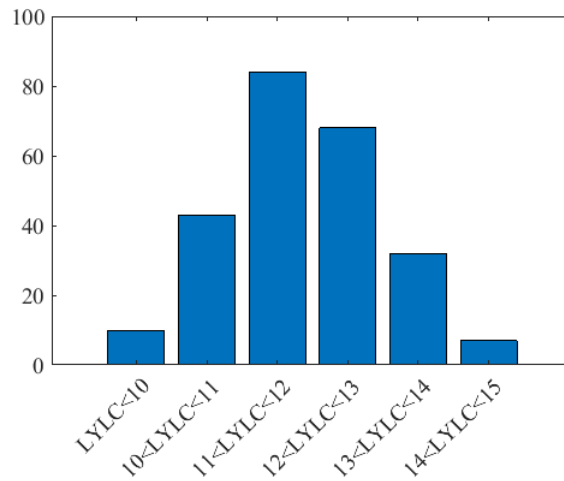


Figure 9.16: Frequency of Vehicle Designs Grouped by Cumulative Number of Life Years Lost (Weighted)

## 9.4 Discussion

In this chapter, the design space exploration of the geometric and material parameters of a front end of a Sedan was undertaken by simulating vehicle to pedestrian crash in MADYMO at the speeds of 40 and 25 km/hr. Three objective functions LYLC, LYLF, and LYLD were used to evaluate the vehicle designs.

### 9.4.1 Injury Metric Sensitivity to Design Variables

The range of injury metrics (Figures 9.17 - 9.26) increased with the impact speed and this is reflected in the increase of the median value of poly-trauma metrics LYLC, LYLF and LYLD with speed (Table 9.3). The peak force generated in the windshield dictates the acceleration imparted to head during the contact with windshield and therefore showed a positive correlation with the HIC36 metric calculated using the head acceleration (Figure 9.17). The injury metric UBrIC which is dictated by the rotational kinematics of the head (angular velocity and angular acceleration) showed a correlation with the bonnet length and bonnet angle at the speed of 40 km/hr. In designs with long bonnet length, the head picks higher angular velocities prior to contact with windshield, and therefore we see higher UBrIC values (Figure 9.18a). In designs with short bonnet length the head might have a larger angular acceleration upon impact with the windshield and lead to higher UBrIC values. Therefore, we see a nonlinear variation for the UBrIC metric with the bonnet length at the speed of 40 km/hr (Figure 9.18a). At speed of 40 km/hr UBrIC increased with bonnet angle (Figure 9.19a). UBrIC was insensitive to bonnet length and angle at the impact speed of 25 km/hr (Figure 9.18b, Figure 9.19b). At both impact speeds UBrIC did not show sensitivity with the stiffness of the windshield and this is consistent with the results predicted by Chen (2017) using THUMS PFEM model (Figure 9.20). No explicit correlation was observed between the injury metric Nij and the design variables (Figure 9.21). The anterior-posterior compression of thorax showed a correlation with the bonnet angle (v7) and from a geometric perspective this correlation is expected (Figure 9.22). The pelvis contact force increased with the bonnet leading edge height (v5) (Figure 9.23) and the femur bending moment decreased with the bonnet lead (v4) length (Figure 9.24). These observations are in

agreement with the results published by Matsui et al. (1998) using injury analysis of field data and pedestrian leg-form impactor tests. The bending moment of tibia with is the injury predictor for the fracture of leg was found to be correlated to the stiffness of the bumper (Bumper force2 (v11) and Bumper def2 (v12)) (Figure 9.25, Figure 9.26). This result is in agreement with the response surface analysis presented by Nie et al. (2013) where the tibial acceleration measured was found to be correlated to bumper stiffness.

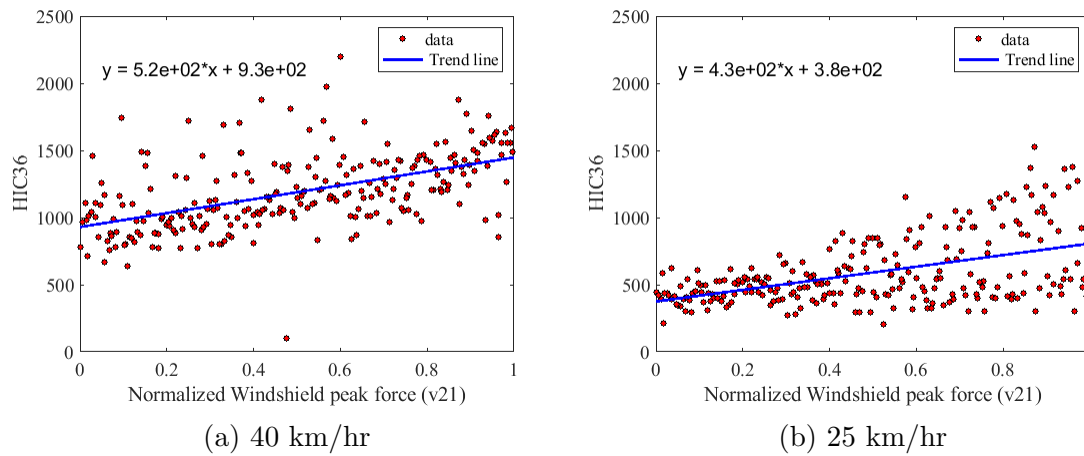


Figure 9.17: Sensitivity of HIC36 With Normalized Windshield Peak Force

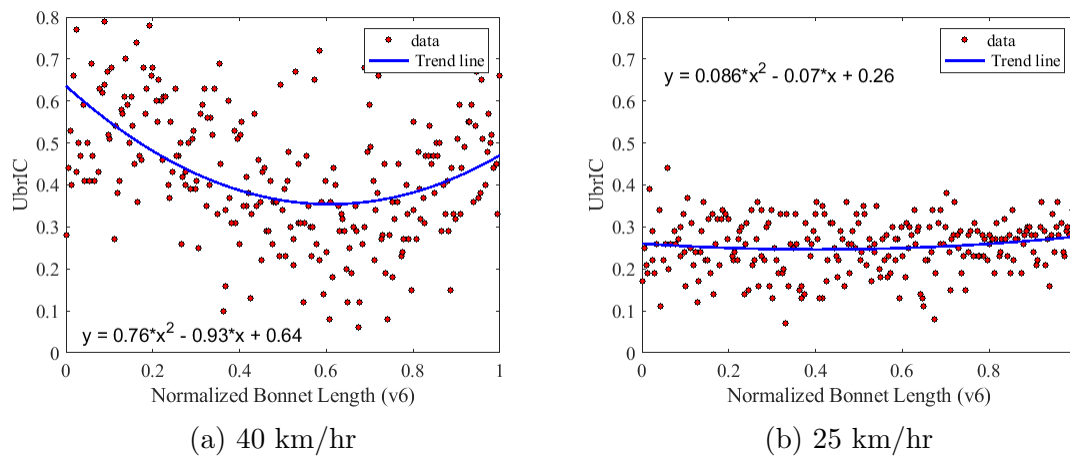
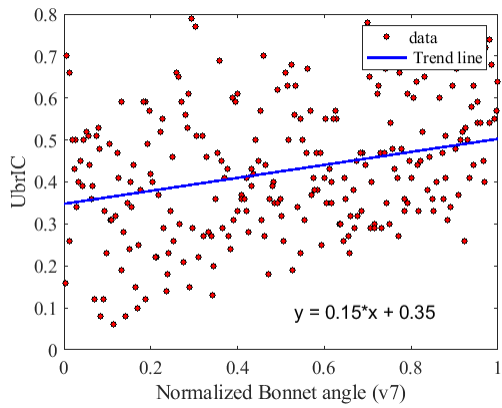
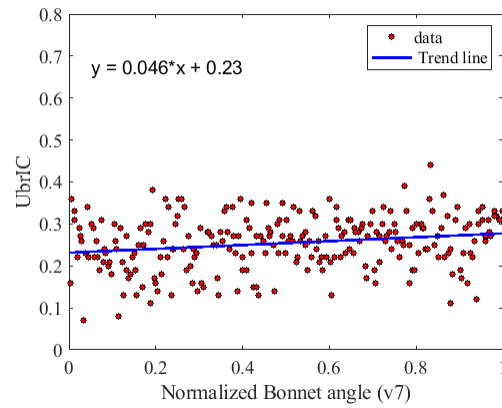


Figure 9.18: Sensitivity of UBriC With Normalized Bonnet Length

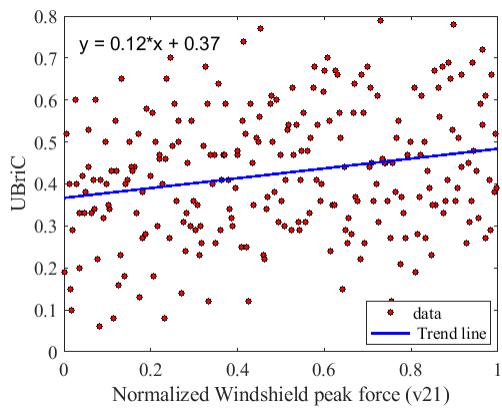


(a) 40 km/hr

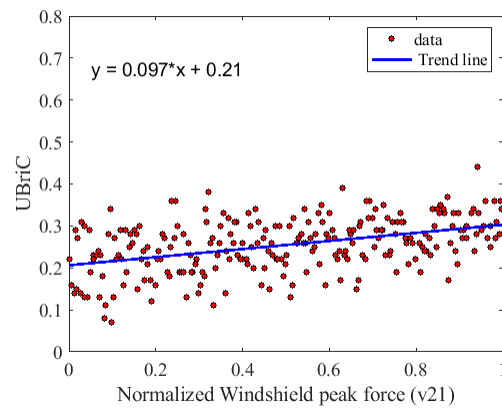


(b) 25 km/hr

Figure 9.19: Sensitivity of UBrIC With Normalized Bonnet Angle

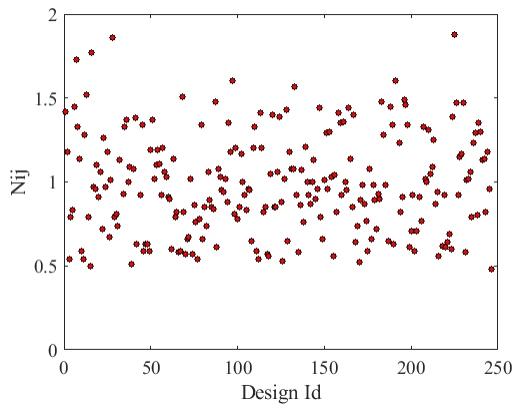


(a) 40 km/hr

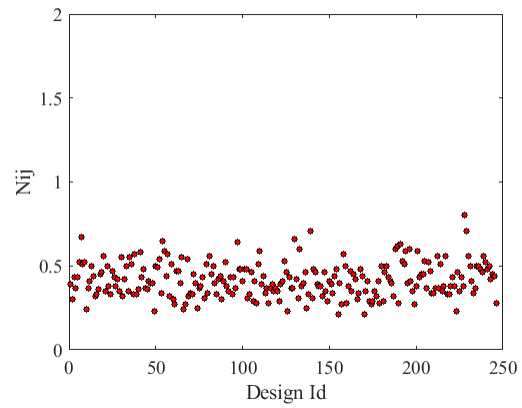


(b) 25 km/hr

Figure 9.20: Sensitivity of UBrIC With Normalized Windshield Peak Force

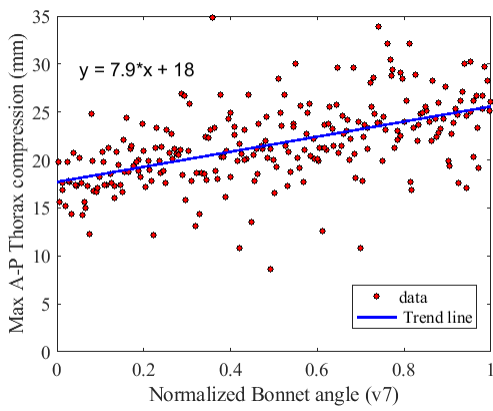


(a) 40 km/hr

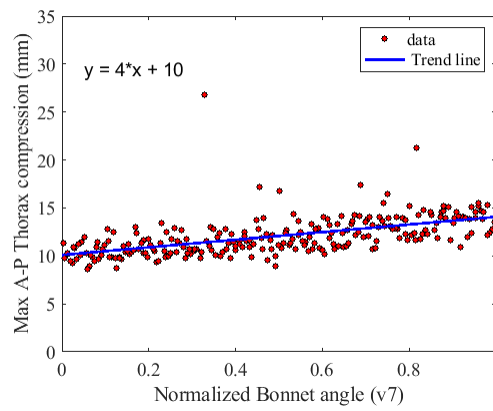


(b) 25 km/hr

Figure 9.21: Range of  $N_{ij}$

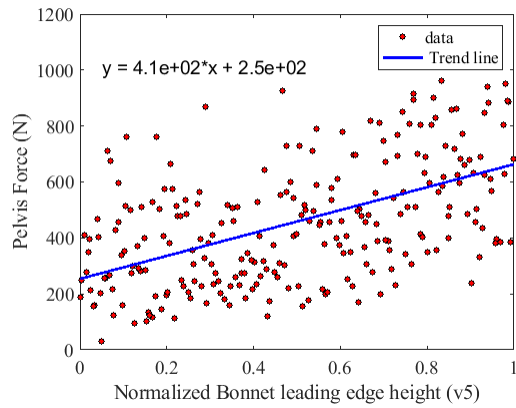


(a) 40 km/hr

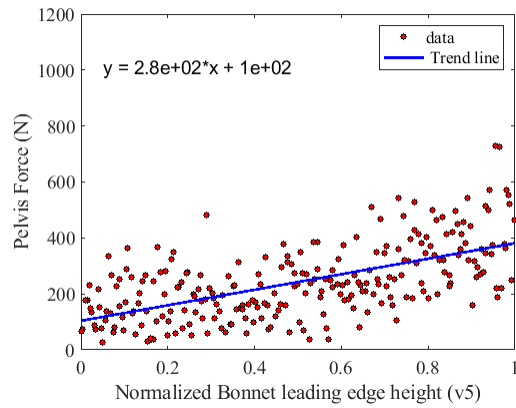


(b) 25 km/hr

Figure 9.22: Sensitivity of Anterior-Posterior Thorax Compression With Normalized Bonnet Angle

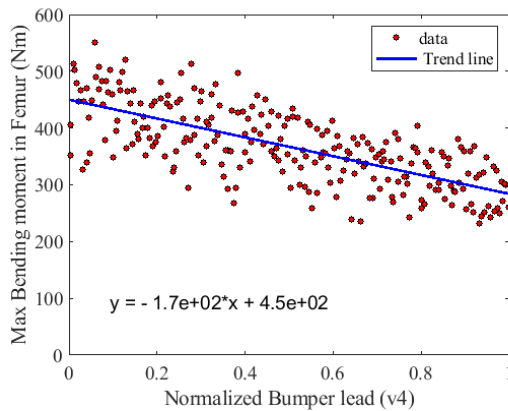


(a) 40 km/hr

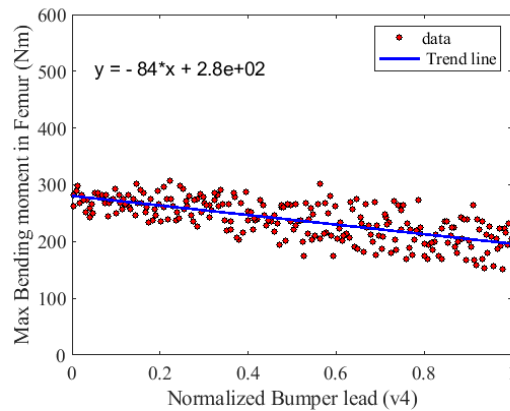


(b) 25 km/hr

Figure 9.23: Sensitivity of Pelvis Contact Force With Normalized Bonnet Leading Edge Height

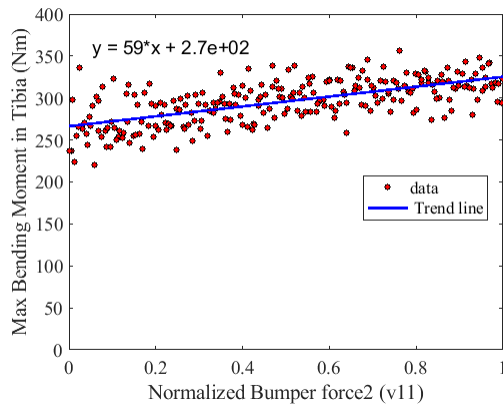


(a) 40 km/hr

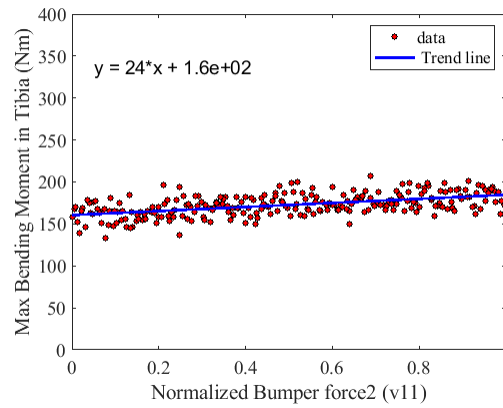


(b) 25 km/hr

Figure 9.24: Sensitivity of Maximum Bending Moment in Femur With Normalized Bumper Lead

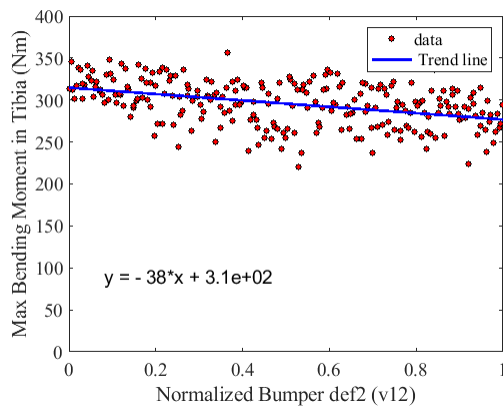


(a) 40 km/hr

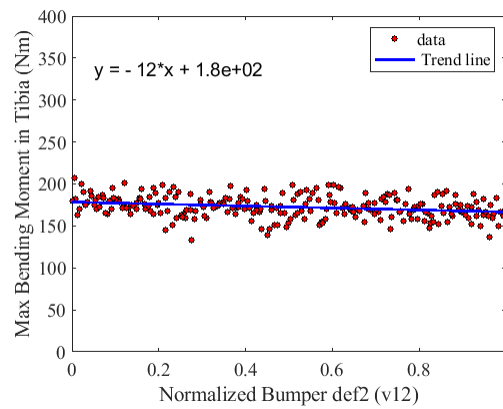


(b) 25 km/hr

Figure 9.25: Sensitivity of Maximum Bending Moment in Tibia With Normalized Bumper Force2



(a) 40 km/hr



(b) 25 km/hr

Figure 9.26: Sensitivity of Maximum Bending Moment in Tibia With Normalized Bumper Def2

## 9.4.2 Best and Worst Designs

Poly-trauma metrics for the best and the worst designs in terms of cumulative life years lost (LYLC) are listed in Table 9.6. The design parameters for each of these designs are listed in Table 9.7. The injury metrics from different body regions for each of these designs are summarized in Table 9.8. Design 25 was the best design in terms of LYLC and LYLF at the speed of 40 km/hr and 25 km/hr (Table 9.6). Design 34 was the worst design in terms of LYLC and LYLF at the speed of 40 km/hr while design 204 was the worst design at the speed of 25 km/hr. It has to be noted that LYLD cannot be treated as an independent metric as the probability of survival goes into the calculation of LYLD (Equation 8.4). Therefore, although for design 34 the LYLF was high, the LYLD was low because of the higher probability of death. When we look at the injury metrics, design 34 and design 205 have similar metrics across the body regions except for the neck ( $N_{ij}$ ) and thorax ( $C_{\max}$  a-p) at the speed of 40 km/hr. The response of the design 34 at 40 km/hr seems to be an outlier for the predictor  $N_{ij}$ . The trend with the injury metrics (Table 9.8) and design variables (Table 9.7) observed from the sensitivity analysis can be seen in all the other body regions except for neck and thorax in design 34.

Table 9.6: Loss Metric Summary for the Best and the Worst Designs

Design	40 km /hr			25 km/hr		
	LYLC	LYLF	LYLD	LYLC	LYLF	LYLD
25*	10.9	3	7.9	8.5	1.7	6.8
34‡	28	24.1	3.8	11.8	3.9	7.9
204†	19.9	12.2	7.7	14.9	6.6	8.4

Table 9.7: Design Parameters for the Best and the Worst Designs

Design	Variable										
	v1	v2	v3	v4	v5	v6	v7	v8	v9	v10	v11
25*	0.76	0.13	0.66	0	0.16	0.67	0.12	0.58	0.96	0.53	0.23
34‡	0.64	0.84	0.79	0.89	0.64	0.35	0.36	0.52	0.35	0.01	0.67
204†	0.41	0.99	0.04	0.94	0.1	0.06	0.83	0.17	0.07	0.77	0.76
	Variable										
	v12	v13	v14	v15	v16	v17	v18	v19	v20	v21	
25*	0.78	0.25	0.32	0.14	0.03	0.63	0.54	0.59	0.25	0.08	
34‡	0.51	0.33	0.92	0.82	0.68	0.87	0.93	0.8	0.63	0.88	
204†	0.72	0.1	0.22	0.42	0.81	0.29	0.29	0.56	0.25	0.94	

Table 9.8: Injury Metric Summary for the Best and the Worst Designs

Impact Speed	40 km /hr			25 km/hr			
	Design ID	25*	34‡	204†	25*	34‡	204†
HIC36		779.5	1432.4	1758.6	295.6	833.7	1364.7
UBrIC		0.06	0.69	0.69	0.08	0.33	0.44
Nij		0.97	6.74	0.91	0.33	0.5	0.53
Thorax AP Cmax (mm)		17.3	34.8	23.7	9.88	11.92	14.8
Pelvis Cont. Force (N)		134.1	496.34	515.74	34.83	241.08	287.12
Femur Bending Moment (Nm)		352.09	303.59	245.05	262.53	205.47	152.37
Tibia Bending Moment (Nm)		269.56	324.34	318.01	163.61	180.38	184.13

\* Best Design at 40 km/hr & 25 km/hr for LYLC and LYLF

‡ Worst Design at 40 km/hr for LYLC and LYLF

† Worst Design at 25 km/hr for LYLC and LYLF

### 9.4.3 Body Region Ranking

The presence of brain injuries almost doubled the life years lost due to fatality at 40 km/hr (Figure 9.11). Brain injuries were the most influential in effecting the number of LYLC, LYLf, and LYLD at 40 km/hr, due to the nature of injuries being both fatal and disabling in nature.

Additionally, in the calculation of NISS the three most severe injuries are taken into account and in calculation of whole body FCI, if a particular dimension is effected by multiple injuries the worst FCI is picked as a conservative estimate. Due to the nature of poly-trauma, omitting a particular body region would not significantly affect the calculation of NISS and WBFCI, if the injuries from the omitted body region were similar in severity and disability to other body regions. This is shown in the relative ranking of body regions where, except for skull, brain, neck and knee, no other body region showed significant influence on the life years lost. Knee injuries almost doubled the life years lost due to disability during the low speed crashes (25 km/hr) (Figure 9.12).

### 9.4.4 Correlation Between FCI and NISS

A negative correlation was observed between the two poly-trauma metrics of WBFCI and NISS at the two speeds considered during the DOE, although the relationship between them varied with speed (Figure 9.6). This correlation may be specific to the design under consideration. Essentially, it means that as the severity of injury increased, so did the disability associated with them. This would suggest that the increase in severity was specific to a body region and therefore we find this negative correlation between WBFCI and NISS.

### 9.4.5 A Hypothetical Scenario of no Head or Brain Injuries

Because head injuries were the most influential in effecting the life years lost at 40 km/hr a hypothetical scenario was considered where irrespective of impact location, the pedestrian model would not suffer any skull/brain injuries. Another DOE was performed following the methodology outlined in this chapter, with omission of head injuries to understand the effect of disabling injuries in the absence of head trauma. Conceptually, this might relate to something like the development of a perfectly performing pedestrian airbag. The range of life years lost due to fatality is considerably reduced in comparison to the case with inclusion of head trauma (Figure 9.27, Figure 9.13). By looking at the interquartile range of life years lost due to disability (Table 9.9), the influence of disabling injuries is quite significant for the vehicle designs in the absence of head trauma.

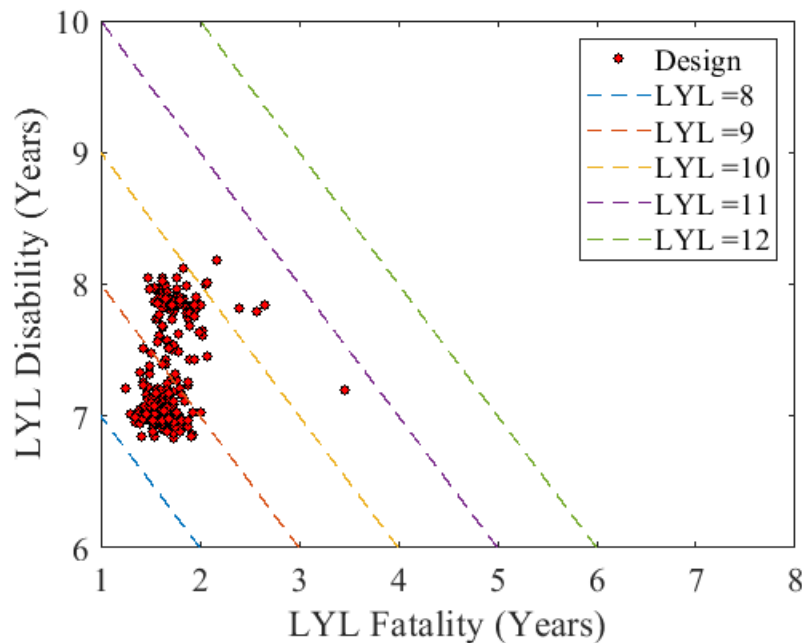


Figure 9.27: DOE Exploration of Life Years Lost in Absence of Head Trauma (Weighted)

Table 9.9: A Comparison of Interquartile Range of Life Years Lost With and Without Head Trauma

Variable	Inter Quartile Range	
	All Injuries	No Head Injury
LYLF	1.21	0.24
LYLD	0.51	0.77
LYLC	1.34	0.92

#### 9.4.6 Effect of End Time on the Best Designs at 40 Km/hr

To check the effect of end time on the poly-trauma metrics LYLC, LYLF and LYLD at 40 km/hr the simulations with LYLC <12 years were rerun with an end time of 260 ms (+60 ms). There was no substantial difference observed in the calculated values of LYLC, LYLF and LYLD with the average difference in LYLD being 0.5 years, average difference in LYLF being 0.4 years and the average difference in LYLD being 0.3 years (Table 9.10). The increase in the poly-trauma metrics was consistent for each vehicle design with the end time.

Table 9.10: Variation in Poly-trauma Metrics with End Time at 40 km/hr for the Best Designs

Cost	LYLC (Years)		LYLF (Years)		LYLD (Years)	
	200 ms	260 ms	200 ms	260 ms	200 ms	260 ms
Design 25	10.8	11.2	3	3.4	8.7	8.9
Design 59	11.2	11.6	3.4	3.7	8.8	9.1
Design 62	11.1	12	3.3	4.2	8.8	9.1
Design 105	11.3	11.7	3.6	4	8.8	9
Design 142	11.3	11.6	3.5	3.9	8.8	9
Design 152	11.7	12.1	3.8	4.2	9	9.2
Design 162	11.1	11.5	3.4	3.8	8.7	8.9
Design 184	11.5	12	3.7	4.2	8.9	9.2
Design 223	11.6	12	3.8	4.2	8.9	9.2
Average	11.3	11.8	3.5	3.9	8.8	9.1

## Chapter 10

### Conclusions

#### 10.1 Concluding Remarks

The goal of this dissertation was to develop a framework to investigate the influence of long-term disability associated with injuries on vehicle design in the context of pedestrian safety. Firstly, a field data analysis was conducted in chapter 3 to identify the most frequently occurring injuries in vehicle to pedestrian crashes in the United States. The injuries observed in chapter 3, were mapped to injury mechanisms and injury risk functions (IRF) surveyed from the literature in chapter 4. The mapping process resulted in 143 unique AIS2+ injuries. These injuries were later binned into specific body regions based on MAIS levels. Head and lower extremities were the two most frequently injured body regions for AIS2+ injuries.

Then in Chapter 6, a multibody pedestrian model UVAPED was developed with virtual sensors capable of calculating the injury metrics across the body regions, for the of evaluation of injury risk (probabilistic). The UVAPED model was validated using component level tests in chapter 6 and was improved to match the biofidelity requirements across the body. Later in chapter 7, the biofidelity of the UVAPED model was evaluated by reconstructing specific PMHS whole-body pedestrian im-

pact conditions using a well characterized buck representing a mid-sized sedan. The UVAPED model performed as good as the most advanced THUMS PFEM in terms of kinematics, bumper forces and injury prediction.

A framework to estimate the poly-trauma metrics of NISS and WBFCI using the frequency of real-world crash patterns has been presented in chapter 8 using Monte Carlo sampling methods. The proposed method exhibited averaging effect in estimation of WBFCI. From a design perspective, the Monte Carlo method of poly-trauma metric evaluation transforms a multi-output design problem into a single-output problem in terms of either NISS or WBFCI and is the first attempt at defining the outcome of poly-trauma using AIS level injuries without resorting to arbitrary thresholds.

To explore the primary objective of understanding the influence of disabling injuries on vehicle design (for pedestrian crashes), a DOE was conducted in chapter 9 using a parametrized vehicle model representing a sedan. Across the design space, the interquartile range of life years lost due to disability (LYLD) was comparable to life years lost due to fatality (LYLF) at the speed of 25 km/hr. The interquartile range of LYLF was almost six times that of the interquartile range of LYLD at 40 km/hr. From this result, it can be concluded that the influence of disabling injuries on vehicle design diminishes as the risk of fatality increases especially at higher speeds of impact. Additionally, it was noted that presence of brain injuries doubled the LYLF compared to injuries to other body regions. In a hypothetical case of no head injuries, the interquartile range of LYLD was almost three times the interquartile range of LYLF at 25 km/hr. This furthers the importance of considering disabling injuries in vehicle design especially while designing countermeasures like hood deployable airbags that can reduce the chance of occurrence of head injuries. Knee ligament injuries were predicted in case of all the vehicle designs, however this might be an artifact of lack

of the biofidelity of knee joint in lateral bending. It is possible that LYLD is currently being overestimated by the model.

## 10.2 Limitations and Future Work

The design space explored in chapter 9 was limited to a 50<sup>th</sup> percentile being struck laterally by the center of a vehicle at two given speeds, therefore the results cannot be generalized to a population. One of the serious limitations of use of FCI as with any other impairment metric is the lack of validation which makes it difficult to estimate if there is any systematic over or under estimation of injury burden (McMurry et al. (2015)). Secondly, FCI assumes that a subject is young (18-34 years), healthy and given appropriate medical care after sustaining an injury. One can expect the older victims to have a worse impairment outcome than predicted by FCI. Additionally, when injuries are aggregated, as in the case of poly trauma, the worst injury in each dimension was used to calculate the overall disability, but multiple injuries in the same dimension are potentially worse than a single injury. Additionally, the FCI reports the disability associated with injuries one year after the occurrence of injury and by using the FCI values in calculating life years lost due to disability we assume that this doesn't improve over time. This could lead to the FCI potentially overestimating the disability outcome associated with an injury. The several mentioned limitations of FCI needs to be addressed going forward to accurately predict the long term effects of injuries.

There is an inherent limitation in the proposed framework for the estimation of WBFCI and NISS which stems from the dependence of sampling AIS level injuries based on body region specific MAIS levels. If the correlation between different injuries is established, this could be considered in the Monte Carlo sampling to improve the

injury prediction in future.

Most of the injury risk functions reported in the literature do not have age as a covariate. Hence, further analysis on the correlation between age and injury severity for different body regions has to be considered to truly understand the injury outcome at a population level.

The biofidelity of the knee complex has to be improved in the UVAPED model to use the injury risk arising from knee during vehicle design. Currently, the prediction of knee injuries from the model is insensitive to changes in vehicle design.

### 10.3 Contributions

The main contribution of this dissertation is the demonstration of the framework for studying the influence of disability associated with injuries on vehicle design which has not been addressed in the field of injury biomechanics. The benefit of the proposed framework is its utility in reporting a single output from a poly-traumatic event to aid in optimization. It is also an improvement over the current methods of defining arbitrary thresholds for injury metrics to define the severity of injuries in various body regions ([Sankarasubramanian et al. \(2016\)](#)). It has to be noted that the framework developed in this dissertation is applicable to any other impact modes such as a frontal, rear or oblique crashes with the caveat of using injury patterns from the particular crash modes. At higher speeds the influence of disabilities is limited on the vehicle design. Despite that it is recommended to use LYLD as a check, especially when injury severity decreases and fatalities decrease as a result of good vehicle design.

A second contribution would be that this dissertation has developed a validated multibody pedestrian model capable of predicting field relevant injury outcomes. It

outclasses the commercially available TNO ellipsoid models in terms of component biofidelity and outputs injury risks from 17 different body regions classified based on injury mechanisms.

Thirdly, the DOE using a 50<sup>th</sup> percentile male pedestrian impact demonstrated the influence of disability associated with injuries on vehicle design especially at low speeds of impact. This is the first step in addressing the long term consequences of injuries.

Lastly, the dissertation provides a summary of injury mechanisms and relevant injury risk functions for injuries resulting from pedestrian crashes.

# Appendices

# Appendix A Model Description

## A.1 Head and Face

The head consists of a single body, Head\_bod, and Head\_bod is connected to HeadOCLC\_bod using a bracket joint, which constrains all the six degrees of freedom, to measure upper neck forces and moments (Figure A.1). Then, HeadOCLC\_bod is connected to C1 via C1-Head\_jnt using a free joint, which does not constrain any degrees of freedom of the two bodies. Instead, the joint generates restraint forces and moments by C0C1\_sdr (RESTRAINT.SIX\_DOF), which is a set of three orthogonal linear springs and torsional springs.

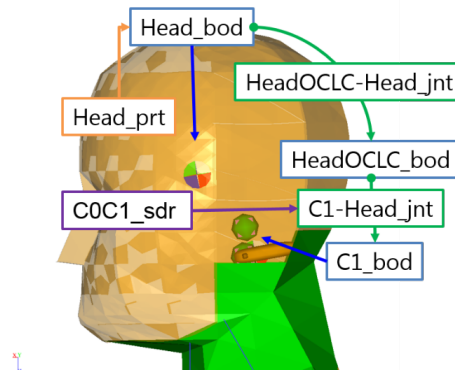


Figure A.1: Schematic of Head and Face in UVAPED Model

## A.2 Neck

The vertebra in the neck was modeled using 2 bodies (one of which represents the vertebrae and another of which acts as a load cell) connected together by a bracket joint to measure internal forces and moments (Figure A.2). Each vertebra is connected to an adjacent one by a free joint (JOINT.FREE). While the free joint does not constrain any degree of freedom of a body, the intervertebral disc was modeled

using 3 linear and 3 torsional springs, which is called RESTRAINT.SIX\_DOF in MADYMO. This modeling scheme was also used for thoracic and lumbar spines.

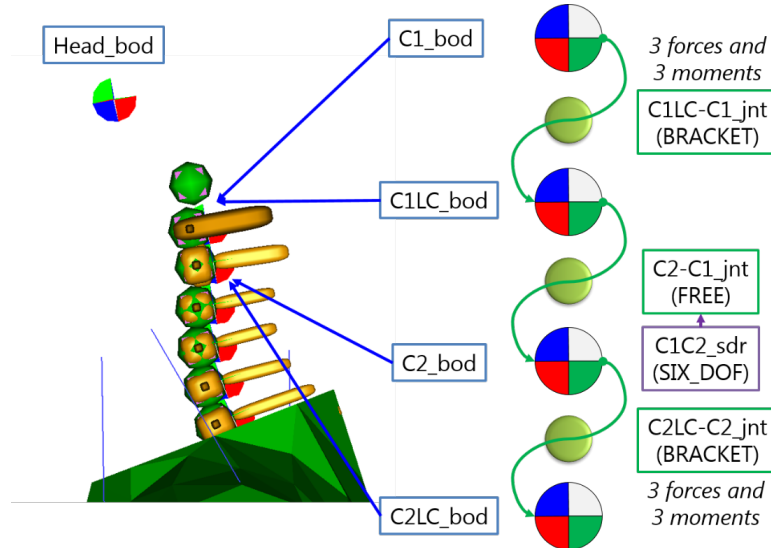


Figure A.2: Schematic of Neck in UVAPED Model

### A.3 Shoulder

The shoulder complex of the UVA pedestrian model is comprised of the arm, scapula, and clavicle connected together by spherical joints, and the clavicle attached to the sternum via a free joint. The sternum was supported by the T3 vertebrae and the scapula was restrained to the T1 and T7 vertebrae (Figure A.3).

### A.4 Thorax

The thorax consists of 4 levels, which has a hoop-like structure, and each level consists of 4 bodies, which are connected to the nearest vertebra in its plane (Figure A.4). For example, the third level of the thorax is comprised of Thorax3Front\_bod, Thorax3L\_bod, Thorax3R\_bod, and Thorax3\_flexbod. The first three bodies were rigid bodies, and those were connected to Thorax3\_flexbod through bracket joints,

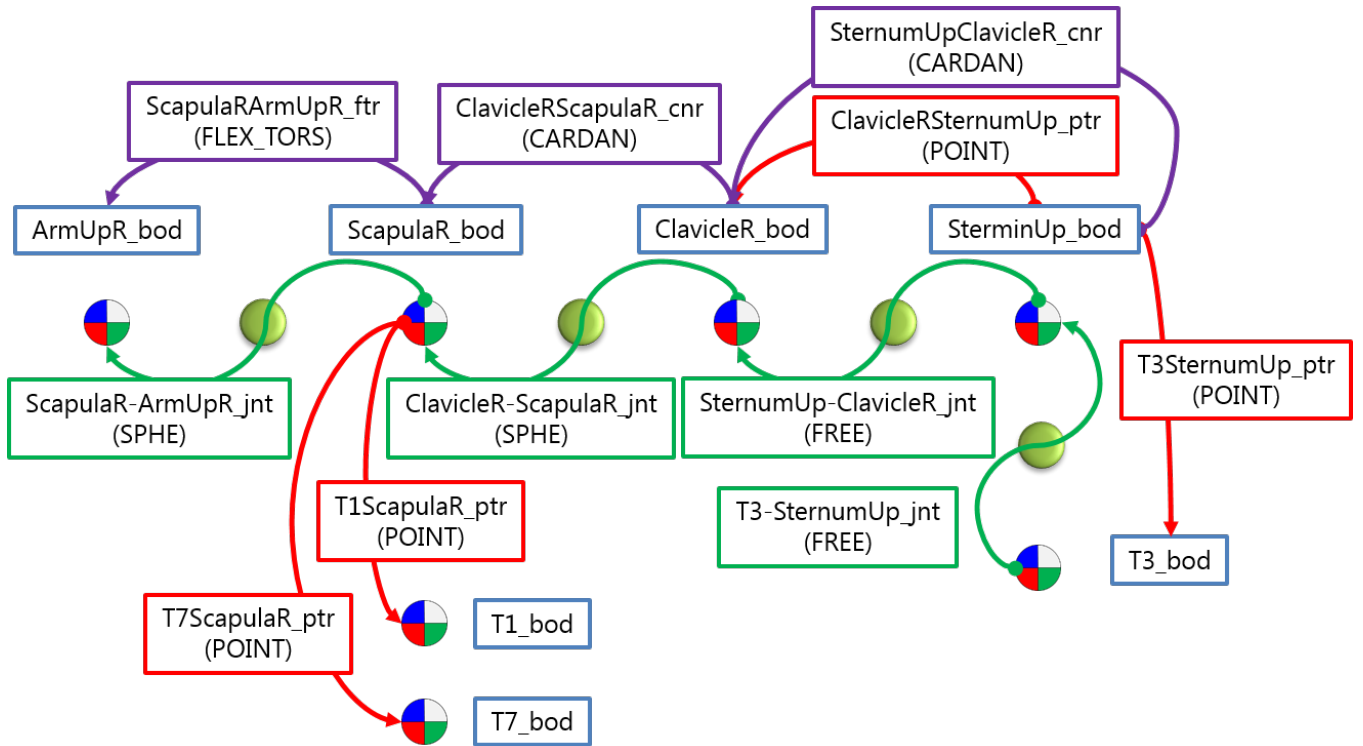


Figure A.3: Schematic of Shoulder Structure

which was a rigid coupling. Point restraints were defined between these three bodies and the T9 vertebral body. These restraints provided mainly axial stiffness, which was along a line connecting each body, e.g., Thorax3Front\_bod, Thorax3L\_bod, and Thorax3R\_bod, and the nearest vertebra, e.g., T9\_bod. Also, the bodies on each hoop were coupled to adjacent levels, e.g., thorax level 4 and thorax level 2. The Thorax3\_flexbod was a deformable body to which all the other bodies were rigidly attached, and the deformation of flexible bodies was represented as a linear combination of three pre-defined three mode shapes (Figure A.5). There was a symmetric mode for anterior posterior deformation and two asymmetric modes for mediolateral deformation. The stiffness of these deformation modes was almost negligible compared to the stiffness provided by point restraints between rigid bodies and the nearest vertebra. The purpose of the flexible body was to fit the geometry of the thorax to positions of

the displaced rigid bodies on a thorax level.

The structure of the abdomen region of the UVAPED model was the same as that of the thorax region. The abdomen consisted of 4 levels similar to the thorax region, and it connected the thoracic and pelvis regions.

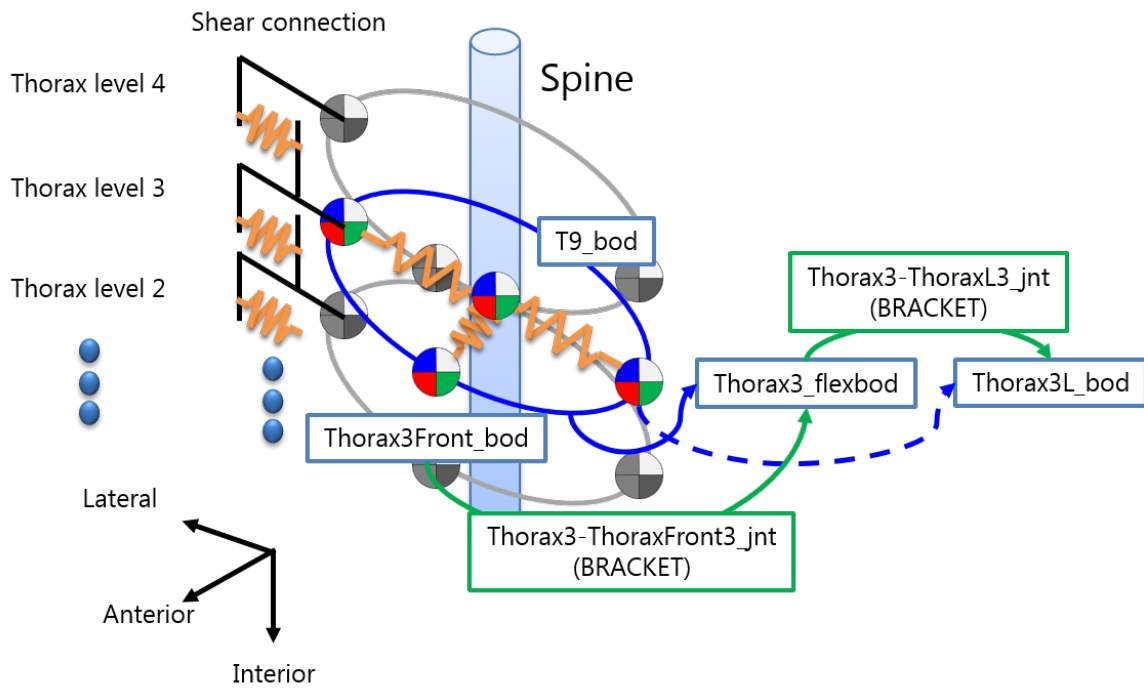


Figure A.4: Schematic of Thorax

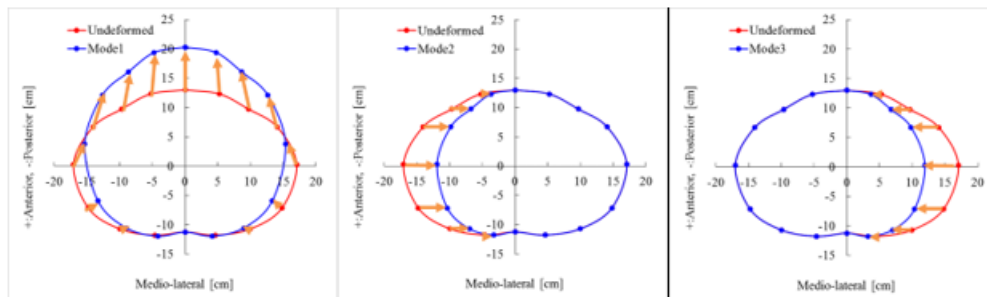


Figure A.5: Mode Shapes of Thorax

## A.5 Pelvis

The Pelvis body connects the spine and lower extremities via the sacrum and hip joint. The Pelvis-Sacrum\_jnt is a BRACKET joint, which constrains all the six degrees of freedoms between pelvis\_bod and sacrum\_bod, and Hip\_jnt is a spherical joint, which constrains relative linear motion between pelvis\_bod and RThigh1\_bod or LThigh1\_bod, which represents proximal thigh region. For the rotational stiffness of the Hip\_jnt, a CARDAN restraint was defined for all the three rotational directions.

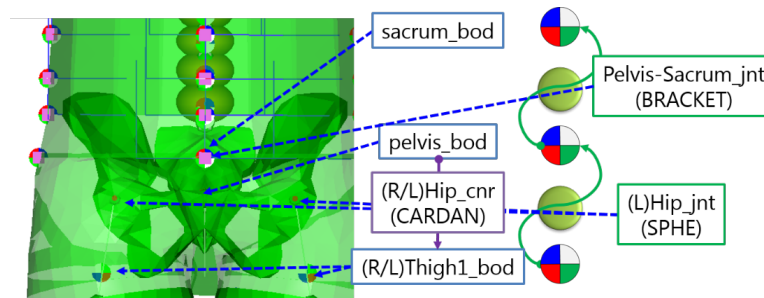


Figure A.6: Schematic of Pelvis

## A.6 Thigh and leg

The joint based models in the lower extremities were converted to beam based models (Figure A.7). Details regarding the modeling approach will be provided in the dissertation and a summary of the approach can be found in (Bollapragada et al. (2016)). The flesh of the lower extremities has been modeled as deformable, similar to the thorax, using a hoop like structure.

## A.7 Knee

The knee complex consists of three bodies; distal thigh body, KneeFX\_bod, and proximal leg body, joined together by RKneePostFX\_jnt and RKneePreFX\_jnt.

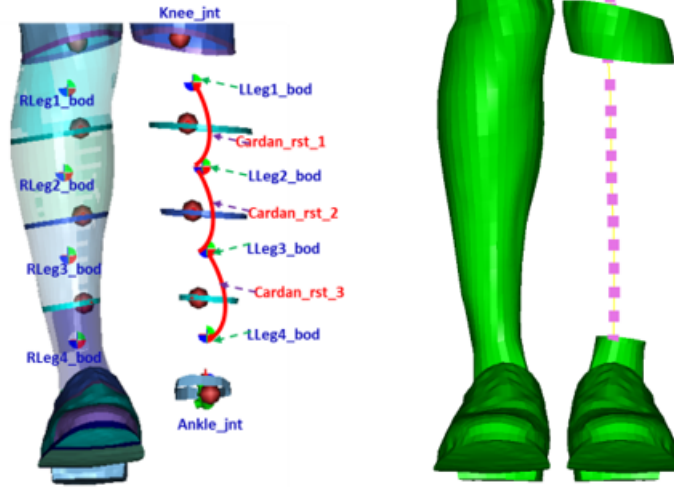


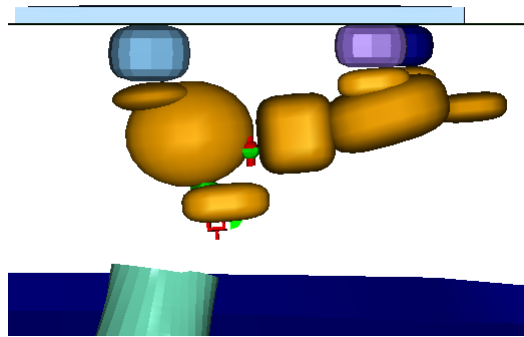
Figure A.7: Lower Extremity Kerrigan (left) UVAPED (right)

Initially, RKneePreFX\_jnt is unlocked and RKneePostFX\_jnt is locked. If the Varus/Valgus rotation reaches a fracture threshold, 16.2 deg, or the lateromedial shear deflection reaches 25.2 mm with fracture enabled model. At the same time, the joint RKneePreFX\_jnt, which connects RKneeFX\_bod and RLeg1\_bod, is locked.

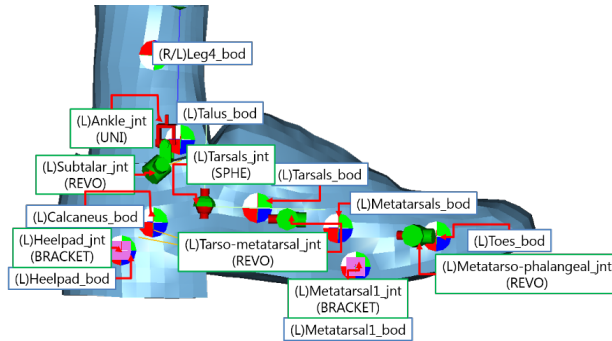
## A.8 Ankle/Foot

The ankle and foot of the UVAPED model, was developed by Hall (1999). It is connected to the distal leg through the Ankle\_jnt. It consists of 7 rigid bodies and 7 kinematic joints per foot. The ellipsoid surfaces of the initial model developed by Hall (1998) were replaced by facet surface for better contact interaction with other surfaces (Figure A.8a and A.8b). The (L)Ankle\_jnt has two rotational degrees of freedom for dorsiflexion/plantarflexion and inversion/eversion (Figure A.8), and the (L)Subtalar\_jnt, which is a REVO joint, provide rotational degree of freedom between (L)Calcaneus\_bod and (L)Talus\_bod. The (L)Tarso-metatarsal\_jnt and (L)Metatarso-phalangeal\_jnt connect (L)Tarsal\_bod, (L)Metatarsals\_bod, and (L)Toes\_bod. The

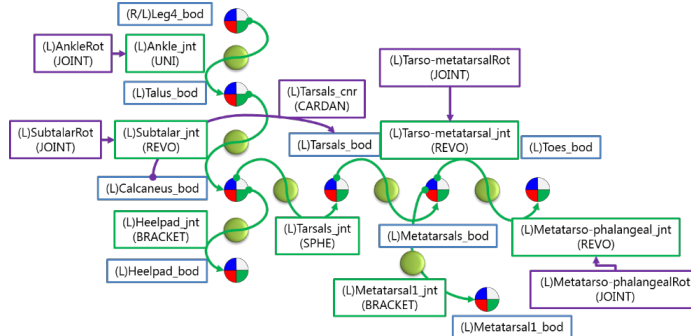
(L)Heelpad\_bod and (L)Metatarsal1\_bod was connected to (L) Calcaneus\_bod and (L)Metatarsals\_bod using (L)Heelpad\_jnt and (L)Metatarsal1\_jnt. All the joints except two BRACKET joints, have stiffness with respect to its degrees of freedom using JOINT or CARDAN restraints.



(a) Ankle and Foot Model Developed by Hall (1999)



(b) (Ankle and Foot Model With Facet Surface



(c) Ankle and Foot Model With Facet surface

Figure A.8: Schematic of Ankle/Foot Structure

# Appendix B Component Validation

## B.1 Head Frontal Impact

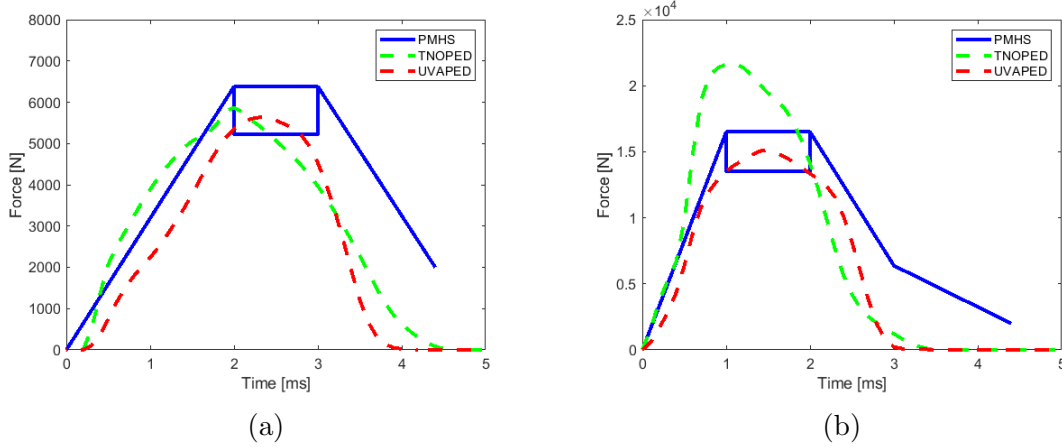


Figure B.1: Head Frontal Impact (Melvin et al. (1985)) (a) 2 m/s (b) 5.5 m/s

## B.2 Forehead drop test

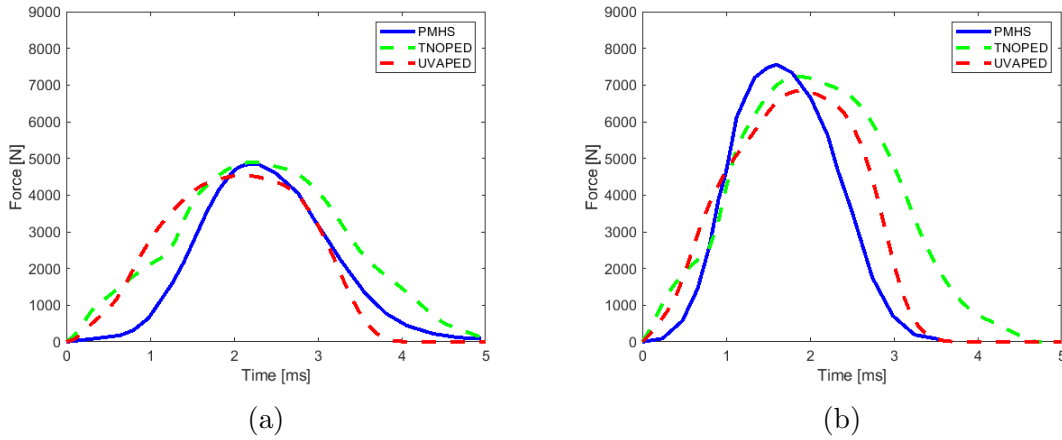


Figure B.2: Forehead Drop Test (Loyd et al. (2012)) (a) 1.1 m/s (b) 2.4 m/s

### B.3 Lateral Shoulder Impact

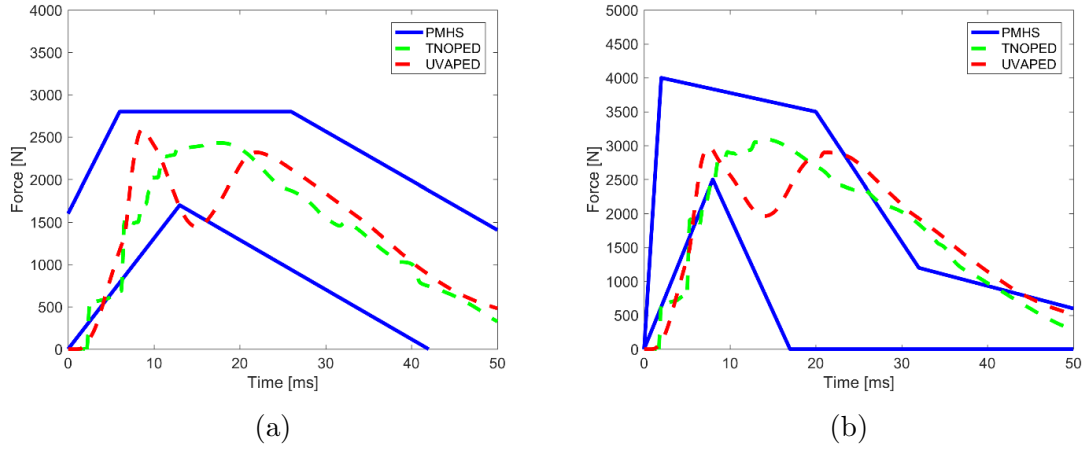


Figure B.3: Lateral Shoulder Impact (ISO (1997)) (a) 4.5 m/s (b) 5.5 m/s

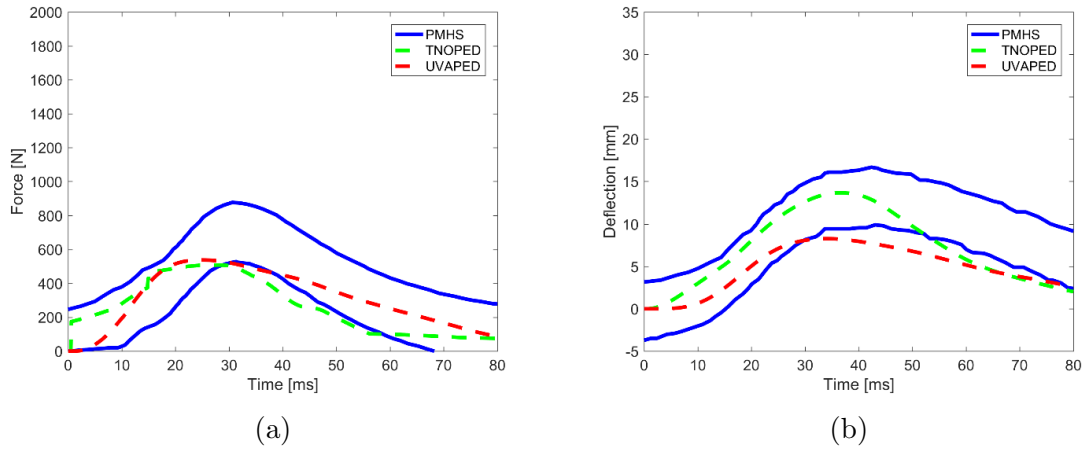
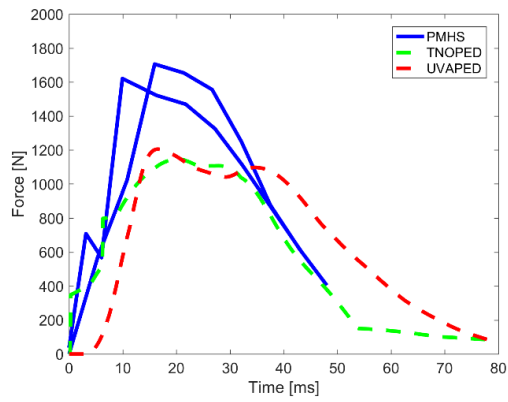
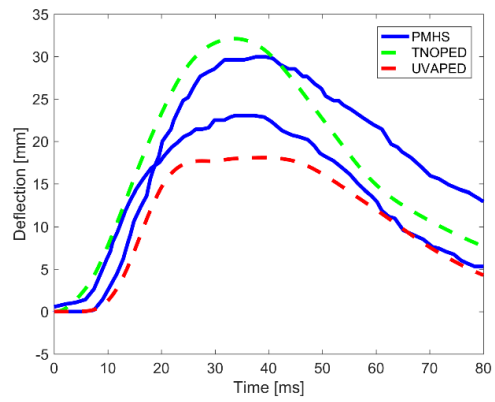


Figure B.4: Lateral Shoulder Impact 1.5 m/s (Compigne et al. (2004))

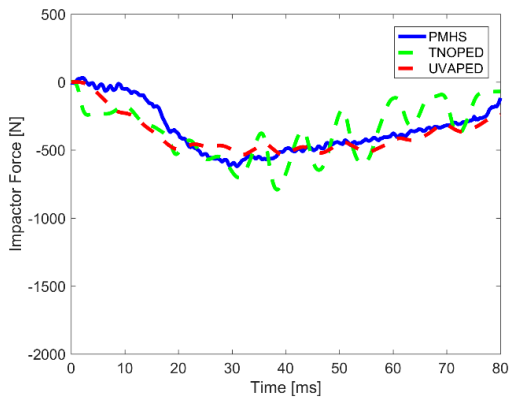


(a)

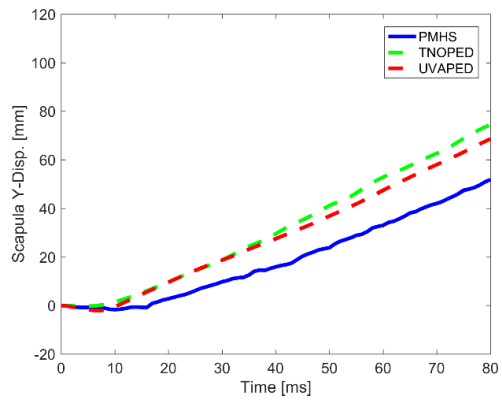


(b)

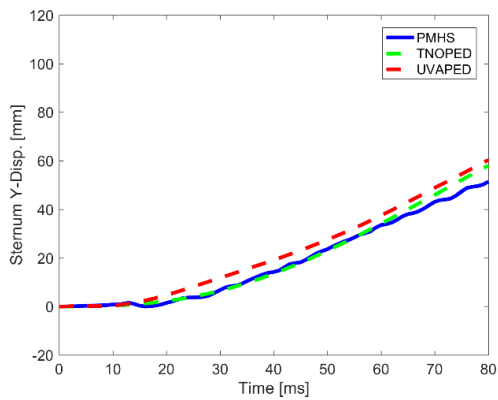
Figure B.5: Lateral Shoulder Impact 3 m/s (Compigne et al. (2004))



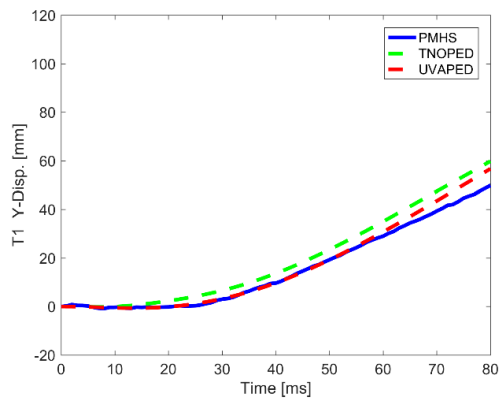
(a)



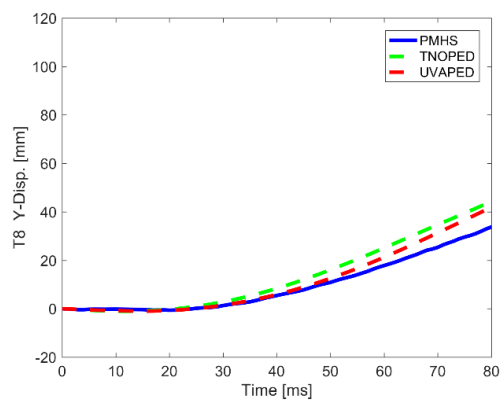
(b)



(c)

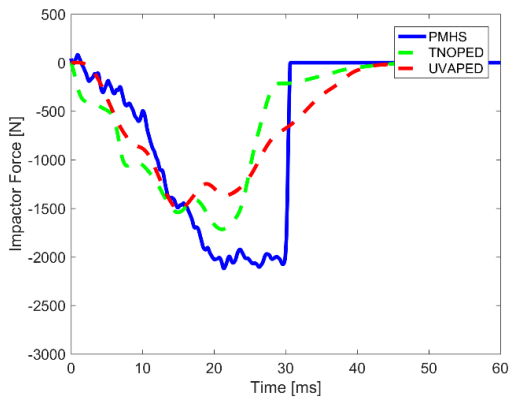


(d)

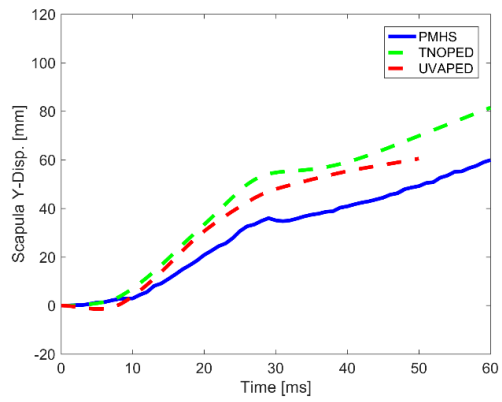


(e)

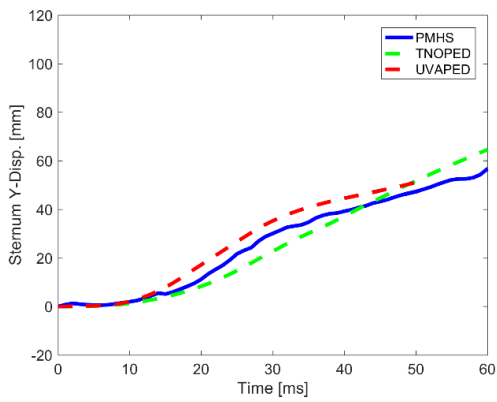
Figure B.6: Lateral Shoulder Impact 1 m/s (Subit et al. (2010))



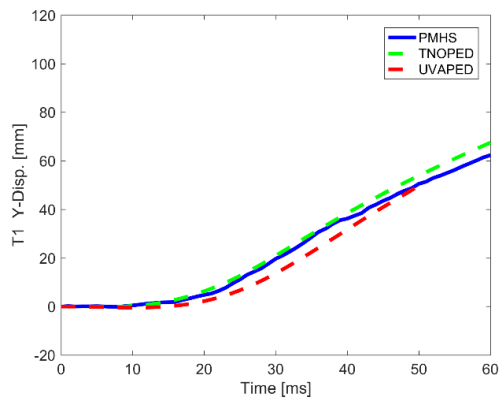
(a)



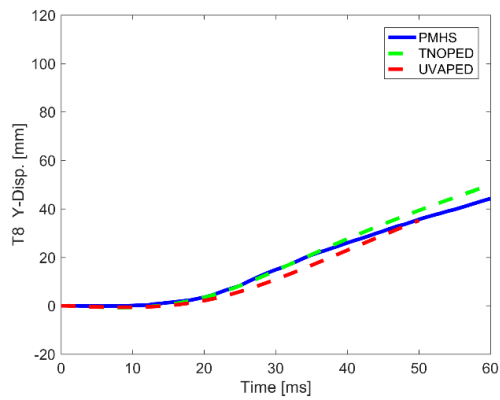
(b)



(c)



(d)



(e)

Figure B.7: Lateral Shoulder Impact 3 m/s (Subit et al. (2010))

## B.4 Frontal Thoracic Impact

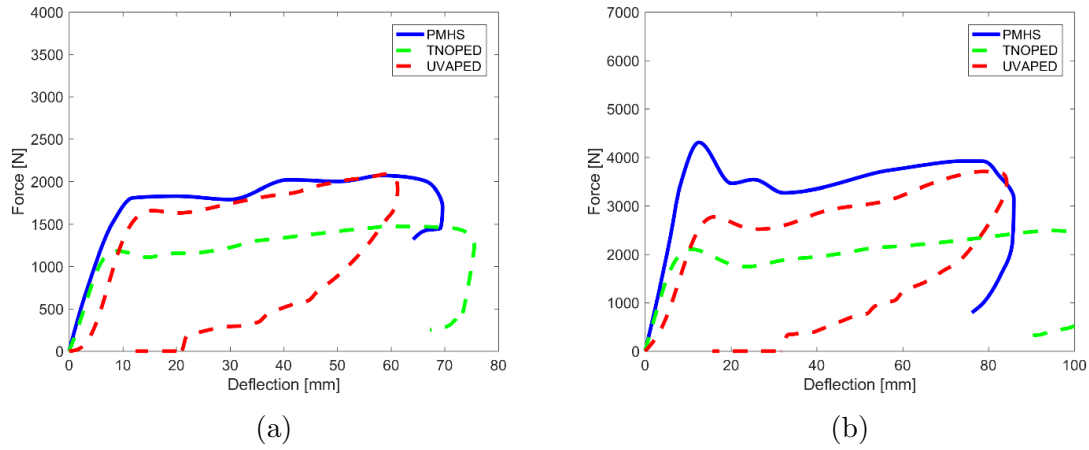


Figure B.8: Frontal Thoracic Impact (Kroell et al. (1971)) (a) 4.3 m/s (b) 6.7 m/s

## B.5 Lateral Thoracic Impact

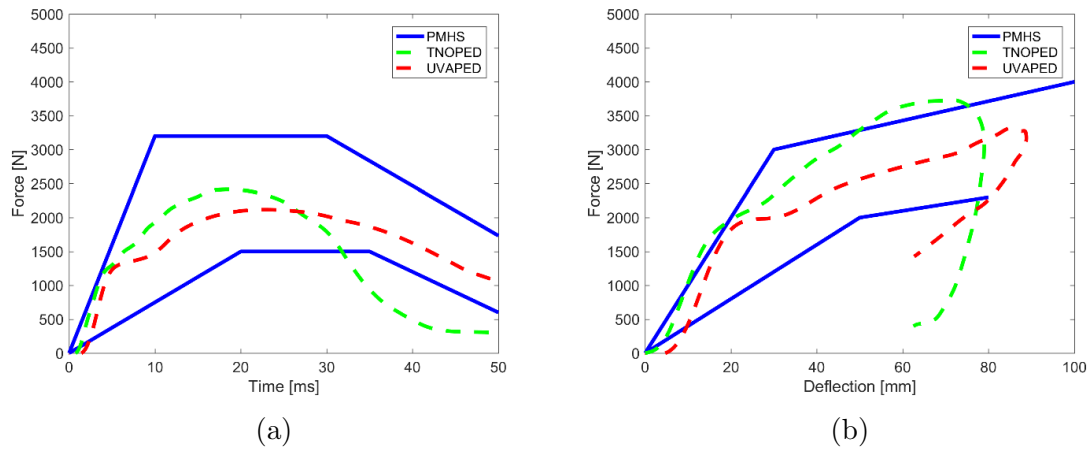
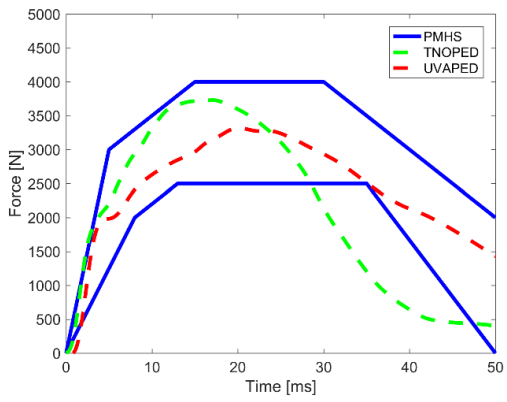
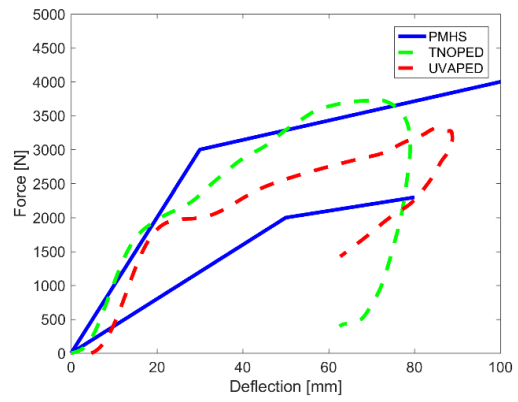


Figure B.9: Lateral Thoracic Oblique Impact (Viano et al. (1989)) 4.4 m/s

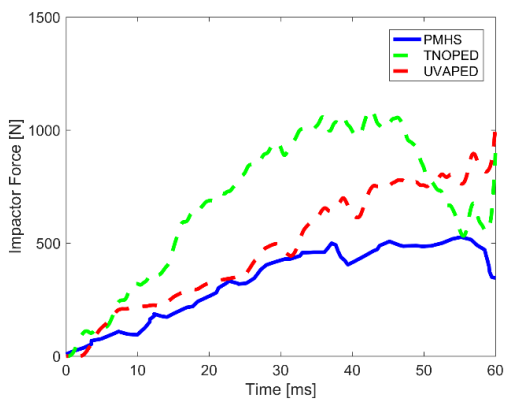


(a)

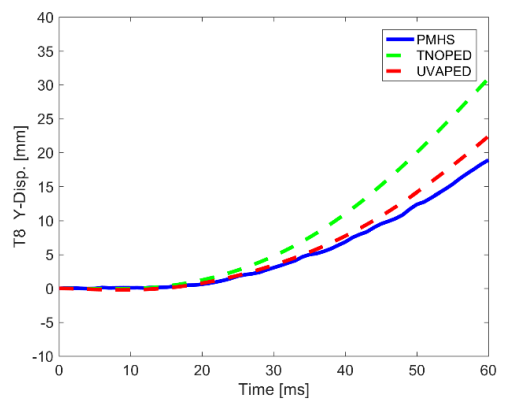


(b)

Figure B.10: Lateral Thoracic Oblique Impact (Viano et al. (1989) 6.5 m/s

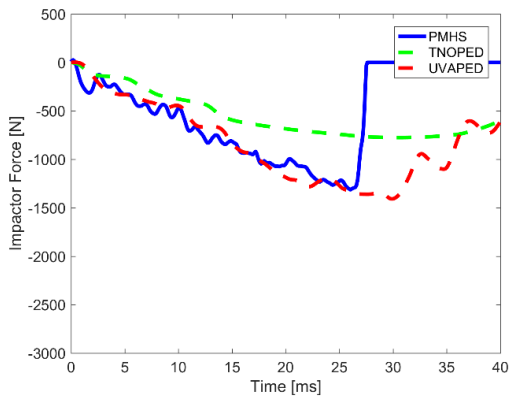


(a)

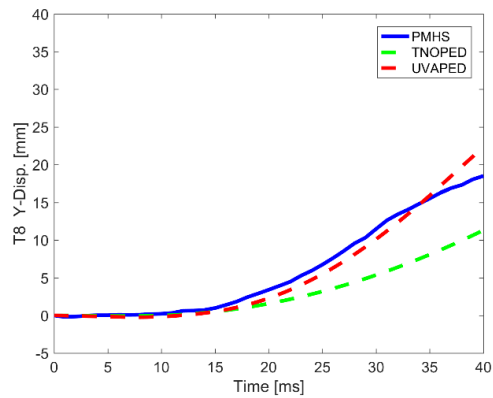


(b)

Figure B.11: Lateral Thoracic Mid Impact (Subit et al. (2010)) 1 m/s

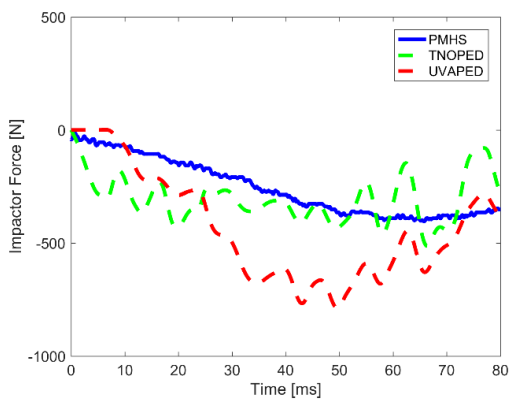


(a)

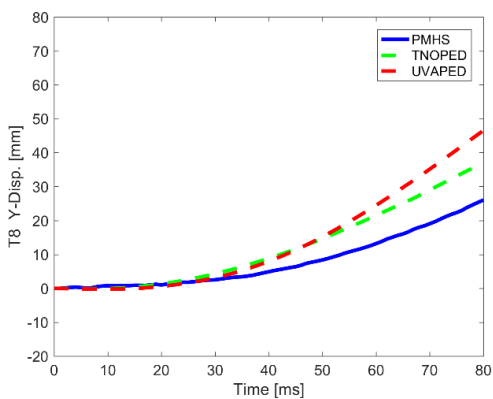


(b)

Figure B.12: Lateral Thoracic Mid Impact (Subit et al. (2010)) 3 m/s

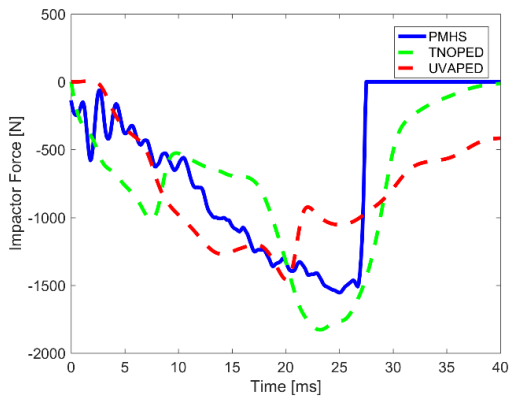


(a)

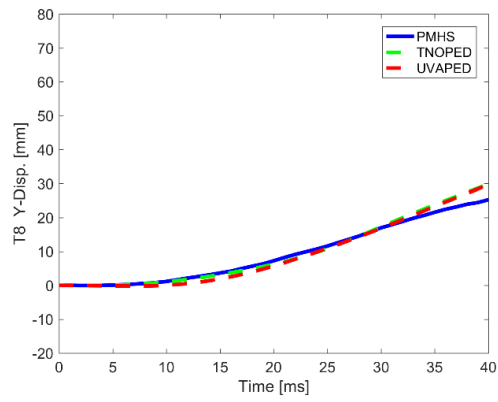


(b)

Figure B.13: Lateral Thoracic Up Impact (Subit et al. (2010)) 1 m/s

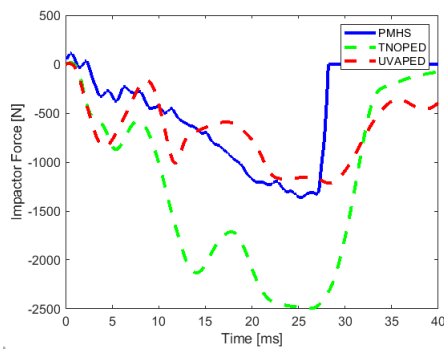


(a)

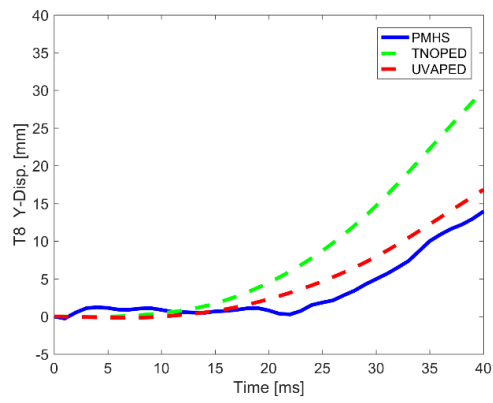


(b)

Figure B.14: Lateral Thoracic Up Impact (Subit et al. (2010)) 3 m/s

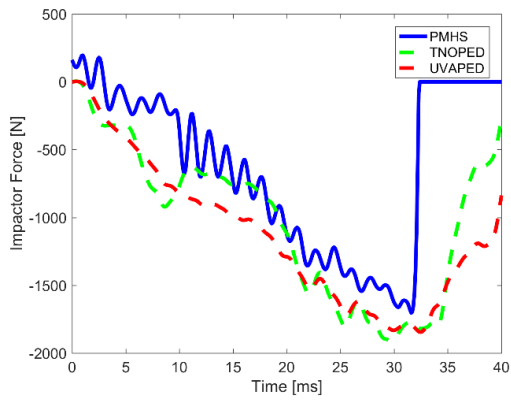


(a)

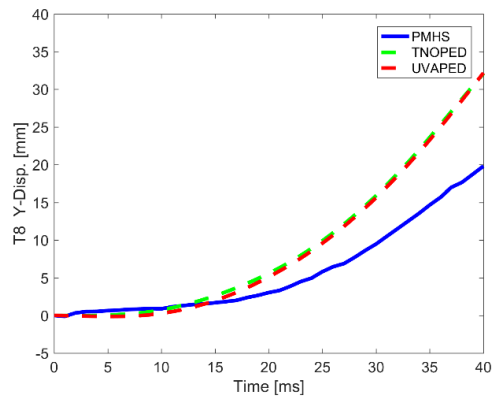


(b)

Figure B.15: Lateral Thoracic AL 15 deg Mid Impact (Subit et al. (2010)) 3 m/s

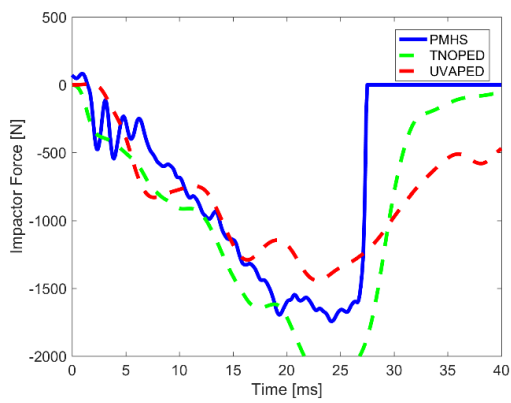


(a)

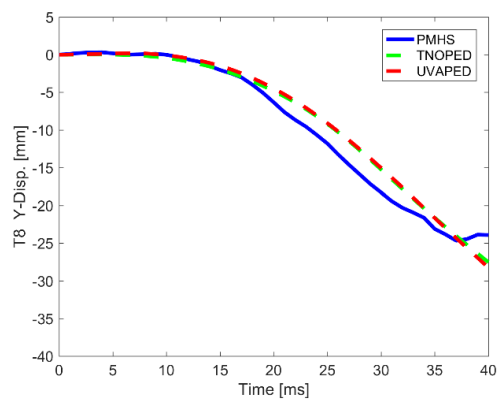


(b)

Figure B.16: Lateral Thoracic AL 15 deg Up Impact (Subit et al. (2010)) 3 m/s



(a)



(b)

Figure B.17: Lateral Thoracic PL 15 deg Mid Impact (Subit et al. (2010)) 3 m/s

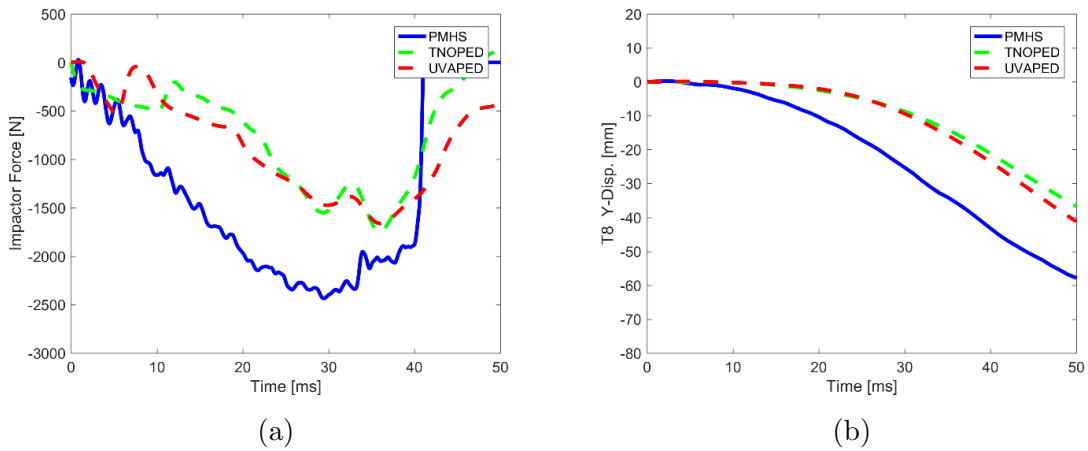


Figure B.18: Lateral Thoracic PL 15 deg Up Impact (Subit et al. (2010)) 3 m/s

## B.6 Abdomen Frontal Impact

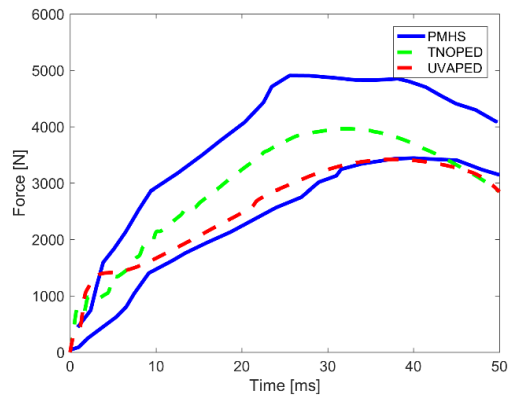


Figure B.19: Abdomen Frontal Impact (Cavanaugh et al. (1986)) 6.1 m/s

## B.7 Abdomen Lateral Impact

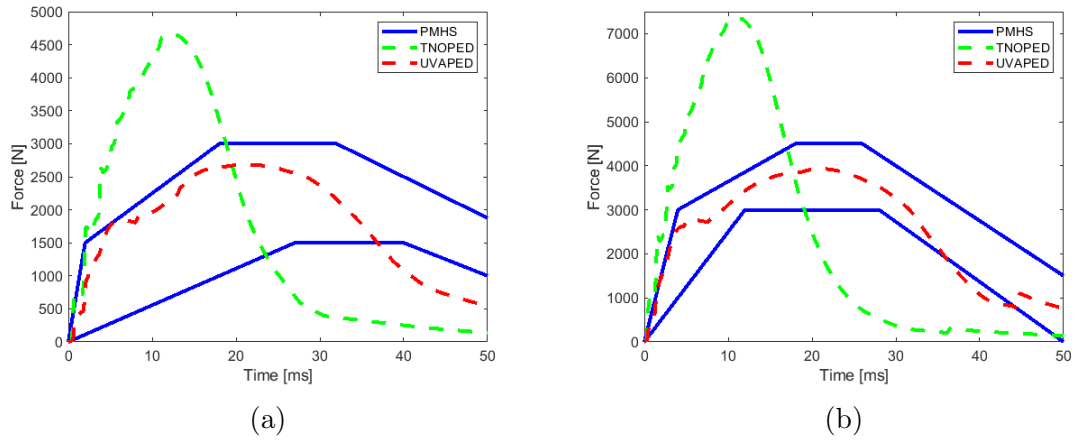


Figure B.20: Abdomen Lateral Impact (Viano et al. (1989)) (a) 4.8 m/s (b) 6.8 m/s

## B.8 Pelvis Lateral Impact

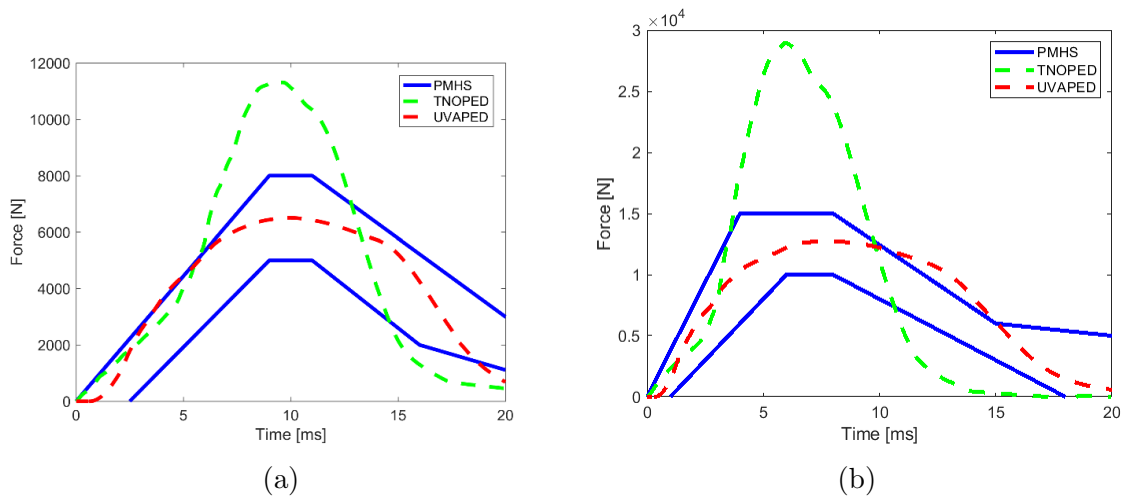


Figure B.21: Pelvis Lateral Impact (Viano et al. (1989)) (a) 4.5 m/s (b) 9.6 m/s

## B.9 Thigh and Leg Three-point Bending

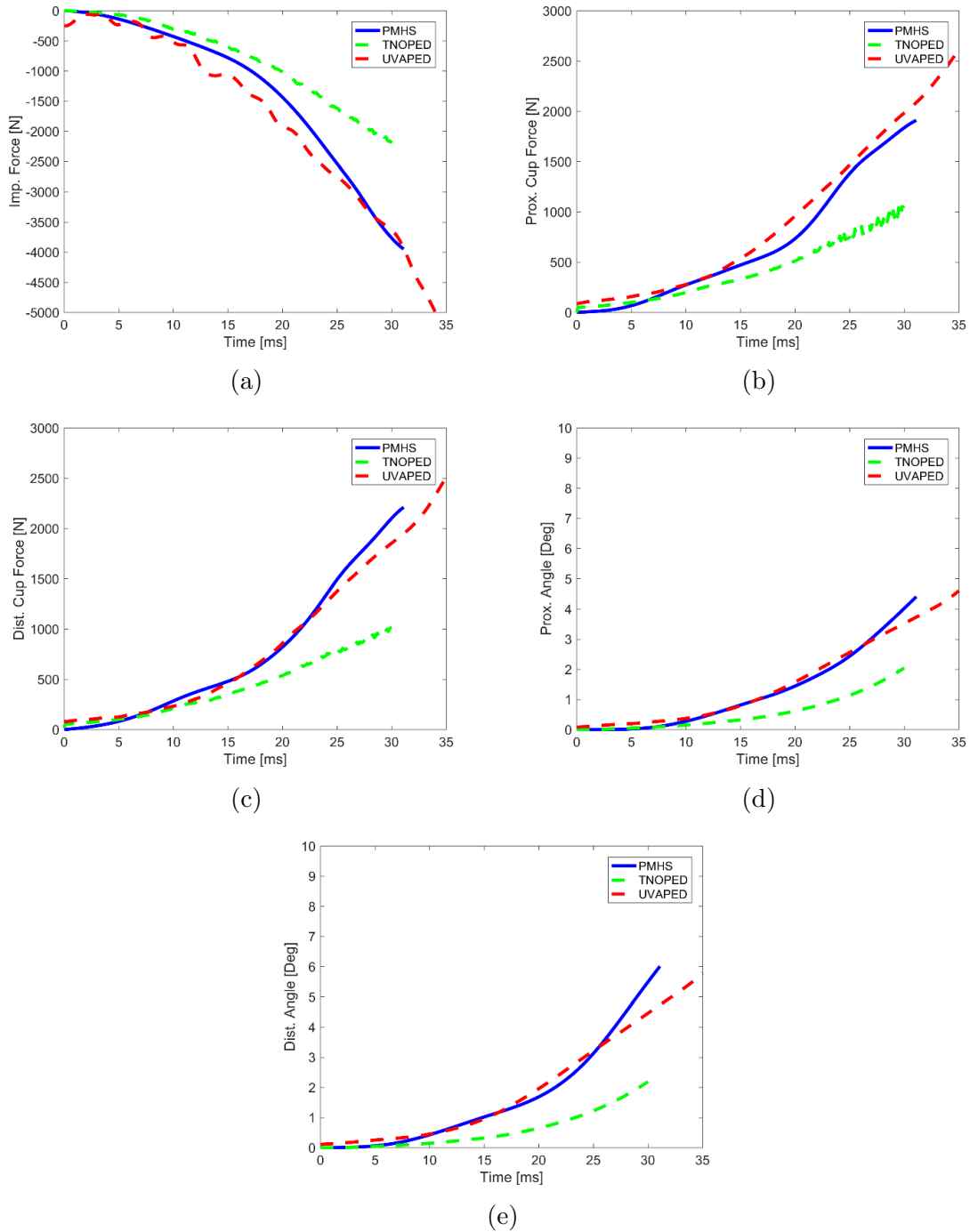


Figure B.22: Mid-Thigh Three Point Bending (Kerrigan et al. (2004)) 1.5 m/s

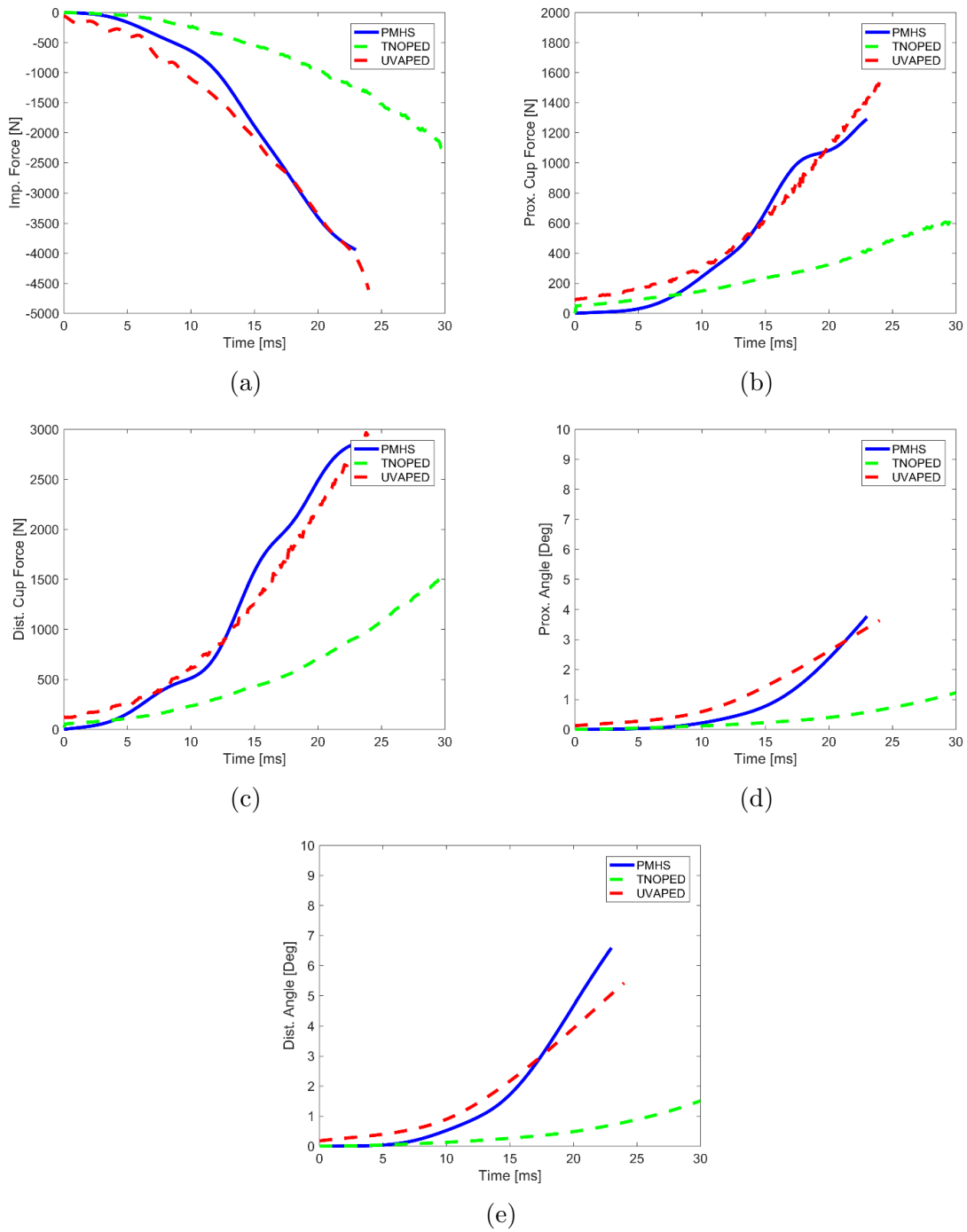
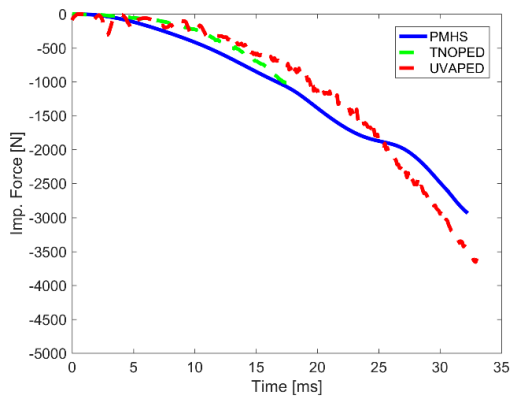
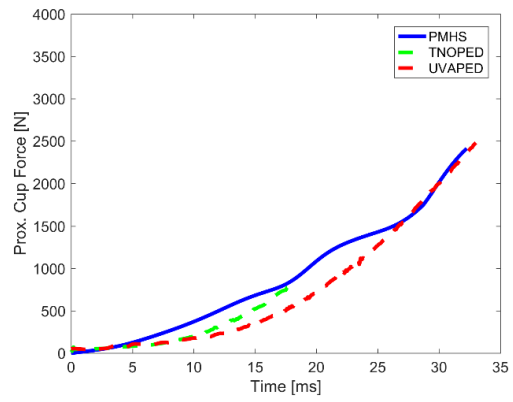


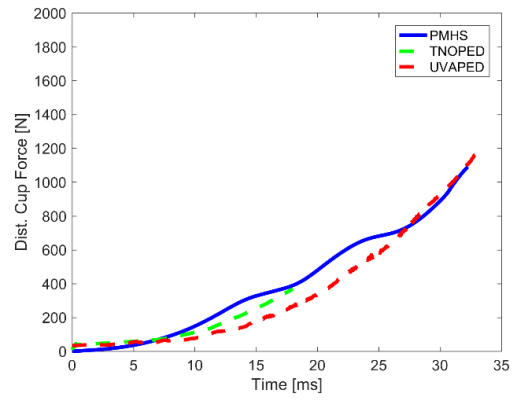
Figure B.23: Distal Thigh Three Point Bending (Kerrigan et al. (2004)) 1.5 m/s



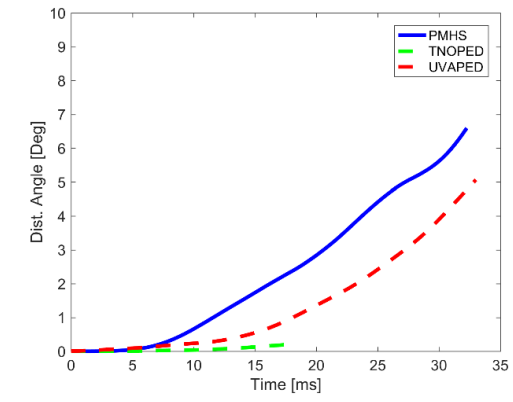
(a)



(b)

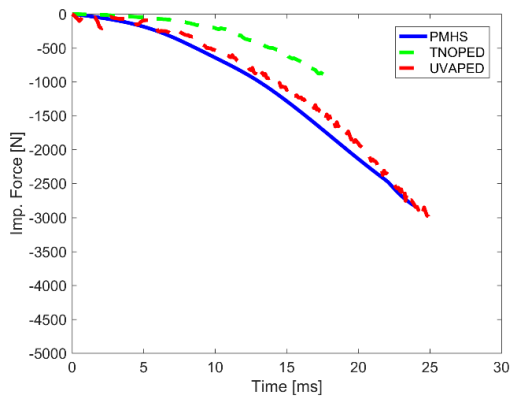


(c)

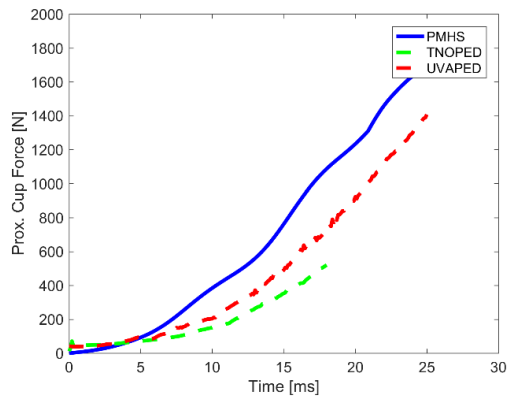


(d)

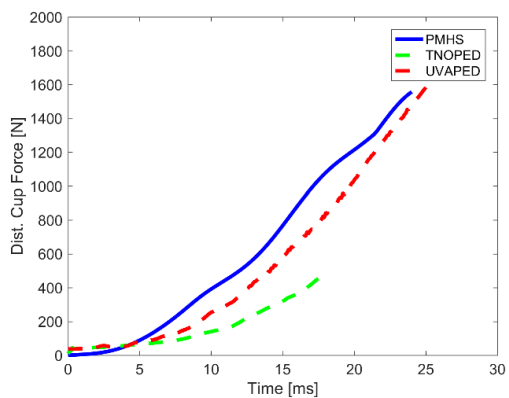
Figure B.24: Proximal Leg Three Point Bending (Kerrigan et al. (2004)) 1.5 m/s



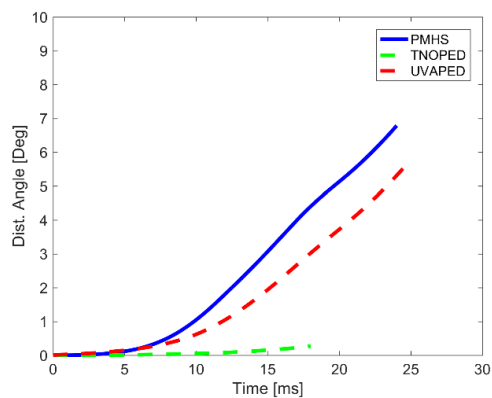
(a)



(b)

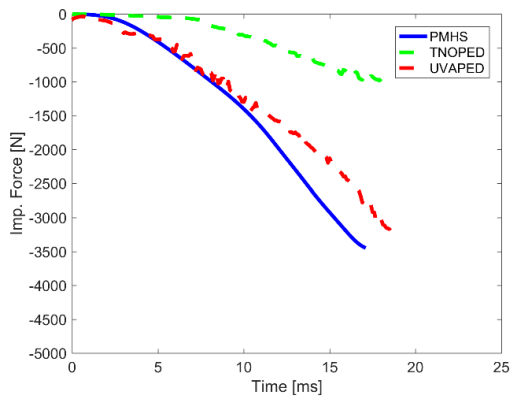


(c)

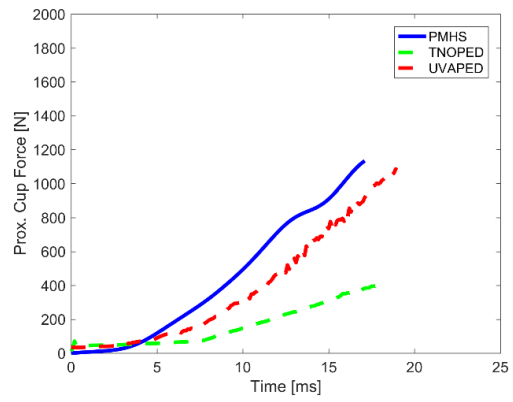


(d)

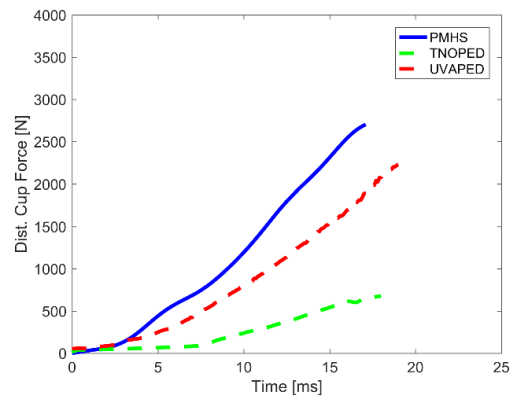
Figure B.25: Mid Leg Three Point Bending (Kerrigan et al. (2004)) 1.5 m/s



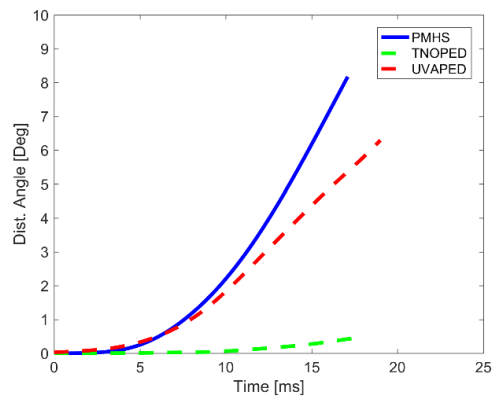
(a)



(b)



(c)



(d)

Figure B.26: Distal Leg Three Point Bending (Kerrigan et al. (2004)) 1.5 m/s

# Appendix C Whole-body evaluation

## C.1 Local Coordinate Systems

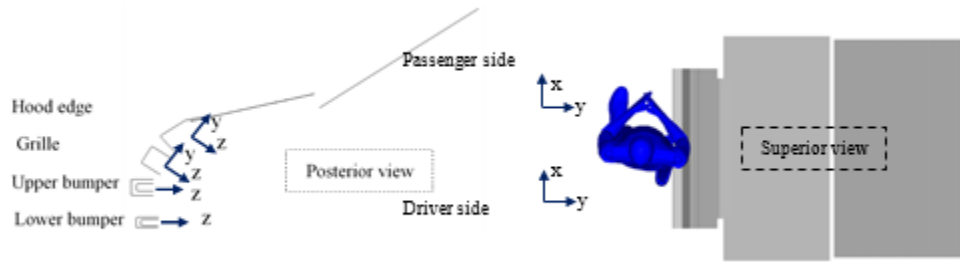


Figure C.1: Force Measurement Location and Coordinate System

The results from three PMHS tests have been summarized in each figure in this appendix. They follow the order V2370 (test 1), V2371 (test2) and V2374 (test3) respectively.

## C.2 Acceleration

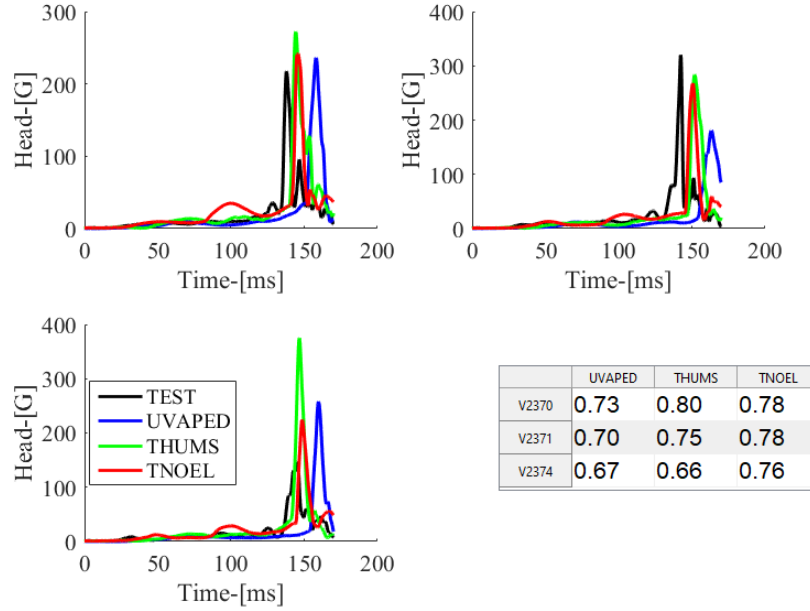


Figure C.2: Head Resultant Acceleration

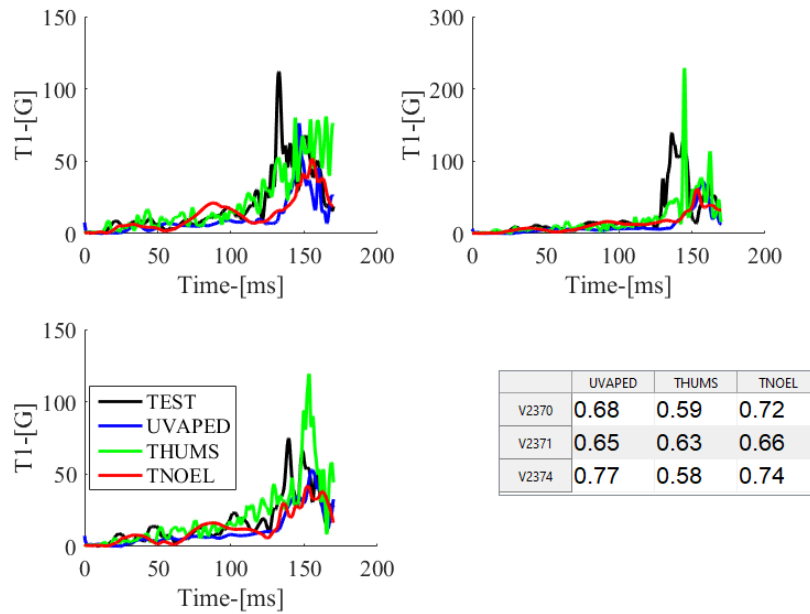


Figure C.3: T1 Resultant Acceleration

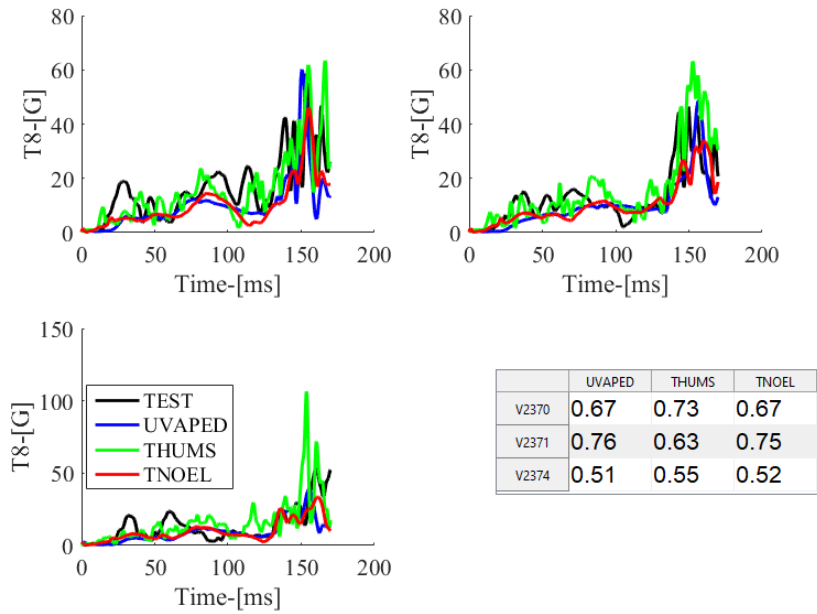


Figure C.4: T8 Resultant Acceleration

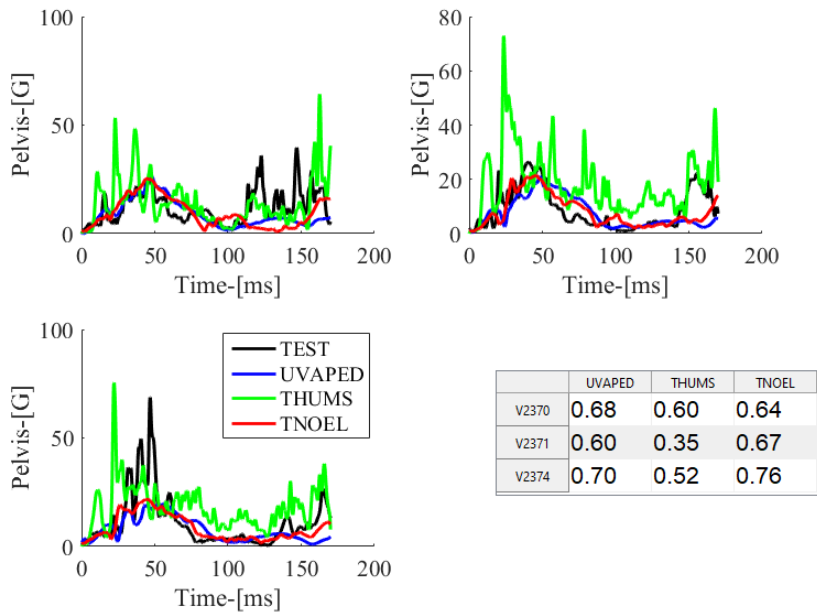


Figure C.5: Pelvis Resultant Acceleration

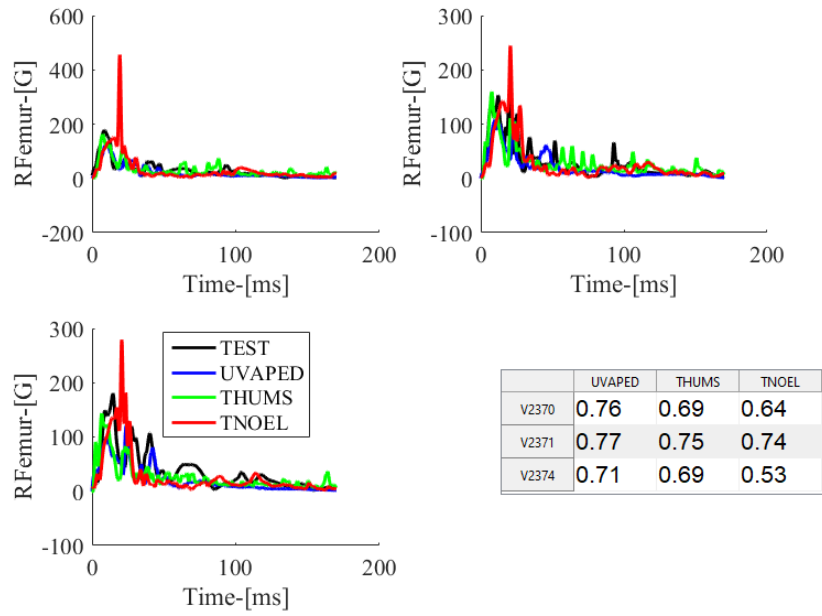


Figure C.6: RFemur Resultant Acceleration

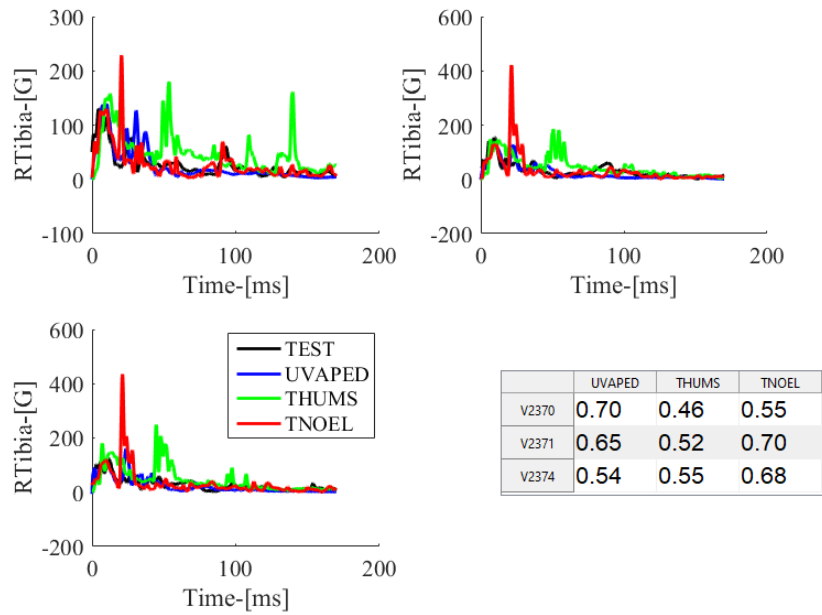


Figure C.7: RTibia Resultant Acceleration

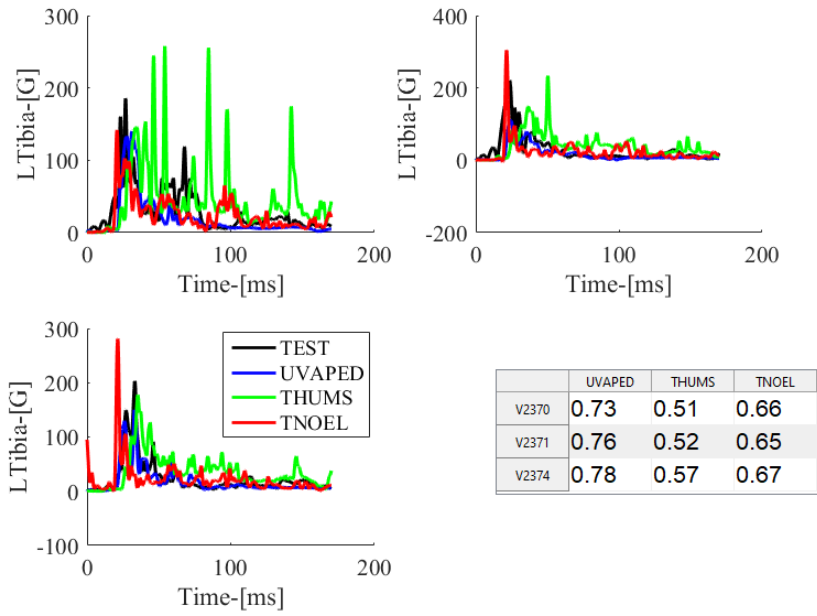


Figure C.8: LTibia Resultant Acceleration

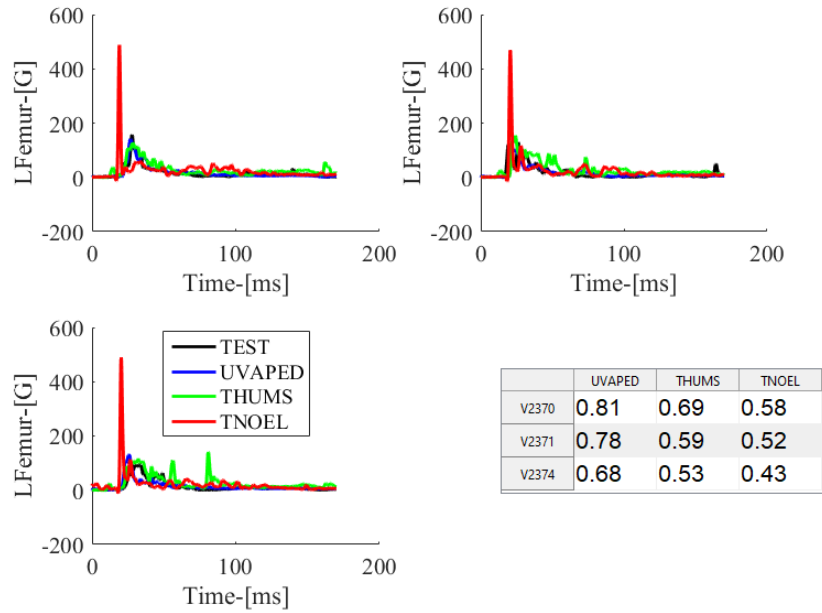


Figure C.9: LFemur Resultant Acceleration

### C.3 Angular velocity (X)

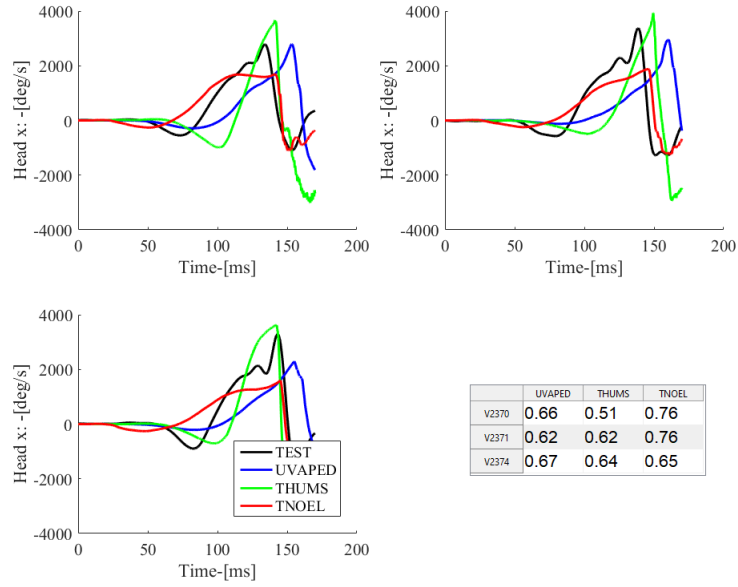


Figure C.10: Head Angular Velocity (X)

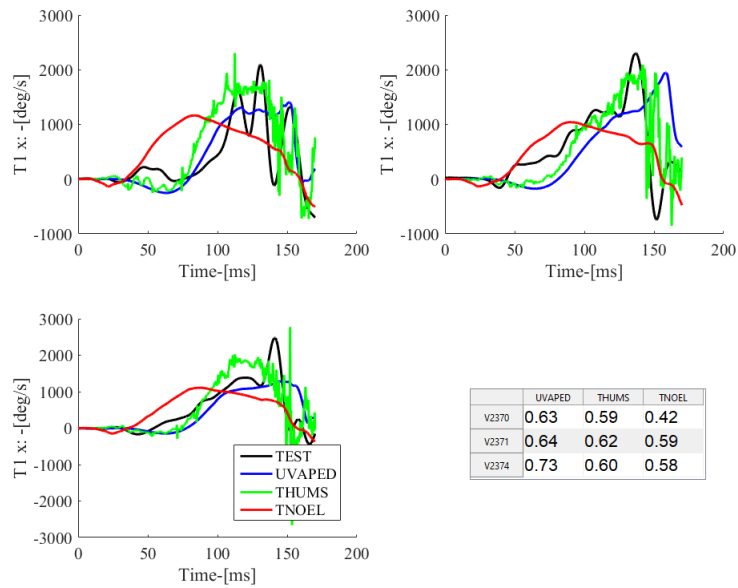


Figure C.11: T1 Angular Velocity (X)

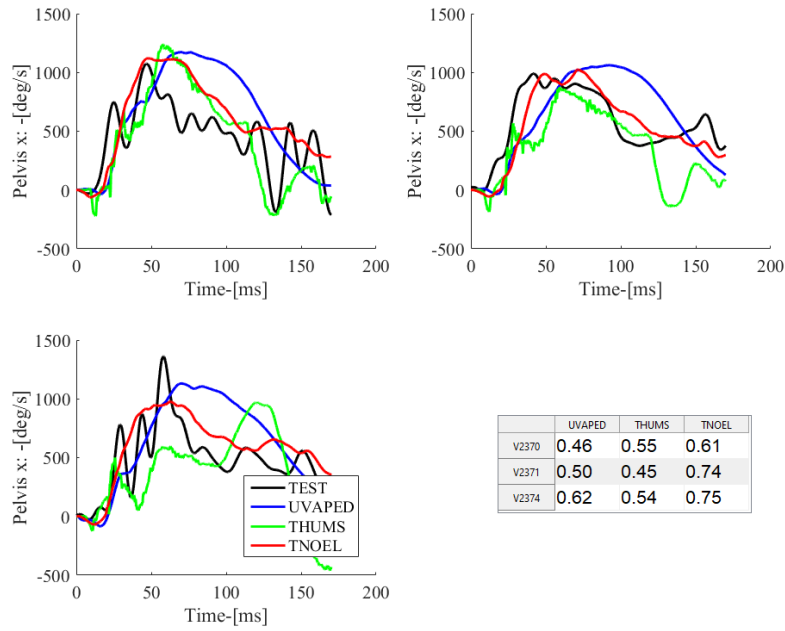


Figure C.12: Pelvis Angular Velocity (X)

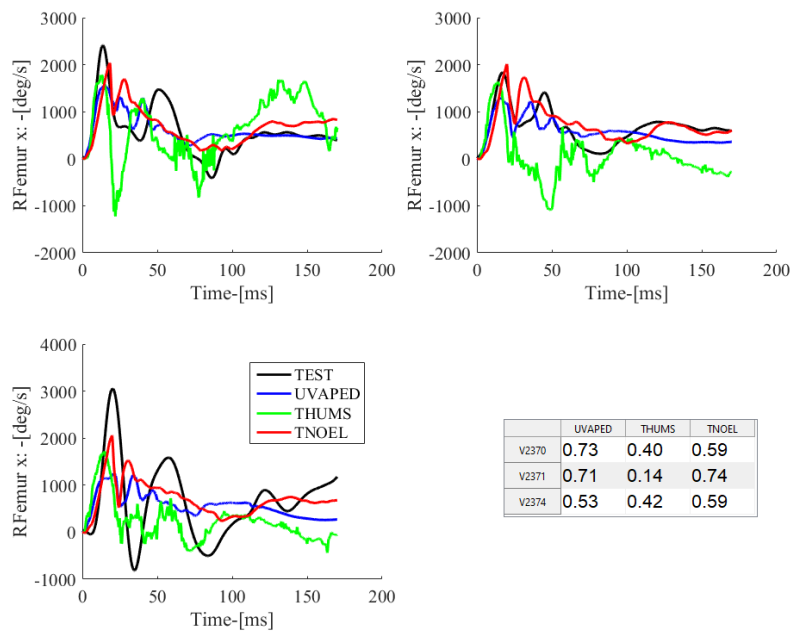


Figure C.13: RFemur Angular Velocity (X)

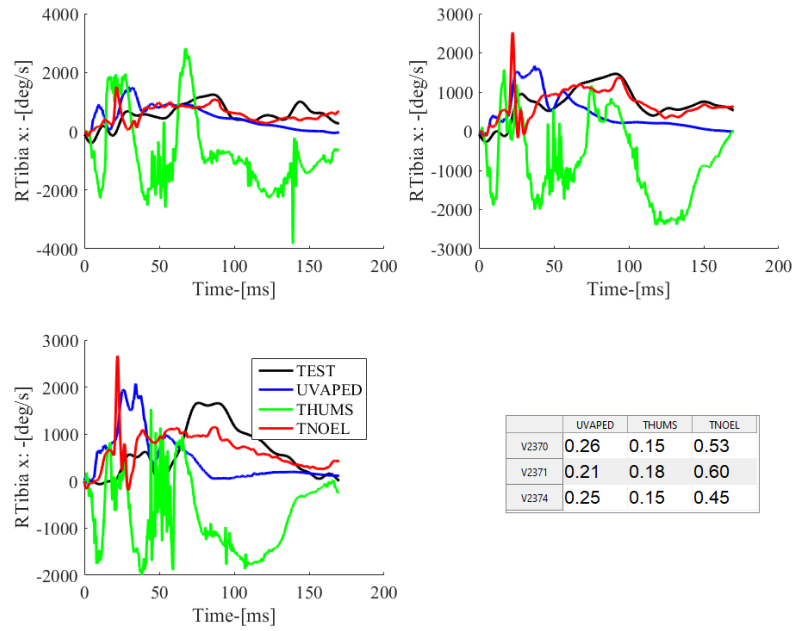


Figure C.14: RTibia Angular Velocity (X)

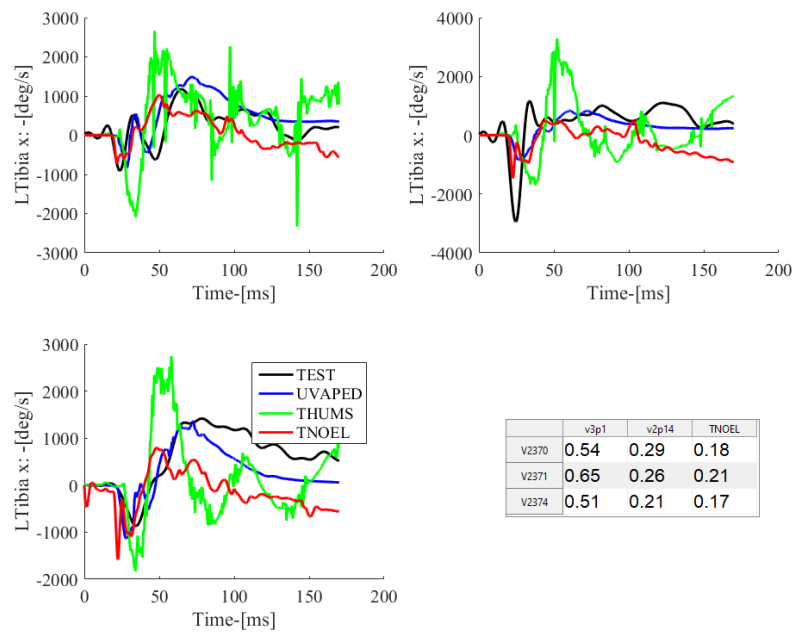


Figure C.15: LTibia Angular Velocity (X)

## C.4 Angular Velocity (Y)

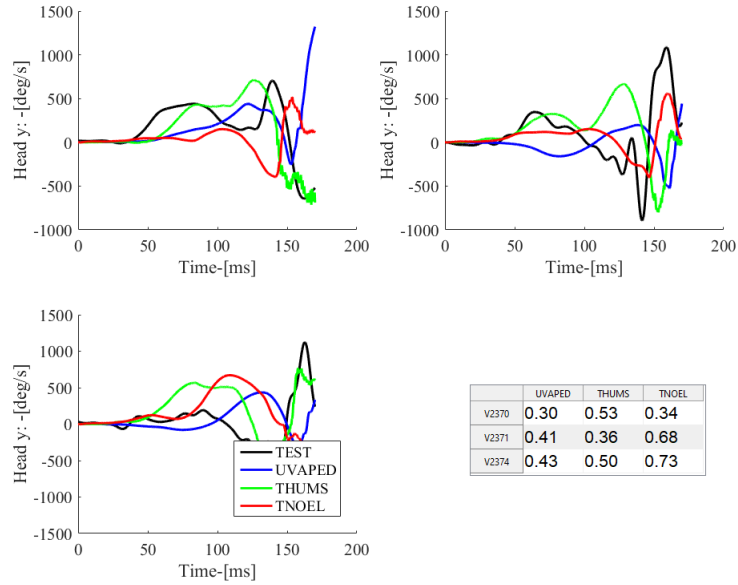


Figure C.16: Head Angular Velocity (Y)

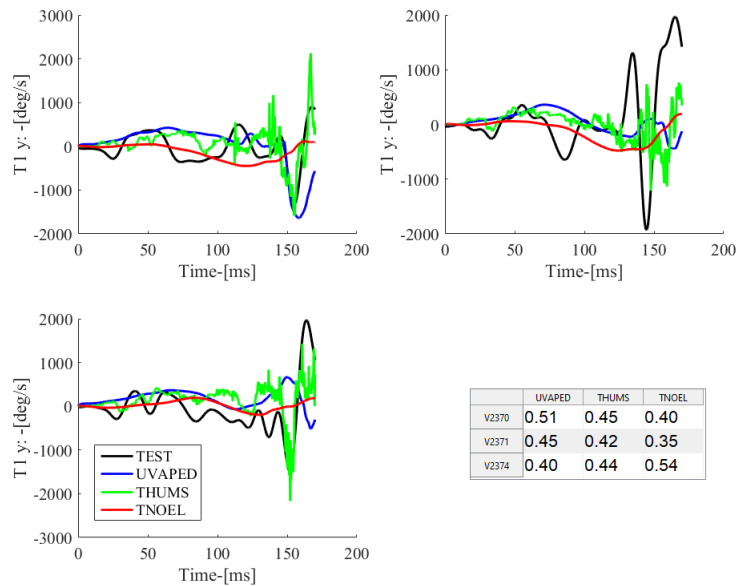


Figure C.17: T1 Angular Velocity (Y)

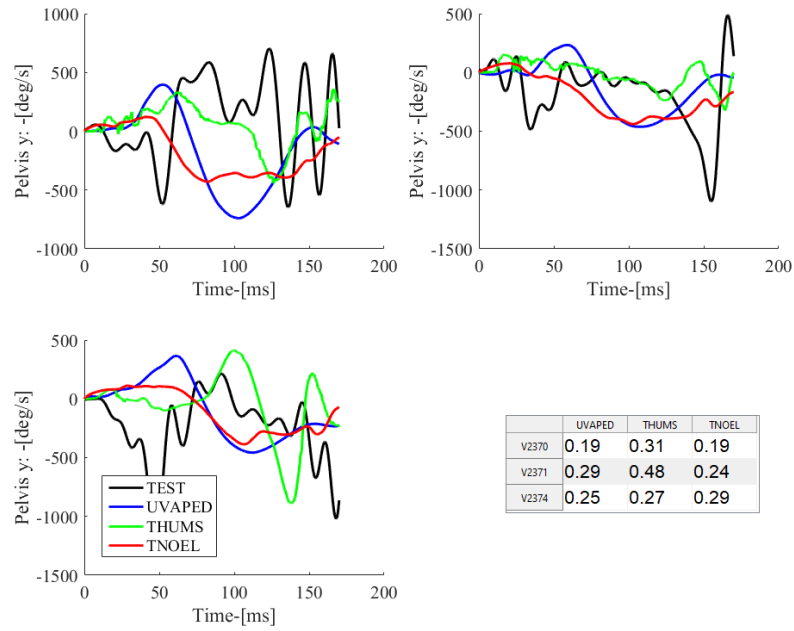


Figure C.18: Pelvis Angular Velocity (Y)

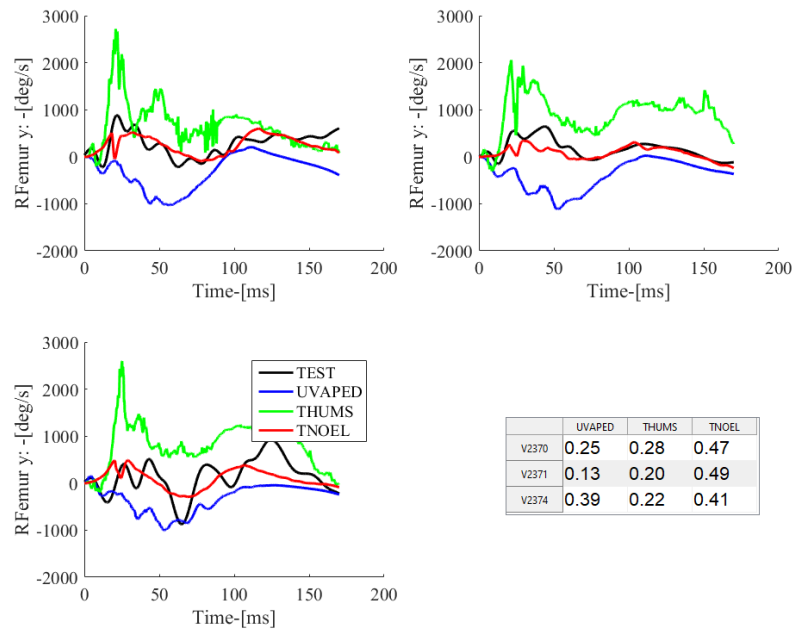


Figure C.19: RFemur Angular Velocity (Y)

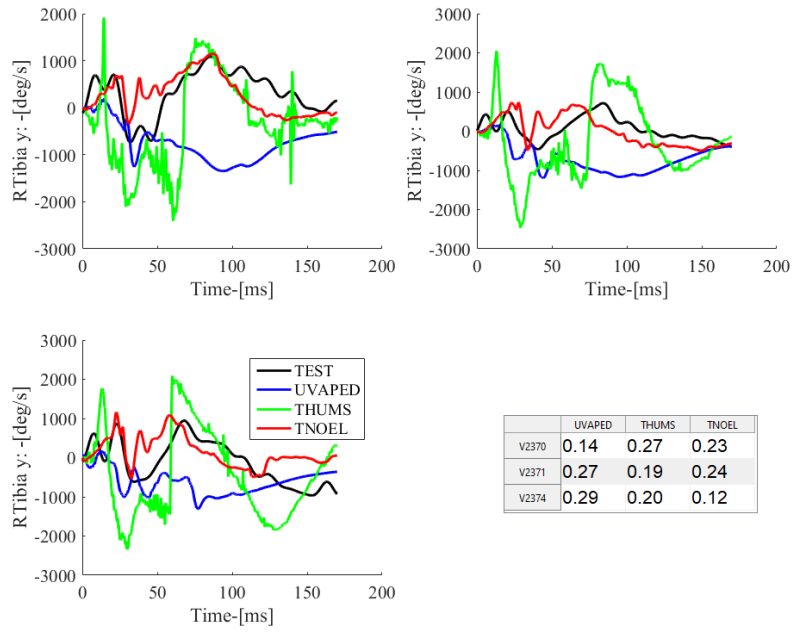


Figure C.20: RTibia Angular Velocity (Y)

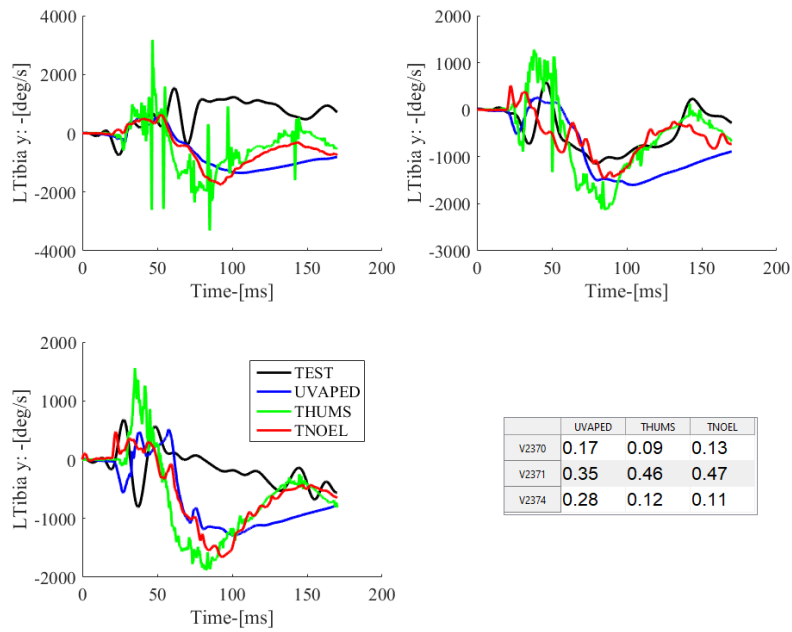


Figure C.21: LTibia Angular Velocity (Y)

## C.5 Angular velocity (Z)

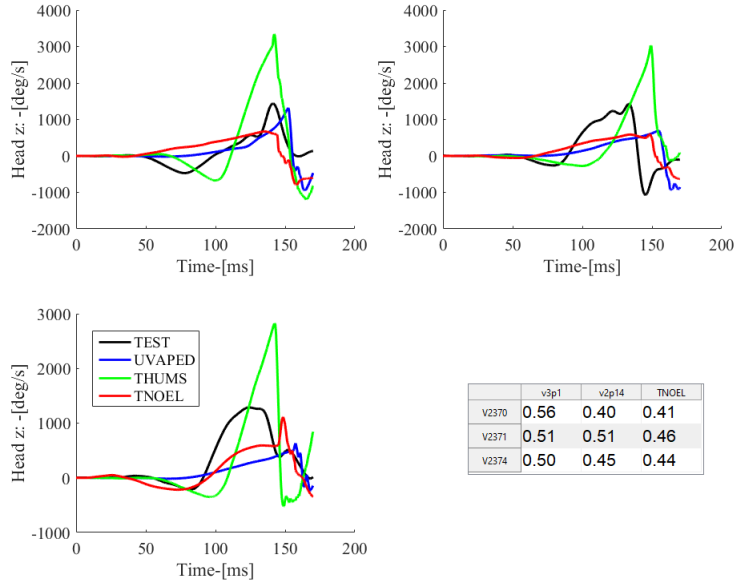


Figure C.22: Head Angular Velocity (Z)

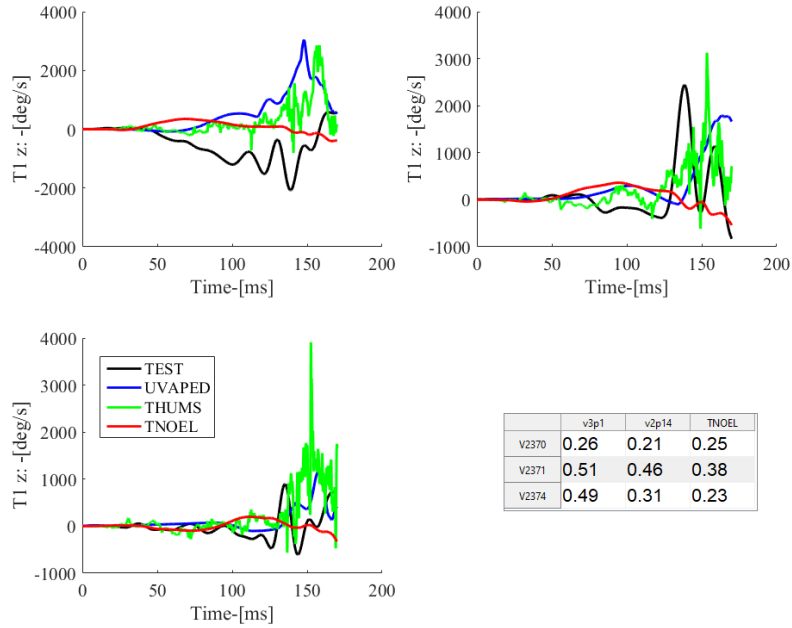


Figure C.23: T1 Angular Velocity (Z)

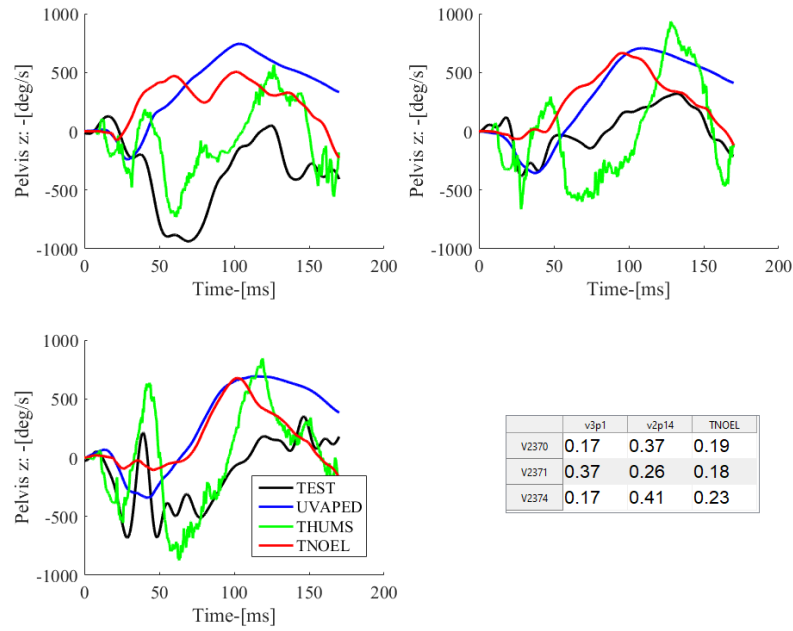


Figure C.24: Pelvis Angular Velocity (Z)

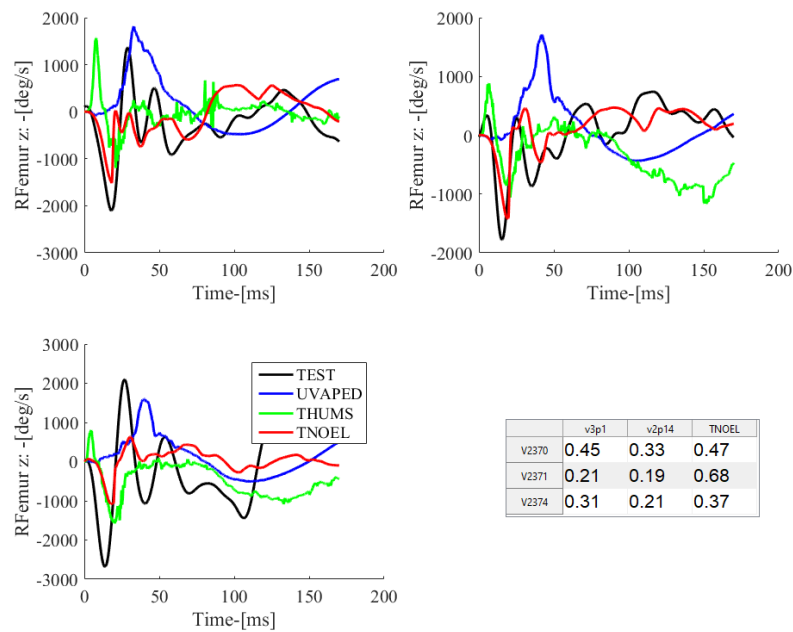


Figure C.25: RFemur Angular Velocity (Z)

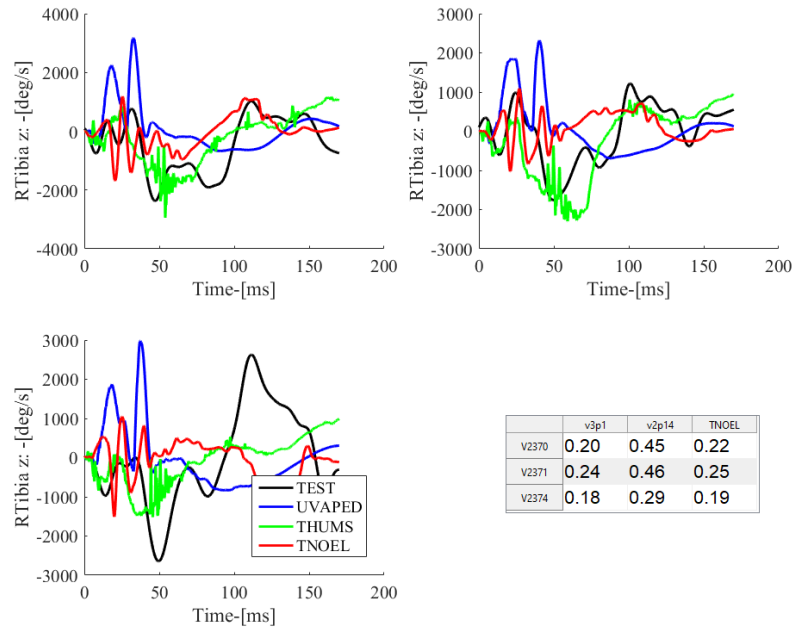


Figure C.26: RTibia Angular Velocity (Z)

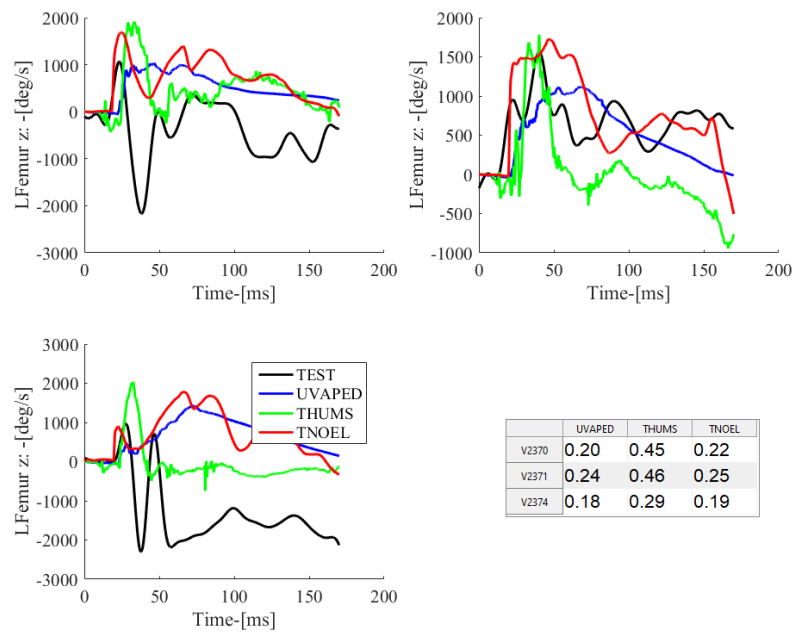


Figure C.27: LFemur Angular Velocity (Z)

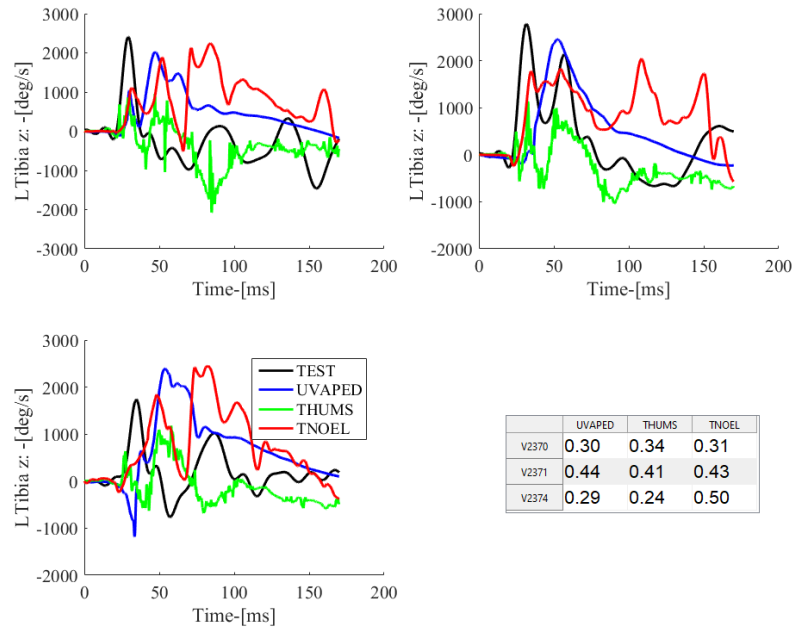


Figure C.28: LTibia Angular Velocity (Z)

## C.6 Contact force (Z)

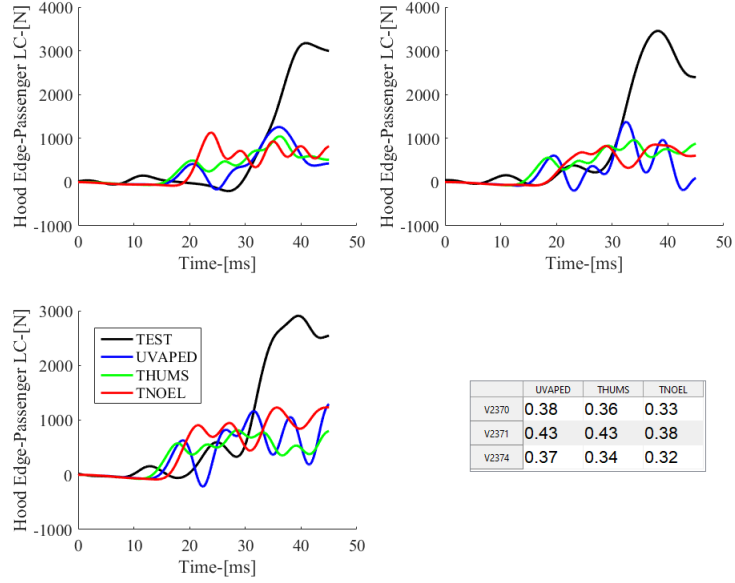


Figure C.29: Hood Edge Passenger Side (Z)

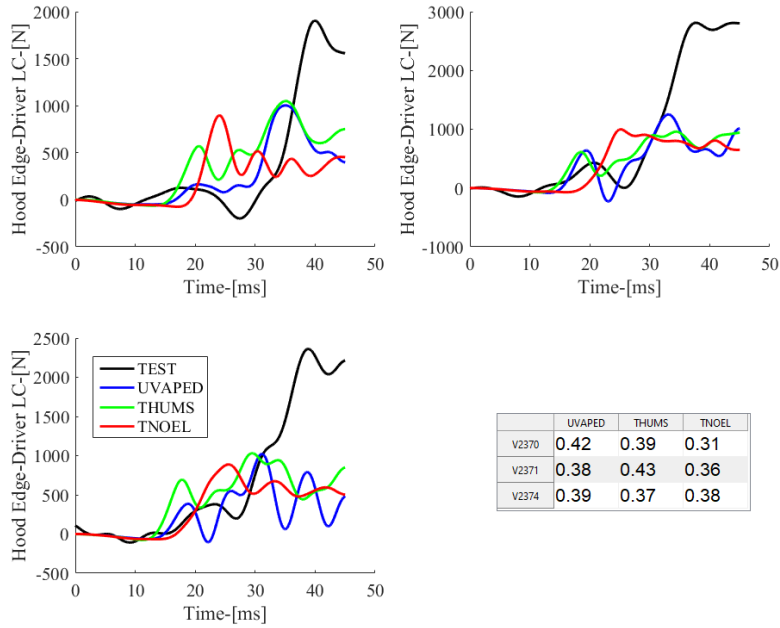


Figure C.30: Hood Edge Driver Side Force (Z)

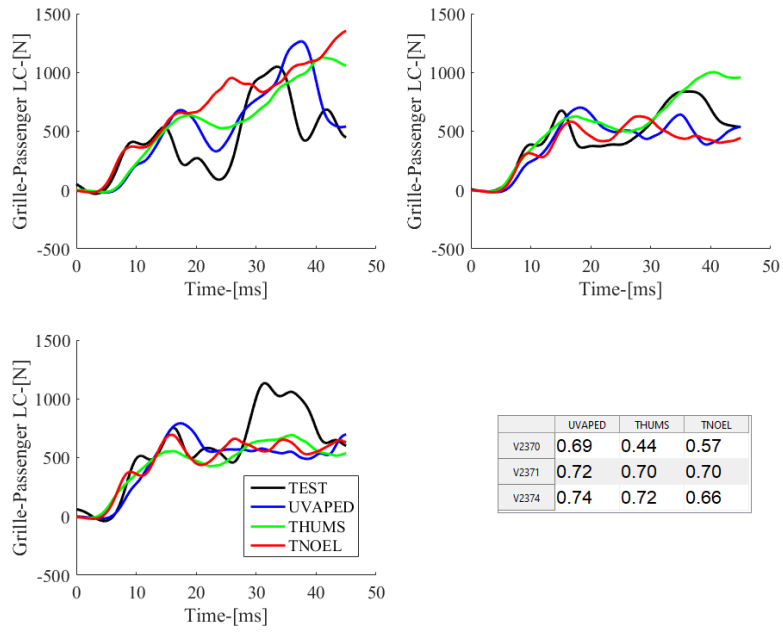


Figure C.31: Grill Passenger Side Force (Z)

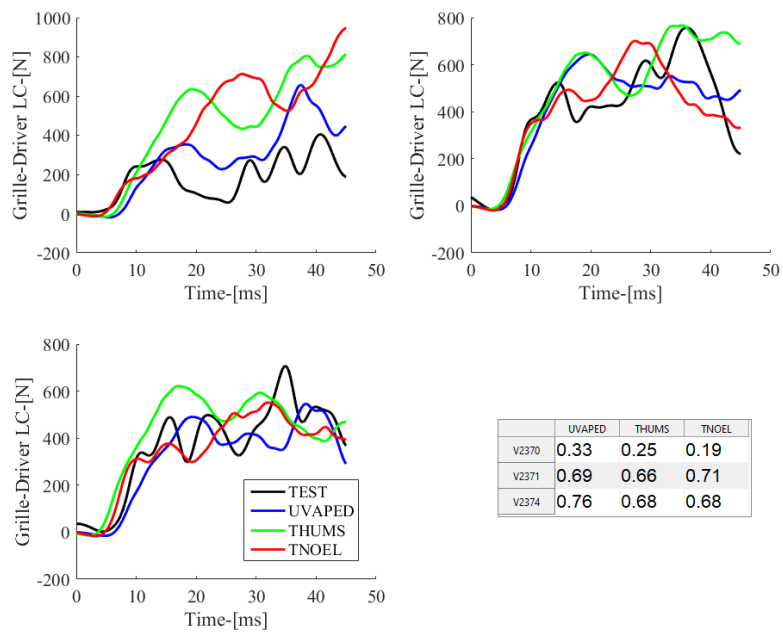


Figure C.32: Grill Driver Side Force (Z)

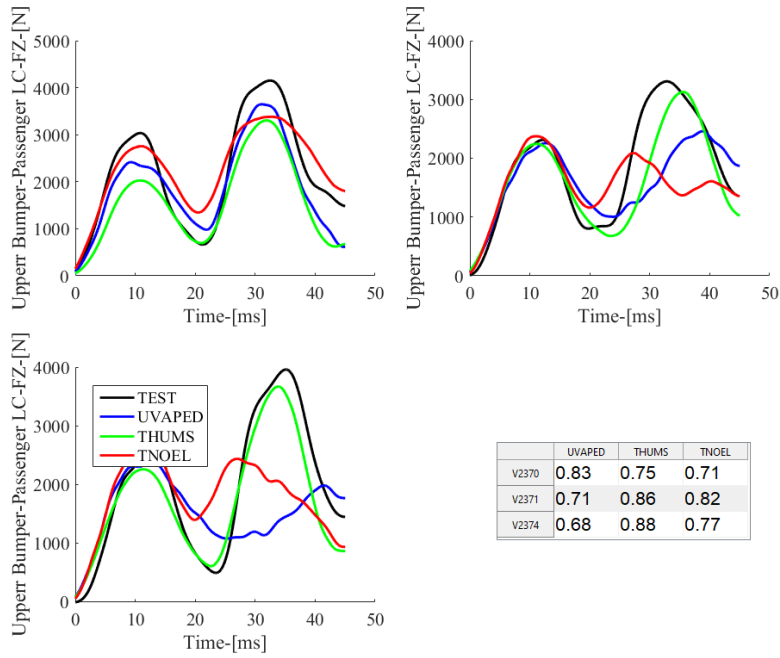


Figure C.33: Upper Bumper Passenger Side Force (Z)

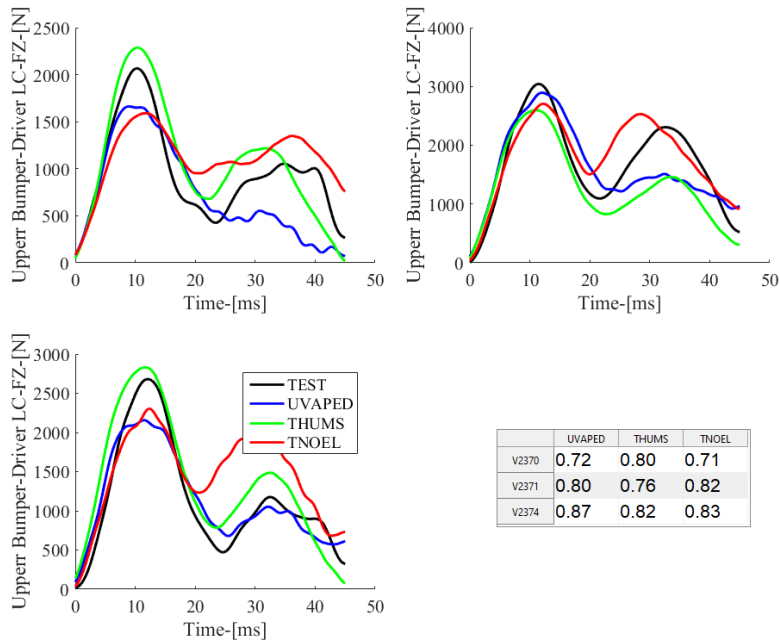


Figure C.34: Upper Bumper Driver Side Force (Z)

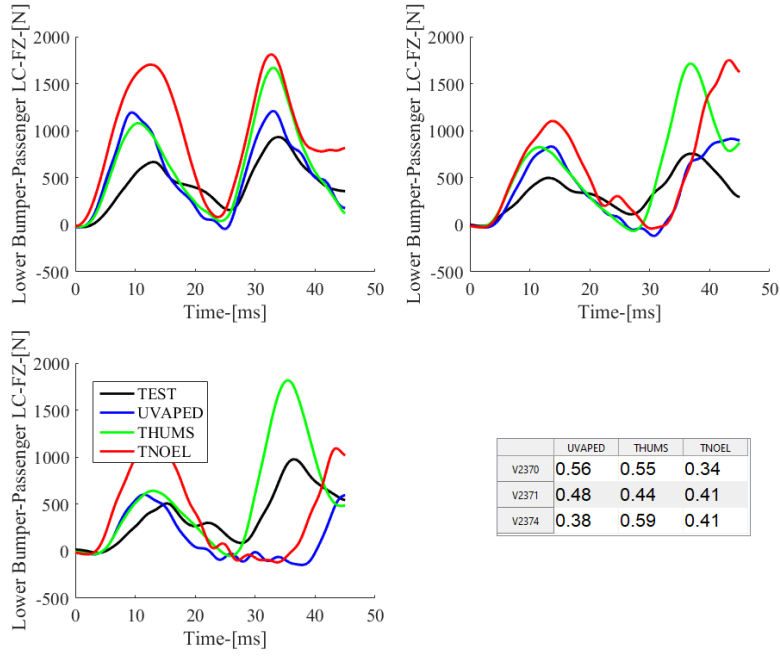


Figure C.35: Lower Bumper Passenger Side Force (Z)

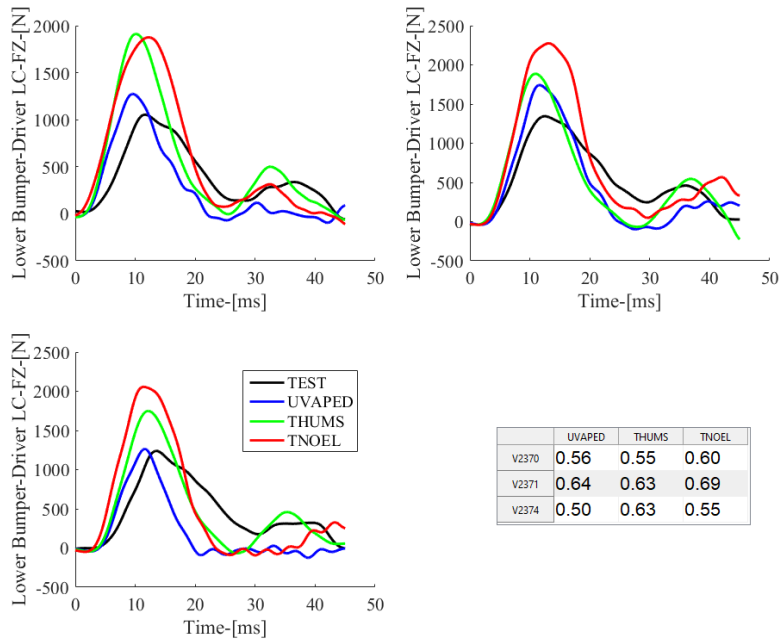


Figure C.36: Lower Bumper Driver Side Force (Z)

## C.7 Contact force (Y)

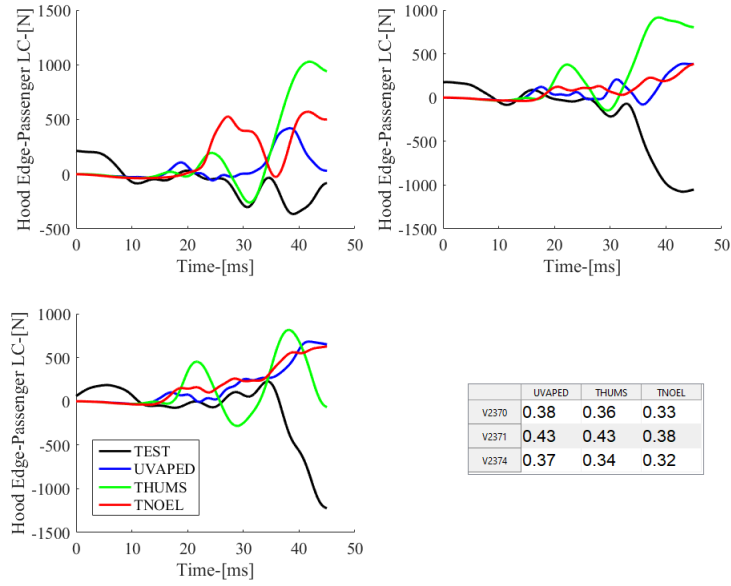


Figure C.37: Hood Edge Passenger Side (Y)

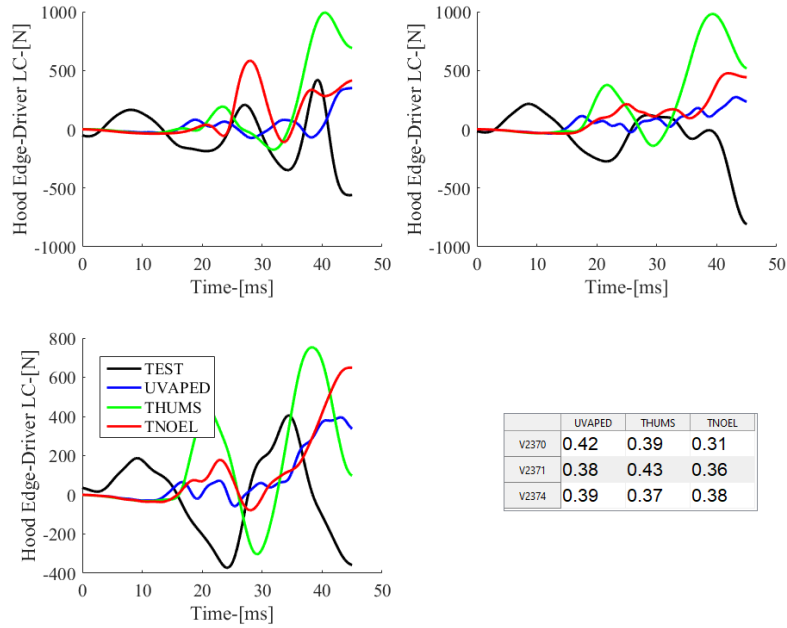


Figure C.38: Hood Edge Driver Side Force (Y)

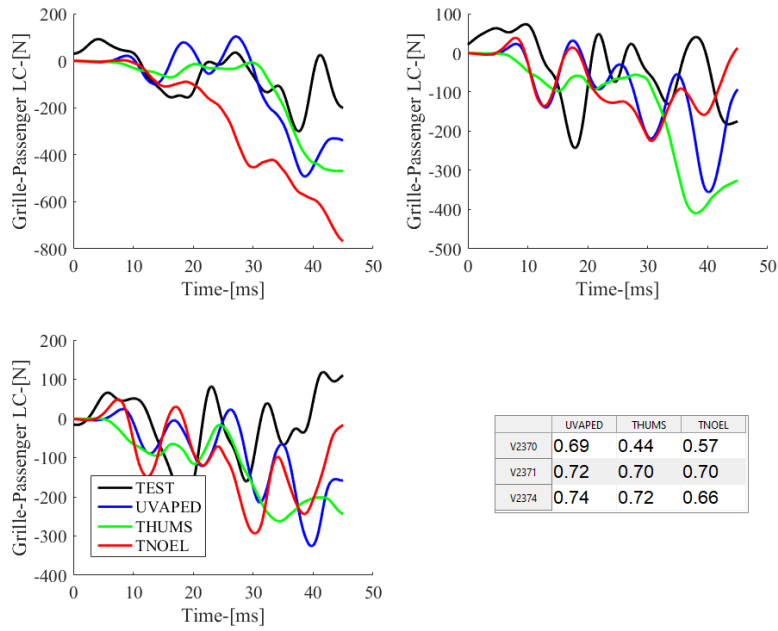


Figure C.39: Grille Passenger Side Force (Y)

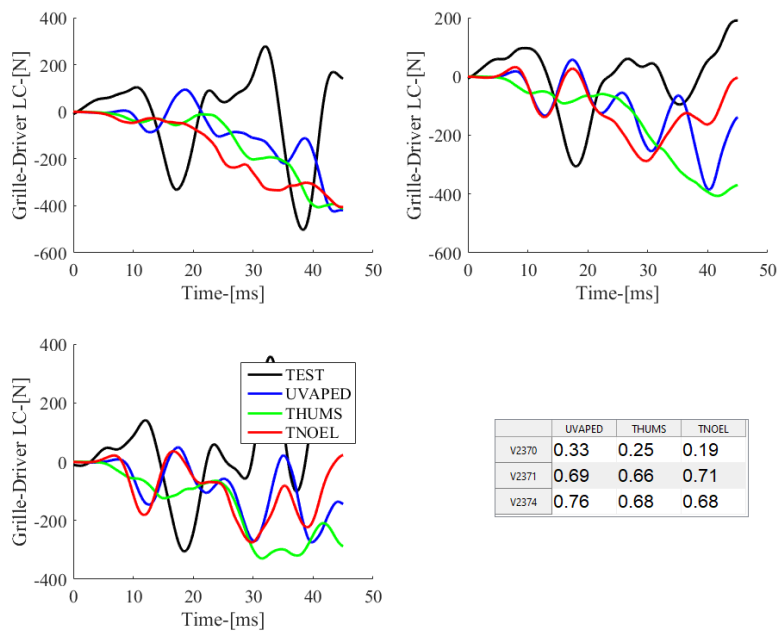


Figure C.40: Grill Driver Side Force (Y)

## Appendix D CIREN Case-Series Analysis

Due to the consideration of multiple injuries during a pedestrian impact, a more comprehensive injury metric was desired to aid the evaluation of the pedestrian protection performance of a vehicle. Additionally, the fidelity of the MADYMO human pedestrian models can be evaluated by understanding the frequency and distribution of injuries occurring in field cases. With the inclusion of impairment (WBFCI) as a loss metric, it was necessary to gauge these outcomes (severity, costs, impairment) against each other. The objective of the current task is to conduct a case series evaluation of the injury distributions and associated losses related to pedestrian crashes that occurred under similar impact scenarios and speeds. An in-depth description of select cases will help further elucidate the potential variation among loss metrics, which may have an impact on the prioritization of potential safety measures. It will also help discern the utility of costs based on maximum AIS injury level (MAIS) as a potential injury metric.

### D.1 Methods

Ten vehicle-to-pedestrian impact cases from the Crash Injury Research and Engineering Network (CIREN) sampled from a total of 67 cases collected at INOVA Fairfax hospital (2002-2007) were analyzed in the current study. Detailed case reviews, crash reconstruction and medical outcomes were available to UVA researchers. The selection criterion for the 10 cases (Table D.1) was based on the impact speed and the anthropometry of the pedestrian and orientation to the vehicle at impact. The desired impact speed was 25 mph with a 50th percentile male pedestrian with a sedan to match the European New Car Assessment Program (Euro NCAP), Global Technical Regulation (GTR) testing standards. Given the convenient nature of this

sample and particular challenge in obtaining precise crash details, the criterion was relaxed to allow for a greater range in anthropometry prior to relaxing acceptable impact speed ranges. In two cases (IDs 32 and 58), the criterion for anthropometry were relaxed as they involved pedestrians who were below the lower quartile range (25th percentile). One case (case 64) was selected to contrast the remaining case series with a different vehicle geometry (i.e., a truck) and age of the struck pedestrian (12 years).

Table D.1: Summary of Included CIREN Cases\*

Case ID	Vehicle Type	Age, years	Height, meter	Weight, kilogram	BMI
6	Sedan	24	1.65 (10)	72.6 (25)	27.7 (50)
8	Sedan	27	1.75 (50)	95.0 (75)	31.0 (75)
16	Sedan	50	1.73 (25)	75.3 (25)	25.2 (25)
17	Sedan	53	1.73 (25)	86.0 (50)	28.7 (50)
23	Sedan	21	1.88 (90)	92.0 (75)	26.0 (50)
27	Sedan	52	1.75 (50)	77.0 (25)	25.1 (25)
32	Sedan	20	1.62 (5)	61.0 (5)	23.2 (25)
33	Sedan	44	1.77 (50)	81.0 (50)	27.1 (50)
58	Sports car	49	1.65 (5)	60.0 (5)	22.0 (5)
64	Truck	12	1.66 (90)	66.0 (85)	24.0 (75)

\*Values in parentheses indicate the closest approximation in percentile value based on the National Health and Nutrition Examination Survey (NHANES) database for US males (McDowell et al. (2008)).

Five out of the 10 cases reported speed estimation based on throw distance measurements. Throw distance is defined as the distance at which the pedestrian lands after being launched into the air by the impacting vehicle. The speed estimated based on throw distance was verified against the data reported from MADYMO simulations (Bhalla et al. (2002)). All the cases were provided with a medical summary containing the findings from X-ray, CT or MRI imaging and the surgical report when

relevant. The cases were also provided with injury coding for all the recorded injuries based on the 1998 AIS scale, vitals of the patient measured on scene and ED, length of hospital stay, ICU stay and ventilator use. Hospital medical costs related to the injury outcomes through the discharge were also reported for each case. A second value for medical costs was estimated from the maximum AIS injury level (MAIS) and compared the average costs reported by [Blincoe et al. \(2014\)](#) to the reported medical costs from each of the CIREN cases under review. The methodology followed by [Blincoe et al.](#) for calculating medical costs was similar to that adopted by WISQARS and described in Task 2, in addition to being completed by the same group from the Pacific Institute for Research and Evaluation (PIRE). It should be noted that the costs reported in CIREN only account for the medical costs incurred until discharge from the hospital and therefore inherently differs from the medical costs reported by [Blincoe et al. \(2014\)](#) and WISQARS, which are principally based on the MAIS injury and also include follow-up costs and various multipliers.

During the case review process all the reported injuries were reviewed with the data reported from the imaging reports and information reported in the surgical notes. When applicable, undocumented or missing injuries from the original CIREN review were added to the relevant case. The 1998 AIS injury codes were updated to the 2008 coding scheme in light of the injury descriptions available from the imaging and OR reports. The Injury Severity Score (ISS) and New Injury Severity Score (NISS) were calculated from the updated list of injuries using the AIS 2005/2008 update. As compared to ISS, some research has shown NISS to be an improved predictor of in-hospital mortality ([Lavoie et al. \(2004\)](#)) and functional recovery after a musculoskeletal injury ([Sutherland et al. \(2006\)](#)).

Using the methods described in Task 2, FCI values were matched to individual injuries to describe the dimensional attributes of functionality and to calculate the

whole body functional losses described in Task 2 (WBFCI). Additionally, the probability of death was calculated for each case using logistic regression equations based on NISS values (Meredith et al. (2002)).

The pedestrian's orientation to the vehicle was verified by comparing the injury severity to impact direction, as well as the scene diagram and reconstruction of impact scenario. The impact location was verified by visually inspecting the damage to the vehicle from the case photographs and correlating them with the anatomy of the body, wrap-around distance, vehicle scuff marks and other physical evidence reported during the original CIREN evaluation. A one-page updated summary of each case was compiled for this task and contains a brief description of incident, vehicle type, anthropometry, injury description, scene diagram, vital signs, cost summary, vehicle photograph and impact locations.

## D.2 Results

Ten pedestrians were struck by vehicles ranging in speeds estimated to be approximately between 20 and 45 miles per hour. On average, these pedestrians suffered 14.3 injuries, ranging between 6 and 26 injuries. The length of a hospital stay averaged 9.7 days, or 12 days when excluding two fatal cases. Single page case reviews for each of the 10 cases is presented in Appendix C. Individually, the medical costs calculated based on the MAIS injury levels (Blincoe et al. (2014)) differed from the medical costs reported by hospitals during the length of initial stay (Figure D.1, Table D.2). In general, the medical costs increased with the number of AIS2+ injuries (Figure D.2).

For the two fatal cases, cost estimates based on MAIS and those reported from hospital data were fairly comparable with differences averaging only \$4,500.

Table D.2: Injury Frequency and Cost Summary

Case ID	Injury (N)	AIS 2+ (N)	Hosp LOS <sup>†</sup>	Hospital Costs, \$	NHTSA Costs*	
					Medical Costs, \$	QALY \$
6	20	8	20	95,591	42,966	732,005
8	6	2	3	20,605	13,947	535,116
16	10	4	16	93,073	13,947	515,116
23	18	8	24	104,397	93,932	3,351,274
32	13	7	6	21,329	41,116	196,133
33	9	2	6	14,843	41,116	397,180
58	12	5	14	71,910	93,932	3,351,274
64	10	1	6	25,295	13,947	535,116
17 <sup>‡</sup>	26	18	1	15,361	11,317	5,244,208
27 <sup>‡</sup>	19	10	1	16,345	11,317	1,506,713
<i>Avg</i>	<i>14.3</i>	<i>6.5</i>	<i>9.7</i>	<i>47,875</i>	<i>37,754</i>	<i>1,636,414</i>
<i>Min</i>	<i>6</i>	<i>1</i>	<i>1</i>	<i>14,843</i>	<i>11,317</i>	<i>196,133</i>
<i>Max</i>	<i>26</i>	<i>18</i>	<i>24</i>	<i>104,397</i>	<i>93,932</i>	<i>5,244,208</i>

\*Based on the 2015 (revised) Blincoe report for costs of MVCs

<sup>†</sup>LOS, length of stay

When accounting for all injuries, the most frequently injured body regions were the lower extremity (inclusive of pelvis) followed by the upper extremities then the head (Figure D.3a). Restricting to moderate or worse (AIS2+) injuries, the lower extremity remains the most frequently injured body region, while the head is the second most injured body region, followed by the upper extremity and thorax (Figure D.3b).

Despite different ages, case ID 58 (49 years) and 23 (21 years) are projected to have the same quality of life year costs (QALY \$, as presented by NHTSA's 2014 Blincoe report) because these costs are based on body region MAIS without consideration of age. A further illustration can be made between cases 17 and 27, which

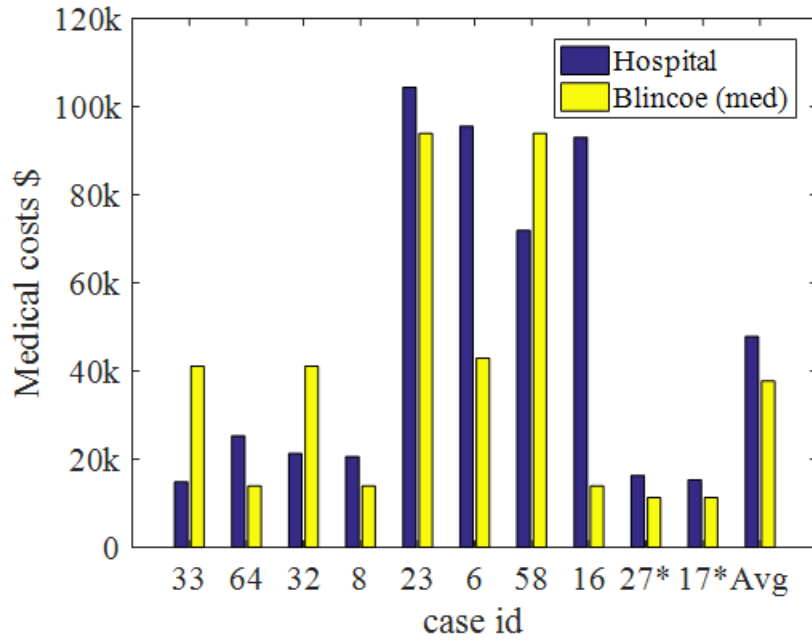


Figure D.1: Comparison of Hospital Costs vs Estimated Costs. (Blincoe et al. (2015))

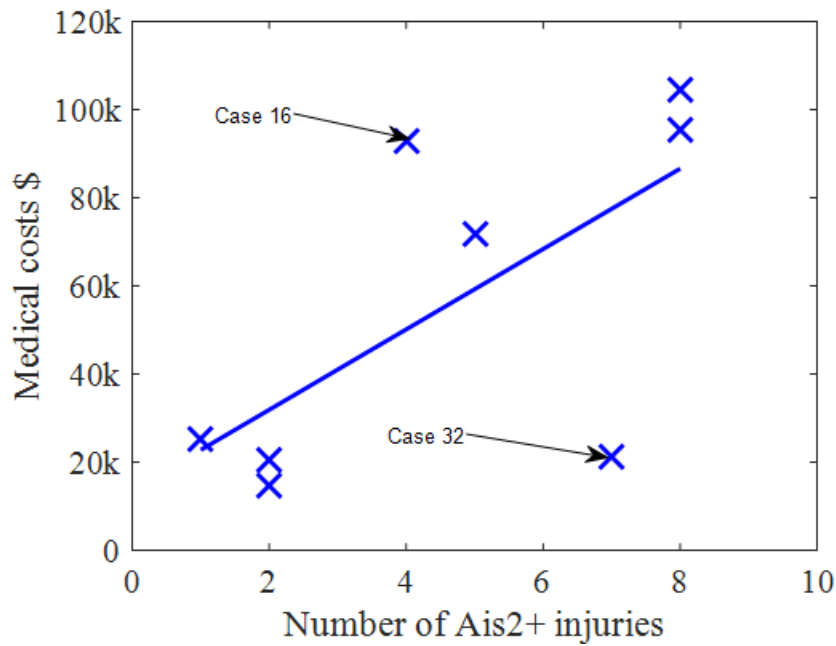


Figure D.2: Hospital Medical Cost vs Number of AIS2+ Injuries (Survivors)

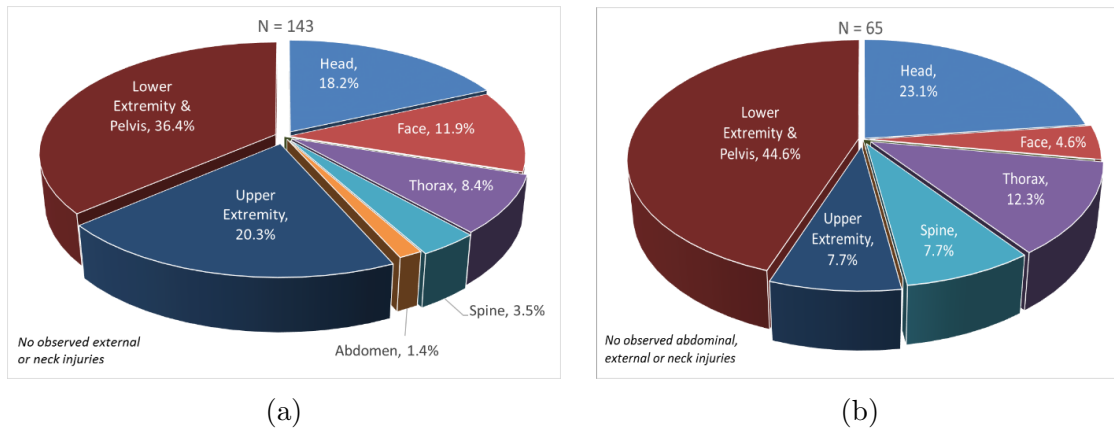


Figure D.3: Frequency Distribution of All (a) and AIS 2+ Injuries Based on Body Region

have similar ages (53 and 52 years, respectively). Both pedestrians sustained critical (AIS 5) injuries, however, the different QALY cost estimates were a result of having incurred the injuries in different body regions (head for case 17, lower extremity and thorax for case 27). In cases of fatality, it may be more sensible to present the statistical value of life, which according to the Blincoe report was estimated at \$9.1 million for 2012 and can be adjusted by the expected remaining years of life. Among non-fatal cases, the largest value of NISS was 34 with a probability of fatality of 17 percent, whereas both non-fatal cases exceeded NISS values of 50 and increased the likelihood of fatality (Table D.3).

The bubble chart in Figure D.4 demonstrates how nine of the ten functional dimensions were affected to some extent among this case series of pedestrians. The size of each bubble represents the average loss for each dimension (in the FCI range of values), and its general frequency by the position on the y-axis. Ambulation was both the most frequently occurring type of impairment (proportion = 0.60) and the largest magnitude of loss (7.84). Vision was the only dimension unaffected. The functional dimensions affected among non-fatal impacts included ambulation, bending

and lifting and cognitive functions, while injuries sustained in the fatal cases affected the functionality in nine of the ten dimensions (Table D.4).

Table D.3: Injury and Disability and Probability of Fatality Scores

Case ID	MAIS 08	NISS	$FCI_{min}$	WBFCI	p(fatality)	
					MAIS 08	NISS
33	3	19	100	100	0.03	0.05
64	2	6	100	100	< 0.01	0.02
32	3	17	100	100	0.03	0.04
8	2	7	92.8	92.9	< 0.01	0.02
23	4	34	87	87	0.13	0.17
6	3	17	92.7	86.9	0.03	0.04
58	4	29	87	82.2	0.13	0.12
16	2	12	81.1	80.7	< 0.01	0.03
27*	5	59	81.1	74.9	0.44	0.68
17*	5	66	60	60	0.44	0.8

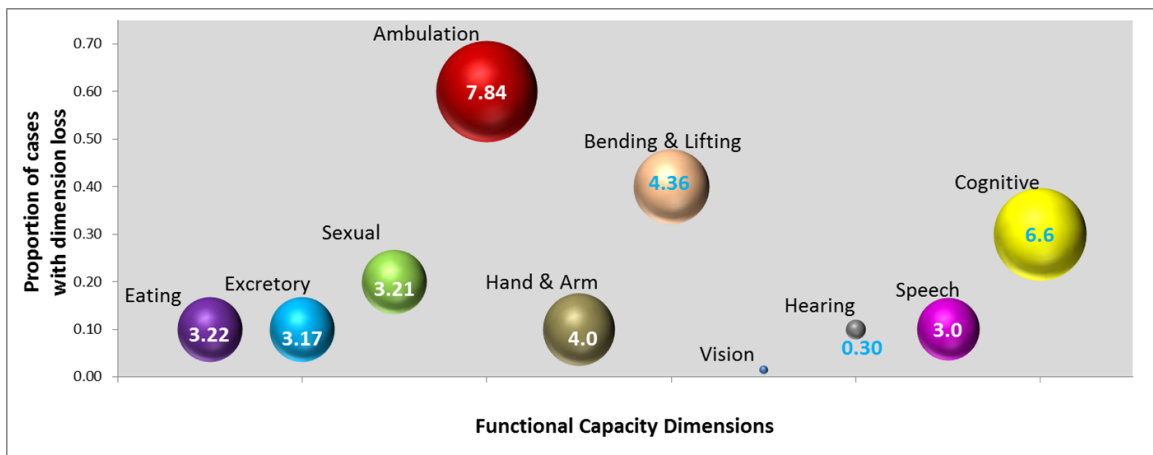


Figure D.4: Proportion and Magnitude of Functional Impairment Among Pedestrian Case Series

Table D.4: Individual Capacity Scores Across The Ten Dimensions of Function, FCI

ID	Eating	Excretory	Sexual	Ambulation	Hand & arm	Bend & lift	Vision	Hearing	Speech	Cognitive
33	100	100	100	100	100	100	100	100	100	100
64	100	100	100	100	100	100	100	100	100	100
32	100	100	100	100	100	100	100	100	100	100
8	100	100	100	93	100	100	100	100	100	100
23	100	100	100	100	100	100	100	100	100	87
6	100	100	100	93	100	93	100	100	100	100
58	100	100	100	93	100	100	100	100	100	87
16	100	100	100	85	100	93	100	100	100	100
27*	100	100	89	85	100	93	100	100	100	100
17*	68	68	79	73	60	78	100	97	70	60
<i>Avg.</i>	<i>97</i>	<i>97</i>	<i>97</i>	<i>92</i>	<i>96</i>	<i>96</i>	<i>100</i>	<i>100</i>	<i>97</i>	<i>93</i>
<i>Min</i>	<i>68</i>	<i>68</i>	<i>79</i>	<i>73</i>	<i>60</i>	<i>78</i>	<i>100</i>	<i>97</i>	<i>70</i>	<i>60</i>
<i>Max</i>	<i>100</i>	<i>100</i>	<i>100</i>	<i>100</i>	<i>100</i>	<i>100</i>	<i>100</i>	<i>100</i>	<i>100</i>	<i>100</i>

\*indicates that the pedestrian involved in the accident succumbed to injuries.

Note that in several instances, the level of detail provided by a series of AIS codes and the complementary predictions for survival or functionality will not convey all of the nuisances and complications that present themselves with any given case. In addition, the available information documented for each case may not capture these nuisances. For example, the acetabular fracture for case ID 64 was not described with enough detail to presume any partial or complement articulation, thus we “code conservatively” (a general rule of AIS coding) resulting in no predicted ambulatory impairment. Similarly, the pelvic fracture described in case 27 (a fatality) is limited in

detail. The mesentery bleed that occurred along with the fracture likely contributed to the fatality more than any other injury, however, that blood loss is not accounted for in the FCI impairment estimation.

When the head or extremities were not injured, the FCI scores indicated none of the dimensions to be affected by impairment (cases 32, 33, 64, Table D.5). If the most severe injury in terms of severity (MAIS) was sustained to the head or extremity body regions, they were also the disabling injuries in terms of FCI (cases 6, 8, 16, 17, 23, 27, 58).

Table D.5: Comparison of Most Severe and Most Disabling Injuries

ID	Severity	Body Region	Injury Description	Max FCI Loss
33	3	Thorax	Pulmonary contusion	100
64	2	Lower Ext.	Acetabulum fracture	100
32	3	Thorax	Pulmonary contusion	100
8	2	Lower Ext.	Tibia shaft fracture	93
23	4	Head	Subdural hematoma	87
6	3	Lower Ext.	Tibia fracture, open	93
58	4	Head	Extradural subdural	87
16	2	Lower Ext.	Tibia plateau	81
27*	5	Lower Ext.	Open book pelvis fx	84
17*	5	Head	Subdural hematoma w/ shift	60

For cases with documented estimates of speed based on throw distance calculations, the estimates fall within the quartile range of speeds described by Searle, which was validated with the aid of MADYMO simulations (Bhalla et al. (2002); Table D.6, Figure D.5). The estimated speed limits were consistently lower than the posted speed limit of 45 mph. In three of the five cases, the estimated speed was close to the target speed of 25 mph. It is interesting to note that although case 17 and

23 presented with a similar estimated impact speed of about 35 mph, the outcome of the events was vastly different, as the pedestrian from case 17 succumbed to injuries whereas the pedestrian from case 23 had functional loss only in the “cognitive” dimension.

Table D.6: Summary of Estimated Vehicle Speed

ID	Throw	Estimated	Estimated	Posted
	distance	Speed	Speed	speed
	(m)	(mph)	(mph)	(mph)
17	20.3	35	56	45
23	NA	37	60	45
27	10.1	25	40	45
32	13.7	27	43	45
58	13.1	27	43	45

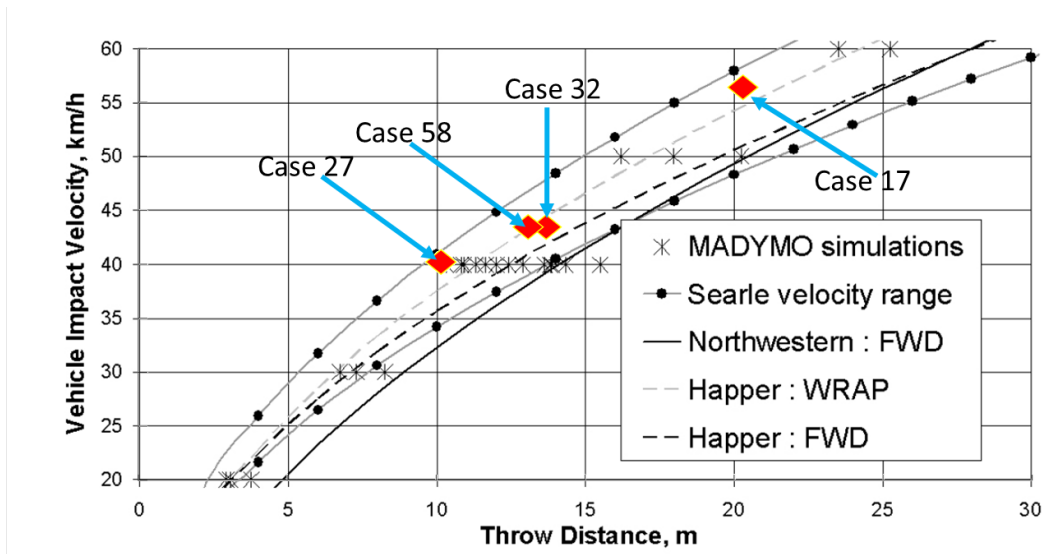


Figure D.5: Comparison of Case Estimated Impact Speed to Reported Corridor Results in Bhalla et al. (2002)

Most of the calculated impact speeds were lower than the posted speed limits and fall within the quartile range of speed vs throw distance corridors (Figure D.5)

verified through MADYMO simulations (Bhalla et al. (2002)). Case 23 and 17 both had the highest estimated speed of 35 mph and suffered from AIS4 and AIS5 level head injuries, indicating that the higher impact speed could be cause of the severe head trauma.

### D.3 Discussion

Average hospital charges to the patients was \$47,875, whereas the average medical costs associated with body region MAIS and estimated by NHTSA (Blincoe et al. (2014)) was \$37,754. Figure A.8 suggests that hospital costs were positively associated with the number of moderate or worse (AIS2+) injuries; however, there are a few “exceptions to the rule”, as demonstrated by cases 16 and 32 which showed contrasting results in relation to the projected averages. Case ID 16 had a disproportionately large hospital charge (\$93,073) despite sustaining “only” four moderate (AIS2+) injuries, whereas the seven AIS 2+ injuries sustained by Case ID 32 resulted in \$21,329 in hospital charges.

The struck pedestrian in Case 16 suffered from fractures to the scapula, humerus, tibia plateau and fibula head resulting in a 16-day hospital stay. The pedestrian case 32 sustained a concussion, adrenal hematoma, pulmonary contusion, and fractures to the maxilla, orbit, L5 transverse process, sacrum, iliac wing and pubic rami. No operations were performed and the length of stay was limited to 6 days prior to being deemed stable and released. Case 16, however, required multiple surgeries to address the fractures to the upper and lower extremities and involved a complication during surgery to depressurize leg compartment syndrome. This suggests that along with the number of multiple AIS2+ injuries the necessity of surgical treatment influences the medical costs associated with the treatment.

Though on average there was an association between medical costs and frequency of AIS2+ injuries, the medical costs from individual cases differed from the estimated NHTSA costs (Blincoe et al. (2014)) based on body region MAIS and irrespective of the number of injuries. However, hospitalized costs were qualitatively similar (approximately \$4,000 greater) to the estimated NHTSA costs when dealing with fatality.

In two cases (IDs 33 and 32), the MAIS was ascribed to a pulmonary contusion. Hospital charges (\$14,843 and \$21,329) were much lower compared to the estimated medical charges from NHTSA (\$41,116). In these cases, the subjects were placed under observation and required no operations, which likely contributed to their lower medical charges. It is also possible that pulmonary contusions are generally associated with lower medical charges compared to other serious (AIS 3) thoracic injuries.

For cases 23 and 58, both pedestrians' most severe injury was sustained in the head body region (AIS 4). The charged hospitalized cost for case 23 was greater than NHTSA's estimated cost by 10%, whereas in case 58 the hospital costs were lower than the estimated cost by 31%. The pedestrian's head in case 23 was operated on to monitor intra-cranial pressure, whereas case 58 only had an operation related to the lower extremity injury while head trauma was simply placed under observation prior to discharge. These differences in the medical costs may be explained by the absence of any surgical procedures to the head.

In case 8 where the maximum severe injury outcome was attributed to tibia and fibular fractures (without any additional AIS2+ injuries). While the hospital charges were greater than the estimated medical costs by 32%, the absolute difference was \$6,658. The difference could be due to the existence of two fractures (tibia and fibula) in the same extremity and resulting treatment for stabilization.

The estimated medical costs for cases 64 and 16 were lower compared to the

hospital costs by 44% (\$11,348) and 85% (\$79,126), respectively. Interestingly, case 64 had only one AIS2+ lower extremity injury and greater cost compared to case 8, that had two AIS2+ injuries to the lower extremity. This discrepancy could be due to a fracture to the pelvic structure that was treated without any surgical intervention. The larger hospital costs in case 16 were likely due to the multiple number of fractures that required surgical intervention in both upper and lower extremities.

In summary, the NHTSA-estimated costs and hospital costs were in close agreement either in the absence of poly-trauma or in the case of mortality. The presence of poly-trauma or surgical intervention in the case of poly-trauma led to a larger difference in costs, with the hospital costs exceeding the estimated medical costs. The average difference in hospital costs and estimated medical costs was 21%, with the hospital costs exceeding the estimated costs.

A reduction in the proportion of upper extremity injuries in the cases of AIS2+ (8%) compared to all injuries (20%) indicate that a large proportion of minor injuries (laceration, contusion and abrasion) were sustained to the upper extremities. The contribution of minor injuries (AIS 1) toward the costs was ignored during the analysis of costs. Amongst moderate (AIS 2+) injuries, the lower extremity (44.6%) was the most frequently injured body region, followed by the head (23.1%), thorax (12.3%), upper extremity and spine (7.7%), which is consistent with the pedestrian injury patterns described among adults in Task 2. The two fatal cases (IDs 17 and 21) involved pelvic injury (AIS 5) and multiple head traumas resulting in NISS scores greater than 50 and a predicted probability of fatality of 0.80 and 0.68, respectively. In case 21 the subject's head hit the a pillar, which is one of the stiffest structures on the front end of the vehicle. Fatality cases also manifested as the most disabling outcomes in terms of FCI scores. The injury distribution of AIS 2+ injuries match the forms of disability outcomes in case of non-fatal injuries with the disabled dimensions being

ambulation, bending and lifting which can be attributed to the extremity injuries and cognitive which can be attributed to the head injuries. Other dimensions like eating, excretory, sexual, hearing and speech were impacted in cases with fatal injury outcomes. Case 17 sustained the worst impairment across all dimensions, due to severe brain damage from impact with the a pillar.

## D.4 Summary

The frequency of AIS2+ injuries were proportional to the medical costs. The estimated medical costs (calculated based on NHTSA [Blincoe et al. \(2014\)](#)), which include readmission costs and the charged hospital costs (reported in CIREN cases) were in close agreement either in the absence of poly-trauma or in the case of fatality. Presence of poly-trauma or surgical interventions led to a larger variation of treatment procedures and a larger variation in costs, with the hospital costs exceeding the estimated medical costs, on average. On a case-by-case basis, the differential between estimated costs (NHTSA) and known hospital charges ranged between \$26,273 and \$79,126, rendering the summarized average costs unreliable. A large proportion of upper extremity injuries were AIS1. Lower extremity and head injuries were the most frequent AIS2+ injuries observed which is consistent with the field data. Estimated higher speed impacts of 35 mph resulted in severe head trauma (AIS 3+). Among the pedestrians who suffered from non-fatal injuries, the dimensions affected by disability were bending and lifting, ambulation and cognitive. The two fatalities involved in this study had a calculated ISS or NISS of greater than fifty with an approximately 0.70 estimated probability of fatality.

## Appendix E MacKenzie's Original Description of FCI Dimension Impairment (1996)

Table E.1: MacKenzie's original Description of FCI Dimension Impairment (1996) - Impairment Levels A,B,C

Major Dimension	Dimensions	Impairment Level		
		A	B	C
Basic Biological Functions	Eating	No limitations	Restrictions in diet or special preparation of foods required because of difficulties chewing, swallowing, or digesting	Tube feeding and/or gastrostomy required
	Excretory Function	No limitations	Controllable excretory difficulty	Moderate incontinence
	Sexual Function	No limitations	Some difficulty due to physical limitations	Severe difficulty due to physical limitations
Mechanical Neuro- musculoskeletal Functions	Ambulation	No limitations	Independent without device but has minor limitations in amount of running or vigorous walking appropriate to age	Independent but may require device; takes more than reasonable amount of time to walk and/or climb stairs
Continued on next page				

**Table E.1 – continued from previous page**

Major Dimension	Dimensions	Impairment Level		
		A	B	C
	Hand & Arm Function	No limitations	Minor limitations in hand function (difficulty with small objects), no limitation in arm function	Major limitation in hand function (difficulty with large objects), no limitation in arm function
	Bending & Lifting	No limitations	Minor limitations in lifting amounts appropriate to age	Major limitations in bending and lifting
Mechanical Sensory Functions	Visual Function	No limitations	No loss in visual activity, but with diplopia	Near normal vision
	Auditory Function	No significant loss; able to hear under everyday listening conditions	Minor difficulty hearing only when listening conditions are less than optimal	Moderate difficulty hearing under everyday listening conditions; usually correctable with hearing aid
	Speech	Can meet all demands necessary for everyday speech and communication	Can meet many to most of the demands necessary for everyday speech	
Cognitive Function	Cognitive Function	No limitations	Hampered or adjusted independence	Aided independence

Table E.2: MacKenzie's original Description of FCI Dimension Impairment (1996) - Impairment Levels D,E,F,G

Major Dimension	Dimensions	Impairment Level			
		D	E	F	G
Basic Biological Functions	Eating				
	Excretory Function	Severe incontinence			
	Sexual Function				
Mechanical Neuro- musculoskeletal Functions	Ambulation	Can walk a minimum of 150 feet but only with assistance	Amount of walking generally limited to 150 feet with or without assistance	Severe difficulty in standing and walking a minimum of 50 feet, including not being able to do it all	
	Hand & Arm Function	No limitation in hand function; minor to moderate limitation in arm function	Complete or near complete loss of function in one but not both limbs	Complete or near complete loss of function in both limbs	
	Bending & Lifting	Cannot bend or lift			
Mechanical Sensory Functions	Moderate-low vision	Visual Function	Severe low vision (legal blindness in USA)	Profound low vision	Total blind-ness

Continued on next page

**Table E.2 – continued from previous page**

Major Dimension	Dimensions	Impairment Level			
		D	E	F	G
	Auditory Function	Severe difficulty hearing even under optimal listening conditions; often, but not always, correctable w hearing aid	Profound to total loss of hearing, non-correctable		
	Speech	Can meet few, if any, of the demands necessary for everyday speech			
Cognitive Function	Cognitive Function	Unconfined dependence	Confined dependence	Complete dependence; limited orientation	

# Appendix F Mapping of AIS Code to Body Region and Injury Metric

Table F.1: Mapping of AIS Code to Body Region and Injury Metric

Body region	Injury Description	specific region	Sev.	AIS 05	Freq	Metric	IRF
Skull	Basilar fx, NFS	skull	3	150200.3	366	HIC15	AIS2-4
	Basilar fx complex	skull	4	150206.4	16	HIC15	AIS2-4
	Skull fx, NFS	skull	2	150000.2	42	HIC15	AIS2-4
	Vault skull fx, closed	skull	2	150402.2	90	HIC15	AIS2-4
	Vault fx comminuted; compound but dura intact; depressed £2cm; displaced	skull	3	150404.3	5	HIC15	AIS2-4
	Vault fx complex; open with torn, exposed or loss of brain tissue	skull	4	150406.4	10	HIC15	AIS2-4
	Brain	Cerebrum laceration >2cm length or depth	brain	4	140686.4	184	uBrIC
Brain stem contusion		brain	4	140204.5	23	uBrIC	AIS2-4
DAI LOC >24 hours NFS		brain	4	161011.5	45	uBrIC	AIS2-4
Brain stem laceration		brain	4	140212.6	1	uBrIC	AIS2-4
Cerebrum contusion NFS		brain	3	140602.3	11	uBrIC	AIS2-4
Cerebrum hematoma, NFS		brain	3	140629.3	82	uBrIC	AIS2-4

Continued on next page

Table F.1 – continued from previous page

Body region	Injury Description	specific region	Sev.	AIS 05	Freq	Metric	IRF
	Cerebrum hematoma epidural or extradural NFS	brain	3	140630.3	12	uBrIC	AIS2-4
	Cerebrum subdural hematoma	brain	3	140650.3	457	uBrIC	AIS2-4
	Cerebrum subarachnoid hemorrhag associated with coma >6 hours	brain	3	140695.3	193	uBrIC	AIS2-4
	Cerebral concussion, loss of consciousness £30 mins	brain	2	161004.2	251	uBrIC	AIS2-4
	Cerebral concussion, loss of consciousness 1-6 hours	brain	3	161006.3	8	uBrIC	AIS2-4
	Cerebral concussion, mild concussion; no loss of consciousness	brain	1	161001.1	508	uBrIC	AIS2-4
	(Oculomotor nerve) NFS	brain	2	130899.2	2	uBrIC	AIS2-4
	(Trochlear nerve) NFS	brain	2	131099.2	1	uBrIC	AIS2-4
	(Trigeminal nerve) NFS	brain	2	131299.2	1	uBrIC	AIS2-4
	(Abducens nerve) NFS	brain	2	131499.2	1	uBrIC	AIS2-4
	(Facial nerve) NFS	brain	2	131699.2	4	uBrIC	AIS2-4
Face	Mandible fx, open, coronoid	face	2	250612.2	2	Force Cnt	2
	Mandible fx, open, body	face	2	250615.2	6	Force Cnt	2
	Mandible fx, open, ramus	face	2	250616.2	1	Force Cnt	2
	Maxilla fx	face	2	250800.2	187	Force Cnt	2

Continued on next page

Table F.1 – continued from previous page

Body region	Injury Description	specific region	Sev.	AIS 05	Freq	Metric	IRF
	Orbital Rim fx, open NFS	face	2	251212.2	2	Force Cnt	2
	Orbital floor blowout fx, closed	face	2	251223.2	96	Force Cnt	2
	Panfacial fracture	face	3	251900.3	3	Force Cnt	2
Neck	Cervical spine Nerve root, single or multiple NFS	C-spine	2	630260.2	2	Nij	AIS2-4
	Cervical spine Brachial Plexus injury NFS	C-spine	2	630299.2	7	Nij	AIS2-4
	Cervical spine disc Dislocation [subluxation], no fracture, no cord involvement NFS	C-spine	2	650204.2	29	Nij	AIS2-4
	Cervical spine fx with or without dislocation but no cord involvement NFS	C-spine	2	650216.2	233	Nij	AIS2-4
	Cervical spine Cord contusion NFS	C-spine	3	640200.3	5	Nij	AIS2-4
	Cervical spine Cord contusion with fx	C-spine	3	640204.3	12	Nij	AIS2-4
	Cervical spine incomplete cord syndrome	C-spine	4	640210.4	10	Nij	AIS2-4
	Cervical spine incomplete cord syndrome with fx	C-spine	4	640214.4	6	Nij	AIS2-4
	Cervical spine complete cord syndrome with fx	C-spine	5	640224.5	1	Nij	AIS2-4
Shoulder	Clavicle fx, shaft open	shoulder	2	750672.2	203	Force Ax	AIS2

Continued on next page

Table F.1 – continued from previous page

Body region	Injury Description	specific region	Sev.	AIS 05	Freq	Metric	IRF
	Scapula fx, neck open	shoulder	2	750962.2	165	Force Ax	AIS2
	Sternoclavicular joint dislocation	shoulder	2	770530.2	2	Force Ax	AIS2
	Shoulder dislocation, open	shoulder	2	771031.2	35	Force Ax	AIS2
Upperarm	Humerus fracture NFS	upperarm	2	751100.2	294	Moment Bend.	AIS2
	Humerus fracture, distal, open	upperarm	3	751372.3	29	Moment Bend.	AIS2
	Upper extremity amputation at or above elbow	upperarm	4	711002.4	1	Moment Bend.	AIS2
	Upper extremity crush injury at shoulder	upperarm	4	713001.4	5	Moment Bend.	AIS2
Lowerarm	Radius fracture NFS	lowerarm	2	752800.2	151	Moment Bend.	AIS2
	Ulna fracture NFS	lowerarm	2	753200.2	147	Moment Bend.	AIS2
	Ulna fracture, proximal, open	lowerarm	3	752174.3	46	Moment Bend.	AIS2
	Radius fracture, distal, open	lowerarm	3	752372.3	36	Moment Bend.	AIS2
wrist	Carpal (wrist) joint dislocation, open	wrist	2	772331.2	5	Force Ax.	AIS2
	Carpus fracture, scaphoid	wrist	2	752451.2	84	Force Ax.	AIS2
	Upper extremity amputation thumb	wrist	2	711005.2	1	Force Ax.	AIS2
Thorax	Rib fx, 2 ribs	thorax	2	450202.2	193	CmaxL or CmaxF	AIS2-4 or AIS2-4

Continued on next page

Table F.1 – continued from previous page

Body region	Injury Description	specific region	Sev.	AIS 05	Freq	Metric	IRF
	Sternum fx	thorax	2	450804.2	49	CmaxL or CmaxF	AIS2-4 or AIS2-4
	Rib fx, >=3 ribs	thorax	3	450203.3	157	CmaxL or CmaxF	AIS2-4 or AIS2-4
	Rib fx, with flail NFS	thorax	3	450209.3	38	CmaxL or CmaxF	AIS2-4 or AIS2-4
	Rib fx, unilateral flail w/ > 5 ribs	thorax	4	450213.4	128	CmaxL or CmaxF	AIS2-4 or AIS2-4
	Diaphragm NFS	thorax	2	440699.2	8	CmaxL or CmaxF	AIS2-4 or AIS2-4
	Brachiocephalic (innominate) vein NFS	thorax	3	420699.3	1	CmaxL or CmaxF	AIS2-4 or AIS2-4
	Lung contusion, NFS	thorax	3	441402.3	320	CmaxL or CmaxF	AIS2-4 or AIS2-4
	Lung laceration, NFS	thorax	3	441414.3	11	CmaxL or CmaxF	AIS2-4 or AIS2-4
	Lung NFS	thorax	3	441499.3	3	CmaxL or CmaxF	AIS2-4 or AIS2-4
	Pericardium hemopericardium without cardiac tamponade or heart injury	thorax	3	441604.3	22	CmaxL or CmaxF	AIS2-4 or AIS2-4

Continued on next page

Table F.1 – continued from previous page

Body region	Injury Description	specific region	Sev.	AIS 05	Freq	Metric	IRF
	Hemopneumothorax, NFS	thorax	3	442205.3	134	CmaxL or CmaxF	AIS2-4 or AIS2-4
	Trachea laceration, NFS	thorax	3	442604.3	1	CmaxL or CmaxF	AIS2-4 or AIS2-4
	Aorta, thoracic NFS	thorax	4	420299.4	11	CmaxL or CmaxF	AIS2-4 or AIS2-4
	Diaphragm laceration, >10cm; with significant tissue loss	thorax	4	440608.4	1	CmaxL or CmaxF	AIS2-4 or AIS2-4
	Esophagus ingestion injury, full-thickness necrosis	thorax	4	440809.4	1	CmaxL or CmaxF	AIS2-4 or AIS2-4
	Hemopneumothorax, major; >1000cc blood loss on at least one side	thorax	4	442206.4	387	CmaxL or CmaxF	AIS2-4 or AIS2-4
Abdomen	Retroperitoneum hemorrhage or hematoma	abdomen	2	543800.2	52	Vcmax, Force1, and Force2	AIS2-3, AIS3-4, and AIS2-3
	Celiac Artery NFS	abdomen	3	520499.3	2	Vcmax, Force1, and Force2	AIS2-3, AIS3-4, and AIS2-3
	Iliac Artery [common, internal, external] and its named branches NFS	abdomen	3	520699.3	13	Vcmax, Force1, and Force2	AIS2-3, AIS3-4, and AIS2-3
	Iliac Vein [common] NFS	abdomen	3	520899.3	2	Vcmax, Force1, and Force2	AIS2-3, AIS3-4, and AIS2-3

Continued on next page

Table F.1 – continued from previous page

Body region	Injury Description	specific region	Sev.	AIS 05	Freq	Metric	IRF
	Vena Cava, inferior NFS	abdomen	3	521299.3	3	Vcmax, Force1, and Force2	AIS2-3, AIS3-4, and AIS2-3
	Superior Mesenteric Artery NFS	abdomen	3	521499.3	14	Vcmax, Force1, and Force2	AIS2-3, AIS3-4, and AIS2-3
	Other named veins NFS e.g., portal, renal, splenic, superior mesenteric	abdomen	3	521699.3	3	Vcmax, Force1, and Force2	AIS2-3, AIS3-4, and AIS2-3
	Aorta, Abdominal NFS	abdomen	4	520299.4	1	Vcmax, Force1, and Force2	AIS2-3, AIS3-4, and AIS2-3
	Bladder laceration, NFS	abdomen	2	540620.2	4	Vcmax, Force1, and Force2	AIS2-3, AIS3-4, and AIS2-3
	Bladder NFS	abdomen	2	540699.2	37	Vcmax, Force1, and Force2	AIS2-3, AIS3-4, and AIS2-3
	Colon (large bowel) NFS	abdomen	2	540899.2	9	Vcmax, Force1, and Force2	AIS2-3, AIS3-4, and AIS2-3
	Duodenum NFS	abdomen	2	541099.2	4	Vcmax, Force1, and Force2	AIS2-3, AIS3-4, and AIS2-3
	Gallbladder NFS	abdomen	2	541299.2	2	Vcmax, Force1, and Force2	AIS2-3, AIS3-4, and AIS2-3
	Jejunum-Ileum (small bowel) NFS	abdomen	2	541499.2	7	Vcmax, Force1, and Force2	AIS2-3, AIS3-4, and AIS2-3

Continued on next page

Table F.1 – continued from previous page

Body region	Injury Description	specific region	Sev.	AIS 05	Freq	Metric	IRF
	Kidney contusion; hematoma NFS	abdomen	2	541610.2	29	Vcmax, Force1, and Force2	AIS2-3, AIS3-4, and AIS2-3
	Kidney laceration NFS	abdomen	2	541620.2	36	Vcmax, Force1, and Force2	AIS2-3, AIS3-4, and AIS2-3
	Kidney NFS	abdomen	2	541699.2	35	Vcmax, Force1, and Force2	AIS2-3, AIS3-4, and AIS2-3
	Liver contusion; hematoma NFS	abdomen	2	541810.2	19	Vcmax, Force1, and Force2	AIS2-3, AIS3-4, and AIS2-3
	Liver laceration NFS	abdomen	2	541820.2	67	Vcmax, Force1, and Force2	AIS2-3, AIS3-4, and AIS2-3
	Liver laceration, simple capsular tears <= 3 cm	abdomen	2	541822.2	24	Vcmax, Force1, and Force2	AIS2-3, AIS3-4, and AIS2-3
	Liver NFS	abdomen	2	541899.2	13	Vcmax, Force1, and Force2	AIS2-3, AIS3-4, and AIS2-3
	Mesentery laceration, NFS	abdomen	2	542020.2	4	Vcmax, Force1, and Force2	AIS2-3, AIS3-4, and AIS2-3
	Mesentery NFS	abdomen	2	542099.2	28	Vcmax, Force1, and Force2	AIS2-3, AIS3-4, and AIS2-3
	Pancreas NFS	abdomen	2	542899.2	8	Vcmax, Force1, and Force2	AIS2-3, AIS3-4, and AIS2-3

Continued on next page

Table F.1 – continued from previous page

Body region	Injury Description	specific region	Sev.	AIS 05	Freq	Metric	IRF
	Rectum NFS	abdomen	2	543699.2	1	Vcmax, Force1, and Force2	AIS2-3, AIS3-4, and AIS2-3
	Spleen contusion; hematoma NFS	abdomen	2	544210.2	15	Vcmax, Force1, and Force2	AIS2-3, AIS3-4, and AIS2-3
	Spleen laceration, simple capsular tears <= 3 cm	abdomen	2	544222.2	12	Vcmax, Force1, and Force2	AIS2-3, AIS3-4, and AIS2-3
	Spleen NFS	abdomen	2	544299.2	61	Vcmax, Force1, and Force2	AIS2-3, AIS3-4, and AIS2-3
	Ureter NFS	abdomen	2	544899.2	1	Vcmax, Force1, and Force2	AIS2-3, AIS3-4, and AIS2-3
	Colon laceration, perforation; full thickness; >=50% circumference	abdomen	3	540824.3	2	Vcmax, Force1, and Force2	AIS2-3, AIS3-4, and AIS2-3
	Liver laceration, moderate, >3cm parenchymal depth; major duct involvement	abdomen	3	541824.3	21	Vcmax, Force1, and Force2	AIS2-3, AIS3-4, and AIS2-3
	Rectum laceration, full thickness; >50% circumference	abdomen	3	543624.3	2	Vcmax, Force1, and Force2	AIS2-3, AIS3-4, and AIS2-3
	Kidney laceration, major, extending through renal cortex	abdomen	4	541626.4	6	Vcmax, Force1, and Force2	AIS2-3, AIS3-4, and AIS2-3
	Liver laceration, major; parenchymal disruption £75% hepatic lobe	abdomen	4	541826.4	16	Vcmax, Force1, and Force2	AIS2-3, AIS3-4, and AIS2-3

Continued on next page

Table F.1 – continued from previous page

Body region	Injury Description	specific region	Sev.	AIS 05	Freq	Metric	IRF
	Spleen laceration, major; involving segmental or hilar vessels	abdomen	4	544226.4	50	Vcmax, Force1, and Force2	AIS2-3, AIS3-4, and AIS2-3
	Stomach injestion injury, full thickness necrosis	abdomen	4	544416.4	1	Vcmax, Force1, and Force2	AIS2-3, AIS3-4, and AIS2-3
	Spleen laceration, massive; hilar disruption producing total devascularization	abdomen	5	544228.5	12	Vcmax, Force1, and Force2	AIS2-3, AIS3-4, and AIS2-3
Lumbar spine	Lumbar spine disc Dislocation [subluxation], no fracture, no cord involvement NFS	lumbar	2	650604.2	17	Force Comp.	AIS2
	Lumbar spine fx with or without dislocation but no cord involvement NFS	lumbar	2	650616.2	431	Force Comp.	AIS2
	Lumbar spine cauda equina contusion with fx	lumbar	3	630606.3	3	Force Comp.	AIS2
	Lumbar spine Cord contusion NFS	lumbar	3	640600.3	3	Force Comp.	AIS2
	Lumbar spine Cord contusion with fx	lumbar	3	640604.3	9	Force Comp.	AIS2
Pelvis	Pelvic ring fracture NFS	pelvis	2	856100.2	650	Force Cnt	AIS2-3
	Acetabulum fracture, complete articular	pelvis	2	856271.2	1	Force Cnt	AIS2-3
	Hip joint dislocation, open	pelvis	2	873031.2	9	Force Cnt	AIS2-3
	Pelvic ring fracture open but NFS	pelvis	3	856101.3	53	Force Cnt	AIS2-3

Continued on next page

Table F.1 – continued from previous page

Body region	Injury Description	specific region	Sev.	AIS 05	Freq	Metric	IRF
	Pelvic ring fracture, complete disruption of posterior arch and pelvic floor NFS	pelvis	4	856171.4	11	Force Cnt	AIS2-3
Femoral Neck	Femur fracture Proximal, femoral neck	femoral neck	3	853161.3	69	Force Ax	AIS3
	Femur fracture Proximal NFS	femoral head or neck	3	853111.3	33	Force Ax	AIS3
	Femur fracture Proximal, trochanteric; intertrochanteric	femoral head	3	853151.3	66	Force Ax	AIS3
	Femur fracture Proximal, femoral head	femoral head	3	853171.3	24	Force Ax	AIS3
Femoral Shaft	Femur fracture shaft, open	femoral shaft	3	853272.3	128	Moment Bend.	AIS3
Knee	Meniscus tear; avulsion NFS	knee	2	840300.2	81	Angle Bend.	AIS2
	Knee Collateral ligament tear	knee	2	840405.2	151	Angle Bend.	AIS2
	Tibia fracture Proximal complete articular; plateau; bicondylar	tibia plateau	2	854171.2	511	Angle Bend.	AIS2
	Knee joint dislocation	knee	2	874030.2	33	Angle Bend.	AIS2

Continued on next page

Table F.1 – continued from previous page

Body region	Injury Description	specific region	Sev.	AIS 05	Freq	Metric	IRF
	Femur fracture Distal partial articular; condylar	femoral condyle	3	853361.3	78	Angle Bend.	AIS2
	Femur fracture Distal complete articular; bicondylar	femoral condyle	3	853371.3	18	Angle Bend.	AIS2
	Femur fracture Distal extra-articular; supracondylar	Distal femur and femoral condyle	3	853351.3	21	Moment Bend.	AIS2
Tibia	Tibia fracture Shaft, simple	tibia shaft	2	854251.2	257	Moment Bend.	AIS2
	Tibia fracture Shaft, complex; comminuted	tibia shaft	2	854271.2	186	Moment Bend.	AIS2
Ankle	Fibula [malleoli] fracture NFS	distal fibula	2	854441.2	151	Angle&Force	AIS2
	Fibula fracture below ankle joint, lateral malleolus open, Weber A open	distal fibula/ankle	2	854454.2	12	Angle&Force	AIS2
	Fibula fracture through ankle joint, Weber B	distal fibula/ankle	2	854461.2	46	Angle&Force	AIS2
	Fibula fracture through ankle joint, Weber B, bimalleolar	distal fibula/ankle	2	854463.2	149	Angle&Force	AIS2
	Talus fracture, extra articular, open	ankle	2	857252.2	29	Angle&Force	AIS2
	Ankle joint dislocation	ankle	2	877130.2	11	Angle&Force	AIS2

Continued on next page

**Table F.1 – continued from previous page**

Body region	Injury Description	specific region	Sev.	AIS 05	Freq	Metric	IRF
	Tibia fracture Distal complete articular	distal tibia	2	854371.2	317	Angle&Force	AIS2
	Fibula fracture above joint, head or neck; Weber C	distal fibula	2	854471.2	707	Angle&Force	AIS2

## Bibliography

- Akiyama, A., M. Okamoto, and N. Rangarajan (2001). Development and application of the new pedestrian dummy. In *ESV Conference, Nagoya*.
- Arregui-Dalmases, C., F. J. Lopez-Valdes, and M. Segui-Gomez (2010). Pedestrian injuries in eight european countries: an analysis of hospital discharge data. *Accident Analysis & Prevention*, 1164–1171.
- Ashton, S. J. (1982). Vehicle design and pedestrian injuries. In J. C. Antony, M. W. Frances, and C. F. Hugh (Eds.), *Pedestrian Accidents*, Chapter 6. New York: John Wileys & Sons Ltd.
- Baker, S. P. and B. O’Neill (1976). The injury severity score: an update. *Journal of Trauma and Acute Care Surgery* 16(11), 882–885.
- Bhalla, K., P. Montazemi, J. R. Crandall, J. Yang, X. Liu, Y. Dokko, Y. Takasaki, Y. Kikuchi, and D. C. Longhitano (2002). Vehicle impact velocity prediction from pedestrian throw distance: trade-offs between throw formulae, crash simulators, and detailed multi-body modeling. In *International Research Council on the Biomechanics of Injury conference*.
- Bhalla, K. S., D. Bose, N. Madeley, J. Kerrigan, J. R. Crandall, D. C. Longhitano, and Y. Takahashi (2003). Evaluation of the response of mechanical pedestrian knee joint impactors in bending and shear loading. In *International Technical Conference on the Enhanced Safety of Vehicles*. National Highway Traffic Safety Administration.
- Blincoe, L., T. R. Miller, E. Zaloshnja, and B. A. Lawrence (2014). The economic and societal impact of motor vehicle crashes, 2010. Technical report.
- Blincoe, L., T. R. Miller, E. Zaloshnja, and B. A. Lawrence (2015). The economic and societal impact of motor vehicle crashes, 2010 (revised). Technical report.
- Bollapragada, V., T. Kim, G. Park, J. Crandall, T. Daniels, and A. Gupta (2016). Development of a multibody human leg model based on beam approximation. In *International Research Council on the Biomechanics of Impact (IRCOBI)*.

- Bose, D. and J. R. Crandall (2008). Influence of active muscle contribution on the injury response of restrained car occupants. In *Annals of Advances in Automotive Medicine/Annual Scientific Conference*, Volume 52, pp. 61. Association for the Advancement of Automotive Medicine.
- Carsten, O. (1986). Relationship of accident type to occupant injuries. final report.
- Carter, E., S. Ebdon, and C. Neal-Sturgess (2005). Optimization of passenger car design for the mitigation of pedestrian head injury using a genetic algorithm. In *7th annual conference on Genetic and evolutionary computation*, pp. 2113–2120. ACM.
- Cavanaugh, J. M., G. W. Nyquist, S. J. Goldberg, and A. I. King (1986). Lower abdominal tolerance and response. In *SAE 861878*.
- Chen, H. (2017). *Evaluating Pedestrian Head Sub-system Test Procedure against Full-scale Vehicle-pedestrian Impact Using Numerical Models*. Ph. D. thesis, University of Virginia.
- Chen, H., D. Poulard, J. R. Crandall, and M. B. Panzer (2015). Pedestrian response with different initial positions during impact with a mid-sized sedan. In *24th International Technical Conference of Enhanced Safety of Vehicles*.
- Compigne, S., Y. Caire, T. Quesnel, and J.-P. Verries (2004). Non-injurious and injurious impact response of the human shoulder three-dimensional analysis of kinematics and determination of injury threshold. Technical report, SAE Technical Paper.
- Cormier, J., S. Manoogian, J. Bisplinghoff, S. Rowson, A. Santago, C. McNally, S. Duma, and J. Bolte (2011). The tolerance of the frontal bone to blunt impact. *Journal of biomechanical engineering* 133(2), 021004.
- Crandall, J. R., K. S. Bhalla, and N. Madeley (2002). Designing road vehicles for pedestrian protection. *Bmj* 324(7346), 1145–1148.
- Crandall, J. R., D. J. Lessley, J. R. Kerrigan, and B. J. Ivarsson (2006). Thoracic deformation response of pedestrians resulting from vehicle impact. *International journal of crashworthiness* 11(6), 529–539.
- Duma, S. M., P. Schreiber, J. McMaster, J. R. Crandall, and C. Bass (2002). Fracture tolerance of the male forearm: the effect of pronation versus supination. *Proceedings of the Institution of Mechanical Engineers, Part D: Journal of Automobile Engineering* 216(8), 649–654.
- EEVC (1998). EEVC working group 17 report—improved test methods to evaluate pedestrian protection afforded by passenger cars. *Delft, the Netherlands: TNO Crash-Safety Research Centre*, 6–8.

- Elliott, J., M. Lyons, J. Kerrigan, D. Wood, and C. Simms (2012). Predictive capabilities of the madymo multibody pedestrian model: Three-dimensional head translation and rotation, head impact time and head impact velocity. *Proceedings of the Institution of Mechanical Engineers, Part K: Journal of Multi-body Dynamics* 226(3), 266–277.
- Eppinger, R., E. Sun, S. Kuppa, and R. Saul (2000). Supplement: Development of improved injury criteria for the assessment of advanced automotive restraint systems-ii. *National Highway Traffic Safety Administration*.
- ETSC (1999). *Safety of Pedestrians and Cyclists in Urban Areas*. The Council.
- Finkelstein, E. A., P. S. Corso, and T. R. Miller (2006). *Incidence and economic burden of injuries in the United States*. Oxford University Press.
- Forman, J. L., H. Joodaki, A. Forghani, P. Riley, V. Bollapragada, D. Lessley, B. Overby, S. Heltzel, and J. Crandall (2015). Biofidelity corridors for whole-body pedestrian impact with a generic buck.
- Forman, J. L., H. Joodaki, A. Forghani, P. O. Riley, V. Bollapragada, D. J. Lessley, B. Overby, S. Heltzel, J. R. Kerrigan, and J. R. Crandall (2015). Whole-body response for pedestrian impact with a generic sedan buck. In *Stapp car crash journal*, Volume 59, pp. 401.
- Funk, J. R., S. C. Srinivasan, J. R. Crandall, N. Khaewpong, R. H. Eppinger, A. S. Jaffredo, P. Potier, and P. Y. Petit (2002). The effects of axial preload and dorsiflexion on the tolerance of the ankle/subtalar joint to dynamic inversion and eversion. Report, SAE Technical Paper.
- Gabler, L. F., J. R. Crandall, and M. B. Panzer (2018). Development of a metric for predicting brain strain responses using head kinematics. *Annals of biomedical engineering*, 1–14.
- Gennarelli, T. A. and E. Wodzin (2006). Ais 2005: a contemporary injury scale. *Injury*, 1083–1091.
- GESAC (2005). Biomechanical response requirements of the thor NHTSA advanced frontal dummy, trauma assessment device development program. Technical report.
- Gold, M. R., D. Stevenson, and D. G. Fryback (2002). HALYS and QALYS and DALYS, Oh My: similarities and differences in summary measures of population Health. *Annual review of public health* 23(1), 115–134.
- Gupta, V. and K. H. Yang (2013). Effect of vehicle front end profiles leading to pedestrian secondary head impact to ground. *Stapp car crash journal* 57, 139.

- Hall, G. W. (1998). *Biomechanical characterization and multibody modeling of the human lower extremity*. Ph. D. thesis, University of Virginia.
- Hall, G. W. (1999). Biomechanical characterization and multibody modeling of the human lower extremity.
- Han, Y., J. Yang, K. Mizuno, and Y. Matsui (2012). Effects of vehicle impact velocity, vehicle front-end shapes on pedestrian injury risk. *Traffic injury prevention* 13(5), 507–518.
- Happee, R., A. Janssen, E. Fraterman, J. Monster, R. Happee, and T. Automotive (2003). Application of MADYMO occupant models in LS-DYNA/MADYMO coupling. In *4th European LS-DYNA Users Conference*, pp. 3–10.
- Hirsch, A. E. and R. H. Eppinger (1984). Impairment scaling from the abbreviated injury scale. In *Proceedings: American Association for Automotive Medicine Annual Conference*, Volume 28, pp. 209–224.
- Hirsch, G. and L. Sullivan (1965). Experimental knee-joint fractures a preliminary report. *ACTA Orthopaedica Scandinavica* 36(4), 391–399.
- Houchens, R., D. Ross, A. Elixhauser, and J. Jiang (2014). Nationwide inpatient sample redesign final report. *Rockville, MD: Agency for Healthcare Research and Quality*.
- Ishikawa, H., J. Kajzer, and G. Schroeder (1993). Computer simulation of impact response of the human body in car-pedestrian accidents. Technical report.
- ISO (1997). Tc22/sc12/wg5, road vehicles-anthropomorphic side impact dummy-lateral impact response requirements to assess the biofidelity of the dummy. Technical report, TR 9790.
- ISO (2002). Pedestrian protection impact test method for pedestrian thigh, leg and knee. Technical report.
- Ito, O., M. Okamoto, Y. Takahashi, F. Mori, M. Meissner, C. Untaroiu, and J. Crandall (2008). Validation of a human FE lower limb model for a child pedestrian against accident data. *JSAE Transaction* 39(1), 21–26.
- Ivarsson, J., D. Lesley, J. Kerrigan, K. S. Bhalla, D. Bose, J. R. Crandall, and R. W. Kent (2004). Dynamic response corridors and injury thresholds of the pedestrian lower extremities. In *Proceedings of the International Research Council on the Biomechanics of Injury conference*, Volume 32. International Research Council on Biomechanics of Injury.

- Kausalyah, V., S. Shasthri, K. A. Abdullah, M. Idres, Q. Shah, and S. Wong (2014). Optimisation of vehicle front-end geometry for adult and pediatric pedestrian protection. *International journal of crashworthiness* 19(2), 153–160.
- Kemper, A. R. (2013). Response corridors for the medial–lateral compressive stiffness of the human arm: Implications for side impact protection. *Accident Analysis and Prevention*, 204–222.
- Kent, R. and J. Patrie (2005). Chest deflection tolerance to blunt anterior loading is sensitive to age but not load distribution. *Forensic science international* 149(2-3), 121–128.
- Kerrigan, J., C. Arregui, and J. Crandall (2009). Pedestrian head impact dynamics: comparison of dummy and pmhs in small sedan and large suv impacts. In *21st international conference on the enhanced safety of vehicles (ESV)*, pp. 09–0127.
- Kerrigan, J., D. Drinkwater, C. Kam, D. Murphy, B. Ivarsson, J. Crandall, and J. Patrie (2004). Tolerance of the human leg and thigh in dynamic latero-medial bending. *International Journal of Crashworthiness* 9(6), 607–623.
- Kerrigan, J., C. Kam, C. Drinkwater, D. Murphy, D. Bose, J. Ivarsson, and J. Crandall (2005). Kinematic comparison of the polar-II and PMHS in pedestrian impact tests with a sport-utility vehicle. In *International Research Council on the Biomechanics of Impact (IRCOBI)*, Volume 33.
- Kerrigan, J. R. (2008a). *A computationally efficient mathematical model of the pedestrian Lower extremity*, Volume 68.
- Kerrigan, J. R. (2008b). *A computationally efficient mathematical model of the pedestrian lower extremity*. ProQuest.
- Kerrigan, J. R., J. R. Crandall, and B. Deng (2008). A comparative analysis of the pedestrian injury risk predicted by mechanical impactors and post mortem human surrogates. *Stapp car crash journal* 52, 527.
- Kerrigan, J. R., D. P. Parent, C. Untaroiu, J. R. Crandall, and B. Deng (2009). A new approach to multibody model development: pedestrian lower extremity. *Traffic injury prevention* 10(4), 386–397.
- King, A. I. (2000). Fundamentals of impact biomechanics: part i-biomechanics of the head, neck, and thorax. *Annual review of biomedical engineering* 2(1), 55–81.
- Kroell, C., D. Schneider, and A. Nahum (1971). Impact tolerance and response of the human thorax. *Society of Automotive Engineers*.

- Kuppa, S. (2004). Injury criteria for side impact dummies. *Washington, DC: National Transportation Biomechanics Research Center, National Highway Safety Administration, US DOT 67.*
- Lavoie, A., L. Moore, N. LeSage, M. Liberman, and J. S. Sampalis (2004). The new injury severity score: a more accurate predictor of in-hospital mortality than the injury severity score. *Journal of Trauma and Acute Care Surgery*, 1312–1320.
- Lawrence, B. A., S. Bhattacharya, E. Zaloshnja, P. Jones, T. R. Miller, P. S. Corso, and C. Steiner (2014). Medical and work loss cost estimation methods for the WISQARS cost of injury module. *Calverton, MD: Pacific Institute for Research and Evaluation (PIRE).*
- Leaf, W. A. and D. F. Preusser (1999). *Literature review on vehicle travel speeds and pedestrian injuries.* US Department of Transportation, National Highway Traffic Safety Administration.
- Lebarbé, M. and P. Petit (2012). New biofidelity targets for the thorax of a 50th percentile adult male in frontal impact. In *Proceedings of the 2012 IRCOBI Conference.*
- Lee, Y., Y. Joo, J. Park, Y. Kim, and H. Yim (2014). Robust design optimization of frontal structures for minimizing injury risks of flex pedestrian legform impactor. *International Journal of Automotive Technology* 15(5), 757–764.
- Leglatin, N., M. Blundell, and G. Blount (2006). The simulation of pedestrian impact with a combined multibody finite elements system model. *Journal of Engineering Design* 17(5), 463–477.
- Li, G., J. Yang, and C. Simms (2017). Safer passenger car front shapes for pedestrians: a computational approach to reduce overall pedestrian injury risk in realistic impact scenarios. *Accident Analysis & Prevention* 100, 97–110.
- Linder, A., A. Clark, C. Douglas, B. Fildes, J. Yang, and L. Sparke (2004). Mathematical modelling of pedestrian crashes: Review of pedestrian models and parameter study of the influence of the sedan vehicle contour. In *Australasian road safety research, policing and education conference*, Volume 8. Monash University.
- Lissner, H., M. Lebow, and F. Evans (1960). Experimental studies on the relation between acceleration and intracranial pressure changes in man. *Surgery, gynecology & obstetrics* 111, 329.
- Lobdell, T., C. Kroell, D. Schneider, W. Hering, and A. Nahum (1973). Impact response of the human thorax: Measurement and simulation. In *Human impact response*, pp. 201–245. Springer.

- Lobo, B., R. Lin, D. Brown, T. Kim, and M. Panzer (2015). Predicting pedestrian injury metrics based on vehicle front-end design. In *International Conference on Internet of Vehicles*, pp. 114–126.
- Loyd, A. M., R. W. Nightingale, Y. Song, J. F. Luck, H. Cutcliffe, B. S. Myers, and C. D. Bass (2012). Impact properties of adult and atd heads. In *International Research Council on the Biomechanics of Impact (IRCOBI)*.
- Mackenzie, E., A. Damiano, J. Ditunno, S. Luchter, and T. Miller (1994). Development of the functional capacity index (FCI). Technical report, U.S. Department of Transportation, National Highway Traffic Safety Administration.
- MacKenzie, E., W. Sacco, S. Luchter, J. Ditunno, C. F. Staz, G. Gruen, D. Marion, and W. Schwab (2002). Validating the functional capacity index as a measure of outcome following blunt multiple trauma. *Quality of Life Research* 11(8), 797–808.
- MacKenzie, E. J., A. Damiano, T. Miller, and S. Luchter (1996). The development of the functional capacity index. *Journal of Trauma and Acute Care Surgery* 41(5), 799–807.
- Martinez, L., L. J. Guerra, G. Ferichola, A. Garcia, and J. Yang (2007). Stiffness corridors of the european fleet for pedestrian simulations. In *20th International Technical Conference on the Enhanced Safety of Vehicles (ESV) National Highway Traffic Safety Administration*, Number 07-0267.
- Matsui, Y., H. Ishikawa, and A. Sasaki (1998). Validation of pedestrian upper legform impact test-reconstruction of pedestrian accidents. In *16th International Technical Conference on Experimental Safety Vehicles-Proceedings*, Volume 1.
- Matsui, Y., A. Wittek, and A. Konosu (2002). Comparison of pedestrian subsystem safety tests using impactors and full-scale dummy tests. Report 0148-7191, SAE Technical Paper.
- McDowell, M. A., C. D. Fryar, C. L. Ogden, and K. M. Flegal (2008). *Anthropometric reference data for children and adults: United States, 2003-2006*.
- McELHANEY, J. H., R. H. HOPPER JR, R. W. NIGHTINGALE, and B. S. Myers (1995). Mechanisms of basilar skull fracture. *Journal of neurotrauma* 12(4), 669–678.
- McMurry, Timothy Land Sherwood, C., G. S. Poplin, M. Segui-Gomez, and J. Crandall (2015). Implications of functional capacity loss and fatality for vehicle safety prioritization. *Traffic injury prevention*, S140–S145.

- Melvin, J. W., A. I. King, and N. M. Alem (1985). Aatd system technical characteristics, design concepts, and trauma assessment criteria. *AATD Task EF Final Report in DOT-HS-807-224 US Department of Transportation, National Highway Traffic Safety Administration, Washington, DC.*
- Meredith, J. W., G. Evans, P. D. Kilgo, E. MacKenzie, T. Osler, G. McGwin, S. Cohn, T. Esposito, T. Gennarelli, and M. Hawkins (2002). A comparison of the abilities of nine scoring algorithms in predicting mortality. *Journal of Trauma and Acute Care Surgery*, 621–629.
- Mertz, H. J. (1984). A procedure for normalizing impact response data. *SAE transactions*, 351–358.
- Meyer, E. and J. Bonnoit (1994). Le choc latéral sur l'épaule: Mise en place d'un protocole expérimental en sollicitation dynamique. *Mémoire de DEA, Université Paris Val de Marne, Faculté de Médecine Pitié-Salpêtrière, Ecole National Supérieure des Arts et Métiers de Paris.*
- Miller, T. R. (1993). Costs and functional consequences of us roadway crashes. *Accident Analysis & Prevention*, 593–607.
- Miller, T. R. (1995). *Databook on nonfatal injury: Incidence, costs, and consequences.* The Urban Insiteute.
- Miller, T. R. (2000). Valuing nonfatal quality of life losses with quality-adjusted life years: The health economist's meow. *Journal of Forensic Economics* 13(2), 145–167.
- Miller, T. R., E. Zaloshnja, B. A. Lawrence, J. Crandall, J. Ivarsson, and A. E. Finkelstein (2004). Pedestrian and pedalcyclist injury costs in the united states by age and injury severity. In *Annual Proceedings/Association for the Advancement of Automotive Medicine*, Volume 48, pp. 265–84. Association for the Advancement of Automotive Medicine.
- Mizuno, Y. (2005). Summary of ihra pedestrian safety wg activities (2005)-proposed test methods to evaluate pedestrian protection afforded by passenger cars. In *Proceedings: International Technical Conference on the Enhanced Safety of Vehicles*, Volume 2005, pp. 15p–15p. National Highway Traffic Safety Administration.
- Mizuno, Y. and H. Ishikawa (2001). Summary of IHRA pedestrian safety WG activities-proposed test methods to evaluate pedestrian protection afforded by passenger cars. In *Proceedings: International Technical Conference on the Enhanced Safety of Vehicles*, Volume 2001, pp. 17–p. National Highway Traffic Safety Administration.

- Nahum, A. M., C. W. Gadd, and D. C. Schneider (1970). Deflection of the human thorax under sternal impact. *Society of Automotive Engineers*.
- Naumann, R. B., A. M. Dellinger, E. Zaloshnja, B. A. Lawrence, and T. R. Miller (2010). Incidence and total lifetime costs of motor vehicle-related fatal and nonfatal injury by road user type, united states, 2005. *Traffic injury prevention*, 353–360.
- Nie, B., Y. Xia, Q. Zhou, J. Huang, B. Deng, and M. Neal (2013). Response surface generation for kinematics and injury prediction in pedestrian impact simulations. *SAE International journal of transportation safety* 1(2), 286–296.
- Nie, B. and Q. Zhou (2016). Can new passenger cars reduce pedestrian lower extremity injury? a review of geometrical changes of front-end design before and after regulatory efforts. *Traffic injury prevention* 17(7), 712–719.
- Osler, T., L. Glance, J. S. Buzas, D. Mukamel, J. Wagner, and A. Dick (2008). A trauma mortality prediction model based on the anatomic injury scale. *Annals of surgery*, 1041–1048.
- Pipkorn, B., C. Forsberg, Y. Takahashi, M. Ikeda, R. Fredriksson, C. Svensson, and A. Thesleff (2014). Development and component validation of a generic vehicle front buck for pedestrian impact evaluation. In *International Research Council on the Biomechanics of Impact (IRCOBI)*.
- Pipkorn, B., R. Fredriksson, S. Oda, Y. Takahashi, S. Suzuki, and M. Ericsson (2012). Development and validation of a generic universal vehicle front buck and a demonstration of its use to evaluate a hood leading edge bag for pedestrian protection. In *International Research Council on the Biomechanics of Injury conference*, Volume 40, pp. 168–181.
- Porta, D., T. Kress, J. Snider, P. Fuller, R. Russell, and J. Hudson (1995). Experimentally-induced frontal bone/facial fractures in human cadavers with a characterization of impact response. pp. 260–268. National Highway Traffic Safety Administration.
- Poulard, D., H. Chen, J. R. Crandall, T. Dzierwonski, M. Pedzisz, and M. B. Panzer (2015). Component-level biofidelity assessment of morphed pedestrian finite element models. In *International Research Council on the Biomechanics of Injury (IRCOBI) Conference*.
- Poulard, D., H. Chen, and M. Panzer (2016). Geometrical personalization of pedestrian finite element models using morphing increases the biofidelity of their impact kinematics. Report 0148-7191, SAE Technical Paper.

- Prasad, P. and H. J. Mertz (1985). The position of the united states delegation to the iso working group 6 on the use of hic in the automotive environment. *SAE transactions*, 106–116.
- Retting, R. and H. Rothenberg (2016). Pedestrian traffic fatalities by state. Report, Governors Highway Safety Association.
- Roberts, B. J., E. Thrall, J. A. Muller, and M. L. Bouxsein (2010). Comparison of hip fracture risk prediction by femoral abmd to experimentally measured factor of risk. *Bone* 46(3), 742–746.
- Rupp, J. D., C. A. Flannagan, and S. M. Kuppaa (2010). Injury risk curves for the skeletal knee–thigh–hip complex for knee-impact loading. *Accident Analysis & Prevention* 42(1), 153–158.
- Sankarasubramanian, H., A. Chawla, S. Mukherjee, and D. Goehlich (2016). Optimisation study on multibody vehicle-front model for pedestrian safety. *International journal of crashworthiness* 21(1), 63–78.
- Sankarasubramanian, H., S. Mukherjee, A. Chawla, and D. Gohlich (2013). A method to compare and quantify threat to pedestrian using injury cost measure. In *International Research Council on the Biomechanics of Impact (IRCOBI)*.
- Santago, A. C., J. M. Cormier, and S. M. Duma (2008). Humerus fracture bending risk function for the 50th percentile male. *Biomedical sciences instrumentation* 44, 231–236.
- Sassi, F. (2006). Calculating QALYs, comparing QALY and DALY calculations. *Health policy and planning* 21(5), 402–408.
- Sears, J. M., L. Blantar, S. M. Bowman, D. Adams, and B. A. Silverstein (2013). Predicting work-related disability and medical cost outcomes: estimating injury severity scores from workers’ compensation data. *Journal of occupational rehabilitation*.
- Sharkey, E., M. Cassidy, J. Brady, M. Gilchrist, and N. NicDaeid (2012). Investigation of the force associated with the formation of lacerations and skull fractures. *International journal of legal medicine* 126(6), 835–844.
- Simms, C. K., T. Ormond, and D. P. Wood (2011). The influence of vehicle shape on pedestrian ground contact mechanisms. In *Proceedings of IRCOBI conference, Poland*.
- Spicer, R. and T. Miller (2010). Uncertainty analysis of quality adjusted life years lost. *Final Report to the National Highway Traffic Safety Administration*.

- Spicer, R. S., T. R. Miller, D. Hendrie, and L. J. Blincoe (2011). Quality-adjusted life years lost to road crash injury: updating the injury impairment index. In *Annals of Advances in Automotive Medicine/Annual Scientific Conference*, Volume 55, pp. 365. Association for the Advancement of Automotive Medicine.
- Stein, M. (1987). Large sample properties of simulations using latin hypercube sampling. *Technometrics* 29(2), 143–151.
- Subit, D., S. Duprey, S. Lau, H. Guillemot, D. Lessley, and R. Kent (2010). Response of the human torso to lateral and oblique constant-velocity impacts. In *Annals of Advances in Automotive Medicine/Annual Scientific Conference*, Volume 54, pp. 27.
- Sullivan, T., A. Haider, S. M. DiRusso, P. Nealon, A. Shaukat, and M. Slim (2003). Prediction of mortality in pediatric trauma patients: new injury severity score outperforms injury severity score in the severely injured. *Journal of Trauma and Acute Care Surgery* 55(6), 1083–1088.
- Sutherland, A. G., A. T. Johnston, and J. D. Hutchison (2006). The new injury severity score: better prediction of functional recovery after musculoskeletal injury. *Value in health*, 24–27.
- Takahashi, Y., M. Ikeda, H. Asanuma, C. Svensson, B. Pipkorn, C. Forsberg, and R. Fredriksson (2014). Full-scale validation of a generic buck for pedestrian impact simulation. In *International Research Council on the Biomechanics of Impact (IRCOBI)*, pp. 730–745.
- Takhounts, E. G., M. J. Craig, K. Moorhouse, J. McFadden, and V. Hasija (2013). Development of brain injury criteria (bric). Report, SAE Technical Paper.
- Takhounts, E. G., R. H. Eppinger, J. Q. Campbell, R. E. Tannous, E. D. Power, and L. S. Shook (2003). On the development of the simon finite element head model. Report, SAE Technical Paper.
- Thunnissen, J., J. Wismans, C. L. Ewing, and D. J. Thomas (1995). Human volunteer head-neck response in frontal flexion: A new analysis. Technical report, SAE Technical Paper.
- TNO (2013). MADYMO human body models manual, release 7.5. Report.
- Trosseille, X., P. Baudrit, T. Leport, and G. Vallancien (2008). Rib cage strain pattern as a function of chest loading configuration. Technical report, SAE Technical Paper.
- UNECE (2008). Global technical regulation No. 9.

- Untaroiu, C. D., D. Bose, Y.-C. Lu, P. Riley, D. Lessley, and M. Sochor (2012). Effect of seat belt pretensioners on human abdomen and thorax: biomechanical response and risk of injuries. *Journal of trauma and acute care surgery* 72(5), 1304–1315.
- Untaroiu, C. D., M. U. Meissner, J. R. Crandall, Y. Takahashi, M. Okamoto, and O. Ito (2009). Crash reconstruction of pedestrian accidents using optimization techniques. *International Journal of Impact Engineering* 36(2), 210–219.
- van Hoof, J., R. de Lange, and J. S. Wismans (2003). Improving pedestrian safety using numerical human models. *Stapp car crash journal* 47, 401.
- Van Rooij, L., K. Bhalla, M. Meissner, J. Ivarsson, J. Crandall, D. Longhitano, Y. Takahashi, Y. Dokko, and Y. Kikuchi (2003). Pedestrian crash reconstruction using multi-body modeling with geometrically detailed, validated vehicle models and advanced pedestrian injury criteria. In *18th ESV Conference*.
- Viano, D. C., I. V. Lau, C. Asbury, A. I. King, and P. Begeman (1989). Biomechanics of the human chest, abdomen, and pelvis in lateral impact. *Accident Analysis & Prevention* 21(6), 553–574.
- Walfisch, G., A. Fayon, C. Tarriere, J. Rosey, F. Guillon, C. Got, A. Patel, and R. Stalnaker (1980). Designing of a dummy’s abdomen for detecting injuries in side impact collisions. Report.
- Wang, Y., T. Kim, Y. Li, and J. Crandall (2015). Neck validation of multibody human model under frontal and lateral impacts using an optimization technique. Technical report, SAE Technical Paper.
- WHO (2013). WHO global status report on road safety 2013: supporting a decade of action. Technical report.
- Wu, T., T. Kim, V. Bollapragada, D. Poulard, H. Chen, M. B. Panzer, J. L. Forman, J. R. Crandall, and B. Pipkorn (2017). Evaluation of biofidelity of THUMS pedestrian model under a whole-body impact conditions with a generic sedan buck. *Traffic injury prevention* 18(sup1), S148–S154.
- Yang, J. (2002). Review of injury biomechanics in car–pedestrian collisions (report to european passive safety network). *Crash Safety Division, Machine and Vehicle Systems, Chalmers University of Technology, SE-412 96*.
- Yang, J., P. Lovsund, C. Cavallero, and J. Bonnoit (2000). A human-body 3d mathematical model for simulation of car-pedestrian impacts. *Traffic Injury Prevention* 2(2), 131–149.
- Zeckhauser, R. and D. Shepard (1976). Where now for saving lives. *Law & Contemp. Probs.* 40, 5.

Zhang, L., K. H. Yang, and A. I. King (2001). Biomechanics of neurotrauma. *Neurological research* 23(2-3), 144–156.

Zhang, Q., J. Kerrigan, M. Kindig, C. Arregui Dalmases, and J. R. Crandall (2013). Axial injury tolerance of the clavicle and the effect of age and gender. In *Injury biomechanics symposium*, pp. 1–17.